AD-A098 120 GHENT RIJKSUNIVERSITEIT (BELGIUM) LAB FOR EXPERIMENTA--ETC F/G 21/5
COOLED, LAMINATED RADIAL TURBINE DEMONSTRATION PROGRAM.(U)
FEB 81 R W VERSHURE, G D LARGE, L J MEYER DAAJ02-77-C-0032
UNCLASSIFIED 21-3684 USAAVRADCOM-TR-81-D-7 NL

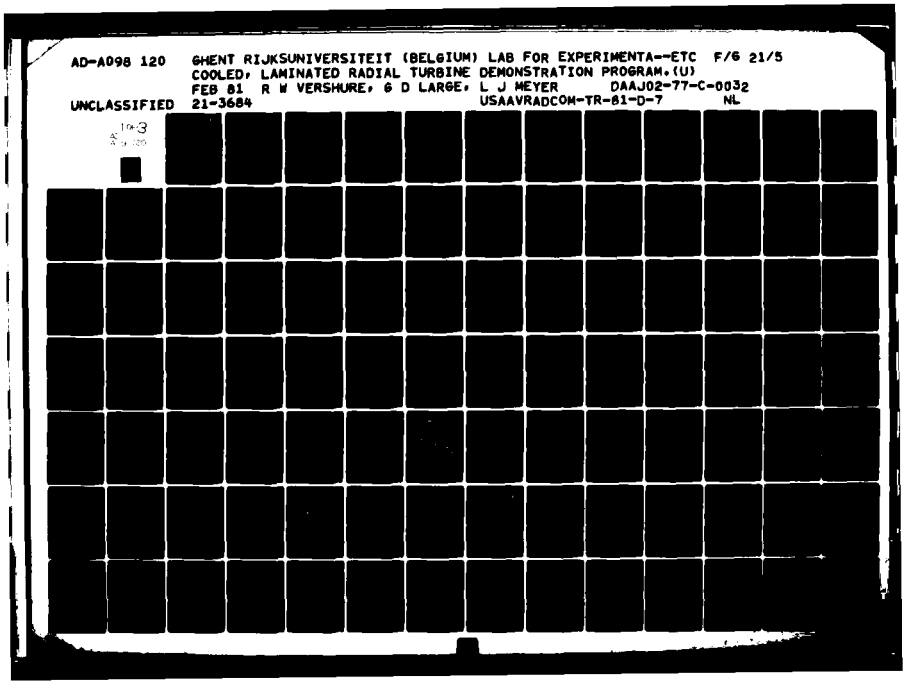

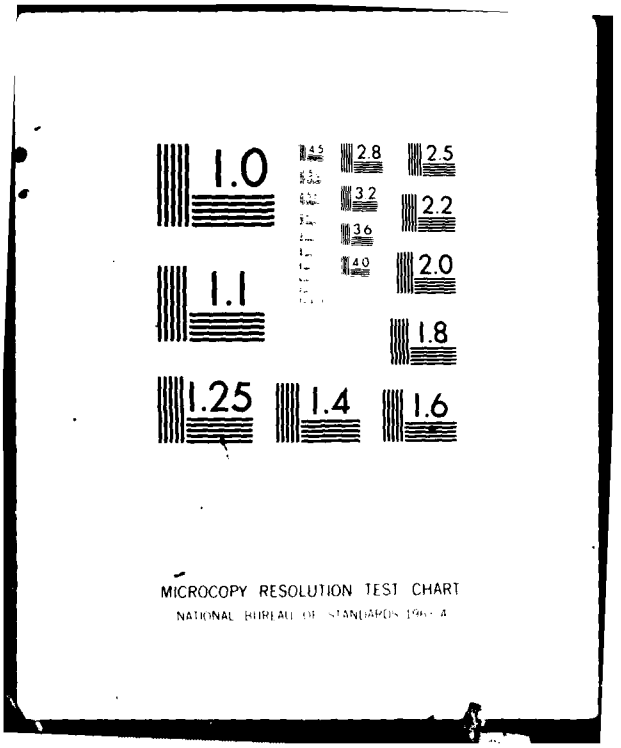
1.0
1.1
1.25
1.4
1.6
1.8
2.0
2.2
2.5
2.8
3.2
3.6
4.0
MICROCOPY RESOLUTION TEST CHART
NATIONAL BUREAU OF STANDARDS 1963-A

USAAVRADCOM-TR-81-D-7

LEVEL II

12

COOLED, LAMINATED RADIAL TURBINE DEMONSTRATION PROGRAM

R. W. Vershure, Jr., G. D. Large, L. J. Meyer, M. J. Egan
GARRETT CORPORATION
AiResearch Manufacturing Co. of Arizona
Phoenix, Ariz. 85034

February 1981

Final Report

Prepared for

APPLIED TECHNOLOGY LABORATORY
U. S. ARMY RESEARCH AND TECHNOLOGY LABORATORIES (AVRADCOM)
Fort Eustis, Va. 23604

APPLIED TECHNOLOGY LABORATORY POSITION STATEMENT

This report provides the documentation for a program which has developed the manufacturing capability for high-temperature cooled radial turbines for small gas turbine engines. The resulting technology is considered feasible and significantly expands the usable cycle conditions under which a radial turbine can be used. The tests and substantiation of this turbine technology are valid and must be considered relative to the text of the test description and the application for the technology. The results of this contract will be used extensively in future high performance small gas turbine engines.

Mr. Jan M. Lane of the Aeronautical Technology Division, Propulsion Technical Area, served as Project Engineer for this effort.

Unclassified

SECURITY CLASSIFICATION OF THIS PAGE (When Data Entered)

REPORT DOCUMENTATION PAGE

READ INSTRUCTIONS BEFORE COMPLETING FORM

1. REPORT NUMBER: USAAVRADCOM TR 81-D-7	2. GOVT ACCESSION NO.
3. RECIPIENT'S CATALOG NUMBER	
4. TITLE (and Subtitle): COOLED, LAMINATED RADIAL TURBINE DEMONSTRATION PROGRAM	5. TYPE OF REPORT & PERIOD COVERED: Final Report
6. PERFORMING ORG. REPORT NUMBER: 21-3684	
7. AUTHOR(s): R. W. Wershure, Jr., G. D. Large, L. J. Meyer, M. J. Egan	8. CONTRACT OR GRANT NUMBER(s): DAAJ02-77-C-0032
9. PERFORMING ORGANIZATION NAME AND ADDRESS: Garrett Corporation, AiResearch Manufacturing Co. of Arizona, Phoenix, Arizona 85034	10. PROGRAM ELEMENT, PROJECT, TASK AREA & WORK UNIT NUMBERS: 62209A; 1L262209AH76; 00; 196 EK
11. CONTROLLING OFFICE NAME AND ADDRESS: Applied Technology Laboratory, US Army Research and Technology Laboratories (AVRADCOM), Fort Eustis, Virginia 23604	12. REPORT DATE: February 1981
	13. NUMBER OF PAGES: 215
14. MONITORING AGENCY NAME & ADDRESS (if different from Controlling Office)	15. SECURITY CLASS. (of this report): Unclassified
	15a. DECLASSIFICATION/DOWNGRADING SCHEDULE

16. DISTRIBUTION STATEMENT (of this Report)

Approved for public release; distribution unlimited.

17. DISTRIBUTION STATEMENT (of the abstract entered in Block 20, if different from Report)

18. SUPPLEMENTARY NOTES

19. KEY WORDS (Continue on reverse side if necessary and identify by block number)

Laminated
Radial Turbine
Turboshaft Engine
Astroloy

20. ABSTRACT (Continue on reverse side if necessary and identify by block number)

A low-cost, high-temperature radial turbine has been developed that demonstrates the technology required to manufacture a small, cooled turbine using photoetched laminates bonded together to form a complete wheel. An advanced long-life and high-performance turbine design is described which uses an iterative optimization procedure to provide a balanced mechanical and aerodynamic design. The calculated bulk heat-transfer effectiveness was [illegible] with operation at 2300°F over a typical Army helicopter mission of [illegible] cycles and with a design life of

DD FORM 1 JAN 73 1473 EDITION OF 1 NOV 65 IS OBSOLETE

Unclassified

SECURITY CLASSIFICATION OF THIS PAGE (When Data Entered)

Block 20. Abstract - continued.

5000 hours. Several wheels were manufactured from precision-rolled Astroloy sheet. The mechanical integrity was demonstrated in a series of proof tests conducted in a whirlpit test facility including overspeed, growth, and burst tests, a stresscoat test, and a 6000-cycle test at overspeed conditions (119-percent design speed) to establish the low-cycle-fatigue characteristics of this rotor.

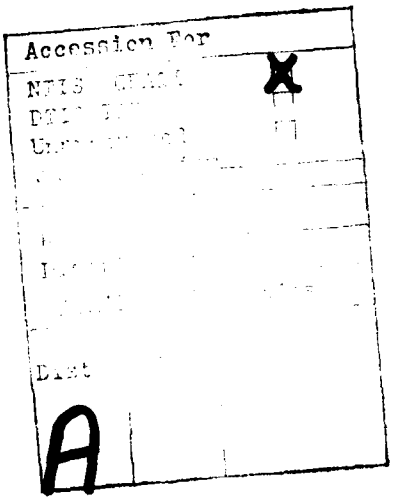

SUMMARY

A small high-temperature cooled radial turbine rotor has been designed for operation at 2300°F and manufactured utilizing the AiResearch laminate process. The laminate design established represents a good balance between aerodynamic and mechanical design which satisfies the major Army design requirements: a design efficiency of 86 percent versus a predicted efficiency of 87.2 percent, a design life of 5000 hours versus a predicted life of 8500 hours in stress rupture, and a low-cycle-fatigue life of 6000 cycles versus a predicted life of 7600 cycles. Also, the maximum metal temperature at the blade tip was held at 1650°F with a bulk average temperature of 1325°F. The inherent flexibility of the laminate process has provided an optimized blade cooling design with a high bulk-metal effectiveness of 0.54.

Three rotors were manufactured in this program using the AiResearch laminate process. During the prototype fabrication, considerable progress was made in optimizing the process to improve producibility and reduce cost. Milestones in the process development include: developing production methods for laminate quality Astroloy sheet; developing an accurate means of measuring chemically milled sheet thickness; developing an improved photochemical machining process utilizing dry-film photoresist; improving cleaning procedures, bond tooling, and bond furnace control; and demonstrating that a hot isostatic press (HIP) cycle can heal porosity and/or unbonded areas and improve yield.

A production cost study was completed for a modest production rate of 50 rotors per month, and the cost to the Government in 1980 was estimated to be $4,250 per wheel. This low manufacturing cost was considered by AiResearch to be well below that of any cast or machined configuration with comparably high cooling and aerodynamic performance. Further cost reductions are considered possible through minimizing the number of laminates by utilizing one-piece end-plates on the inlet portion of the rotor and on the exducer and shaft extension, and by developing a plated boron coating method to replace the Borofuse® boriding process used.

A series of whirlpit tests was conducted to evaluate the mechanical integrity of the rotor. These tests included overspeed, growth, and burst testing up to 126-percent speed and Stresscoat testing to evaluate stress concentrations. A 6000-cycle test was successfully completed in a whirlpit test facility at 119 percent of design speed (87 krpm) to assess the low-cycle-fatigue characteristics of the rotor. Periodic fluorescent penetrant and dimensional inspections of the rotor were conducted during and after the cyclic testing, and the turbine rotor was free of defects and was dimensionally stable throughout the testing.

PREFACE

This final report was submitted by AiResearch Manufacturing Company of Arizona, a division of The Garrett Corporation, under Contract DAAJ02-77-C-0032. The effort was sponsored by the Applied Technology Laboratory, U.S. Army Research and Technology Laboratories (AVRADCOM), Fort Eustis, Virginia, with Mr. Jan M. Lane as the contracting officer's technical representative. Mr. R. W. Vershure, Jr., of AiResearch was technically responsible for the work. He was assisted by G. D. Large, Aerodynamic Design; L. J. Meyer and J. C. Mays, Heat Transfer; D. G. Finger, Stress Analysis; and M. J. Egan, Advanced Materials and Process Engineering.

TABLE OF CONTENTS

TABLE OF CONTENTS

TABLE OF CONTENTS

LIST OF ILLUSTRATIONS

LIST OF ILLUSTRATIONS (Contd)

LIST OF ILLUSTRATIONS (Contd)

LIST OF ILLUSTRATIONS (Contd)

LIST OF ILLUSTRATIONS (Contd)

LIST OF ILLLUSTRATIONS (Contd)

LIST OF TABLES

SECTION I

INTRODUCTION

This report provides the results of the Cooled Laminated Radial Turbine Demonstration Program, which was conducted under Contract DAAJ02-77-C-0032 between the Applied Technology Laboratory and AiResearch. The objective of this 38-month program was to demonstrate the manufacturing technology required to economically fabricate a cooled, high-temperature, radial turbine with sufficient mechanical integrity and aerodynamic performance to meet future Army requirements for a reliable, low-cost, high-performance, small gas turbine engine. The program included the design, fabrication, and mechanical integrity testing of a small air-cooled, laminated, high-pressure, radial turbine wheel. The AiResearch laminate manufacturing process was used to fabricate the turbine rotor. In this process, photoetched laminates were bonded together to form a complete wheel. This program included mechanical property testing of the wheel blanks and definition of the final process specification and materials specification to be used. Several wheels were manufactured from Astroloy sheet material, and mechanical integrity testing was conducted in a series of proof tests utilizing a whirlpit test facility.

SECTION II

DESIGN

AERODYNAMIC DESIGN

Cycle Requirements

The conceptual engine configuration established for the cooled radial turbine is based on combining the characteristics of the advanced 10/1 centrifugal compressor with the radial turbine requirements of this program. The result is a 3-lb/sec class turboshaft engine with the following turbine design point requirements:

Rotor Inlet Total Temperature, °F	= 2300
Total-to-Total Pressure Ratio, $P_{R_{t-t}}$	= 3.30
Inlet Corrected Flow, $w\sqrt{\theta}/\delta$, lb/sec	= 0.633
Physical Speed, N, RPM	= 73,379
Corrected Speed, $N/\sqrt{\theta}$, RPM	= 31,811
Total-to-Total Efficiency, η_{t-t}	= 0.860

Preliminary Design Considerations

The preliminary turbine aerodynamic design was based on an optimization study which established the attainable turbine efficiency as a function of rotor inducer tip speed and blade number. The optimization technique was developed specifically for highly loaded radial turbines which are tip-speed-limited due to the limitations of currently available materials. The effect of rotor tip speed on attainable turbine efficiency is best illustrated by relating the efficiency to a stage work coefficient, defined as the ratio of imposed work level to the inducer tip speed squared ($\psi_{stage} = gJ\Delta H/U_2^2$). Figure 1 shows these characteristics based on the test results of an in-house research turbine. The variation of stage work coefficient was achieved by varying turbine corrected speed while maintaining design-point pressure ratio. At 100 percent design speed, optimum tip speed and peak efficiency are achieved. However, at higher or lower speeds, performance decreases primarily due to rotor inlet incidence. At 80 percent of design corrected speed (positive incidence with respect to rotor rotation), the total-to-total efficiency decrement is 4.5 points for an increase in stage work coefficient from 0.90 to 1.33. Of the total efficiency decrement, analysis shows that 3.4 points can be attributed to rotor inlet incidence. The remaining 1.2 points are a result of higher stator loss and lower rotor reaction. Conversely, at higher than design speeds (higher than optimum tip speed) stator loss decreases and rotor reaction increases,

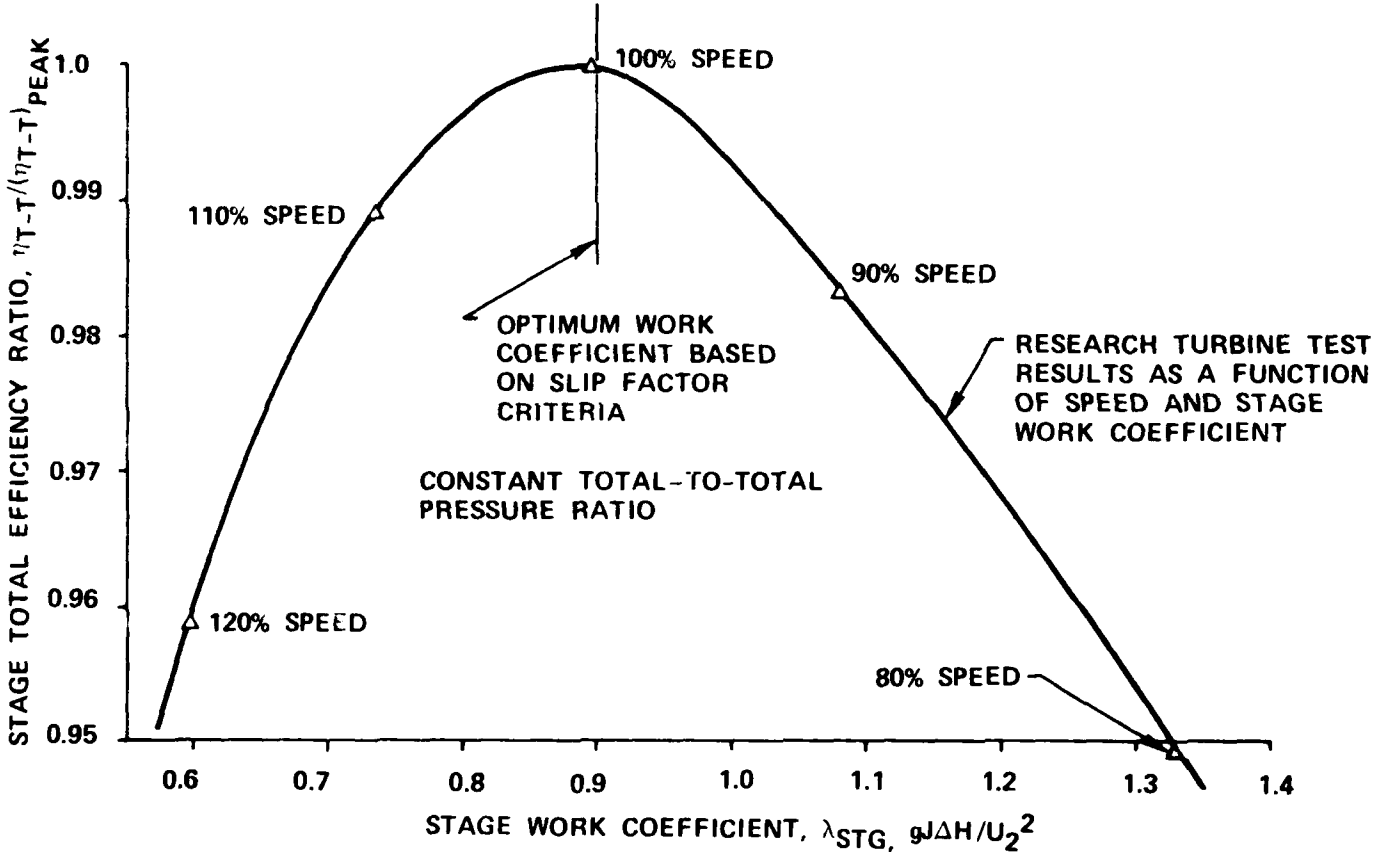

Figure 1. Effect of Stage Work Coefficient on Peak Turbine Efficiency.

resulting in a lower overall performance decrement. If the centrifugal compressor slip factor criteria developed by Stanitz[1] are applied to this turbine, the optimum stage work coefficient is 0.90, which correlates well with the observed peak efficiency (where approximately zero exit swirl was obtained).

Normally the designer is not faced with designing a turbine with a higher than optimum tip speed. Therefore, high work radial turbines will be tip-speed-limited, and positive rotor inlet incidence losses will predominate.

To reduce the rotor inlet incidence losses associated with high work radial turbines, three approaches are feasible. The first is to adjust the inducer-to-exducer work split to allow optimum rotor inlet conditions to be reestablished. In principle, peak efficiency could be maintained under these conditions; however, in practice this solution merely transfers the losses to the downstream interturbine duct and turbine stages (due to the increase in rotor exit kinetic energy and swirl). This does not imply that a favorable trade-off between rotor inducer loss and interturbine duct loss is not possible by adjusting the inducer-to-exducer work split; however, this type of analysis was beyond the scope of the current program. The second and desirable approach is similar to the above, except now the requirement for radial rotor blade elements is relieved. Under these conditions, the turbine-interturbine duct system optimization would then be a function of rotor inlet blade angle. This type of analysis would be the logical choice for investigating future aerodynamic performance increases for the cooled turbine. The third approach, and the one selected for optimizing the cooled radial turbine for this program, is based on radial blade elements, assumes that the downstream stages are co-rotating, and does not consider the influence of the interturbine duct. Under these conditions, analysis shows that an optimum vector diagram for tip-speed-limited radial turbines can be achieved which will maximize turbine efficiency. This is accomplished by minimizing the total losses between rotor inlet incidence and exit swirl losses. This analysis is considered desirable for the present design even though a counter rotating downstream turbine would be utilized and the rotor exit tangential component would not be lost. First, this procedure increases the turbine efficiency relative to zero exit swirl, and in doing so, maintains high rotor reaction. Secondly, the magnitude of rotor exit swirl introduced by this method will not arbitrarily favor the turbine efficiency at the expense of unduly increasing the interturbine duct loss.

3
B

(1) Stanitz, J. D., "Some Theoretical Aerodynamic Investigations of Impellers in Radial and Mixed Flow Centrifugal Compressors," Trans. ASME, Vol. 74, No. 4, May 1952.

The latter optimization procedure was applied to the cycle requirements of the cooled radial turbine for a range of rotor tip speeds and blade numbers during the preliminary design phase of the program. The results are presented in Figure 2. Based on rotor life requirements, mechanical analysis indicates that the maximum allowable rotor tip speed is 1880 feet per second. At this condition, 14 blades are required to achieve the efficiency goal of 86.0 percent.

The optimized one-dimensional vector diagram for the selected turbine configuration is presented in Figure 3. The average exit swirl angle is -21.96 degrees. Figure 4 shows the variation of interstage duct loss coefficient as a function of average rotor exit swirl (based on Reference 2 data) normalized by the minimum value measured. In Dovzhik's experiment, the inlet conditions were based on uniform temperature and pressure and the duct endwalls were straight. Available AiResearch duct data is based on actual rotor exit conditions (inlet duct conditions) with moderately curved endwalls and radius ratios between turbines. Since the current engine conceptual layout indicates that the cooled radial turbine interstage duct will not require struts, a minimum loss coefficient of 0.20 was used to estimate the duct loss with -21.96 degrees of rotor exit swirl. With an exit absolute critical velocity ratio (V/Acr') of 0.403, the calculated interstage duct loss is 1.61 ($\Delta P/P$).

The preliminary meridional flow path corresponding to the one-dimensional vector diagram is shown in Figure 5. In order to minimize rotor blade surface area required for cooling, and in addition, minimize rotor weight and inertia, a separate analysis was conducted to determine the minimum rotor axial length required to achieve satisfactory rotor blade velocity distribution.

For tip-speed-limited designs, the highly loaded regions of the rotor are predominantly in the inducer region. Therefore, an overall rotor blade loading parameter similar to the Zweifel loading coefficient utilized for axial rotors is currently not utilized due to the lack of meaningful correlations. An alternate approach for evaluating the solidity requirements of the radial rotor is to examine the mean line loading distribution through the rotor over a range of exducer lengths. The entire blade height through the rotor is treated as a stream tube and the continuity equations, together with an estimated rotor blade angle distribution, determine the rotor meanline relative velocity distribution. The condition of zero absolute vorticity

(2) Dovzhik, S. A., and V. M. Kartavenko, "Measurement of the Effect of Flow Swirl on the Efficiency of Annular Ducts and Exhaust Nozzles of Axial Turbomachines," Fluid Mechanics Soviet Research, Vol. 4, No. 4, July-August 1975.

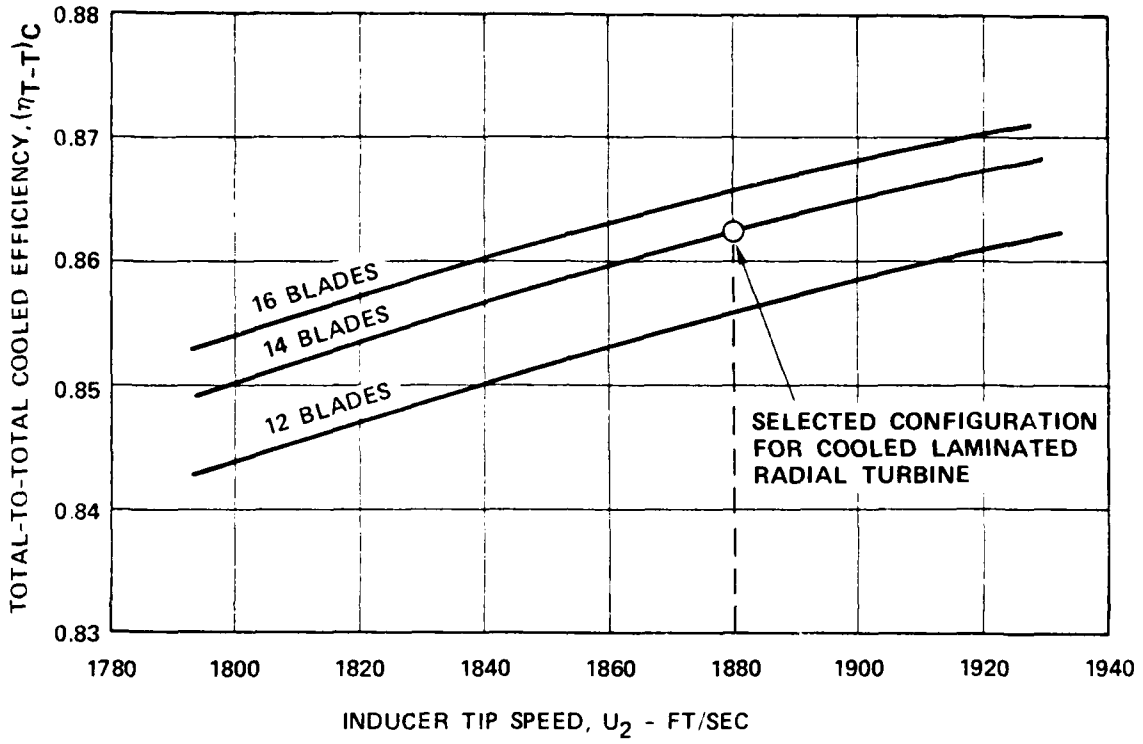

Figure 2. Variation of Turbine Efficiency with Tip Speed and Blade Number.

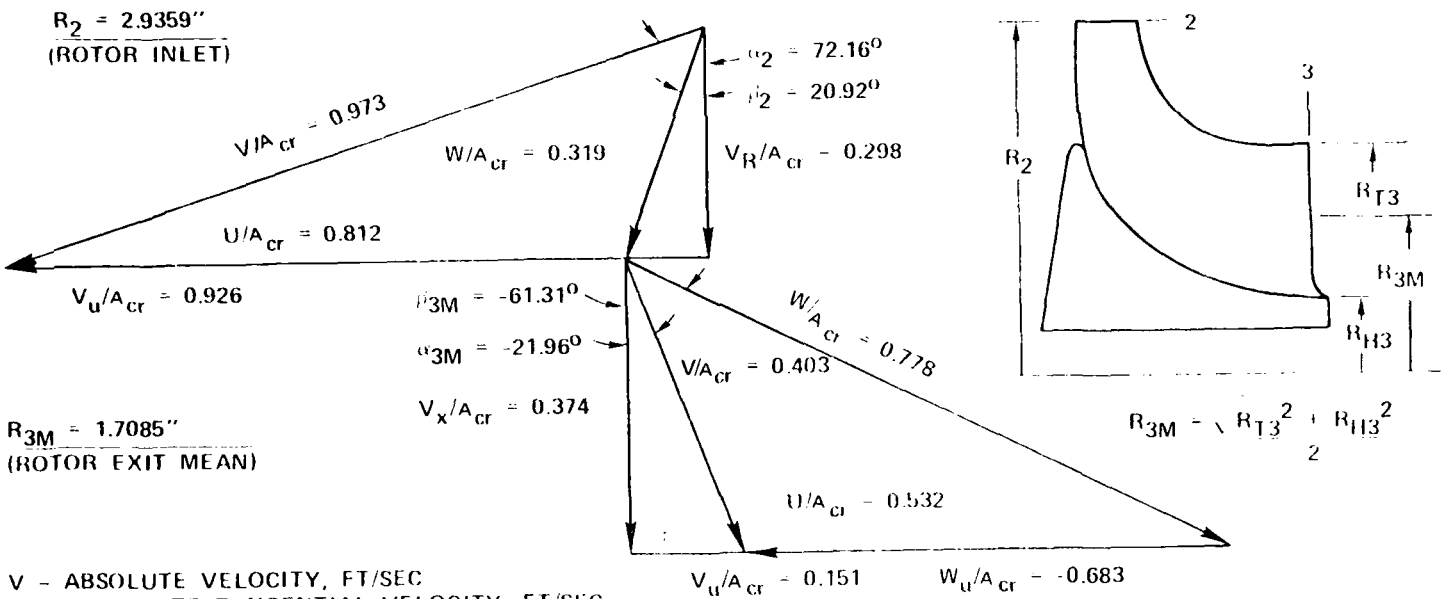

V = ABSOLUTE VELOCITY, FT/SEC
V_u = ABSOLUTE TANGENTIAL VELOCITY, FT/SEC
U = ROTOR WHEEL SPEED, FT/SEC
W = RELATIVE VELOCITY, FT/SEC
W_u = RELATIVE TANGENTIAL VELOCITY, FT/SEC
α = ABSOLUTE FLOW ANGLE, DEGREES
β = RELATIVE FLOW ANGLE, DEGREES
$A_{cr})_2$ = 2314.27 FT/SEC
$A_{cr})_{3M}$ = 2055.76 FT/SEC

$\lambda_{2,OPT} = V_{u2}/U_3 = 1.140$
$\lambda_{2,I}$ = 0.857 (FROM SLIP FACTOR CRITERIA)
$\lambda_{3M} = V_{u_{3M}}/U_{3M} = -0.151$
$K = R_{3M}/R_2 = 0.5819$
$\lambda_{STG} = \lambda_{2,OPT} - K^2 (\lambda_{3M})$

Figure 3. Optimized One-Dimensional Vector Diagram.

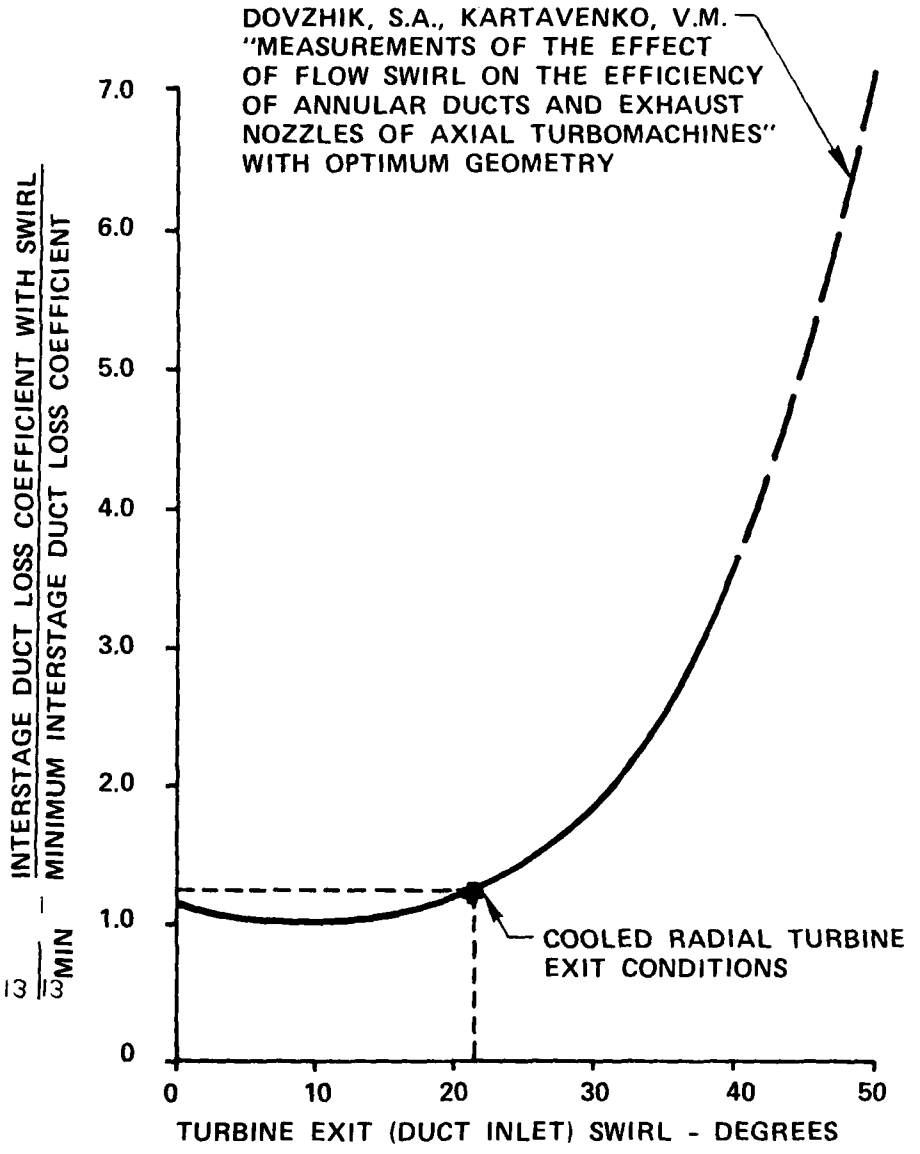

Figure 4. Effects of Swirl on Interstage Duct Loss Coefficient (From Ref. 2).

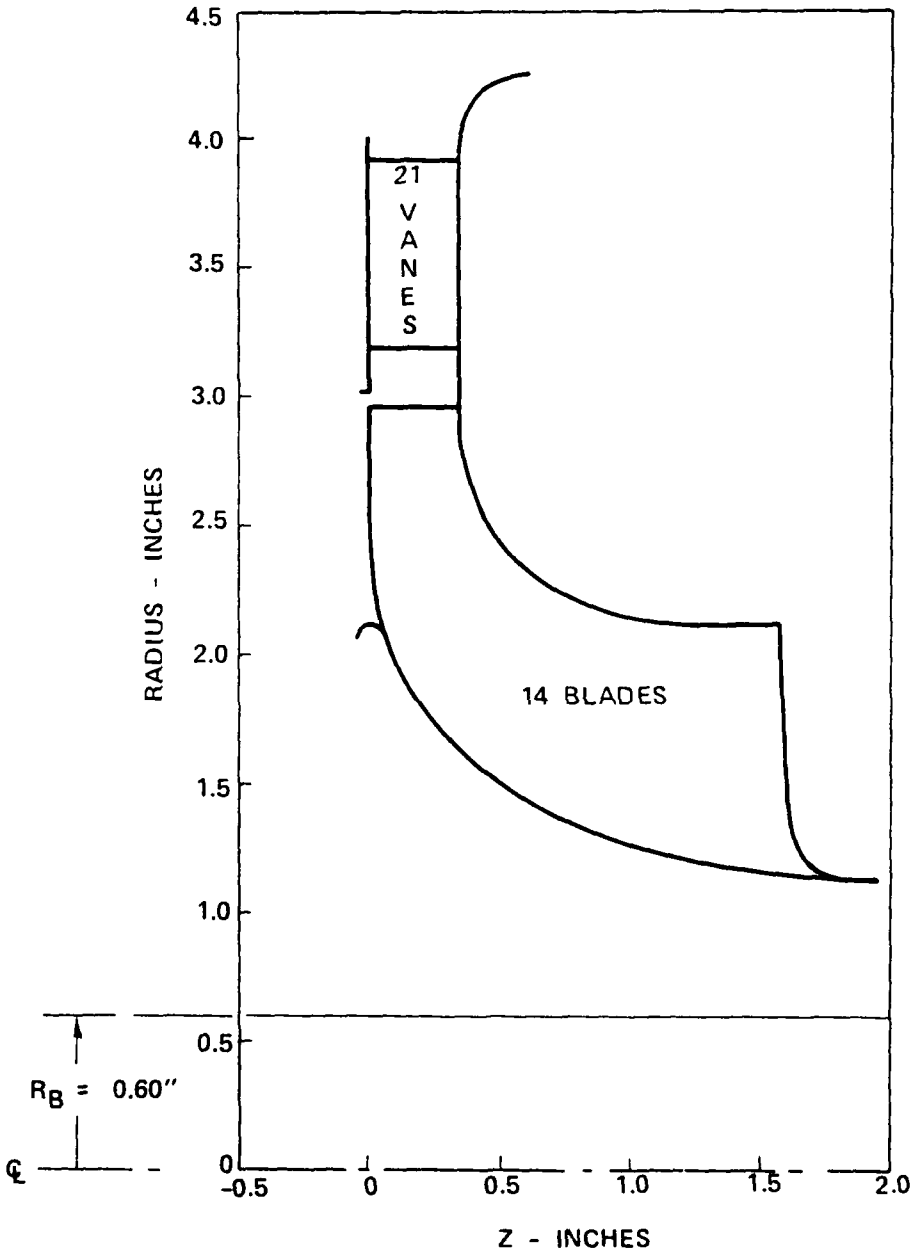

Figure 5. Preliminary Turbine Flow Path for Cooled Radial Turbine.

can then be used to arrive at an estimated blade-to-blade loading. This was accomplished for the cooled rotor turbine flow path, and the results indicated that an axial length of 1.62 inches would produce satisfactory blade-to-blade loading. The calculated velocity distribution for this condition is presented in Figure 6.

Turbine Efficiency Prediction

The turbine performance prediction is based on the aerodynamic design conditions that result from the cycle objective, optimized vector diagram, and turbine meridional flow path. These conditions are summarized in Table 1. Due to the complex flow in radial turbines, the maximum attainable efficiency is generally correlated with a specific speed parameter. Specific speed relates turbine shaft speed, volumetric flow, and isentropic stage work in the following manner:

$$N_S = \frac{N(Q_3)^{1/2}}{(H)^{3/4}}$$

where N = rotational speed, rpm

Q = volume flow rate, ft^3/sec

H = isentropic specific work, ft

Although alternate approaches to evaluating the basic profile and secondary losses occurring in the radial turbine are feasible, and indeed desirable, these alternate methods do not offer any real advantage at this time, since the real flow phenomena occurring in the turbine cannot be accurately modeled. However, current development in flow visualizations (LDV) and 3-dimensional viscous flow calculation techniques should significantly increase the capabilities for correlating radial turbine internal losses.

NASA has conducted extensive analytical and experimental investigations to determine the relationship of specific speed to radial turbine efficiency[3,4]. The test results[4] showed that an efficiency level of 0.925 is attainable for relatively low stage work radial turbines. This data is shown as a dashed line in Figure 7 for an average axial and radial clearance of 0.010 inch and 2.0×10^5 Reynolds number. When this data is

(3) Rohlik, Harold E., "Analytical Determination of Radial Inflow Turbine Design Geometry for Maximum Efficiency," NASA TN D-4384, 1968.

(4) Kofskey, Milton G.; and Nusbaum, William J., "Effects of Specific Speed on Experimental Performance of a Radial-Inflow Turbine," NASA TN D-6605, 1972.

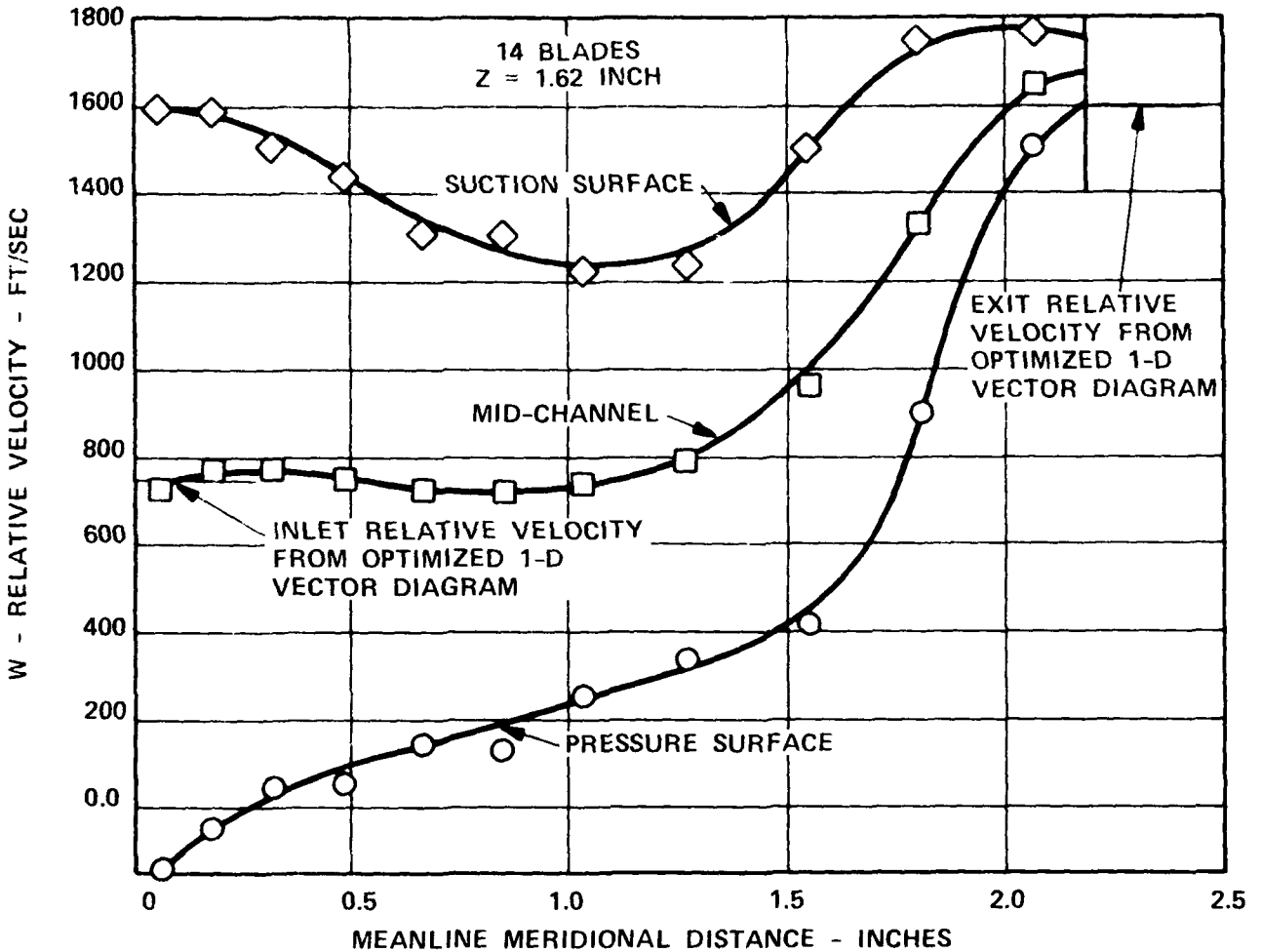

Figure 6. Preliminary Meanline Loading for Rotor Solidity Study.

TABLE 1. AERODYNAMIC DESIGN CONDITIONS.

Rotor inlet total temperature, °F	2300
Total-to-total pressure ratio	3.30
Inlet corrected flow, $W\sqrt{\theta}/\delta$, lb/sec	0.633
Rotational speed, N, rpm	73,379
Corrected speed, $N/\sqrt{\theta}$, rpm	31,811
Stage work, ΔH, Btu/lb	170.25
Corrected stage work, $\Delta H/\theta$, Btu/lb	32.0
Rotor inlet tip speed, U_2, ft/sec	1880
Stage work coefficient, λ_{stg}	1.206
Stage total-to-total efficiency, η_{t-t}	0.860
Specific speed, $\frac{NQ^{1/2}}{(J\Delta H_{ID})^{3/4}}$	69.0

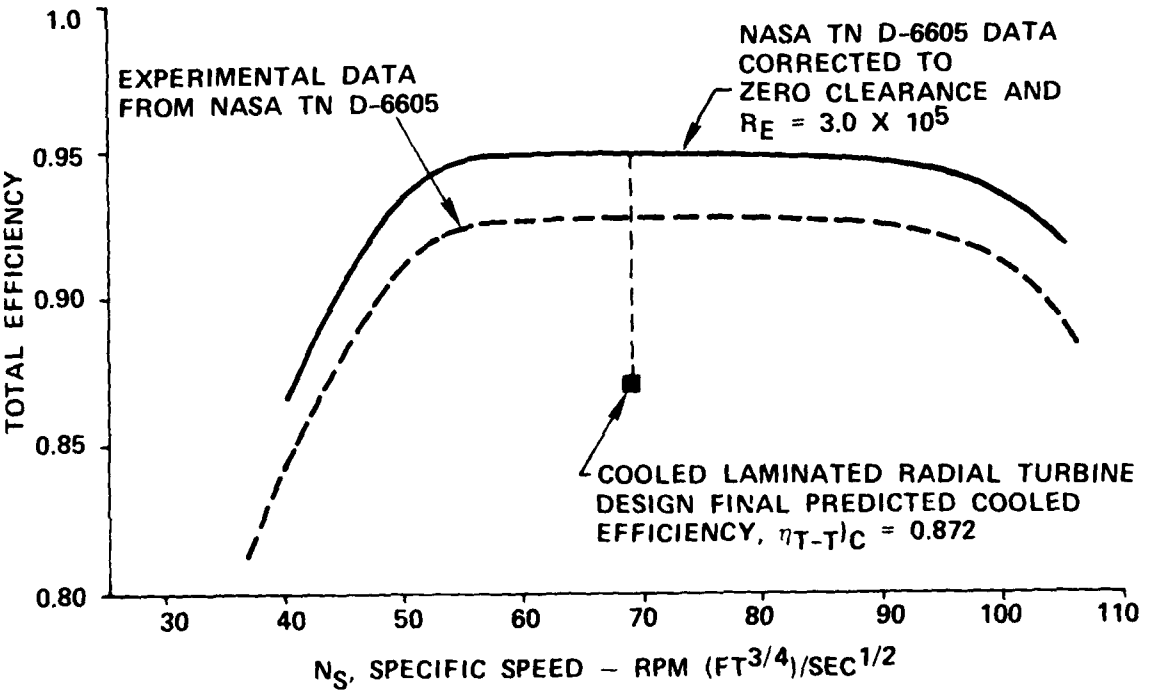

Figure 7. Specific Speed Correlation For Radial Turbines.

corrected to zero clearance with AiResearch correlations and the tested Reynolds number is increased to 3.0×10^5, the NASA test data is then represented by the solid line in Figure 7. Once the turbine maximum efficiency level is determined, additional turbine efficiency decrements will depend on the required operating conditions and mechanical constraints imposed. The efficiency decrements associated with the cooled radial turbine configuration are outlined below.

- The specific speed (N_S) of the cooled turbine design is 69.0. The efficiency decrement due to the effects of friction and secondary and mixing losses in the stator and rotor amounts to 5.2 points.

- The basic efficiency obtained from the specific speed curve is next corrected for Reynolds-number effects. The efficiency correlation is based on NASA radial turbine test results(5). Good agreement with the experimental data was established with the following relationship:

$$\frac{1 - \eta_T}{1 - \eta_{Base}} = 0.40 + 0.6 \left(\frac{R_e}{R_{e,Base}} \right)^{-1/5}$$

where

η_t = corrected total efficiency

$\eta_{T,Base}$ = base efficiency from specific speed curve

R_e = calculated Reynolds number, $\frac{W}{R_T \mu}$

$R_{e,Base}$ = base Reynolds number of specific speed curve, 3.0×10^5

The calculated Reynolds number for the cooled radial turbine is 3.5×10^5. Correcting the base efficiency for Reynolds number effects results in an efficiency increment of 0.1 point.

- Rotor inlet incidence losses are calculated from the optimized turbine vector diagram in the following manner:

$$\lambda_{2,opt} = \frac{\lambda_{2,i} + (1/K^2)\ \lambda_{stage}}{1 + 1/K^2} \left[\begin{matrix} \text{Optimum inlet work} \\ \text{coefficient} \end{matrix} \right]$$

(5) Nusbaum, William J., and Charles A. Wasserbauer, "Experimental Performance Evaluation of a 4.59-Inch Radial-Inflow Turbine Over a Range of Reynolds Number", NASA TN D-3835

$$\frac{\eta_{opt}}{\eta_{Base}} = \frac{1}{1 + \frac{\eta_{Base}}{2\lambda_{stage}} (\lambda_{2,opt} - \lambda_{2,i})^2}$$

[Ratio of efficiency with incidence to base efficiency from specific speed correlations]

where

$\lambda_{2,i}$ = inlet work coefficient for zero incidence loss

λ_{stage} = stage work coefficient

K = radius ratio between rotor exit and rotor inlet.

The calculated incidence loss is 2.80 points.

- The effect of rotor shroud clearance is based on correlations derived from References 6 and 7 and on in-house test results. The peformance penalties are a function of both axial and radial clearance. Based on 0.012-inch axial and radial clearances, the resultant efficiency decrement is 2.30 points.

- Additional rotor clearance effects are present with rotor scallops. The performance effects as a function of backface clearance have recently been evaluated for the GTP305-2 turbine. The size and scallop depth of this turbine are similar to the subject turbine. Analysis of the GTP305-2 backface seal design indicated the minimum allowable clearance was 0.030 inch. Applying the GTP305-2 clearance correlation to the cooled turbine design results in an efficiency decrement of 0.9 points. The correlation is shown in Figure 8.

- The performance effects of blade number are based on in-house and published Pratt and Whitney data[8]. For the AiResearch units, the 10 splitter blades were

(6) Penny, N., "Rover Case History of Small Gas Turbines," SAE Paper No. 634A, Jan. 1963.

(7) Futral, S. M. , Jr., and D. E. Holeski, "Experimental Results of Varying the Blade-Shroud Clearance in a 6.02 Inch Radial-Inflow Turbine," NASA TN D-5513, 1970.

(8) Calvert, G. S., and U. Okapuu, "Design and Evaluation of a High-Temperature Radial Turbine," Phase I Final Report, USAAVLABS Technical Report 68-69, U.S. Army Aviation Materiel Laboratories, Ft. Eustis, Va., Jan. 1969, AD 688164.

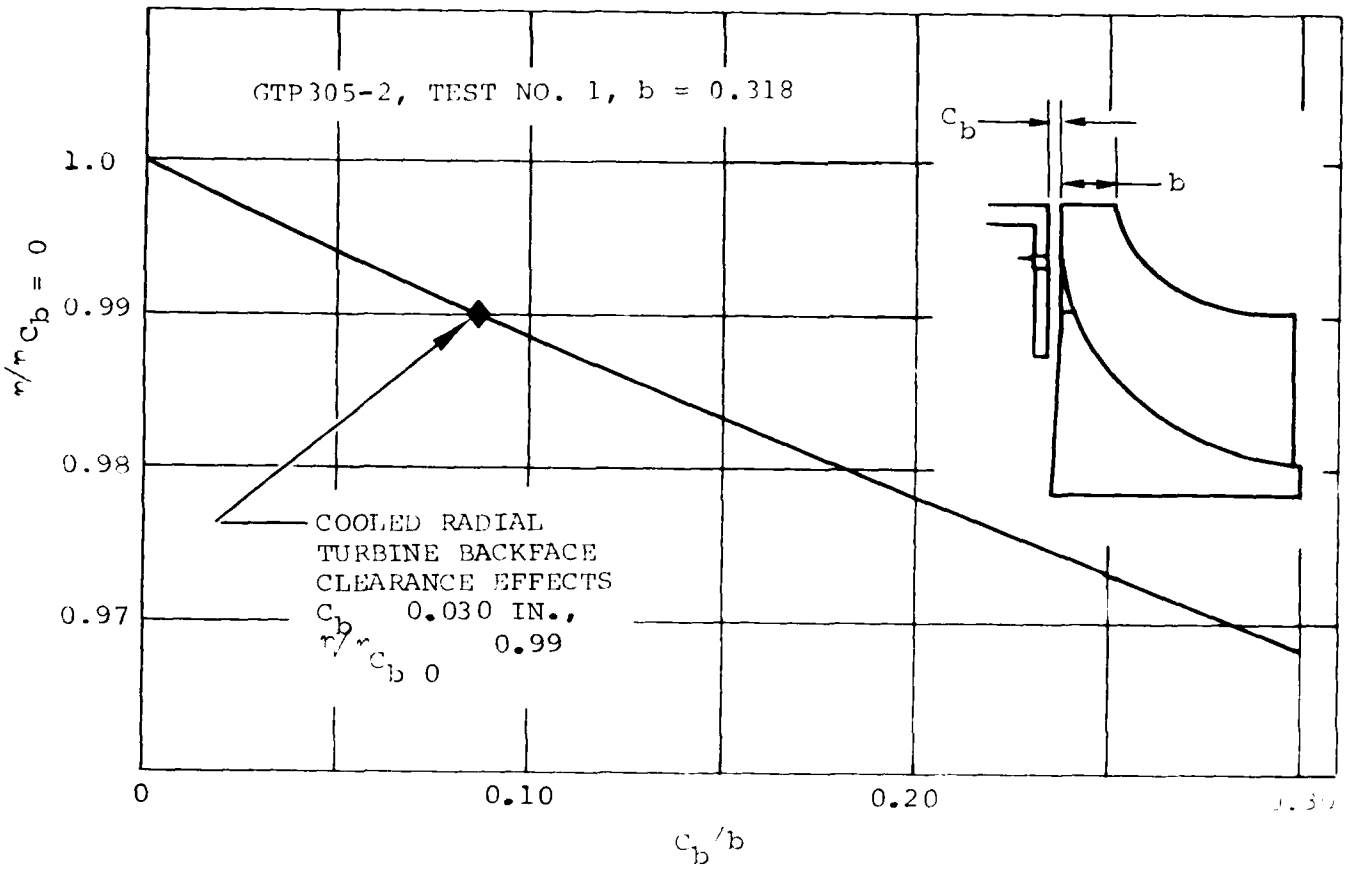

Figure 8. Performance Effects of Rotor Backface Clearance.

removed; for the Pratt and Whitney data, the number of whole blades was changed. The AiResearch data was run at essentially zero rotor inlet incidence and rotor exit swirl at the 20-blade condition. The resultant change in turbine efficiency, therefore, represents the effect of increased blade loading as the blade number is reduced for a given work requirement. For 14 blades, the efficiency decrement is 0.5 point.

- The disk friction losses along the rotor backface are estimated based on the results of the investigation conducted in Reference 9. This work is fully described in Reference 10. The performance penalty for rotor backface disk friction is 0.30 point.

The predicted aerodynamic efficiency up to this point is 0.881 percent. However, the exducer cooling flow requirement has resulted in a significant increase in blade thickness as compared to a conventional uncooled radial rotor. With the final thickness distribution, the exducer hub normal thickness is 0.1838 inch and the exducer tip thickness is 0.0788 inch, compared to 0.1400 and 0.030 inch for typical uncooled rotors. Currently, no test data is available to assess the effect of exducer trailing-edge blockage on radial turbine performance, although rotor exit survey data indicates that the radial turbine is less sensitive than axial turbines of comparable size. In order to assess the effect of increased rotor trailing-edge blockage, a mixing loss calculation was performed for both the cooled radial turbine and the previously tested GTC36-200 radial turbine. Both turbines are designed for 14 blades, and the performance level of the GTC36-200 matches the NASA peak efficiency. The mixing loss calculations were based on the results of Reference 11. The analysis accounted for the dump loss associated with the sudden expansion occurring at the trailing edge, based on the blade thickness alone. The distribution of calculated loss is shown in Figure 9 as a function of percent of blade height. As expected, the loss level is higher over the entire blade height for the cooled turbine. The mass average loss for the GTC36-200 turbine is 1.5 percent ($\Delta P/P$) compared to 2.72 percent for the cooled turbine, or an increase of

---

(9) Daily, J. W., and R. E. Nece, "Chamber Dimensions Effects on Induced Flow and Frictional Resistance of Enclosed Rotating Disks," J. Basic Eng., Vol. 82, No. 1, Mar. 1960, pp 217-232.

(10) "Turbine Design and Application," NASA SP-290, Vol. 2, pp. 131-138.

(11) Benedict, R. P., N. A. Carlucci, and S. D. Swetz, "Flow Losses in Abrupt Enlargements and Contractions," Journal of Eng. for Power, Jan. 1966, pp. 73-81.

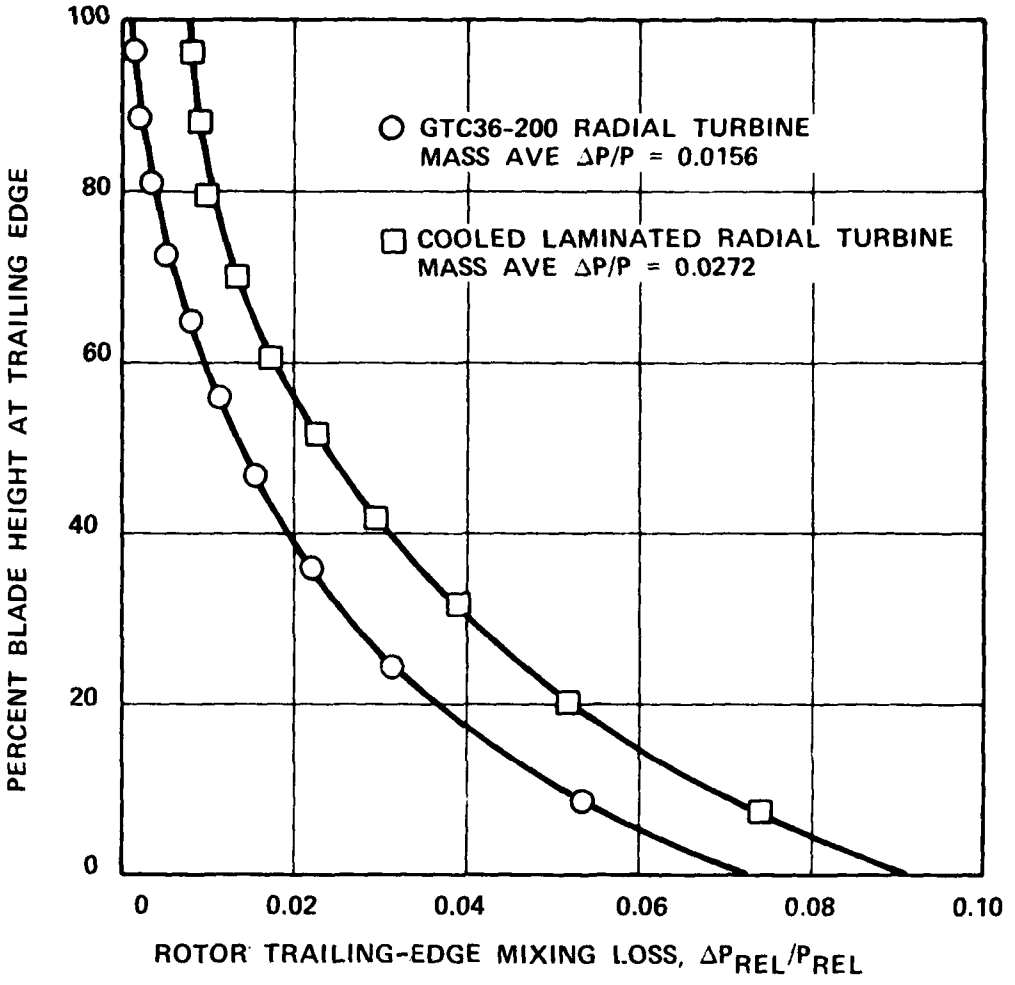

Figure 9. Effect of Trailing-Edge Blockage on Mixing Loss.

1.16 percent. Converting this increase in relative total pressure loss to an overall efficiency change results in a decrement of 0.90 point. The final predicted aerodynamic efficiency is therefore 0.872 percent.

The effects of cooling flow on turbine performance are usually accounted for in the following manner. All rotor internal and disk cooling flows are assumed to do no work in passing through the turbine. In addition, pumping work to accelerate the rotor-cooling flows to wheel speed is charged to the turbine as an efficiency penalty. For the preliminary turbine configuration, the rotor internal cooling flow penalty was based on pumping the flow to rotor exit mean wheel speed since a trailing-edge discharge scheme was proposed. However, during the detail design phase, the cooling flow scheme was modified. The final scheme is shown in Figure 27 and results in all the cooling flow discharging to the rotor shroud and backface clearance regions. Test data evaluating the effects of tip discharge is not available for radial turbines, but has been evaluated for axial turbines at AiResearch. In-house test data shows that the cooled turbine efficiency either remains fairly constant or rises slightly up to 3.0-percent internal cooling. This characteristic is attributed to a reduction in tip clearance losses, which offsets the required internal pumping. The same beneficial effects are expected to occur in the radial turbine, especially in the exducer region where similarities between the axial and radial turbine blading are the greatest.

For the backface cooling flow, test results from both the GTC36-200 and GTP305-2 showed that the work done by the cooling flow, due to acceleration through the rotor, offsets the required pumping along the rotor backface. This conclusion is based on two methods of calculating the turbine efficiency. The first method derives the turbine work based on the thermodynamic mixing of both cooling and mainstream flows. The second method is based on calculating the turbine work from the momentum equation by integrating the rotor exit survey data and calculating the rotor inlet tangential velocity from a constant stator loss coefficient obtained with no cooling. Figure 10 shows the effects of rotor backface cooling flow for the GTP305-2 radial turbine.

On the basis of the preceding discussion, the rotor cooling flow penalties will be offset, and no net change in efficiency would result between cooled and uncooled rotors. The turbine efficiency prediction is summarized in Table 2.

Detailed Aerodynamic Design

The aerodynamic and mechanical optimization procedure developed for the cooled radial turbine detail design is shown in Figure 11. As indicated, the procedure is iterative, and in order to achieve an acceptable aerodynamic and mechanical design, all elements in the design system must be satisfied.

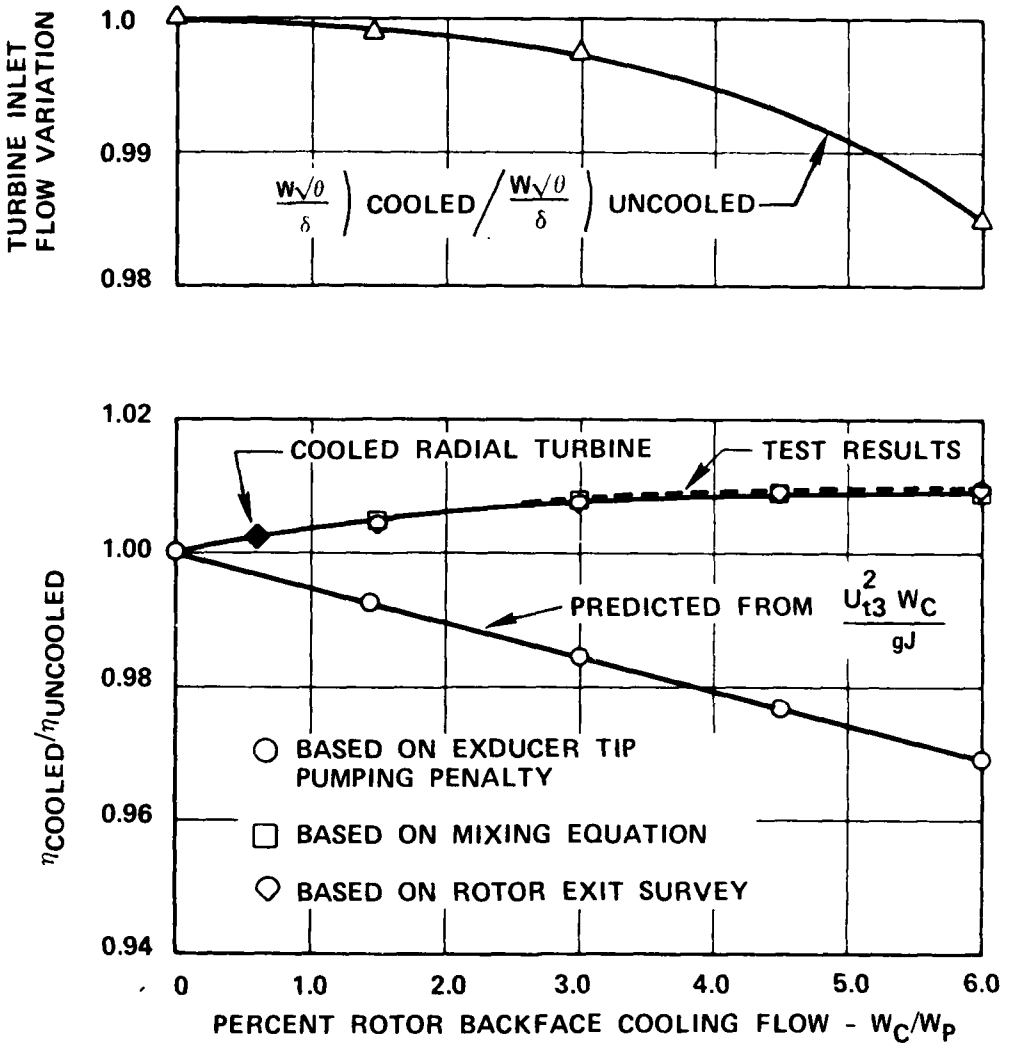

Figure 10. Effects of Rotor Backface Cooling on Turbine Performance.

TABLE 2. COOLED TURBINE EFFICIENCY PREDICTION.

Aerodynamic Efficiency		
	η_{t-t}	$\Delta\eta_{t-t}$
Base efficiency from specific speed correlation - Figure 7	0.948	
Reynolds Number effect at $R_E = 3.5 \times 10^5$	0.949	+0.1 pt
Rotor inlet incidence effects	0.921	-2.8 pts
Rotor shroud clearance effects at 0.012 inch clearance	0.898	-2.3 pts
Rotor backface clearance effects at 0.030 inch clearance - Figure 8	0.889	-0.9 pt
Blade number effects with 14 blades	0.884	-0.5 pt
Rotor backface disk friction effects	0.881	-0.3 pt
Rotor exit blockage effects	0.872	-0.9 pt
Final predicted aerodynamic efficiency	0.872	

Cooled Efficiency		
	$\eta_{t-t)Cooled}$	$\Delta\eta_{t-t}$
Rotor backface cooling for 0.60 percent cooling flow	0.872	0.0
Rotor internal cooling flow at 4.94 percent cooling flow	0.872	0.0
Final predicted cooled efficiency	0.872	
Design requirement	0.860	

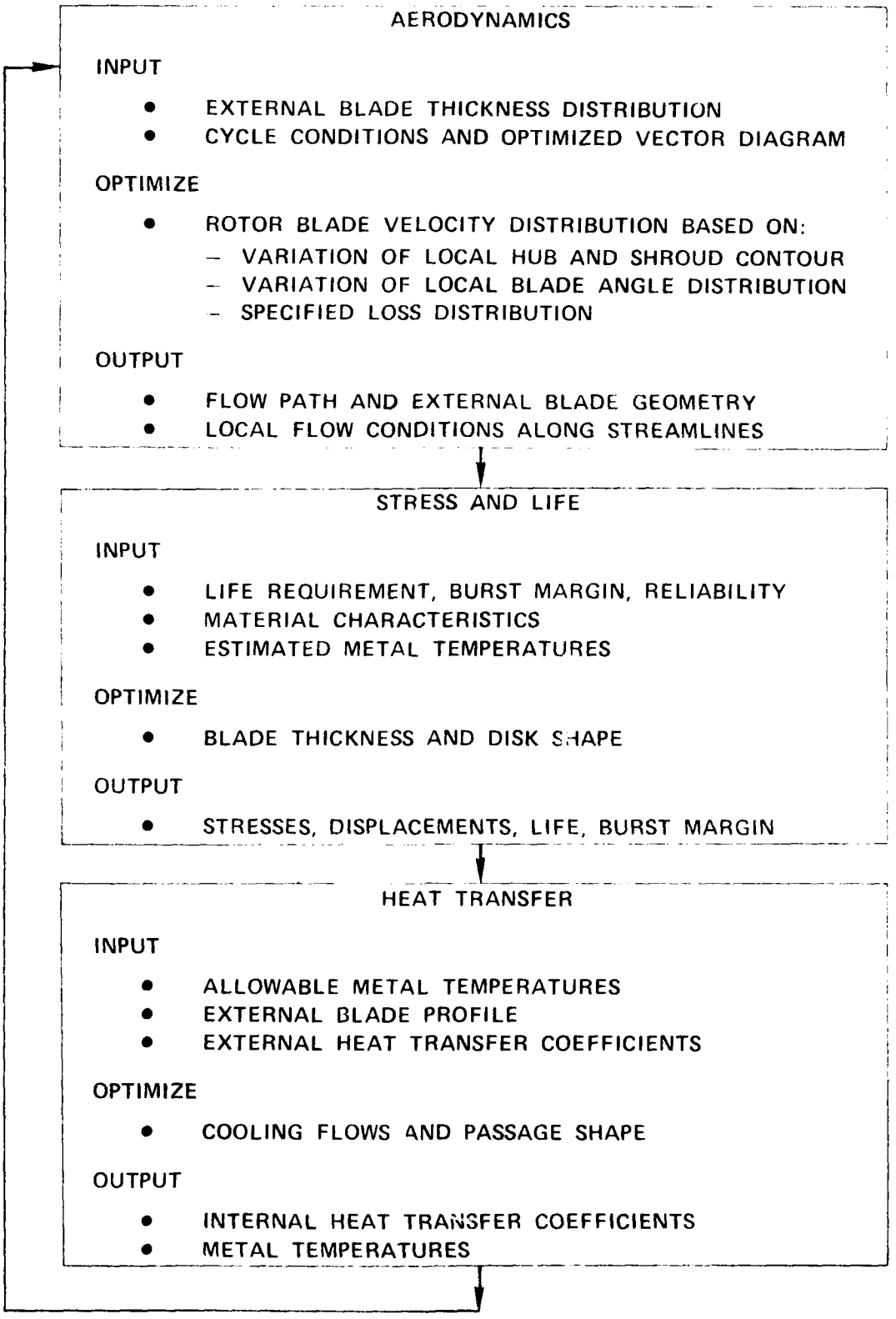

Figure 11. Aerodynamic and Mechanical Optimization Procedure.

Aerodynamically, the design procedure consists of two basic elements: the radial blade geometry definition and internal blade velocity distribution.

Rotor Blade Geometry Definition

The detailed design of the rotor begins with establishment of rotor Z-section thickness distributions from the results of preliminary stress, heat transfer, and aerodynamic analyses. The thickness is specified at four rotor Z-locations: at Z = 0, Z = "D", an intermediate location, and at the rotor exducer as shown in Figure 12.

A preliminary estimate of the rotor hub and shroud contour is then defined from an analytical curve fitting with specified coordinates established from the one-dimensional vector diagram. A good initial estimate of the contours can be obtained by adjusting the curve fit until a uniform meridional rotor area distribution is achieved. To complete the initial definition of the rotor geometry, a blade angle definition is established. Since the rotor blade elements are radial, specification of a blade angle as a function of axial distance automatically defines the blade angle at all radii for that axial location. In order to perform the internal rotor flow analysis, the level and distribution of losses in the rotor must be specified. The level of losses is determined from the efficiency analysis described earlier. The distribution of losses, both in the through-flow and radial directions, is more difficult to establish. Due to the lack of detailed knowledge of the internal rotor flow field, the losses in the through-flow direction are assumed linear. For the radial direction, previous rotor exit survey results show that the radial loss characteristics for radial turbines exhibit certain similar characteristics. That is, in the hub region, the losses are low (due to lower loading level) and progressively increase to about 80 percent of the blade and then are fairly uniform to the rotor tip. For the cooled radial turbine, a radial loss distribution based on recent test data from the GTP305-2 radial turbine was utilized. The loss level was then adjusted to agree with the predicted performance level of the cooled turbine. The loss parameter is defined as

$$Q = e^{-\left(\frac{\Delta S}{Cp}\right)} = \left(\frac{P_1}{P_o}\right)^{\frac{\gamma-1}{\gamma}} \Big/ \left(\frac{T_1}{T_o}\right)$$

where P_o, T_o are the total pressure and total temperature at the initial state and P_1, T_1 are similar properties at the final state. The radial loss distribution used for the cooled radial turbine is presented in Figure 13.

With the preceding input data, the radial rotor geometry program curve fits the four-station thickness distributions along equally spaced meridional streamlines. A number of

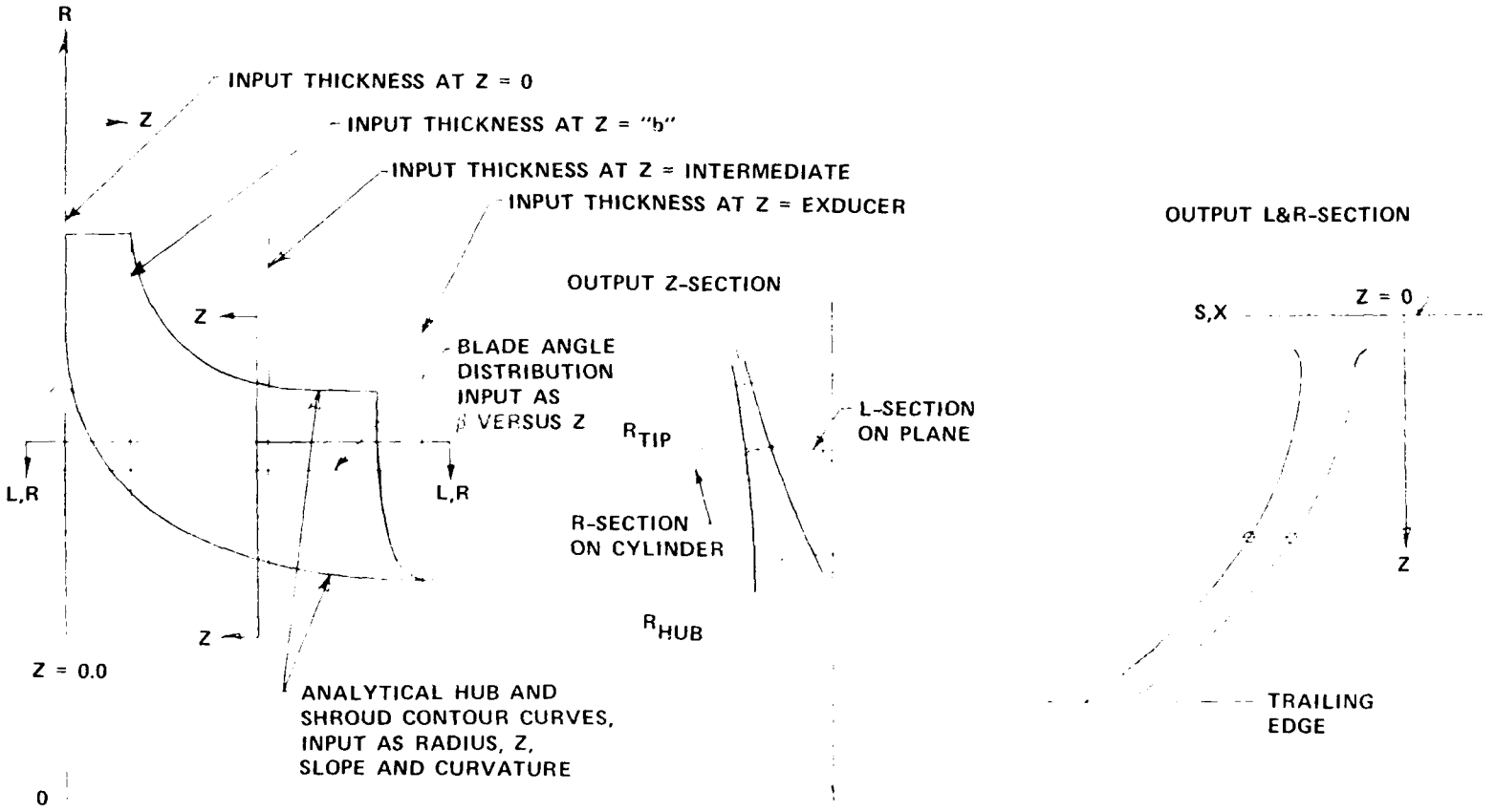

Figure 12. Input and Output from Rotor Geometry Program.

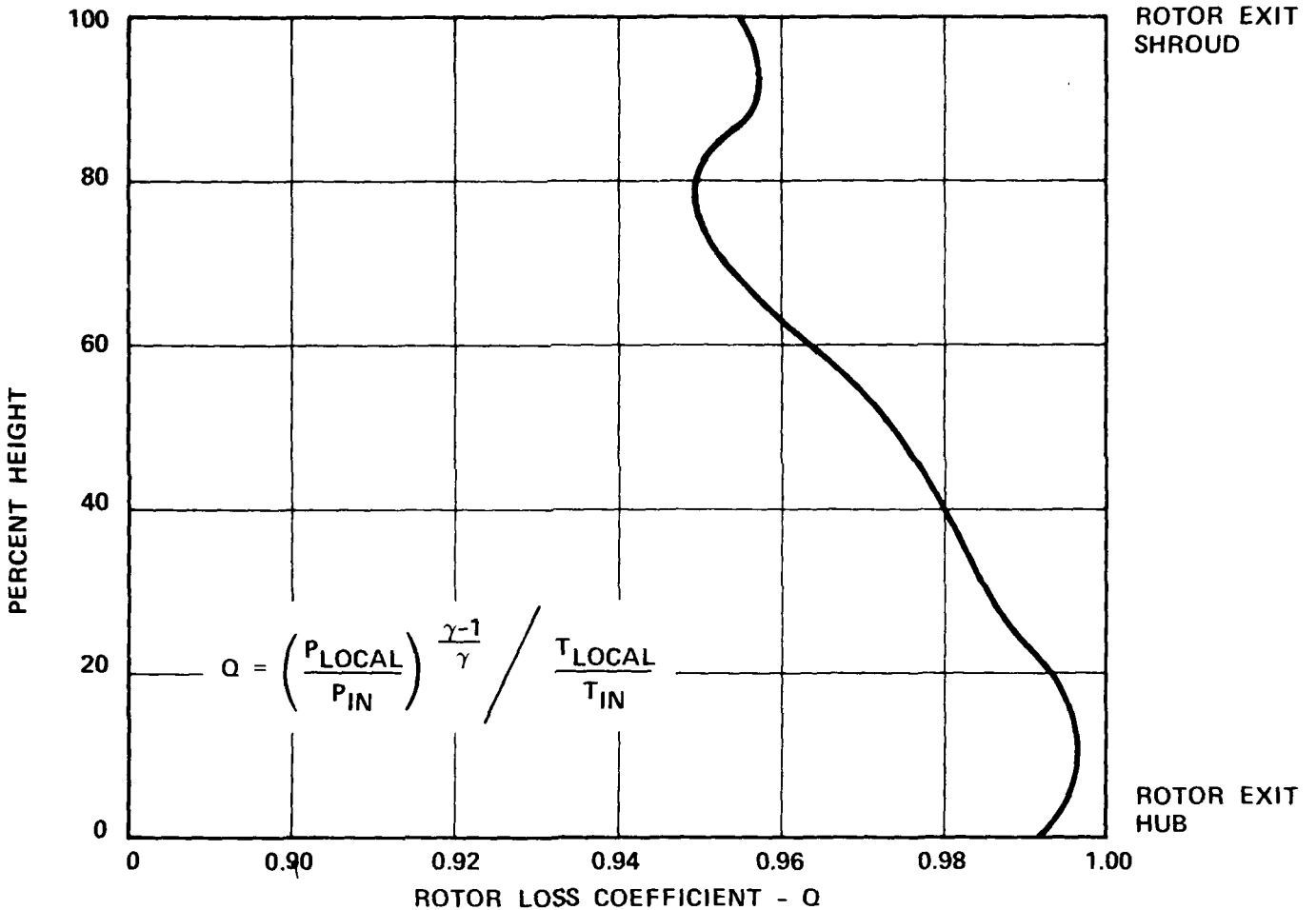

Figure 13. Rotor Radial Loss Distribution Based on GTP305-2 Turbine.

analytical curve fit options are available in order to match the required thickness distribution throughout the entire rotor flow path. To define input for mechanical and aerodynamic analysis, the geometry program interpolates the required variables along specified quasi-orthogonals in the through-flow direction. The quantities at the intersection of the streamline and quasi-orthogonals are then output to mechanical and flow analysis computer programs. The radial rotor geometry program also has the capability of providing coordinates for three types of sections at any location in the flow path. These sections are designated as Z, L, and R. The Z and L sections are normally used to manufacture and inspect the rotor blade external profile. However, for the cooled laminated turbine, the Z sections will be generated for each rotor laminate (increments of 0.020 inch) and the required internal cooling flow geometry will be defined on each laminate. The R section shows the true blade shape for a specified constant radius and is used to obtain the rotor throat dimensions. Figure 12 defines and shows the relationship between the three sections. The final rotor blade geometry that satisfies the mechanical requirements and produces acceptable aerodynamic blade velocity distributions is presented in Figures 14 through 16.

Rotor Internal Flow Analysis

The criterion for determining aerodynamically acceptable blade profiles is the manner in which the profile directs the gas flow from known inlet to known exit conditions, i.e., the blade loading. Acceptable blade loadings are characterized by:

- High reaction from inlet to exit. This condition is initially established at the rotor meanline by maintaining 50-percent reaction in the one-dimensional vector diagram optimization.
- Monotonically increasing mid-channel velocities along all streamlines.
- Minimum suction-surface diffusion, followed when possible by rapid accelerations.

Parameters that are adjusted to achieve these characteristics for a given thickness and loss distribution are: (a) the local change in rotor blade angle distributions, (b) the meridional area distribution, and (c) the shape and curvature of the hub and shroud contours. Characteristically, for highly loaded rotors the rotor inlet incidence results in large local suction and pressure surface diffusion in the inducer region. In addition, due to the lower turning and streamline curvature associated with the exducer hub regions, optimization of the rotor velocity distribution is primarily concerned with minimizing the high turning and curvature effects in the exducer mean and shroud regions.

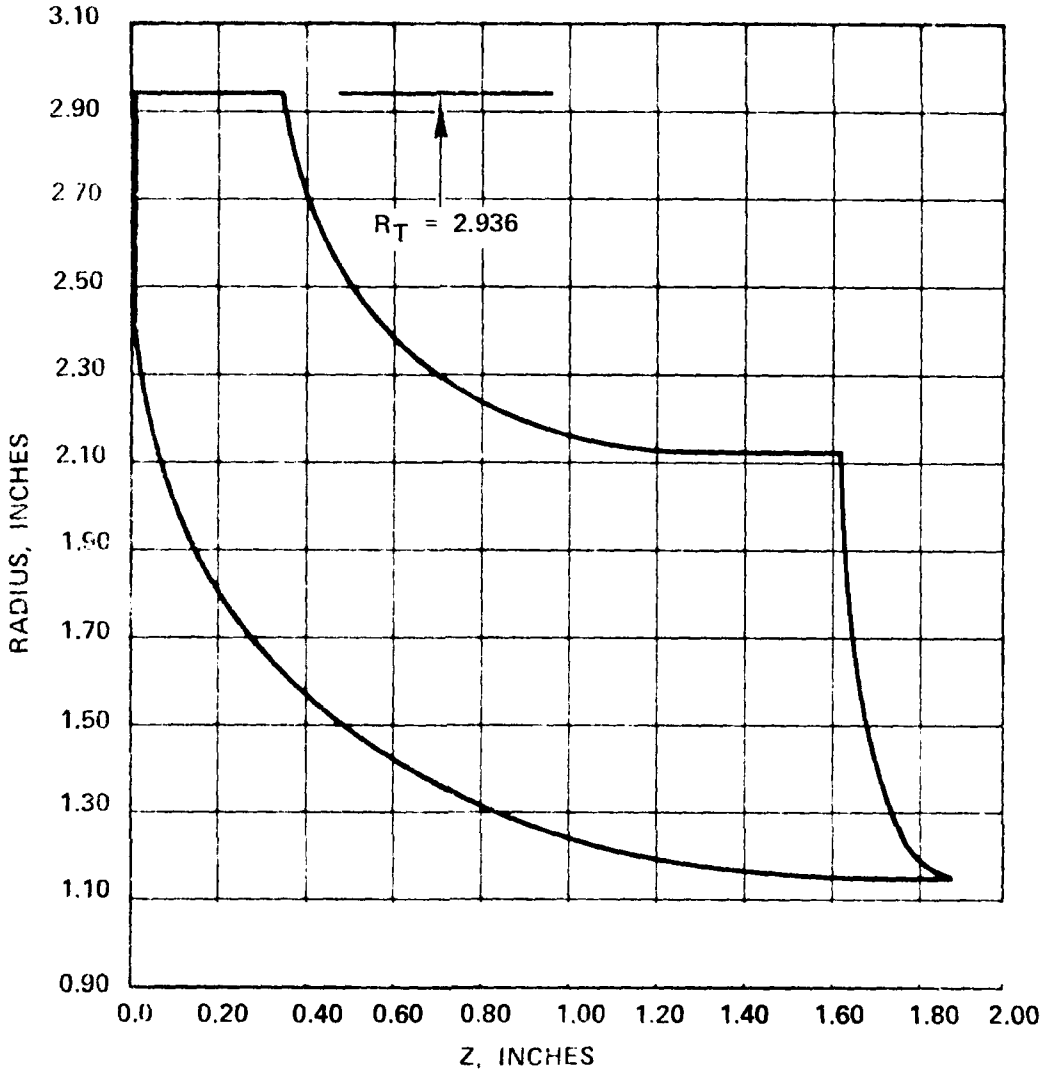

Figure 14. Final Rotor Meridional Flow Path.

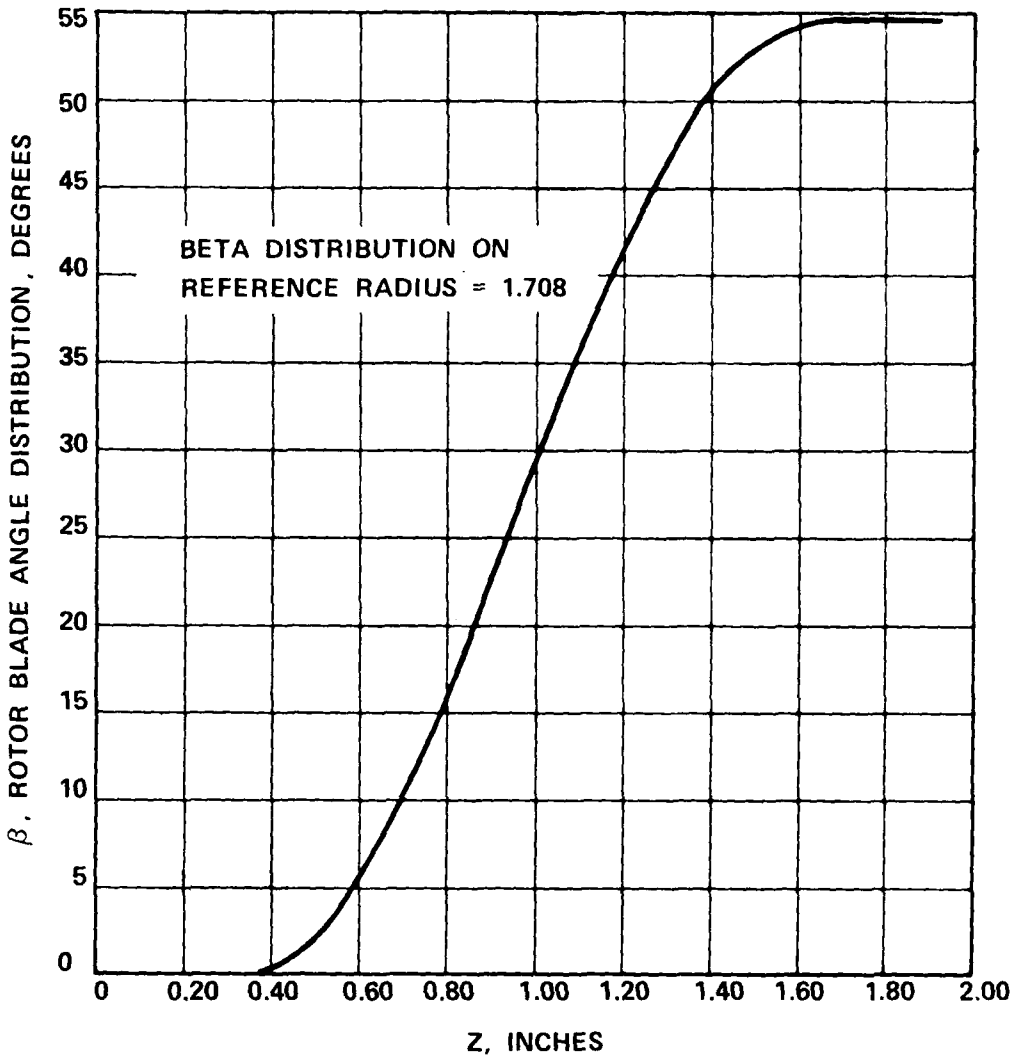

Figure 15. Final Rotor Blade Angle Distribution.

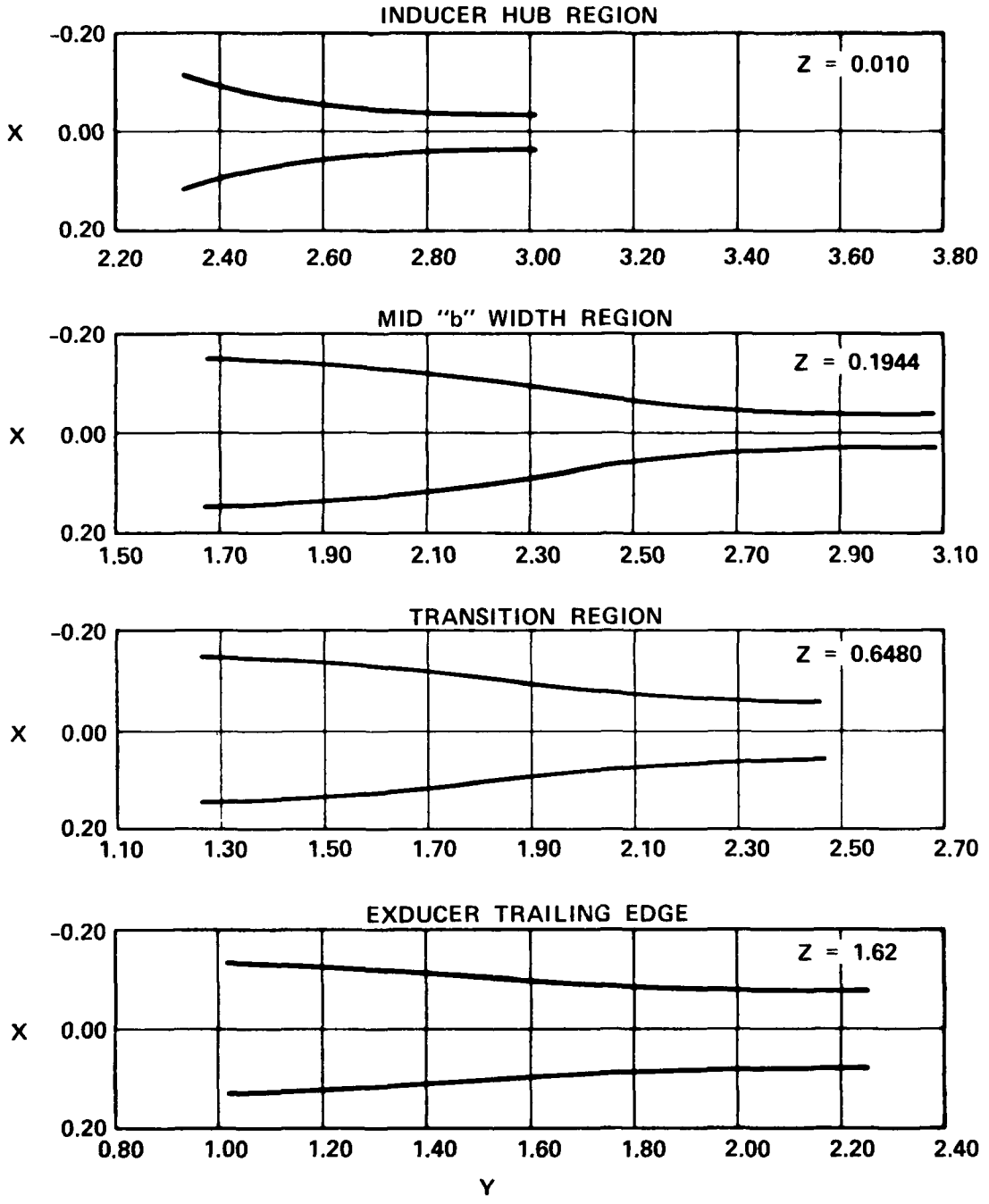

Figure 16. Z-Section with Final Geometry.

The design process is initiated with the geometry and loss distribution established from the geometry program. The radial equilibrium equation is then solved with the AiResearch compressible flow analysis program. This program solves the radial equilibrium equation by satisfying the equations of continuity, momentum, and energy in the meridional plane with circumferential averaging similar to References 12 and 13. Blade surface velocities are then computed from the local rate of change of moment of momentum and the condition of zero absolute vorticity. A number of iterations between the geometry program and flow analysis program are usually necessary to achieve satisfactory blade loading for each thickness distribution specified.

The final rotor blade loadings, with the thickness distribution that satisfies rotor blade stress and internal cooling flow requirements, are presented in Figures 17, 18, and 19 for the rotor hub, meanline, and shroud streamlines. As discussed previously, high loading in the inducer region is unavoidable. However, the remaining portions of the blade surface show acceptable characteristics. The rotor inlet and exit vector diagrams for these three streamlines are presented in Figure 20.

(12) Smith, L. H., Jr., "The Radial-Equilibrium Equation of Turbomachinery," Journal of Eng. for Power, Jan. 1966, pp. 1-12.

(13) Katsanis, T., "Use of Arbitrary Quasi-Orthogonals for Calculating Flow Distribution in the Meridional Plane of a Turbomachine," NASA TN D-2546, Dec. 1964.

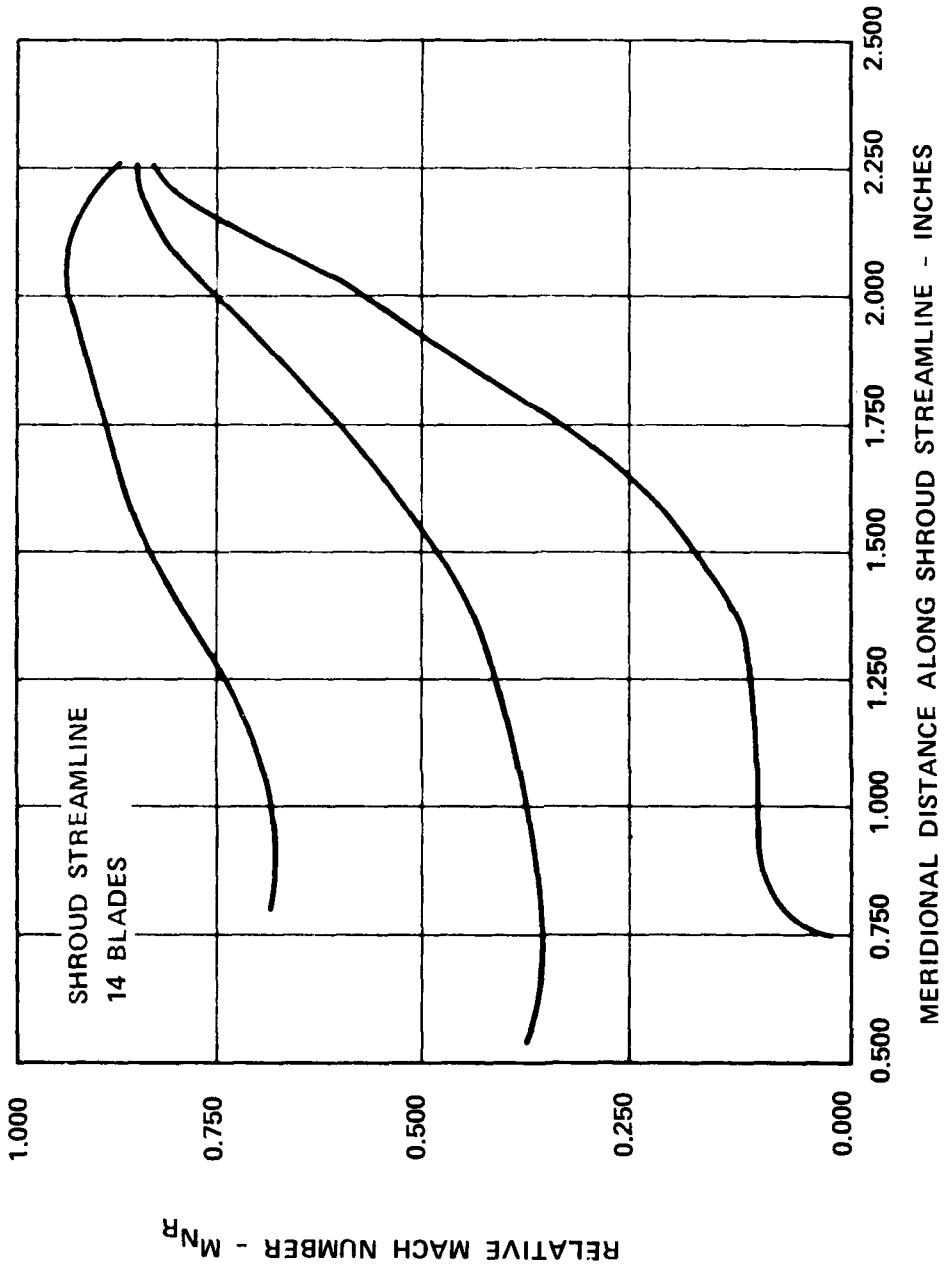

Figure 17. Shroud Streamline Loading with Final Geometry.

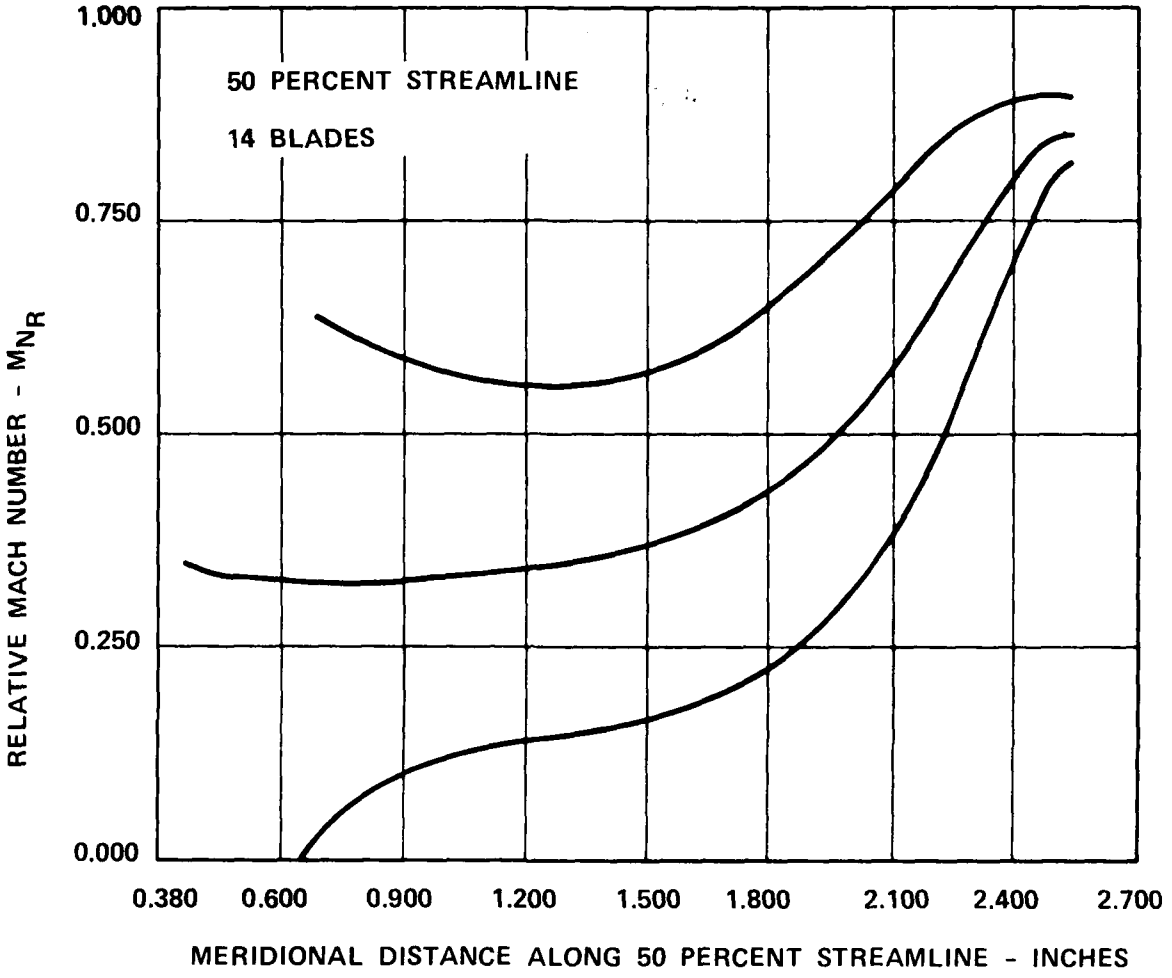

Figure 18. Fifty-Percent Streamline Loading with Final Geometry.

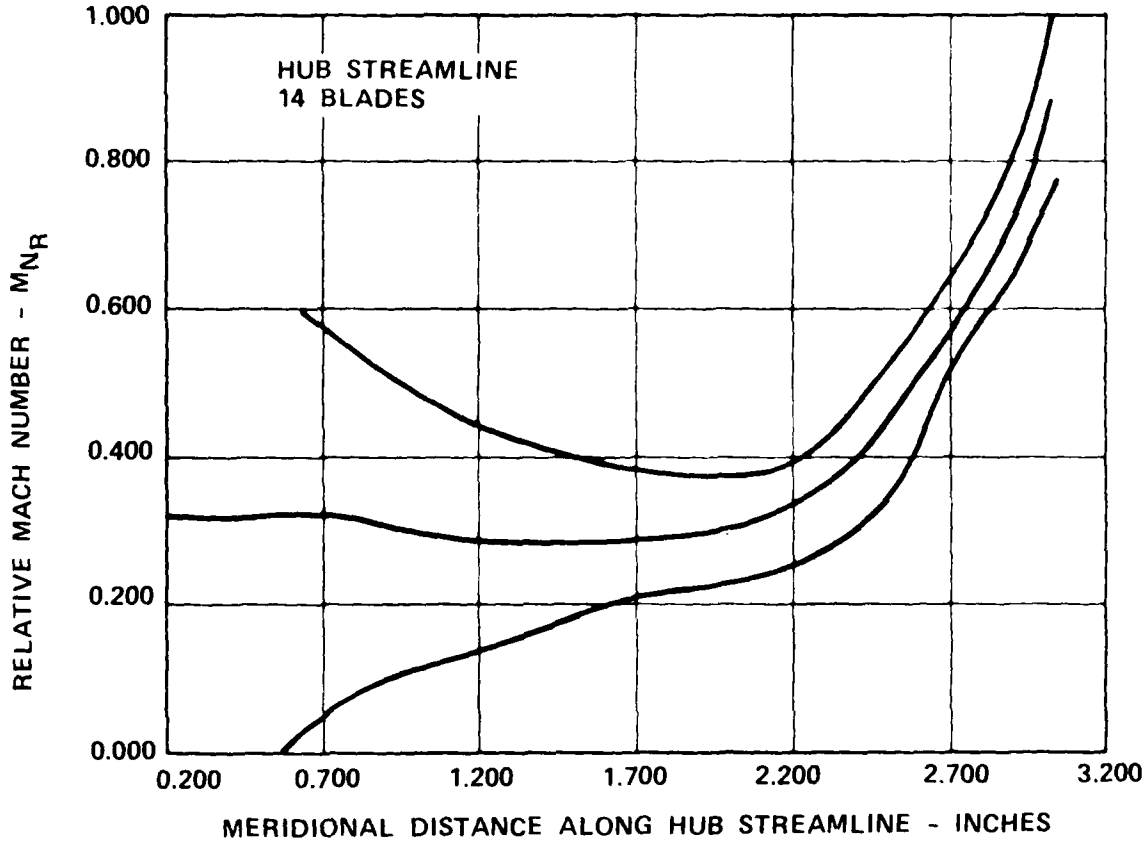

Figure 19. Hub Streamline Loading with Final Geometry.

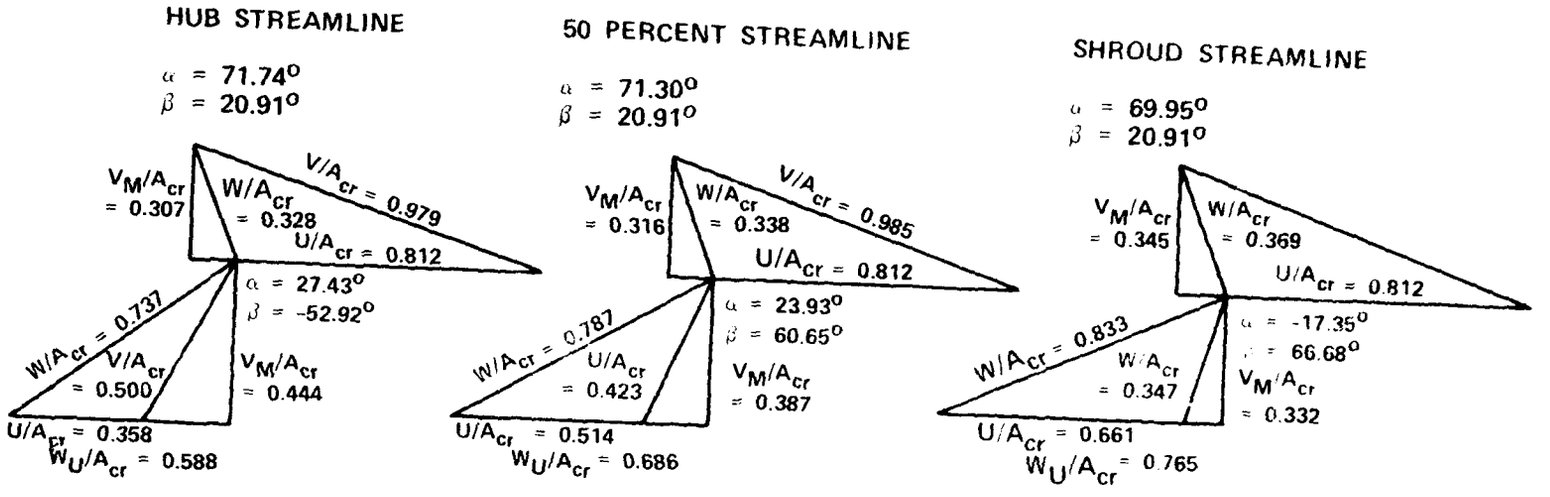

INLET RADIUS	= 2.9359 IN.
EXIT RADIUS	= 1.150
A_{cr}, INLET	= 2314.25 FT/SEC
A_{cr}, EXIT	= 2054.6 FT/SEC

INLET RADIUS	= 2.9359 IN.
EXIT RADIUS	= 1.6375 IN.
A_{cr}, INLET	= 2314.25 FT/SEC
A_{cr}, EXIT	= 2053.15 FT/SEC

INLET RADIUS	= 2.9359 IN.
EXIT RADIUS	= 2.125 IN.
A_{cr}, INLET	= 2314.25 FT/SEC
A_{cr}, EXIT	= 2058.28 FT/SEC

Vm = MERIDIONAL VELOCITY, FT/SEC

$= (V_x^2 + V_R^2)^{1/2}$

V_x = AXIAL (Z) COMPONENT

V_R = RADIAL (R) COMPONENT

Figure 20. Vector Diagram From Final Flow Solution.

HEAT TRANSFER AND COOLING AIRFLOW DESIGN

Laminated Turbine Wheel Cooling Circuit Design

The laminated, cooled radial turbine has been designed to operate in a 3-lb/sec airflow class engine that develops approximately 550 horsepower under sea-level, standard day conditions. The cycle parameters pertinent to the cooling circuit design at maximum power operation are tabulated below.

Rotor Inlet Temperature	= 2300°F
Speed	= 73,380 rpm
Core Flow	= 3.173 lbs/sec
Compressor Discharge Temp.	= 723°F
Compressor Discharge Pressure	= 167.7 psia

Estimates have been made for rotor cooling flow supply conditions based on the engine configuration anticipated for this application. These estimates yielded values of 137.2 psia inlet pressure and 750°F inlet temperature.

The cooling requirements for any conceptual scheme depend on three variables: (a) the operating environment and stress level, (b) the required life and mission, and (c) the material properties. The turbine rotor has been designed for a life of 5000 mission hours with 1000 of these at full rated power. Early in this program, an estimate of required cooling was made based on Astroloy laminate strength and life requirements. The required cooling temperature difference, based on uncooled blade metal temperatures, ranged from 200°F to 500°F, thereby illustrating the need for an efficient and sophisticated system. Laminated construction offers features with which a highly effective design can be achieved. Potential features for a high-performance cooling circuit design include:

- Heat transfer augmentation with:
  - Pin fin arrays
  - Ribs oriented parallel or perpendicular to the flow direction
  - Impingement
  - General surface roughness
- Flow control with:
  - Metering orifices
  - Flow guides
  - Dust holes
  - Cross passage bleed to eliminate stagnant areas
  - Passage size flexibility

All of the potential cooling circuit configurations have the main cooling supply passage location and orientation in common. To maintain the integrity of each individual laminate during machining, handling, and bonding procedures, a completely continuous circumferential passage is not possible anywhere in the rotor. Figure 21 is a possible laminate layout at a location that would section a circumferential manifold in a cast design. This figure illustrates the requirement for mechanical ties between inner and outer portions of the laminate. Although only a small number of ties are necessary from an assembly standpoint, the separate supply passage for each of the 14 blades and the resulting 14 ties represents a better design choice. Separate supply passages and orifices offer the potential for balancing blade flows after in-process flow checks; and the additional ties aid load transfer from the rim to the bore of the wheel. Cooling air supplied to each blade discharges from the supply passage into a saddle region cavity from which it is distributed to various circuits in the blade through metering areas.

Cooling Scheme Iterations

Several iterations were necessary to properly allocate cooling flows where needed, without waste, and to maintain structural integrity in the design. It was also necessary to minimize steep thermal gradients to avoid excessive thermal stress. The aim throughout the design phase was to maximize the cooling effectiveness without undue complexity. The evolutionary changes in the design to the final configuration are described in the subsequent paragraphs.

Two-Passage, Single-Pass, Meridional-Flow Configuration

A two-passage, single-pass, meridional-flow configuration is shown in Figure 22. The first passage flows radially outward, cooling the forward portion and leading-edge region of the blade, and then flows in a meridional direction, exiting at the outer part of the trailing edge. The second passage flow enters at the hub, flows in a meridional direction, cooling the lower portion of the blade, and exits out the inner part of the trailing edge. Pin fins are used in all areas where additional heat transfer is required. The density of the pin spacing is varied to maintain low thermal gradients in the blade walls.

Advantages of this scheme are:

- Good cooling efficiency and flexibility
- Coolant discharge at a low radius
- No interpassage coolant-flow distribution problems

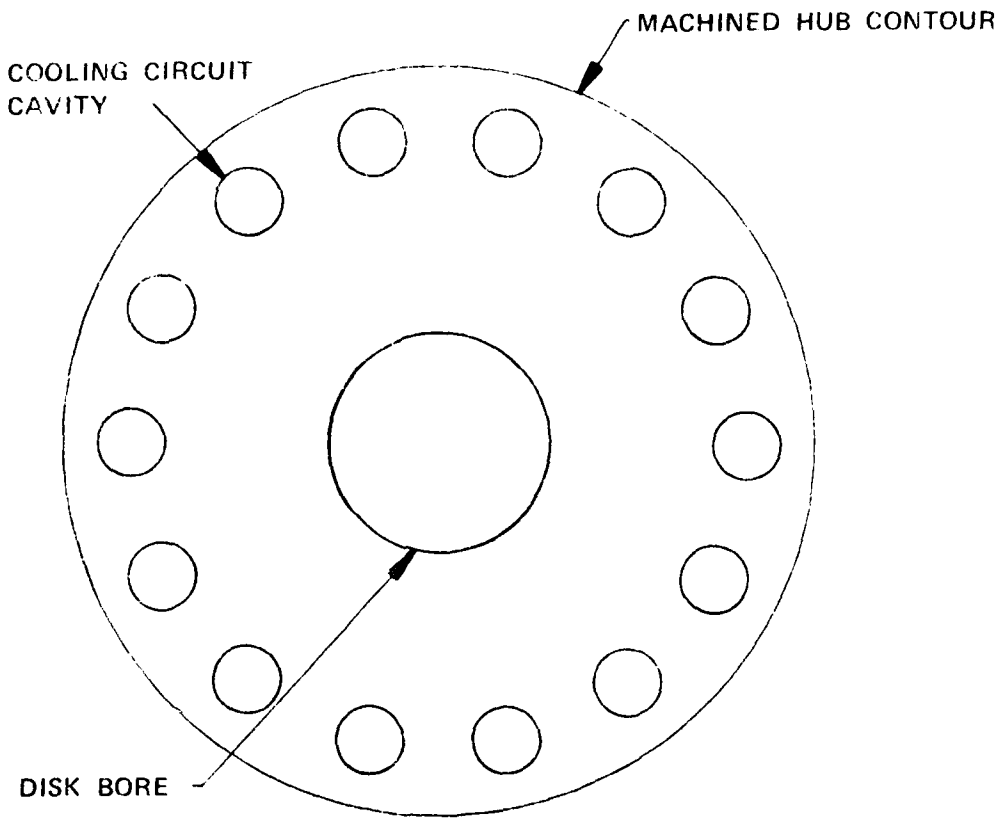

Figure 21. Possible Laminate Section at Cooling Manifold Locations.

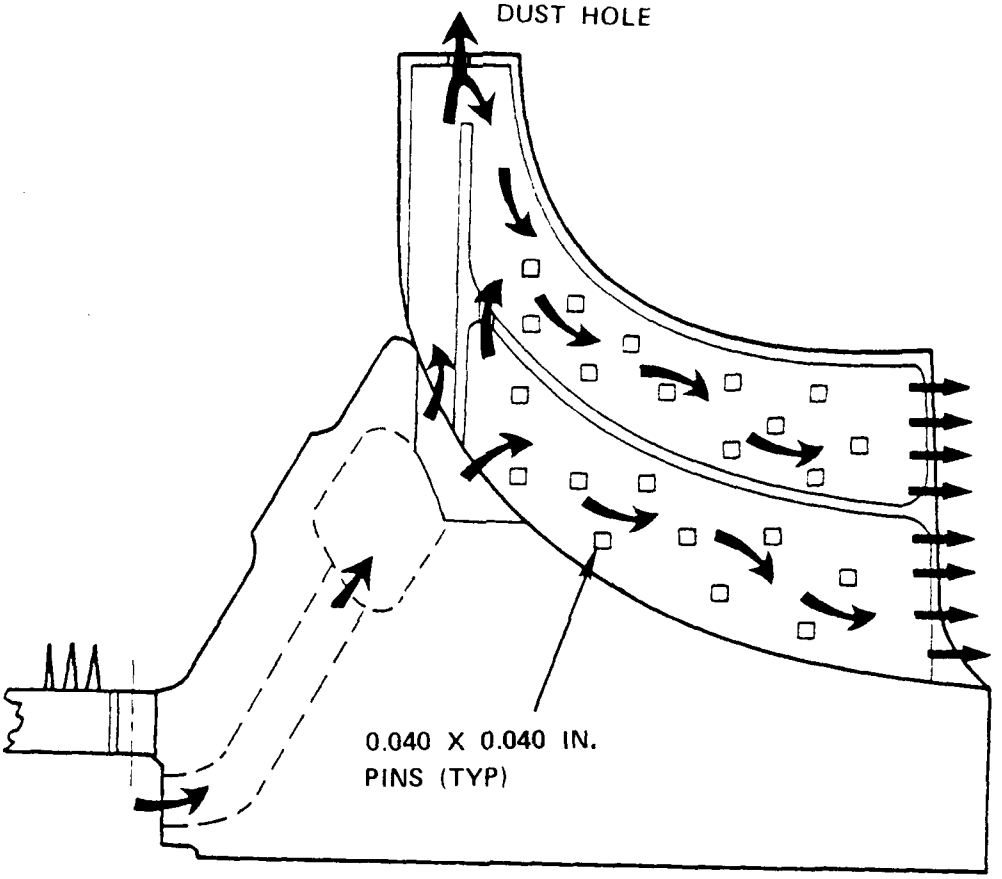

Figure 22. Two-Passage, Single-Pass, Meridional-Flow Configuration.

- Extended surfaces permitting variation of inside heat-transfer coefficients, giving better temperature distributions

- Relatively light weight, reducing stresses in the disk.

Figure 23 shows a typical blade section at a radius of 2.1 inches. The laminate boundaries are shown along with the maximum cooling passage width that the blade thickness would permit. The blade thickness is a function of both mechanical and aerodynamic requirements. Initially, this was considered to be the maximum allowable blade width. It can be seen in Figure 23 that, because of the width restriction and also due to the high turning angle of the blade, meridional flow becomes very restricted in the exducer region of the blade. For this reason it was deemed desirable to revise the cooling configuration.

Multiple-Passage, Single-Pass Meridional/Radial Flow Configuration

Because of the meridional flow restrictions discussed above, the cooling configuration shown in Figure 22 was revised to a multiple-passage, single-pass, meridional/radial flow configuration as shown in Figure 24.

The first passage is cooled as follows: Flow enters at the hub and flows radially outward, cooling the forward and leading-edge regions. Flow is then baffled in a meridional direction, cooling the upper portion of the inducer section, and then exits at the tip along the shroud line. Additional flow is bled into this region to scrub any potential area of stagnant flow. Pin fins are used as required throughout this passage. Flow for the next passage enters at the hub and travels in a meridional direction, cooling the lower portion of the inducer. At about mid-chord, the flow is turned radially outward, discharging at the tip along the shroud line. The last three passages are fed at the hub, flow radially outward, and discharge at the tip along the shroud line.

Pin fins are used as required to give desired temperature levels and gradients. The radial flow passages in the exducer region of this configuration eliminate the problems associated with meridional flow in the previous design. Test data is available which indicates that flow discharged along the shroud line, as used in this concept, tends to reduce the effective clearance between the rotor tip and shroud, giving improved aerodynamic efficiency.

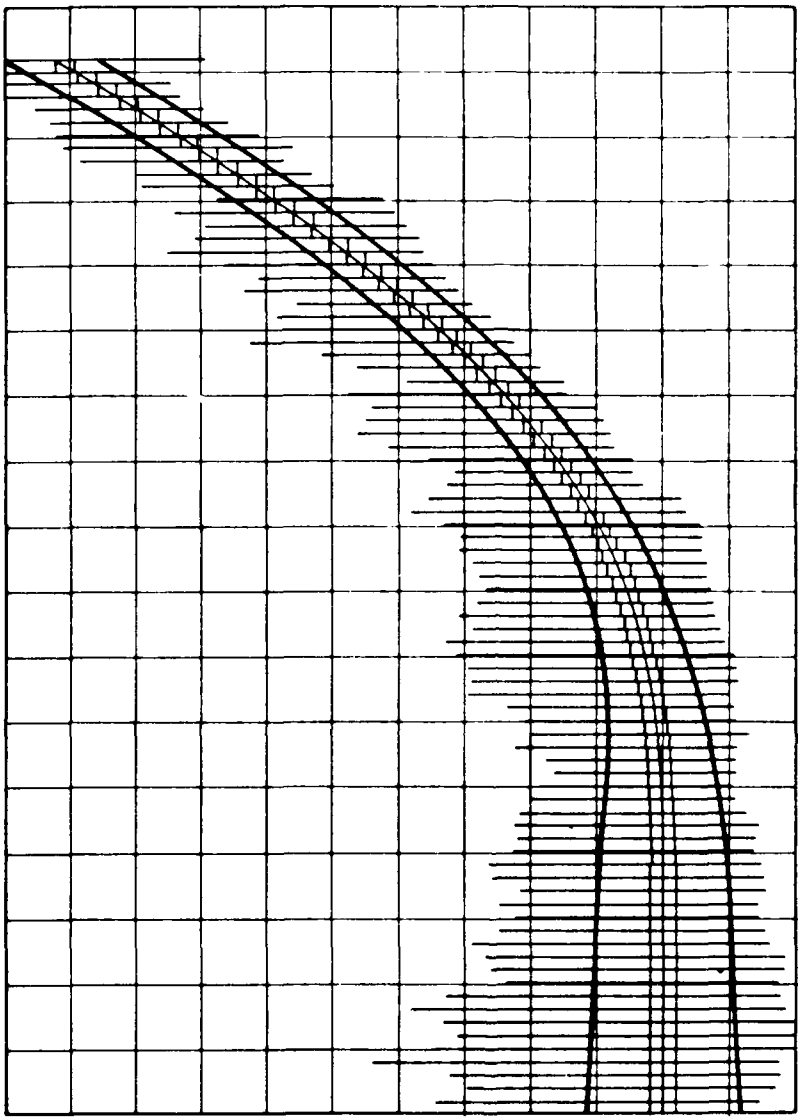

Figure 23. Typical Blade Section at R = 2.1.

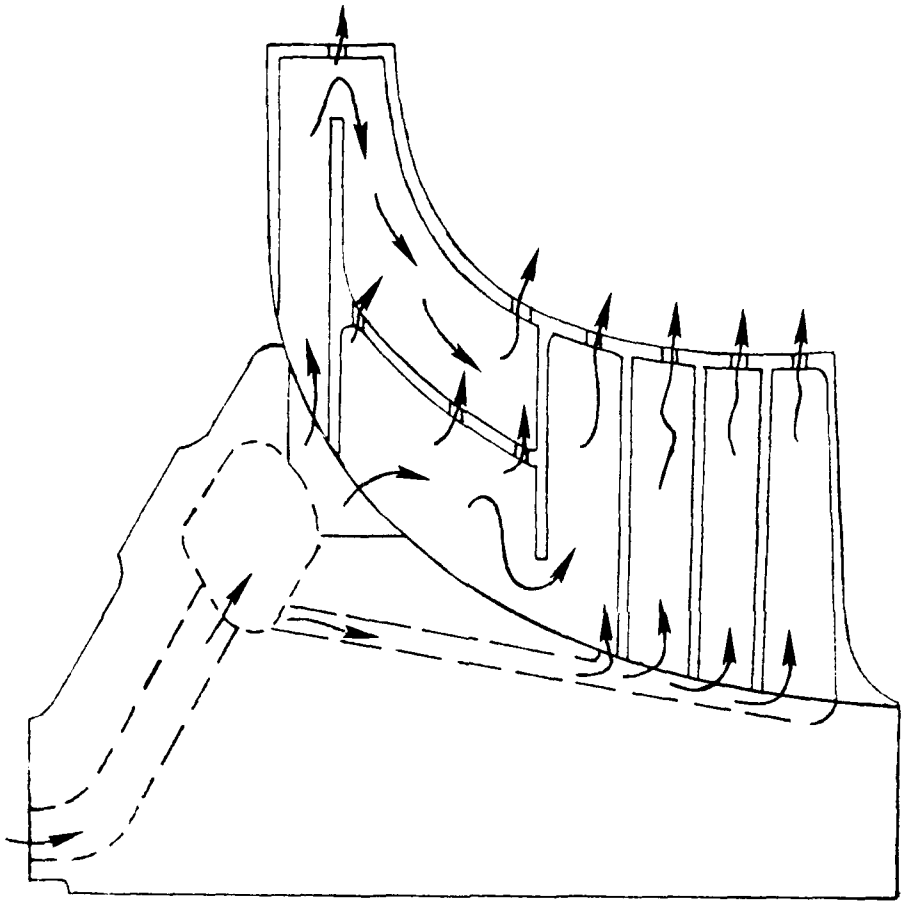

Figure 24. Multiple-Passage, Single-Pass, Meridional/ Radial Flow Configuration.

Early in the design of this configuration, it was found that a very high level of coolant-side heat transfer was required in the leading-edge region which could not be obtained with the methods shown. The leading-edge region was thus modified as shown in Figure 25.

Multiple-Passage, Single-Pass, Meridional/Radial Flow Configuration With Modified Leading-Edge Region

The cooling passage in the leading-edge region in this approach was modified, as shown in Figure 25, to give higher coolant velocities and thus higher heat transfer than the previous design. However, the degree of heat transfer necessary to reduce the metal temperatures to acceptable levels could still not be obtained. The leading edge was subsequently redesigned to incorporate impingement cooling as shown in Figure 26.

Multiple-Passage, Single-Pass, Impingement-Cooled, Leading-Edge, Meridional-Flow Inducer and Radial-Flow Exducer

In order to obtain the high levels of coolant-side heat transfer required at the tip, impingement cooling was incorporated as shown in Figure 26.

Part of the air from the forward passage is directed through three metering orifices at high velocities, striking the leading edge and giving high heat-transfer coefficients. This "spent" impingement air is then discharged through slots along the shroud line and back face. The remainder of the forward passage air is directed radially inward along a meridional path to cool the upper half of the inducer section. This air is then baffled in a radially outward direction before discharging through slots along the shroud line. The lower part of the inducer region is cooled the same as previously described.

The exducer region of this blade configuration consists of radial passages, separately fed at the hub, flowing outward and discharging along the shroud line. However, further analysis of this design indicated that an excessive amount of cooling air would be required. In the initial design phase, the blade thickness limitations imposed by the aerodynamic design restricted axial flow through the exducer. However, after further iterations between the mechanical and aerodynamic requirements, it was found that a slight increase in blade thickness could be tolerated to permit a small amount of axial flow in the exducer. A serpentine exducer region, as shown in Figure 27, was then considered.

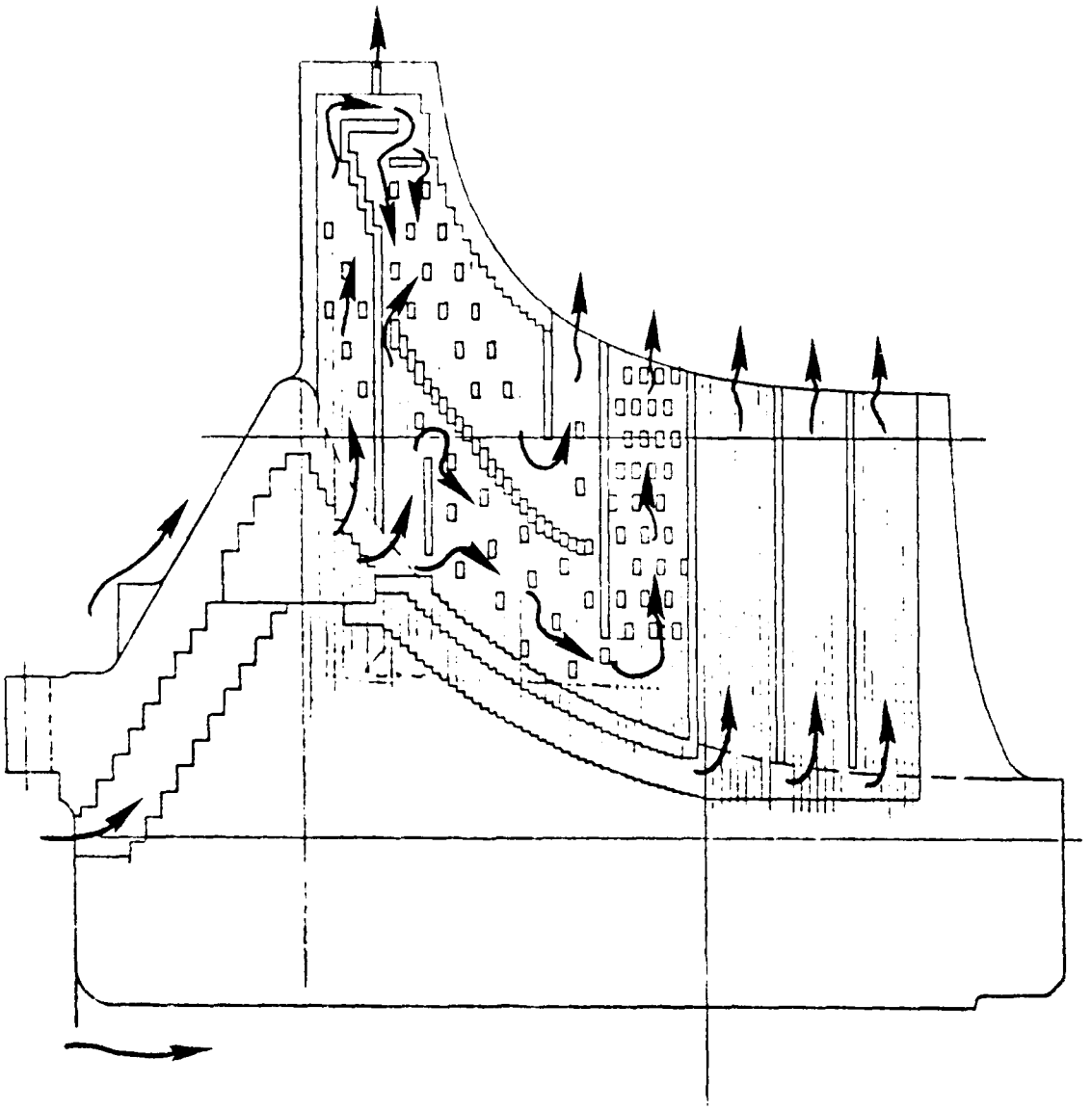

Figure 25. Multiple-Passage, Single-Pass, Meridional/ Radial Flow Configuration with Modified Leading-Edge Region.

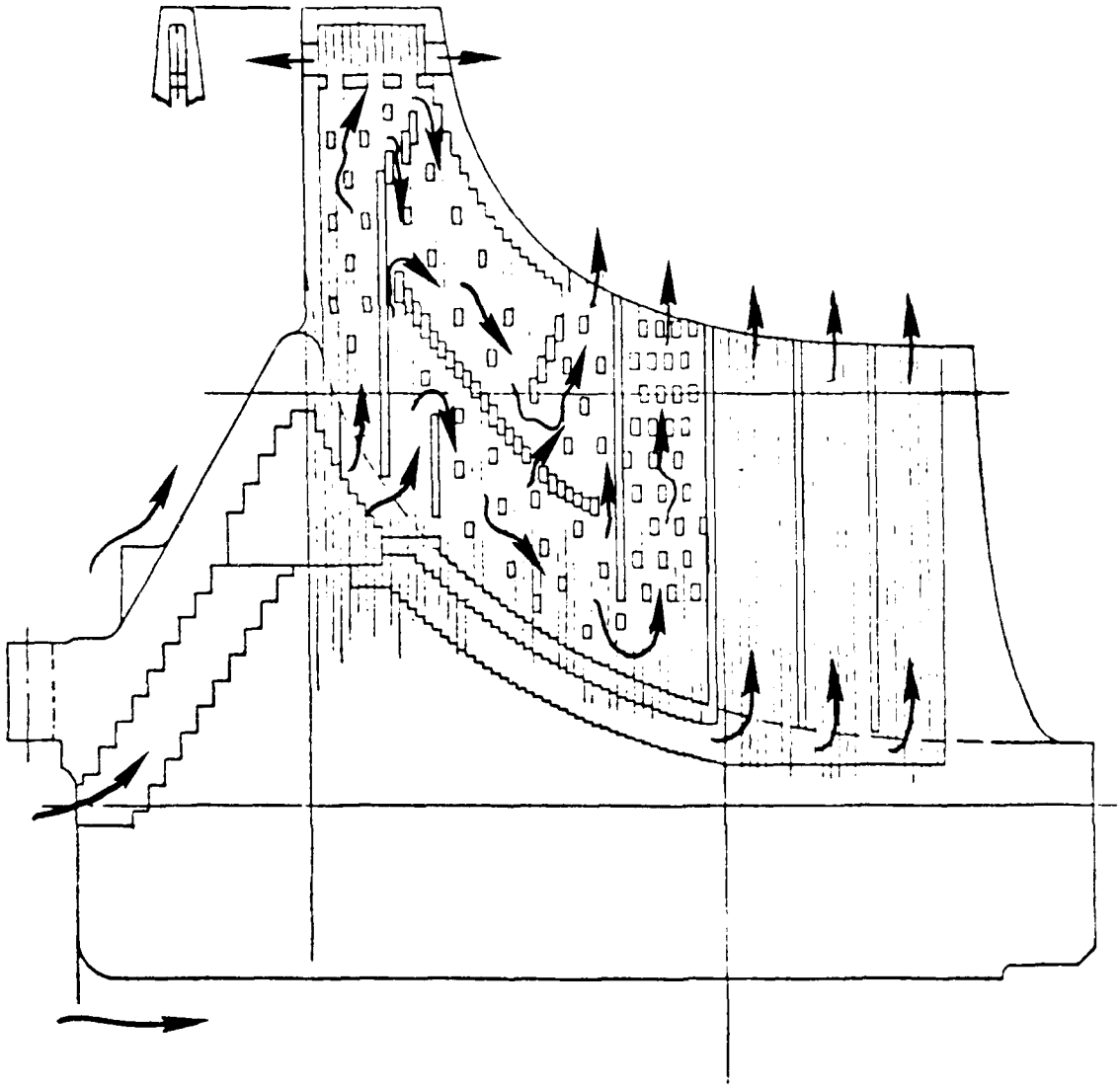

Figure 26. Impingement-Cooled Leading Edge. Low Thermal Gradient Side Wall Inducer Cooling, Radial Cooled Exducer.

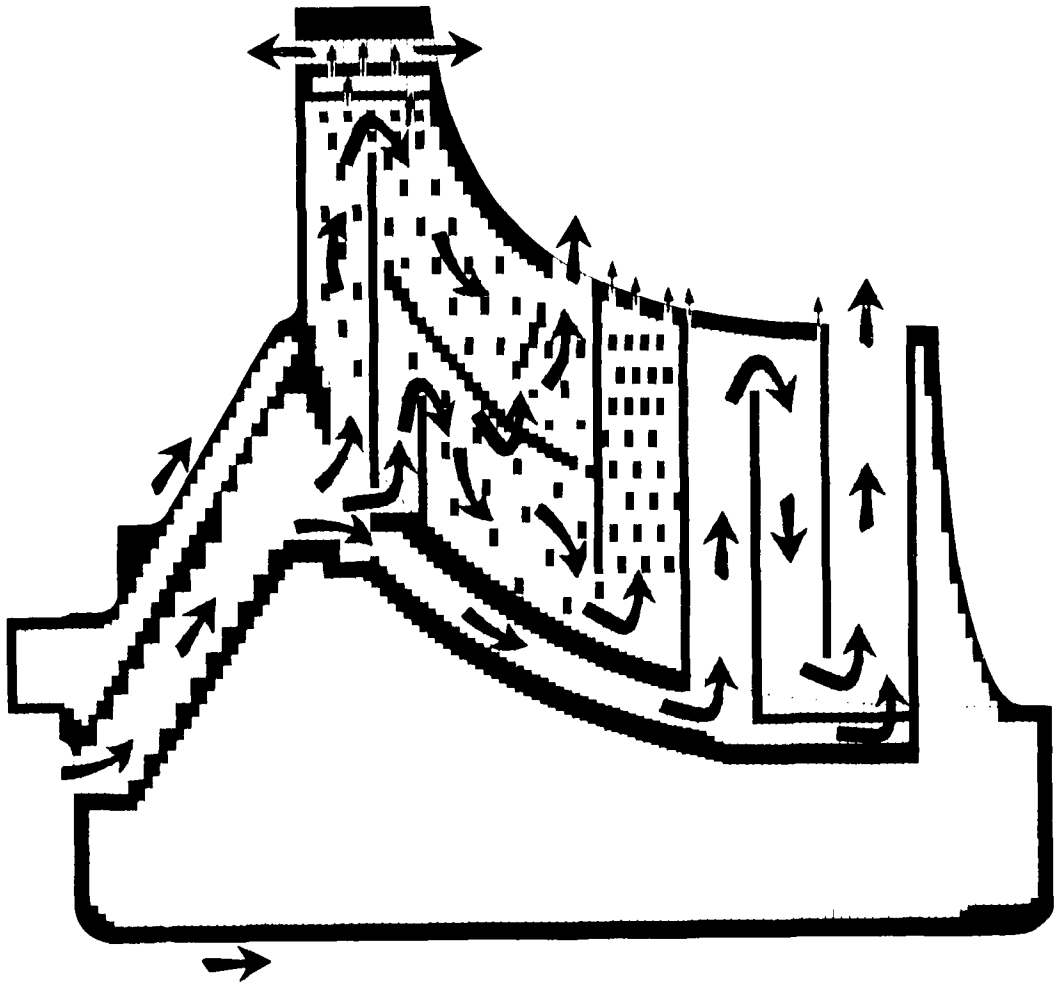

Figure 27. Impingement-Cooled Leading Edge, Meridional-Flow Inducer and Serpentine Exducer Configuration.

Multiple-Passage, Impingement-Cooled Leading Edge, Meridional-Flow Inducer, and Serpentine-Cooled Exducer

In order to get better cooling efficiency in the exducer region of the blade, a serpentine configuration has been used as shown in Figure 27. The serpentine is a three-pass configuration entering at the hub and exiting along the shroud line. The inducer design configuration is the same as discussed in the previous section.

The analyses of the inducer and exducer sections of the blade are discussed in detail in subsequent sections. This concept appears to meet all thermal and stress requirements and has thus been selected as the final configuration.

Analysis

Design Considerations

External thermal boundary conditions for the radial turbine blades were calculated at the maximum power design condition from aerodynamic data and airfoil geometry. The computation was performed using the standard AiResearch computer program based on cylinder in crossflow and turbulent flat plate correlations. Values of surface heat-transfer coefficient and adiabatic wall temperature are calculated along eleven streamlines from the blade inlet to blade exit on both pressure and suction sides of the airfoil. A spanwise flat inlet temperature profile was assumed for the analysis. Tables 3 and 4 present the calculated values interpolated onto an R by Z grid for convenience in the analysis. Some grid values are actually outside the blade outline and may appear to be inconsistent.

The heat-transfer and pressure-drop characteristics of typical laminated blade construction passages are higher than for smooth passages by varying amounts depending upon laminate orientation and flow direction. Prediction of these characteristics for rough passages is a difficult problem, which has not been treated experimentally or analytically. A literature search was conducted by AiResearch to scan for geometries similar to those produced in laminated structure passages, which were studied in detail. Experimental work on thread-like roughness has been extensive and has been utilized to develop correlations for friction factor increases and heat-transfer augmentation in regular rough-surfaced passages.(14,15,16,17) These correlations have been used in cooling circuit design of the

---

(14) Sams, E.W., "Experimental Investigation of Average Heat Transfer and Friction Coefficients for Air Flowing in Circular Tubes Having Square Thread Type Roughness", NACA RME52D17, Lewis Flight Propulsion Lab., June 1952.

(15) Kolar, V., "Heat Transfer in Turbulent Flow of Fluids Through Smooth and Rough Pipes", International Journal of Heat and Mass Transfer, Vol. 8, No. 4, Apr. 1965, pp. 639-653.

(16) Furber, B.N., and D.N. Cox, "Heat Transfer and Pressure Drop Measurements in Channels with Whitworth Thread Form Roughness", Journal of Mechanical Engineering Science, Vol. 9, No. 5, Dec. 1967, pp. 339-350.

(17) Norris, R.H., "Some Simple Approximate Heat Transfer Correlation for Turbulent Flow in Ducts with Rough Surfaces", ASME Winter Meeting, Dec. 1970, printed in ASME Publication G76 (1970), "Augmentation of Convective Heat and Mass Transfer".

TABLE 3. RADIAL LAMINATED COOLED BLADE BOUNDARY CONDITIONS - ADIABATIC WALL TEMPERATURES.

HIGH TEMPERATURE COOLED RADIAL TURBINE (LAMINATED)
NEW HUB CONTOUR 9/21/77

INTERPOLATED PRESSURE SIDE GRID TEMPERATURES (DEGREES F)
(ALL GRID COORDINATES IN INCHES)

K COORDINATES	Z COORDINATES									
	0.0000	.2000	.4000	.6000	.8000	1.0000	1.2000	1.4000	1.6000	1.8000
1.0000	1832.8	1824.2	1817.3	1812.8	1810.7	1803.2	1798.3	1795.3	1791.6	1795.2
1.2000	1837.6	1831.4	1822.9	1813.5	1808.1	1804.1	1800.1	1796.6	1792.3	1796.8
1.4000	1850.1	1837.1	1824.4	1816.2	1815.4	1815.7	1812.5	1808.7	1807.5	1807.3
1.6000	1856.0	1841.3	1833.4	1834.0	1832.5	1832.9	1829.1	1825.3	1823.4	1820.8
1.8000	1864.5	1852.5	1853.0	1850.9	1849.8	1850.1	1849.7	1846.2	1840.3	1843.4
2.0000	1872.4	1872.6	1869.8	1874.0	1872.7	1871.9	1869.2	1866.7	1861.1	1861.6
2.2000	1845.5	1905.3	1894.2	1891.6	1894.3	1889.1	1881.6	1876.1	1872.7	1868.8
2.4000	1930.0	1915.2	1921.9	1917.1	1905.1	1897.0	1884.7	1875.5	1873.0	1868.8
2.6000	1946.1	1951.3	1946.6	1938.4	1918.4	1906.9	1887.6	1878.7	1873.4	1869.0
2.8000	1979.6	1978.5	1976.8	1956.8	1935.9	1915.1	1888.8	1882.4	1873.5	1868.9
3.0000	1998.8	1998.8	1997.1	1984.9	1968.6	1954.5	1929.6	1883.4	1881.9	1873.1

INTERPOLATED SUCTION SIDE GRID TEMPERATURES (DEGREES F)
(ALL GRID COORDINATES IN INCHES)

P COORDINATES	Z COORDINATES									
	0.0000	.2000	.4000	.6000	.8000	1.0000	1.2000	1.4000	1.6000	1.8000
1.0000	1838.1	1821.7	1815.0	1810.3	1808.1	1800.6	1795.6	1792.9	1790.1	1794.1
1.2000	1834.8	1828.8	1820.5	1811.5	1806.0	1801.7	1797.3	1794.2	1791.1	1795.8
1.4000	1846.6	1834.2	1822.3	1814.2	1812.8	1812.1	1808.1	1805.6	1806.6	1806.4
1.6000	1852.2	1838.5	1830.8	1830.8	1828.4	1827.4	1822.9	1821.2	1822.6	1820.1
1.8000	1860.3	1843.0	1849.3	1846.4	1843.7	1842.6	1842.2	1840.7	1839.9	1843.2
2.0000	1867.7	1867.7	1864.7	1867.9	1865.1	1862.8	1860.8	1861.2	1860.9	1861.8
2.2000	1889.4	1887.8	1887.9	1883.7	1882.2	1876.6	1872.7	1871.1	1871.9	1868.7
2.4000	1920.6	1917.4	1914.2	1906.5	1892.8	1884.4	1875.4	1870.5	1870.4	1867.6
2.6000	1935.5	1940.8	1936.7	1928.3	1907.2	1895.0	1878.0	1872.6	1870.0	1867.6
2.8000	1960.9	1961.3	1960.4	1944.5	1923.9	1903.8	1879.0	1876.0	1869.9	1867.4
3.0000	1964.0	1965.6	1950.2	1950.7	1945.0	1933.1	1911.0	1876.8	1875.8	1869.7

TABLE 4. RADIAL LAMINATED COOLED BLADE BOUNDARY CONDITIONS - EXTERNAL HEAT-TRANSFER COEFFICIENTS.

HIGH TEMPERATURE COOLED RADIAL TURBINE (LAMINATED)
NEW HUB CONTOUR 9/21/77

INTERPOLATED PRESSURE SIDE GRID HEAT TRANSFER COEFFICIENTS (BTU/HR-FT2-F)
(ALL GRID COORDINATES IN INCHES)

R COORDINATES	Z COORDINATES									
	0.0000	.2000	.4000	.6000	.8000	1.0000	1.2000	1.4000	1.6000	1.8000
1.0000	156.01	158.76	155.84	157.95	160.10	172.83	202.27	232.21	256.90	264.11
1.2000	155.58	156.38	157.31	149.47	150.42	161.85	190.78	242.24	261.97	265.47
1.4000	147.48	156.49	154.96	149.35	167.15	170.18	208.68	253.16	270.36	264.81
1.6000	137.31	143.41	160.66	173.19	165.41	167.94	202.73	251.62	269.81	269.74
1.8000	118.38	142.42	172.55	162.10	150.28	163.03	202.18	242.20	265.72	265.19
2.0000	134.66	136.16	154.36	137.71	111.04	135.60	209.85	254.50	267.33	268.48
2.2000	63.90	113.36	126.37	87.61	80.87	151.67	246.32	273.06	276.53	273.53
2.4000	149.34	127.47	111.59	70.65	65.67	97.43	211.16	265.82	271.36	272.57
2.6000	165.11	129.22	130.44	115.61	86.12	96.52	187.83	247.48	268.52	272.33
2.8000	7.71	7.70	7.16	101.52	75.12	97.37	178.97	225.95	267.27	272.13
3.0000	929.81	929.81	803.22	477.54	77.83	66.67	135.61	218.37	228.50	267.51

INTERPOLATED SUCTION SIDE GRID HEAT TRANSFER COEFFICIENTS (BTU/HR-FT2-F)
(ALL GRID COORDINATES IN INCHES)

R COORDINATES	Z COORDINATES									
	0.0000	.2000	.4000	.6000	.8000	1.0000	1.2000	1.4000	1.6000	1.8000
1.0000	188.33	182.12	175.80	179.09	181.02	187.95	203.83	218.29	227.37	230.41
1.2000	191.76	185.68	179.58	165.69	167.29	177.55	199.12	224.86	229.58	231.61
1.4000	206.03	191.00	172.26	165.66	181.69	204.24	228.88	237.99	235.43	234.44
1.6000	212.48	188.60	185.85	204.45	214.88	227.30	238.34	233.34	231.07	231.25
1.8000	213.41	205.93	216.81	222.86	235.04	242.59	242.67	236.42	221.39	219.05
2.0000	230.31	234.70	238.05	246.86	247.20	248.38	243.84	237.60	218.80	219.58
2.2000	265.67	293.23	265.19	264.20	297.69	285.00	263.59	246.68	231.79	226.55
2.4000	391.75	316.34	304.06	326.47	314.83	301.25	273.33	246.12	237.21	229.47
2.6000	391.74	405.43	380.08	364.90	333.62	316.66	276.77	253.41	239.82	230.31
2.8000	436.67	453.45	506.71	429.17	377.62	327.70	279.37	260.72	240.70	230.51
3.0000	699.09	583.46	483.40	461.98	426.04	403.41	343.75	263.36	239.19	239.88

radial laminated turbine wheel. [illegible] over hydraulically smooth values varied from 60 percent to 480 percent for friction factor and 25 percent to 140 percent for heat-transfer coefficient, depending on the ratio of passage roughness height to hydraulic diameter.

Total pressure losses due to turning in complex cooling circuit geometries can be significant for predicting flow rate and thermal performance. The geometric parameters of passage total bend angle, bend radius, and aspect ratio were used to predict dynamic head losses at various points in the cooling flow circuits.

The various cooling schemes studied, including the final selection, have a variety of geometric features compatible with, or made possible by, laminated construction. Pin fins are of rectangular cross section and can be located in arrays of varying density as desired, including interrupted arrays. The minimum areas of metering holes and dust or cross-passage bleed holes are limited by current laminate etching technology. However, these areas can be easily varied above the minimum value. Passage height is also easily varied above a minimum value to achieve the desired changes in flow velocity for any circuit portion in the design.

An examination of the alternative schemes presented for the radial turbine blade cooling circuit design, including the final configuration selected, accentuates the importance of in-depth analysis to obtain desired flow distributions in a multiplicity of passages connected in series and parallel. The general approach for solving flow distribution problems at AiResearch, which has been utilized for the laminated radial turbine, is a computerized compressible flow network analysis. The procedure considers the impact of heat transfer between the coolant and passage surfaces for fixed external boundary conditions, fluid friction effects, the effect of passage rotation about a reference axis, passage area changes including sudden turns, expansions and contractions, and variation in fluid transport properties. Boundary conditions at the passage exit and inlet supply locations are used with the geometry to define the flow distribution. In conjunction with the solutions obtained defining fluid temperatures and pressures within the cooling circuit, a one-dimensional heat conduction solution yields passage inner and outer wall surface temperatures at discrete points along each fluid passage centerline. These solutions for blade wall temperature have been used to make accurate estimates of final steady-state blade temperatures that will occur at the maximum power operating condition. The resultant blade metal temperatures were used for stress and life analyses.

Passage exit boundary conditions were established by the aerodynamic solution. Blade tip static pressures are plotted in Figure 28 as used in compressible flow analysis of the blade circuits.

Blade Inducer Region

The cooling circuit, as pictured in Figure 29, requires coolant flow in the amount of 4.94 percent of compressor discharge flow to effectively cool the blade to temperature levels that are acceptable from a life-prediction standpoint. The individual flow splits to each portion of the blade are indicated. The sizes of the holes noted in Figure 30 are listed in Table 5.

The inducer upper circuit includes an outward radial pass and then splits the flow into an impingement portion at the leading edge and an inward radial pass portion. The impingement feature is preceded by turbulence promotion devices and orificing and is followed by axial flow discharged in two directions. The radially inward passage employs pin-fin heat-transfer promotion and a flow guide, which allows for tip discharge without introducing regions of stagnant flow behavior. Impingement at the leading edge provides the high level of coolant-side heat-transfer coefficients necessary to obtain acceptable metal temperatures. The "spent" air after impingement discharges axially through slots along the shroud line and back face. Coolant discharged at the shroud line tends to reduce the effective gap between the blade and the shroud and hence improves aerodynamic performance. Coolant discharged at the back face correspondingly tends to fill the gap between the blade hub and the adjacent part and produces a similar aerodynamic performance improvement.

These impingement coolant discharge locations result in a straight-through passage that can be visually inspected and cleaned easily. A severe rub could occur on either the shroud or hub line if axial clearances are not properly established. However, it is doubtful that a severe rub could occur on both the shroud and hub in any given wheel. If a severe rub occurs, the coolant discharge passage could be partially or completely closed, thus restricting coolant discharge at that location. This presents another advantage of this design since the system will work reasonably well with either the hub or shroud discharge location completely closed. Further, the blockage can be easily removed at overhaul. Another advantage of this leading-edge cooling scheme is that the blade will remain integral even with severe leading-edge erosion or damage.

Coolant temperature increases in the flow direction because of heat transfer to the coolant. This fact is taken into account by orienting the coolant flow direction in the upper inducer region from an area of higher external gas temperature

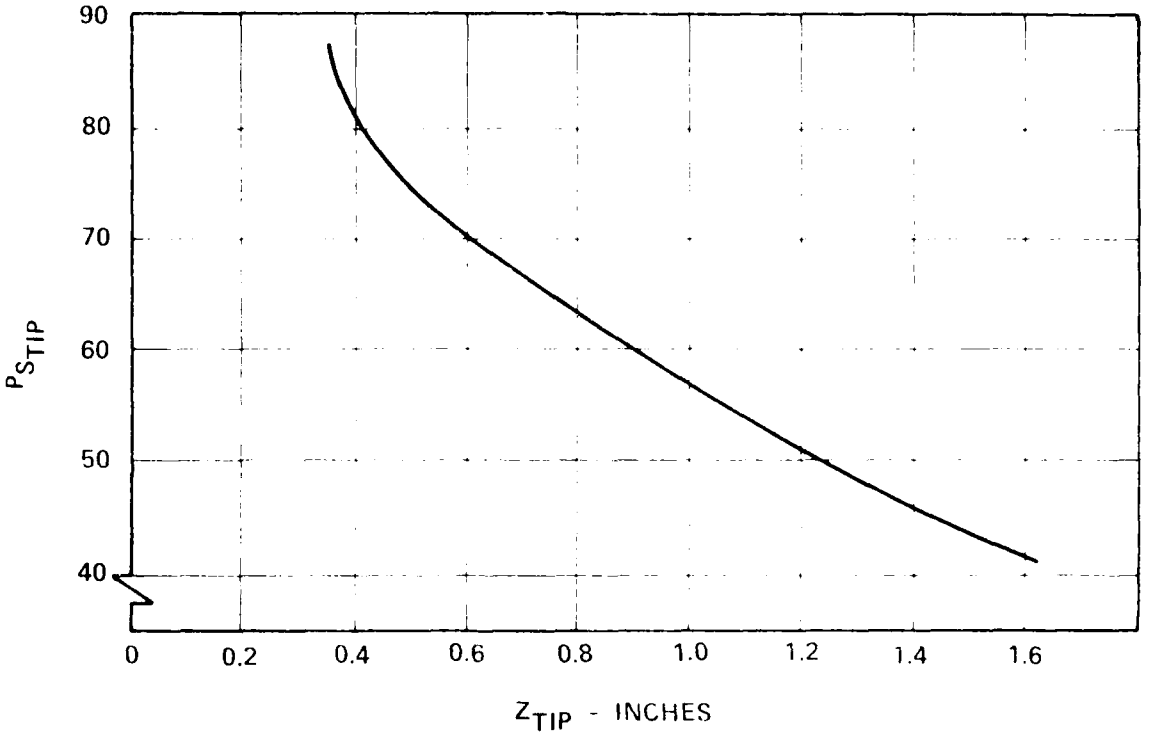

Figure 28. Radial, Cooled, Laminated Turbine Blade Tip P_{Static}.

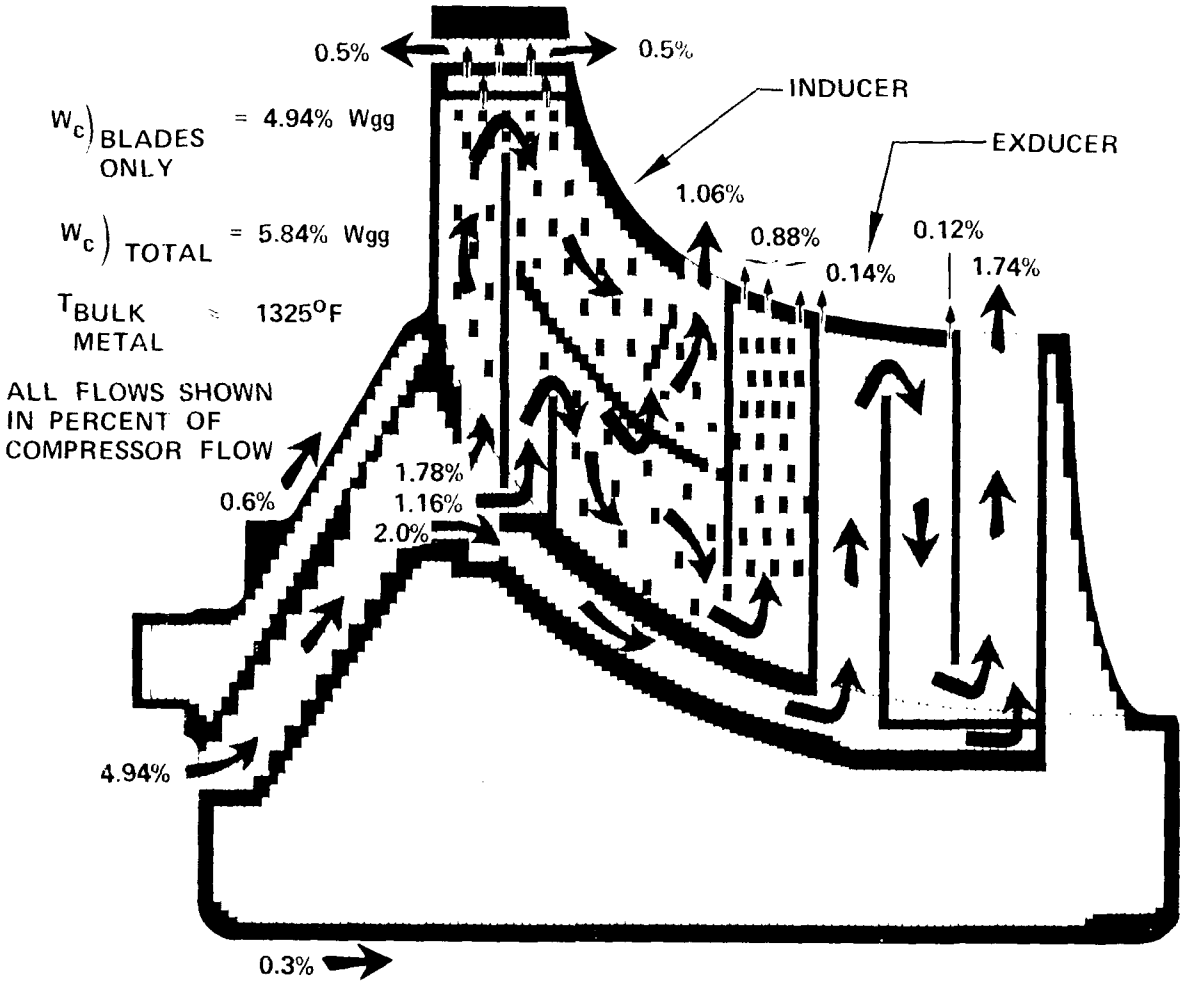

Figure 29. Cooling Geometry (See Figure 30 and Table 5 for Holes Sizes).

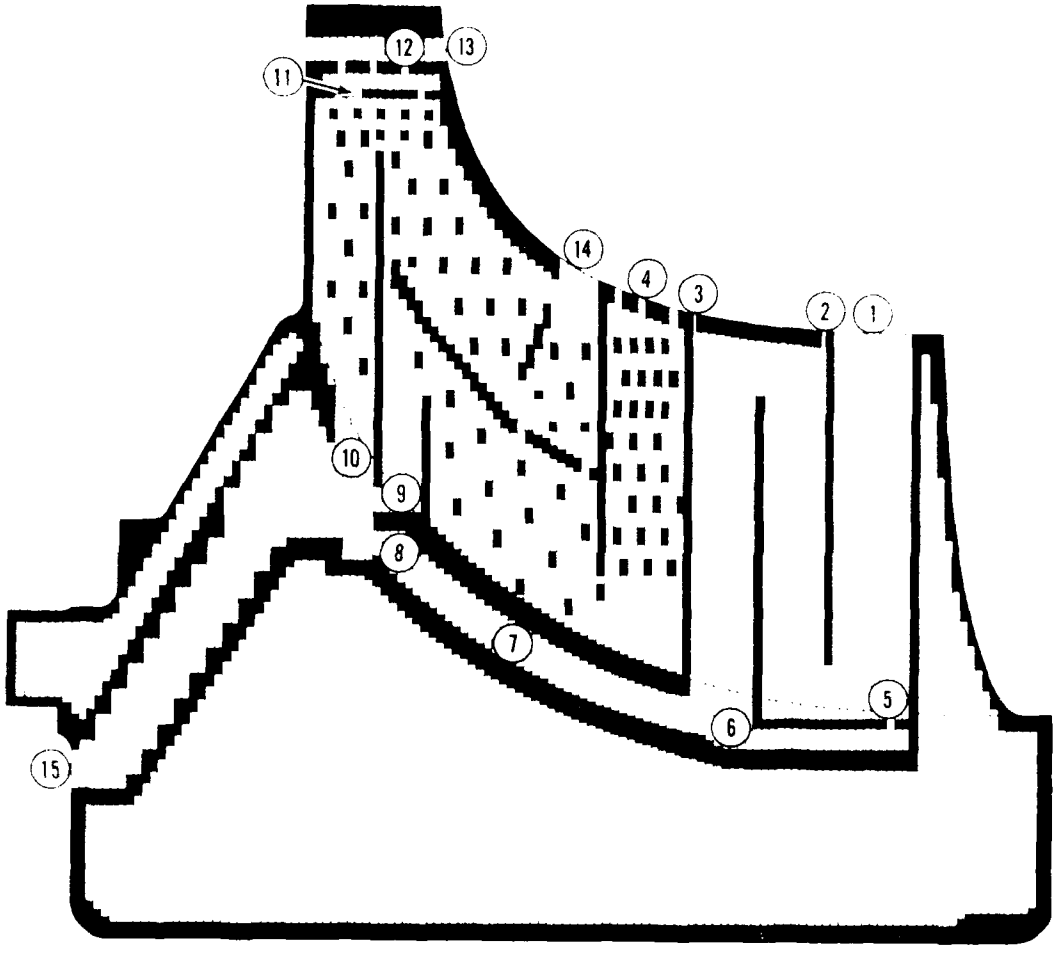

Figure 30. Hole Geometry (See Table 5 for Hole Sizes).

TABLE 5. HOLE SIZES (See Figure 30).

[illegible]	[illegible]	Size
1	[illegible]	[illegible]
2	[illegible]	[illegible]
3	[illegible]	[illegible]
4	[illegible]	[illegible]
5	[illegible]	[illegible]
6	[illegible]	[illegible]
7	[illegible]	[illegible]
8	[illegible]	[illegible]
9	[illegible]	[illegible]
10	[illegible]	[illegible]
11	[illegible]	[illegible]
12	[illegible]	[illegible]
13	[illegible]	[illegible]
14	[illegible]	[illegible]
15	[illegible]	[illegible]

at the leading edge inward to an area of lower gas temperature. With this orientation, the required cooling capacity decreases as the cooling capability decreases, thus facilitating attainment of low thermal gradients in the walls. Extended surfaces to further promote low thermal gradient walls are also available where required.

The inducer lower cooling passage guides a metered amount of flow over pin-fin arrays of varying densities, as determined by temperature requirements, and discharges at the blade tip. It also supplies regulated quantities of bleed to the upper passage at locations where stagnation would otherwise occur. A total of 2.94 percent of compressor discharge flow is used for cooling in the inducer section. See Figure 31 and Table 6 for boundary conditions and the one-dimensional metal temperatures at selected stations.

Blade Exducer Region

The cooled exducer uses a total of 2.0 percent of core flow supplied in equal portions to each blade by a separate passage in the wheel hub. The passage extends from the saddle region cavity aft, just below and parallel to the blade hub line, up to the third circuit pass location as shown in Figure 29. The third pass supply section carries 20 percent of the total exducer cooling flow, bypassing the first two passes, and meters it into the trailing-edge cooling pass to lower the bulk temperature at this point in the circuit and raise the mass average velocity. Dust holes at the tip region of the first and second passes are positioned in otherwise stagnant corners and are half-etched single laminates, which pass 0.13 percent and 0.12 percent of core flow respectively.

The initial exducer cooling design utilized a three-passage, single-pass scheme primarily because the blade curvature was expected to rule out axial flow at any region of the exducer that would be required for other designs. Solutions for the most forward of the three passages indicated that the restriction placed on minimum passage height of 0.028 inch due to etching limitations prevented attainment of an optimum design. A design with passage height tapering significantly below this would be required to raise flow velocities high enough to overcome a loss in effectiveness due to coolant temperature rise and increasing external thermal load. Pin-fin heat-transfer augmentation was not appropriate because of the reduction in interlaminate flow communication with increasing blade turning angle. Increased blockage obtained by replacing alternate laminates was investigated as a means to increase flow velocity but was found to be ineffective because of reduction in coolant-side surface area. To reduce blade tip temperatures to acceptable levels would have required excessive amounts of cooling flow, on the order of 3.3 percent of core flow, and radial metal temperature gradients would be unnecessarily high.

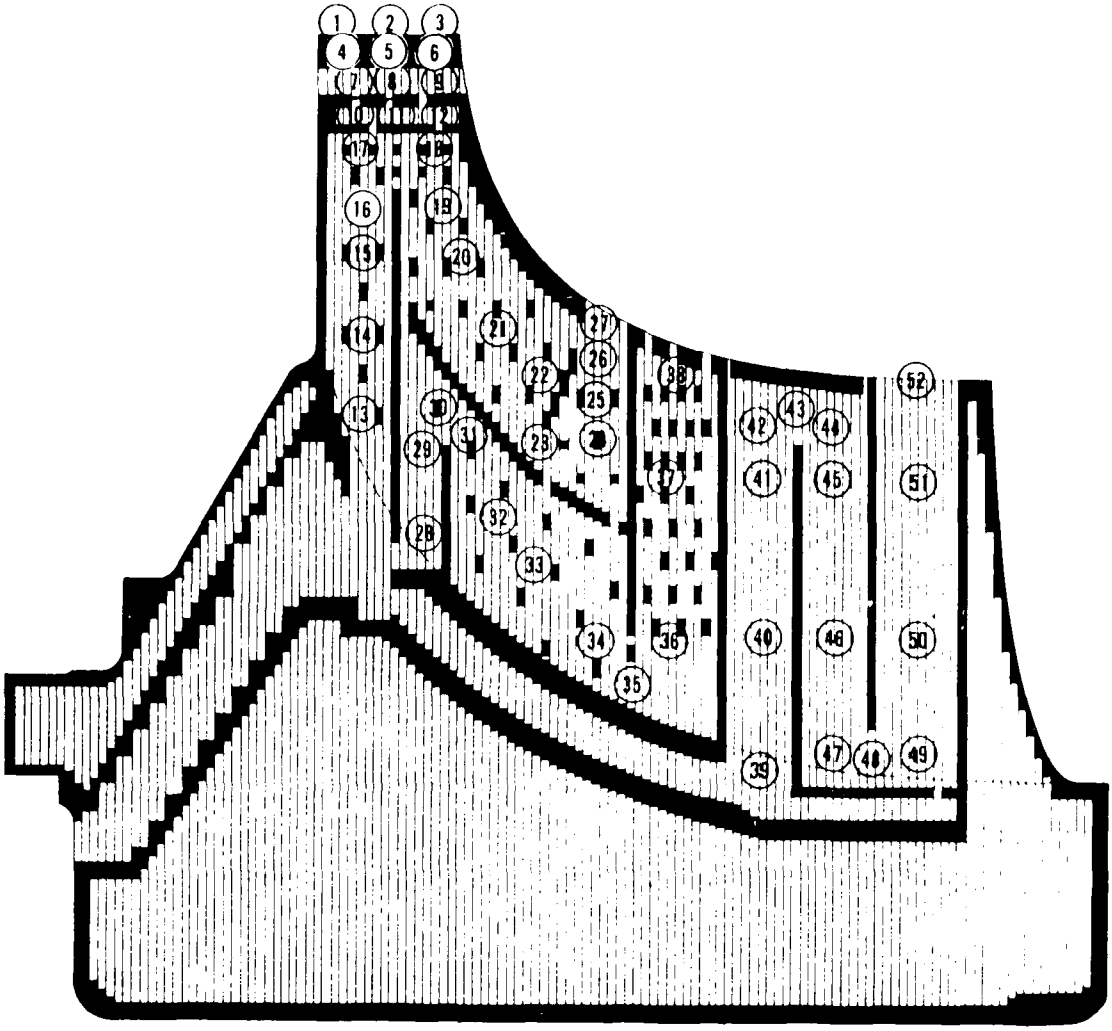

Figure 31. Estimated Metal Temperatures (See Table 6 for Values at Station Locations Indicated by "O").

TABLE 6. ESTIMATED METAL TEMPERATURE AND BOUNDARY CONDITIONS AT STATION LOCATIONS INDICATED BY "O" ON FIGURE 31.

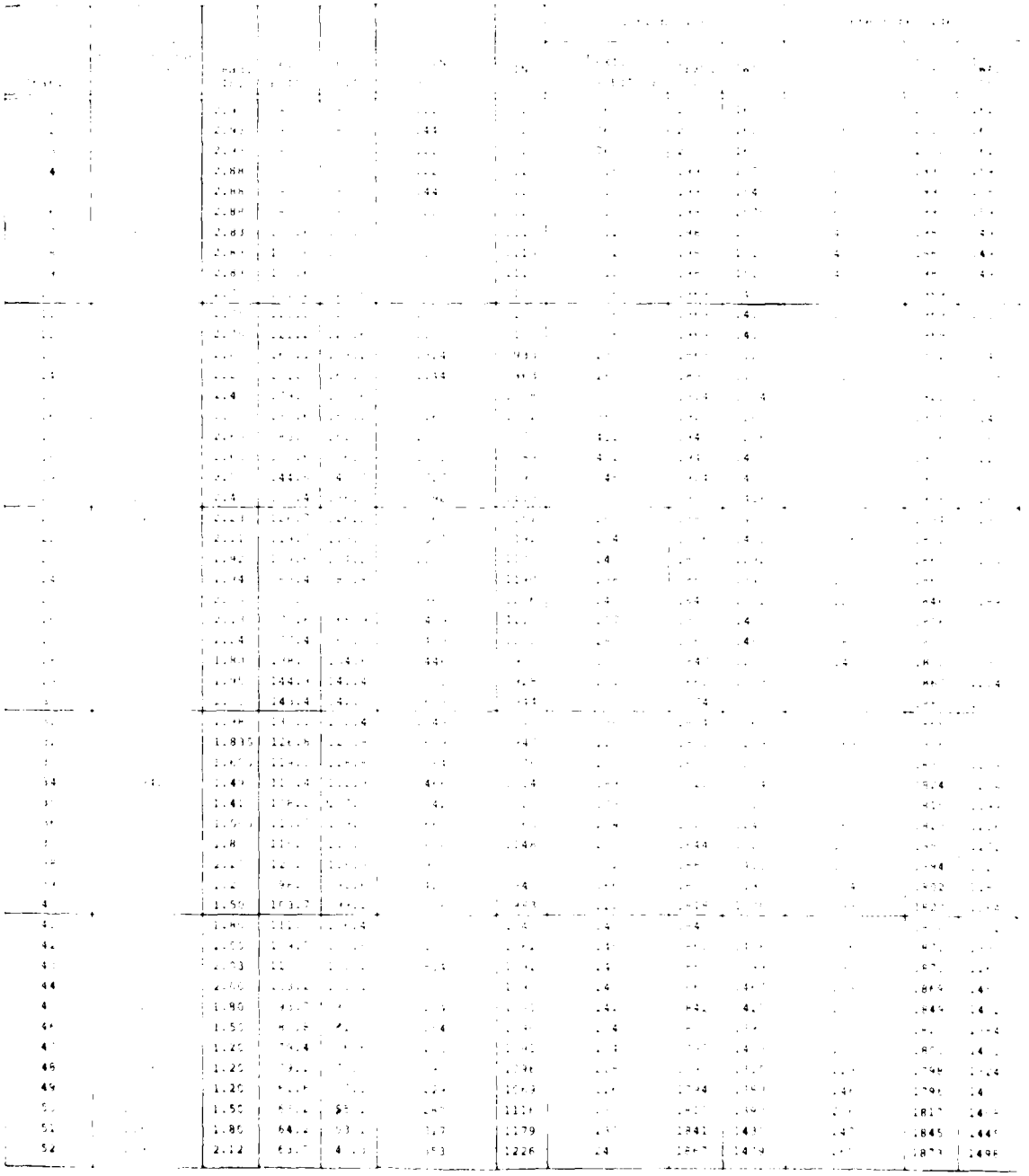

A serpentine three-pass design was selected, as shown in Figure 29, over the three-passage design because of its greater thermal efficiency. The serpentine scheme offers reduced wall temperature thermal gradients and requires 60 percent less cooling flow than the three-passage design to produce similar peak metal temperatures. The greater thermal efficiency is derived primarily from the higher average flow velocities and the second-pass orientation with flow in the direction of decreasing external gas temperature. The third pass augmentation flow balances wall temperatures evenly between all three passes.

Axial flow is required in two locations at crossover points between passes. The second of these is at the hub line where blade turning is small, the passage height is maximum, and therefore no restriction is presented to flow between laminate slots. Examination of the tip crossover location from pass one to pass two indicated a limitation on axial flow with preliminary design blade tip thicknesses. It was found that a slight thickening of the blade aerodynamic profile in this region, as shown in Figure 32, would provide the targeted free area or peak-to-peak gap of 0.015 inch. This increase in blade thickness had negligible impact on aerodynamic blockage or loading and was accomplished without an increase in the blade tip wall thickness, which would add unnecessary load to the blade root.

Figure 31 and Table 6 present analytical results for the serpentine exducer design at the maximum power operating condition, including coolant temperatures and pressures, internal heat-transfer rates, external boundary conditions for suction and pressure sides, and blade wall temperatures. The results shown are for a portion of the total number of discrete stations along the passage flow length and correspond to the locations shown in the schematic. The passage inlet and exit pressure losses are not shown but are reflected in the results presented.

Summary of Results

The blade inducer and exducer pressure- and suction-side wall temperatures calculated in the cooling circuit analysis and presented in Table 6 do not reflect the influence of transverse heat conduction along the blade surfaces. The degree to which this conduction affects temperatures calculated on a one-dimensional basis depends on the severity of the temperature gradient. This is significant, of course, in regions such as near the hub line and near the inducer tip. Adjustments have been made based on examination of the local gradients, the overall cooling circuit design, and related experience with radial wheel designs. These are represented in the overall hub and blade isotherms presented in Figures 33 and 34, which were used for stress and life analyses of the turbine wheel.

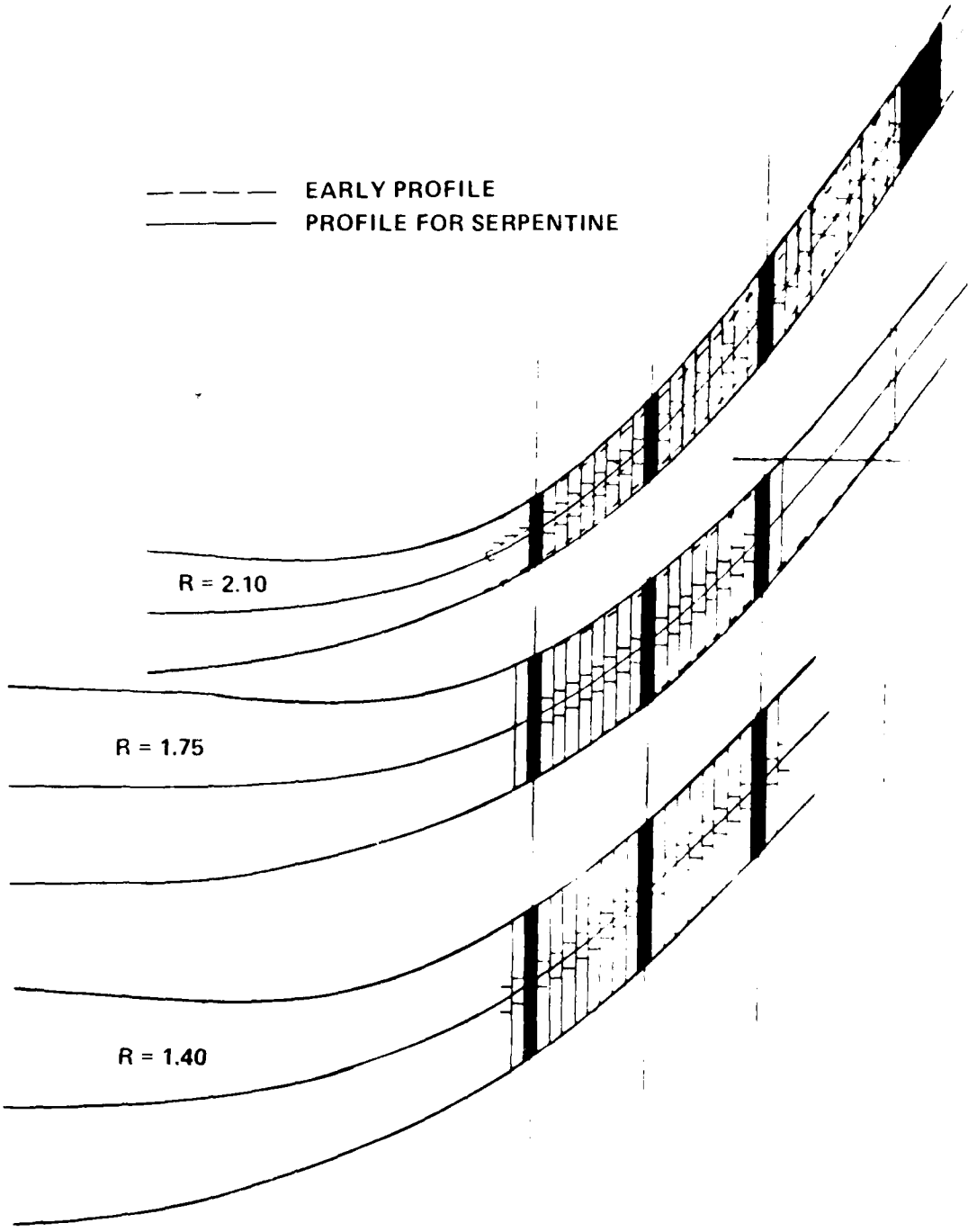

Figure 32. Blade Exducer Thickness for Serpentine Design.

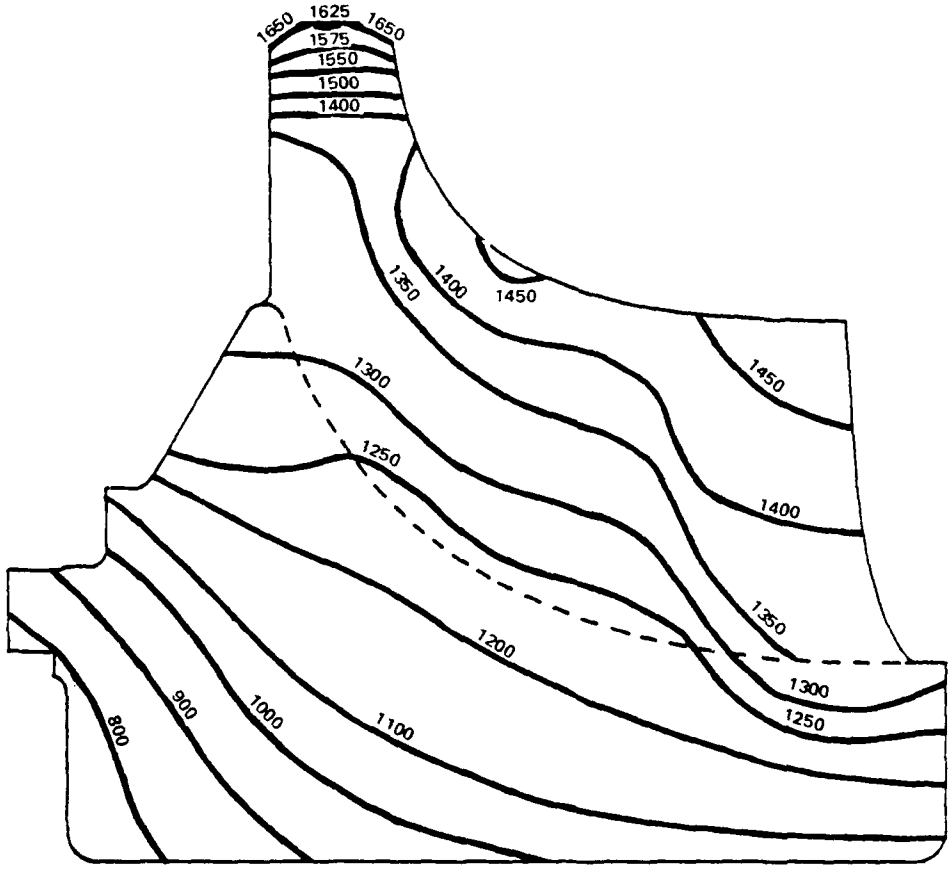

Figure 33. Hub and Suction Side Isotherms.

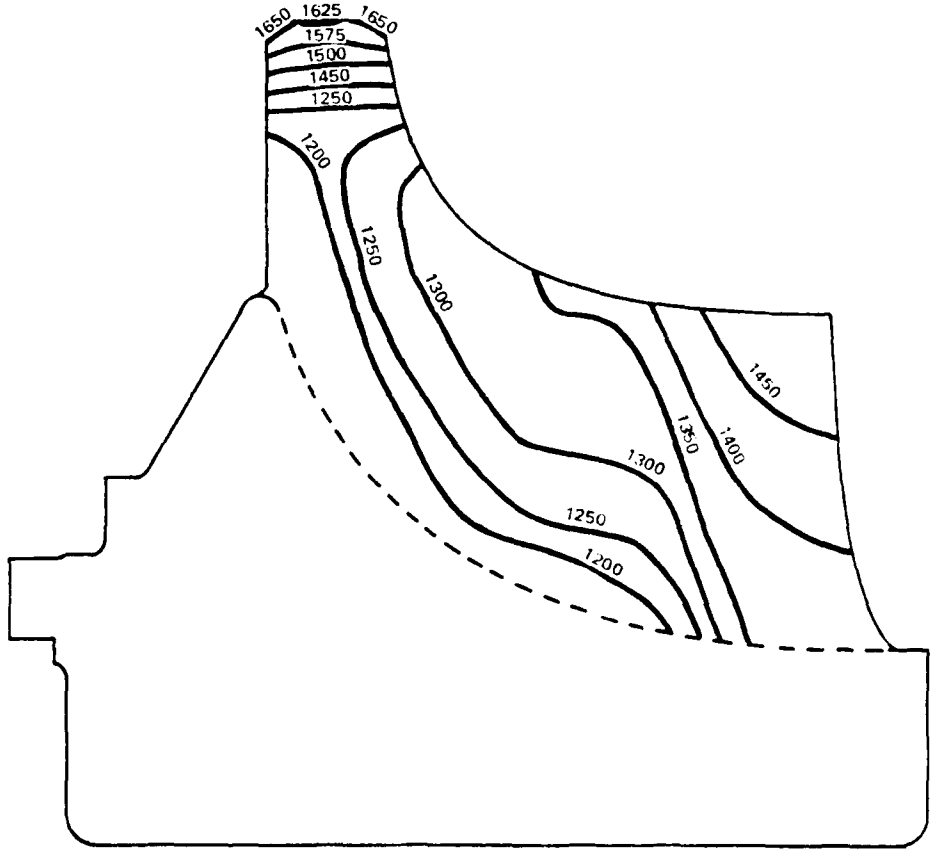

Figure 34. Pressure Side Isotherms.

Conclusions

The final cooling circuit design has achieved all of the basic program objectives:

- Temperature levels throughout the blades will permit achievement of the stress-rupture and creep life goals.
- Thermal gradients throughout have been minimized in order to control thermal stresses.
- Maximum metal temperature at the blade tip has been held to a value (1650°F) that will reduce hot-corrosion damage to an acceptable level throughout the duty cycle.
- The cooling flow has been effectively used. A basic metal effectiveness of 0.54 was obtained based on the relative gas inlet temperature and a cooling flow of 4.94 percent. This compares favorably with the effectiveness of 0.58 calculated for the axial flow laminated turbine designed for the TFE731 blade, which uses 5.88 percent cooling flow.(18,19)
- Each blade is served by a separate cooling passage so that damage to one circuit will have no effect on the other blades and the flow to each blade can be measured during manufacture.
- Design cooling flows can be adjusted rather simply by changing individual laminates for growth versions.
- The total flow to each blade can be metered at the inlet by either plugging or opening the passage.

---

(18) Vershure, R.W., Jr., H.R. Fisk, and J.A. Vonada, "Demonstration of a Cooled Laminated Integral Axial Turbine", AIAA Paper 77-949. Reprinted in Journal of Aircraft, Vol. 15, No. 11, pp. 735-742, 1978.

(19) Vershure, R.W., Jr., "Engine Demonstration Testing of a Cooled Laminated Axial Turbine", AIAA Paper 79-1229, June 1979.

MECHANICAL DESIGN

Introduction

The design of the subject turbine wheel was an iterative process by optimizing or compromising the following aerodynamic and structural constraints:

- Turbine Efficiency
- Aerodynamic Blockage
- Burst Margin
- Cooling Flow
- Blade Stress Rupture Life
- Creep Life
- Low-Cycle Fatigue Life
- High-Cycle Fatigue Life
- Blade Erosion/Corrosion Life

The mechanical design process was initiated by approximating a blade thickness distribution based primarily on stress-rupture estimates for the blades. Temperatures, stresses, burst margin, blade stress-rupture lives, and blade natural frequencies were computed using this preliminary thickness distribution. Based on these results, modifications were made to the disk and blades and were fed back into the design loop. After a number of iterations, the final configuration evolved. Table 7 shows the physical properties and Figure 35 illustrates the final wheel configuration.

TABLE 7. WHEEL PROPERTIES.

Material	Astroloy Sheet (0.020 inch)
Weight	5.0 lbs
No. of blades	14
Polar moment of inertia	0.024 lb-in.-sec^2
Average tangential stress	82.8 ksi
Burst factor (design)	0.85
Minimum expected UTS (1200°F)	167 ksi
Burst margin (minimum)	31 percent
Design speed	73,380 rpm

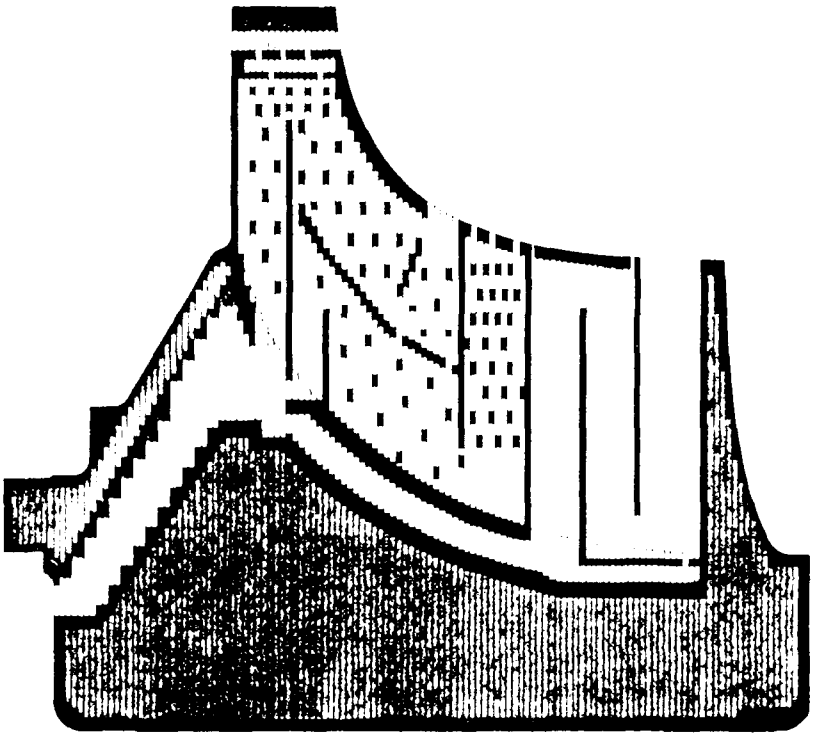

Figure 35. Final Wheel Configuration.

Blade Configuration

The final blade configuration is the result of cooling-flow optimization studies as described previously, stress-rupture and fatigue life, and aerodynamic considerations. Experience gained from other AiResearch radial wheel engine programs was utilized in the design of the blade root fillets and the blade trailing-edge contour. These regions have consistently demonstrated low-cycle-fatigue problems during service operation. Modifications, which have been incorporated into this design, have dramatically increased the life of radial wheels in the field. These modifications included a recontoured blade trailing edge to reduce stresses in the blade trailing-edge root fillet radius. These reduced trailing-edge fillet stresses are clearly evident in Figures 36 through 38. The radii in the blade roots and in the disk saddle region have been optimized to minimize the root stresses along the entire length of the blade and disk interface.

A minimum blade normal wall thickness of 0.020 inch has been maintained to ensure blade integrity. The pin fins and cooling passage dividers in the blade are spaced in close proximity to prevent any panel vibration problems within the blade.

Disk Configuration

The disk geometry was determined by burst requirements, fatigue life, and creep considerations. However, the design was also influenced by physical constraints which limited the diameter of the bore to accommodate a front drive shaft; and the size of the front curvic coupling was restricted to allow the use of standard grind tooling.

The proposed configuration was modified considerably to reduce localized stresses and to provide adequate burst margin by reducing the cooling air plenums and passageways. The front curvic and balance ring were also included in the design to account for their adverse effects on burst margin and tangential stresses at the disk bore. The aft shaft extension was not included in the design because it is relatively isolated from the rest of the wheel and its elimination simplifies attachment to the arbor for whirlpit testing. The cooling air inlet holes were made elliptical to reduce the stress concentration in this region. The major axis is in the tangential direction with a 2:1 ellipse ratio.

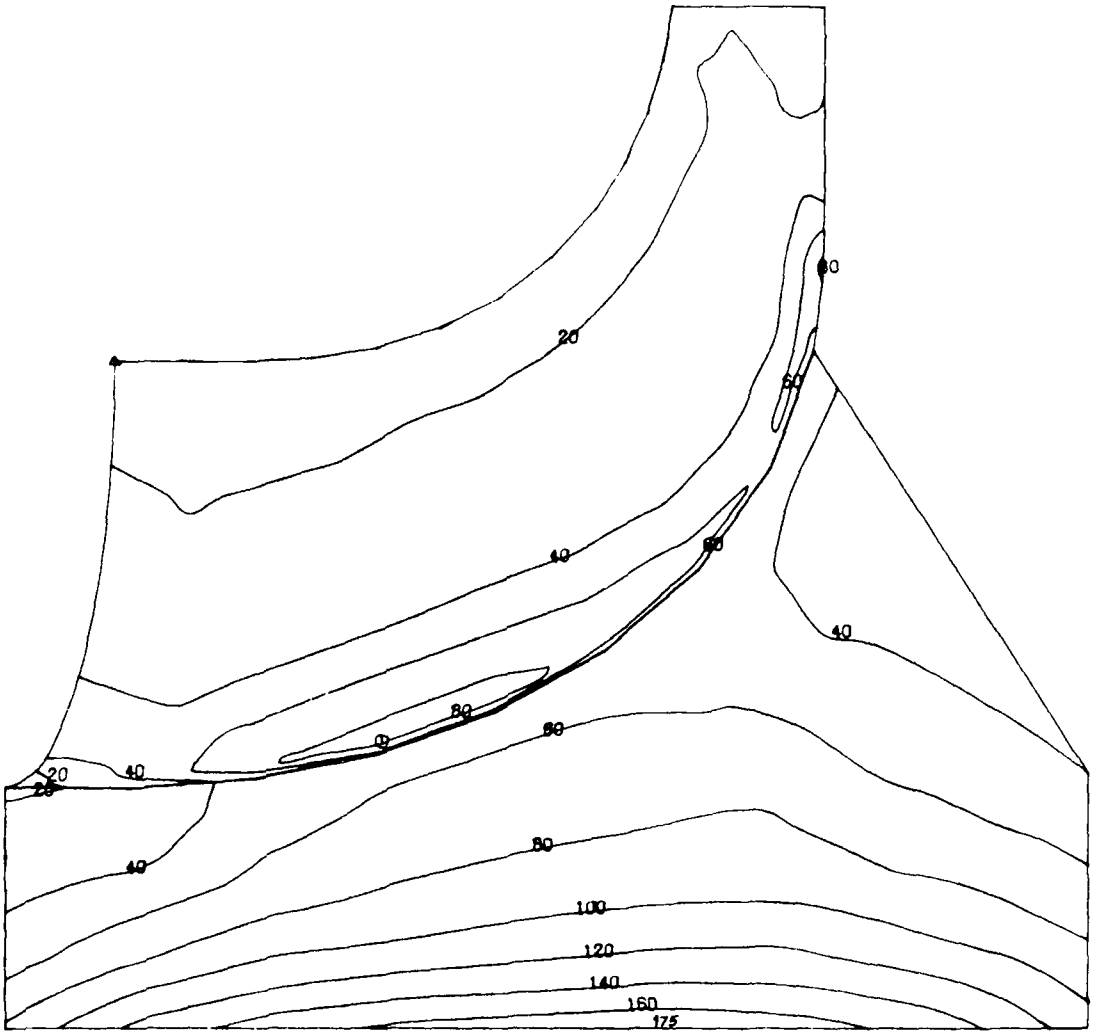

Figure 36. 3-D Equivalent Stresses (KSI) for Combined Effects of Rotation (73,380 rpm) and Temperatures on Blade Pressure-Side Surface and Corresponding Disk (View Rotated 180°).

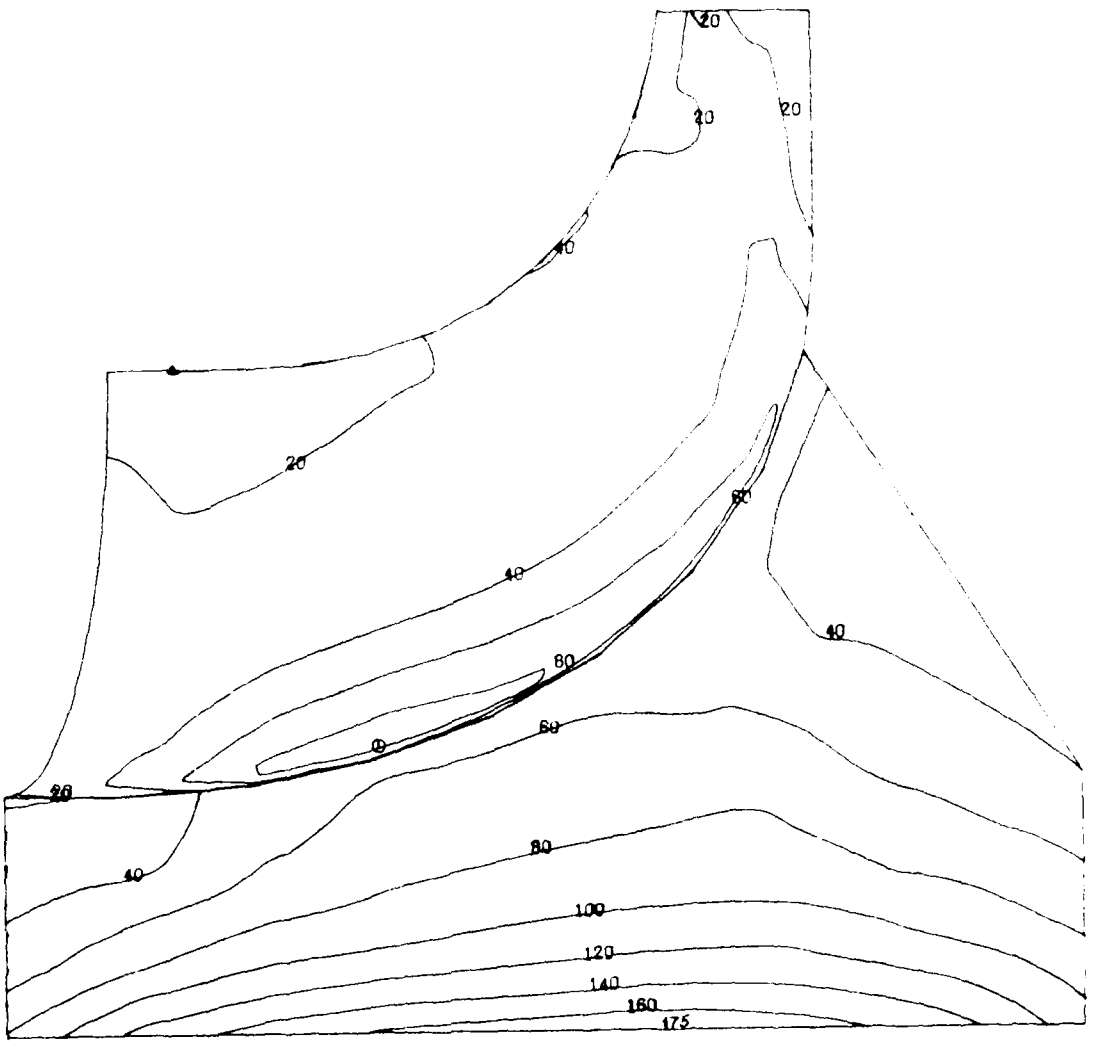

Figure 37. 3-D Equivalent Stresses (KSI) for Combined Effects of Rotation (73,380 rpm) and Temperatures on Blade Suction Surface and Corresponding Disk (View Rotated 180°).

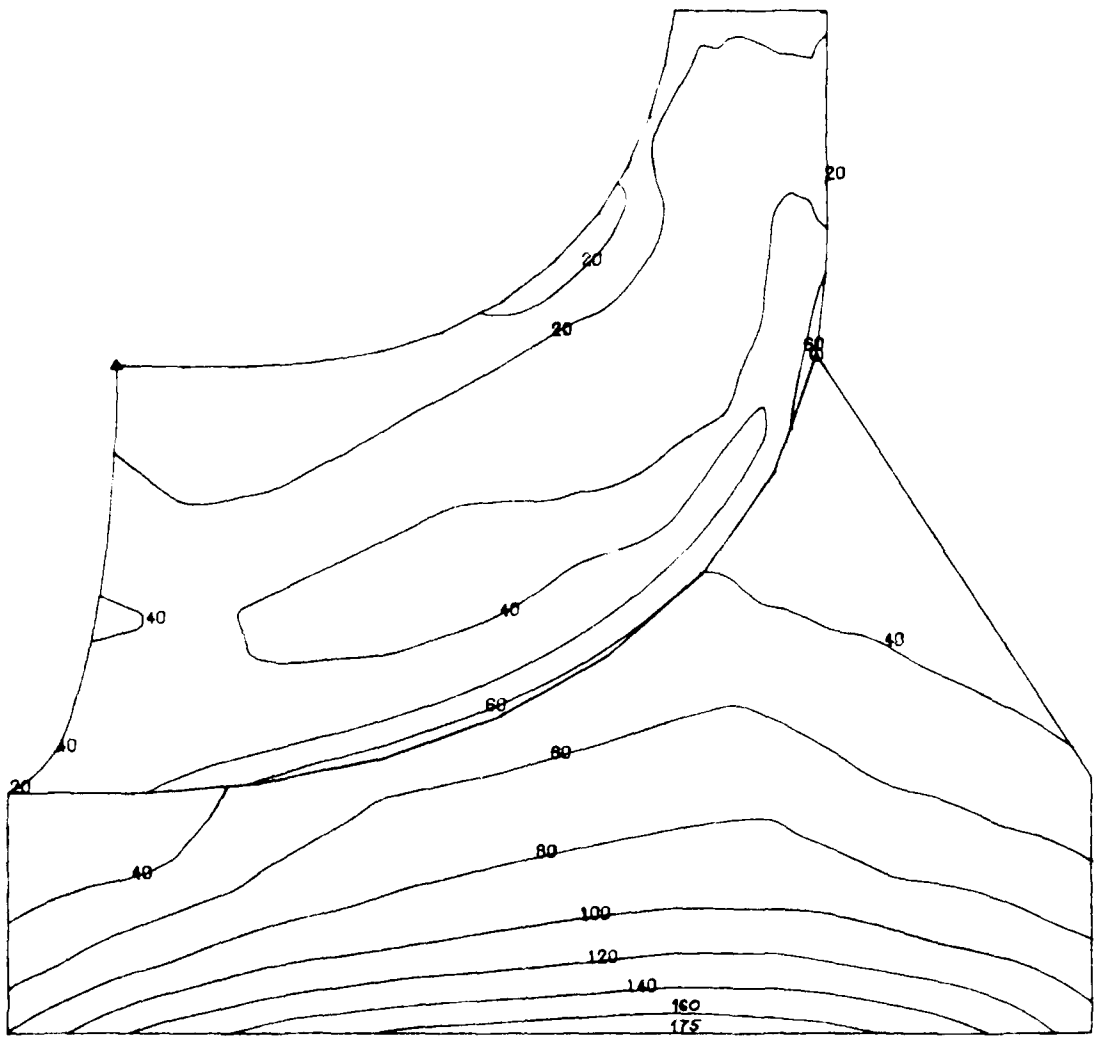

Figure 38. 3-D Equivalent Stresses (KSI) for Combined Effects of Rotation (73,380 rpm) and Temperatures Inside of Blade Pressure-Side Cooling-Passage and Corresponding Disk (View Rotated 180°).

Results of Stress Analysis

Both two- and three-dimensional finite-element models were used in the analysis of the subject wheel. The 2-D finite-element program models the blades as plane stress axisymmetric elements and cannot simulate the blade curvature and stress concentration effects in the blade roots. The cooling passageways and plenums could be modeled accurately with the 2-D program, whereas their incorporation in the 3-D model would have added undue complexity. Therefore, the 2-D model was used primarily for calculating disk stresses and burst margin, and the 3-D program was used for calculating blade stresses. Figure 39 illustrates the 2-D finite-element model and Figures 40 and 41 depict the 3-D model.

Two-dimensional stresses caused by rotation are included in Figures 42 to 44. The stresses were calculated for an engine speed of 73,380 rpm, at room temperature. The stress isopleths in these figures do not completely account for the stress concentrations around the cooling passageways. "Stress Concentration Factors"(20) was used to calculate stress concentrations in the disk near the cooling passageways. The region of the disk that showed the maximum concentrated stress is near the cooling air inlet holes. To reduce the concentrated stresses to acceptable levels, the circular inlet holes were changed to ellipses. The 2-D computer analysis revealed an average tangential stress of 82.8 ksi, which when used in conjunction with a burst factor of 0.85 and a minimum ultimate tensile stress of 167 ksi, results in a burst margin of 31 percent at 1200°F.

Equivalent stresses from the 3-D finite-element model are included in Figures 45 through 47, for rotation at 73,380 rpm. Figure 45 depicts the stresses on the pressure surface of the blade and the corresponding disk stresses. Figure 46 illustrates the stresses on the suction surface of the blade and the corresponding disk stresses. Lastly, Figure 47 shows the internal blade stresses on the pressure side cooling-passage surface with corresponding disk stresses. These 3-D results compare well with the 2-D equivalent stresses in Figure 44, except that the blade root stresses are lower in the 2-D analysis because this stress model cannot account for the stress concentrations in this region.

To evaluate the steady-state thermal stresses for the wheel, temperatures from the heat transfer and cooling airflow design section of the report were included in the 3-D finite-element model (Figures 48 and 49). The 3-D equivalent stresses

(20) Peterson, R.E., "Stress Concentration Factors", John Wiley and Sons, New York, 1974.

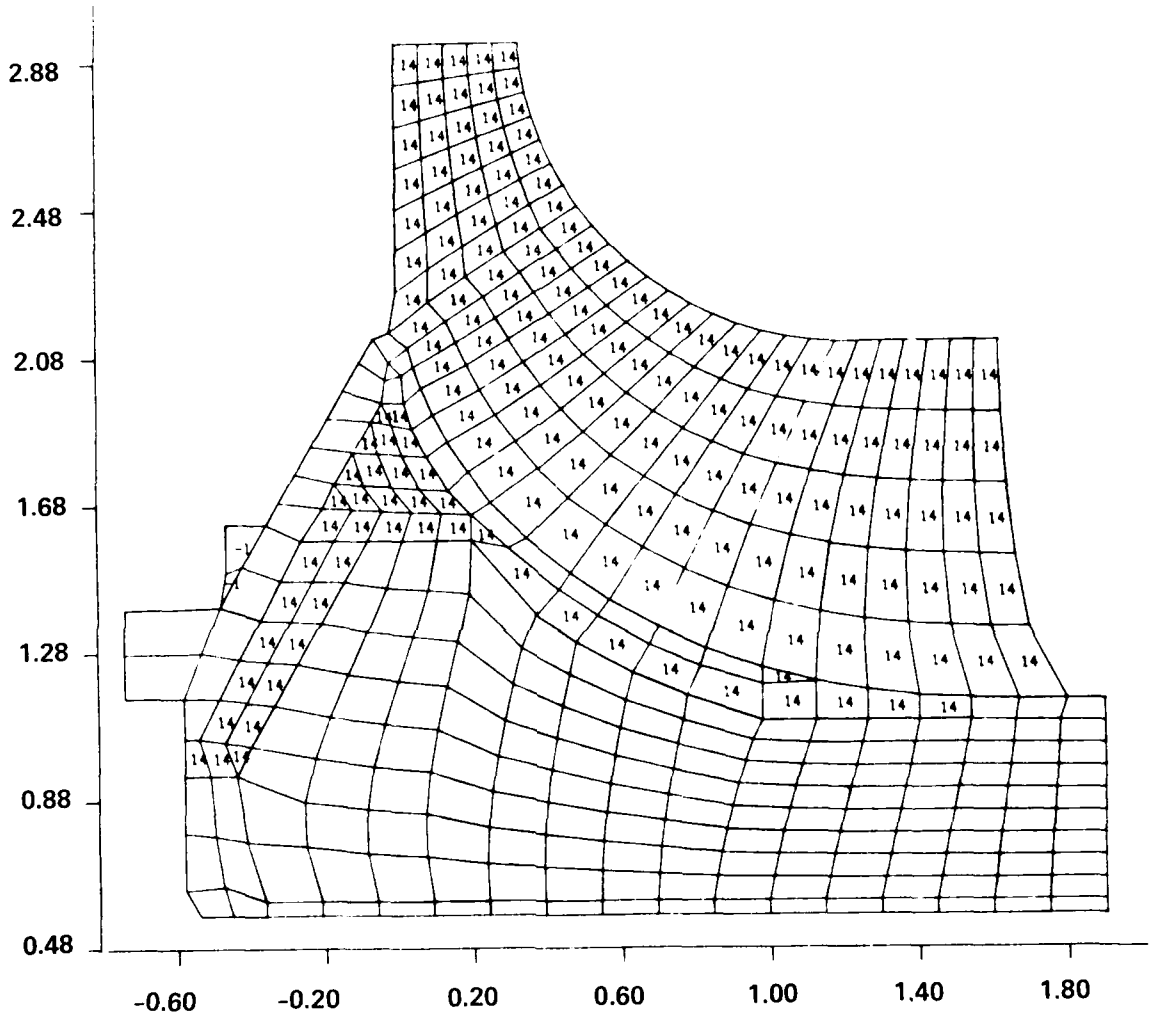

Figure 39. 2-D Finite-Element Model.

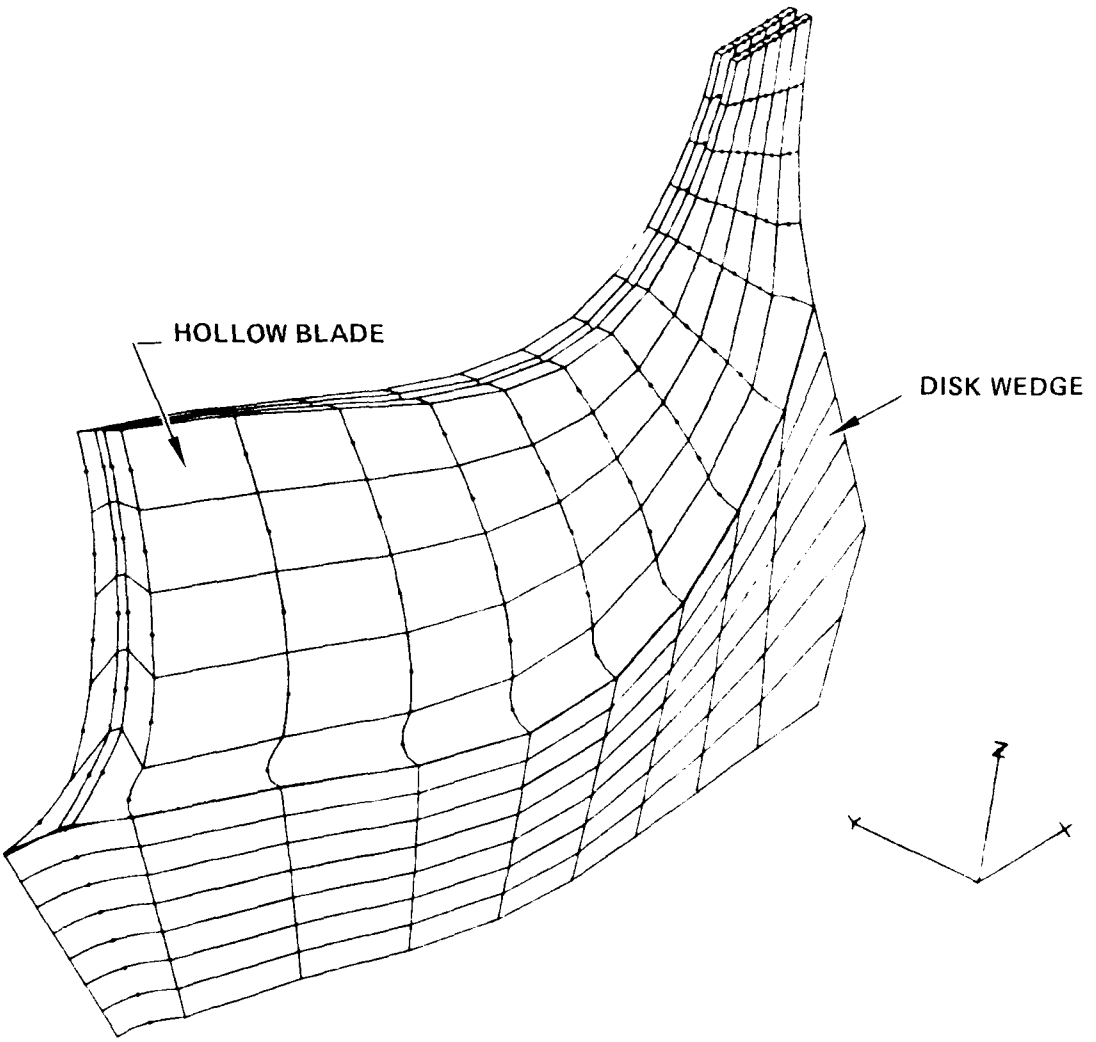

Figure 40. 3-D Finite-Element Model.

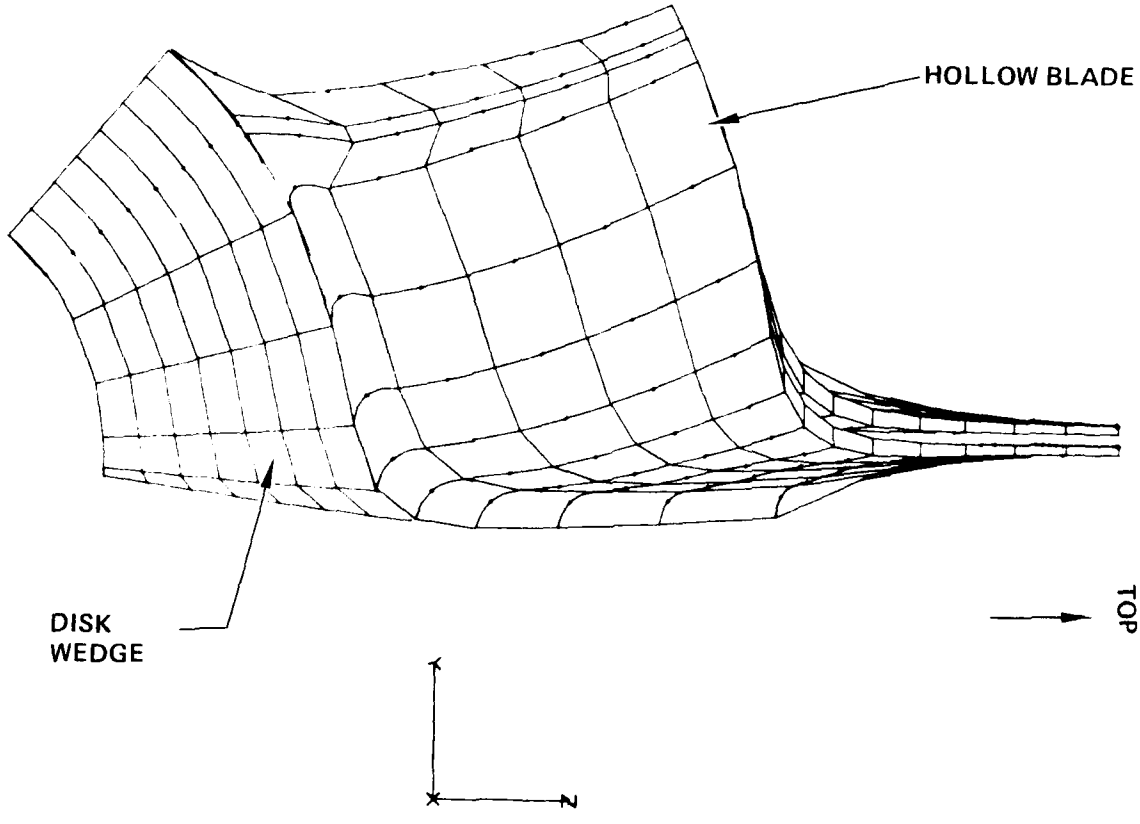

Figure 41. 3-D Finite-Element Model.

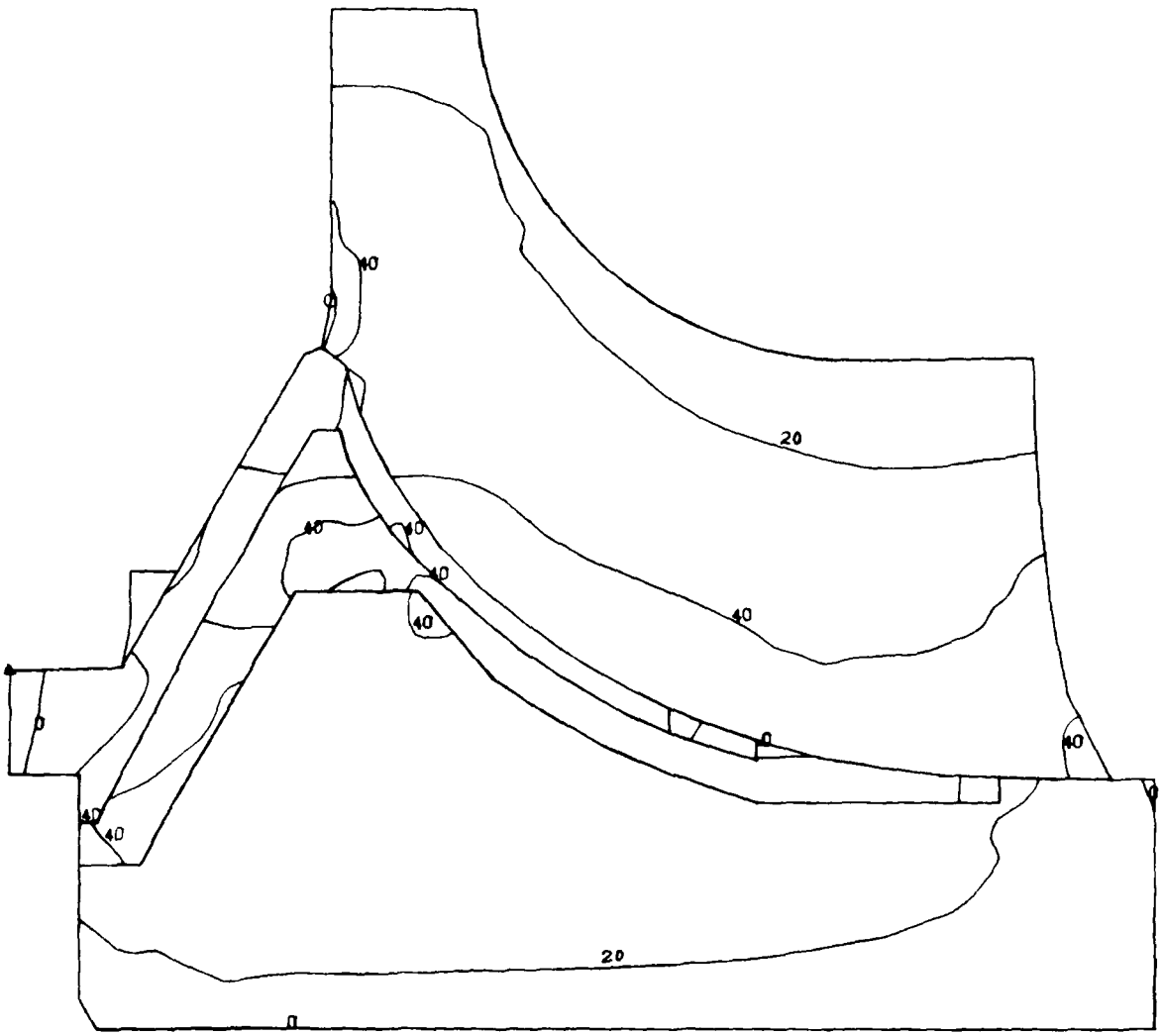

Figure 42. 2-D Radial Stresses (KSI) at 73,380 rpm and Room Temperature.

12
F

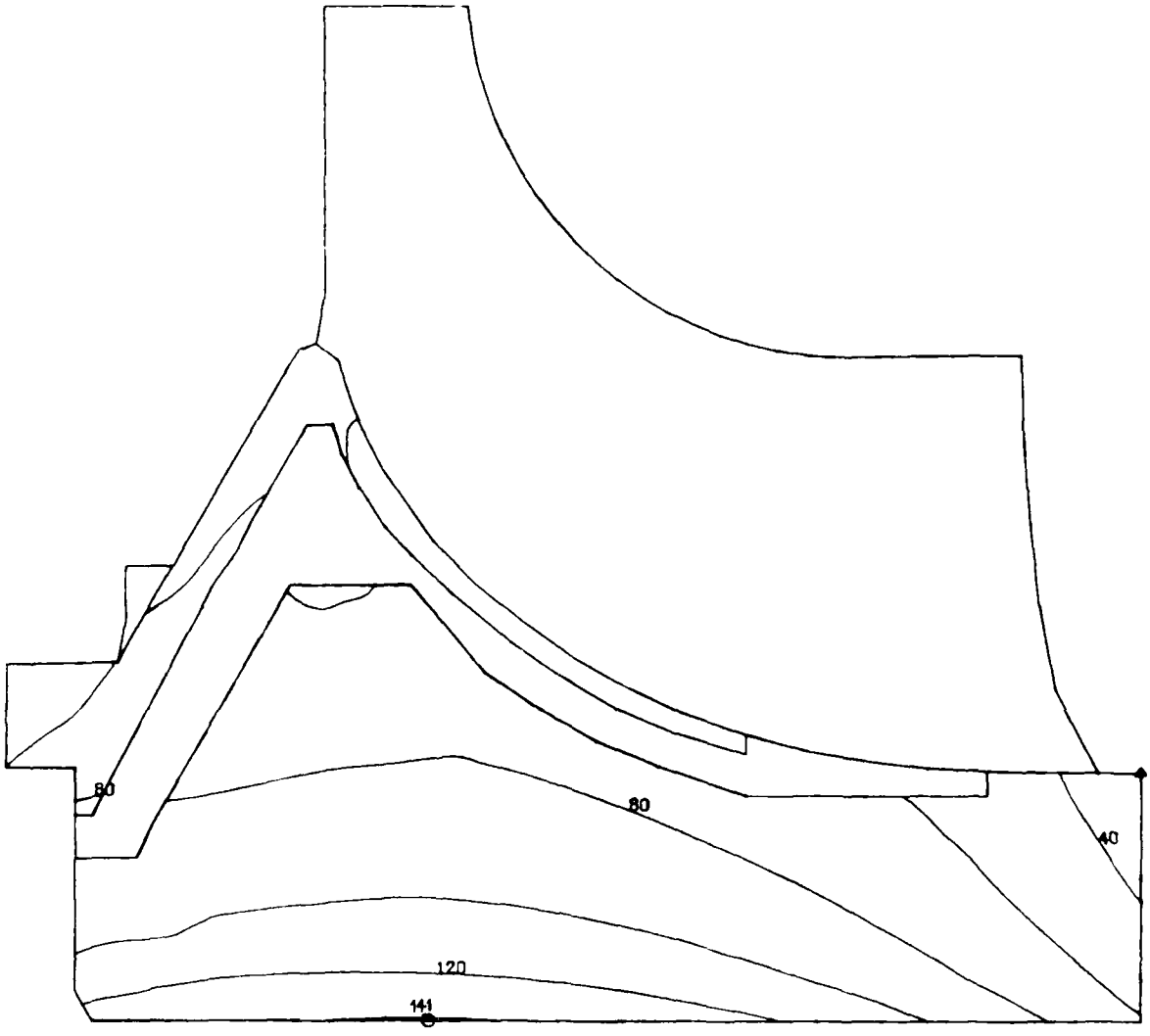

Figure 43. 2-D Tangential Stresses (KSI) at 73,380 rpm and Room Temperature.

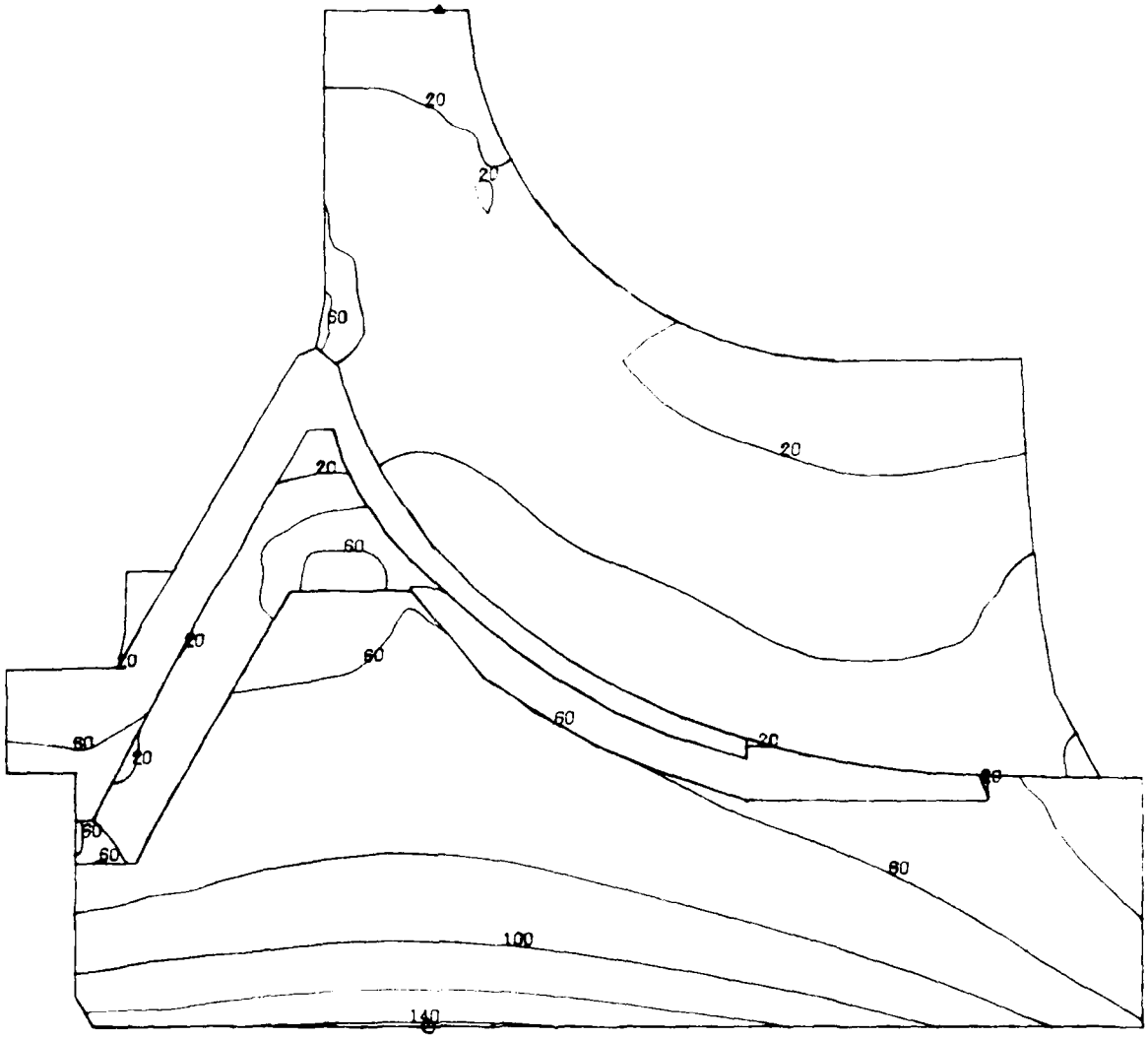

Figure 44. 2-D Equivalent Stresses (KSI) at 73,380 rpm and Room Temperature.

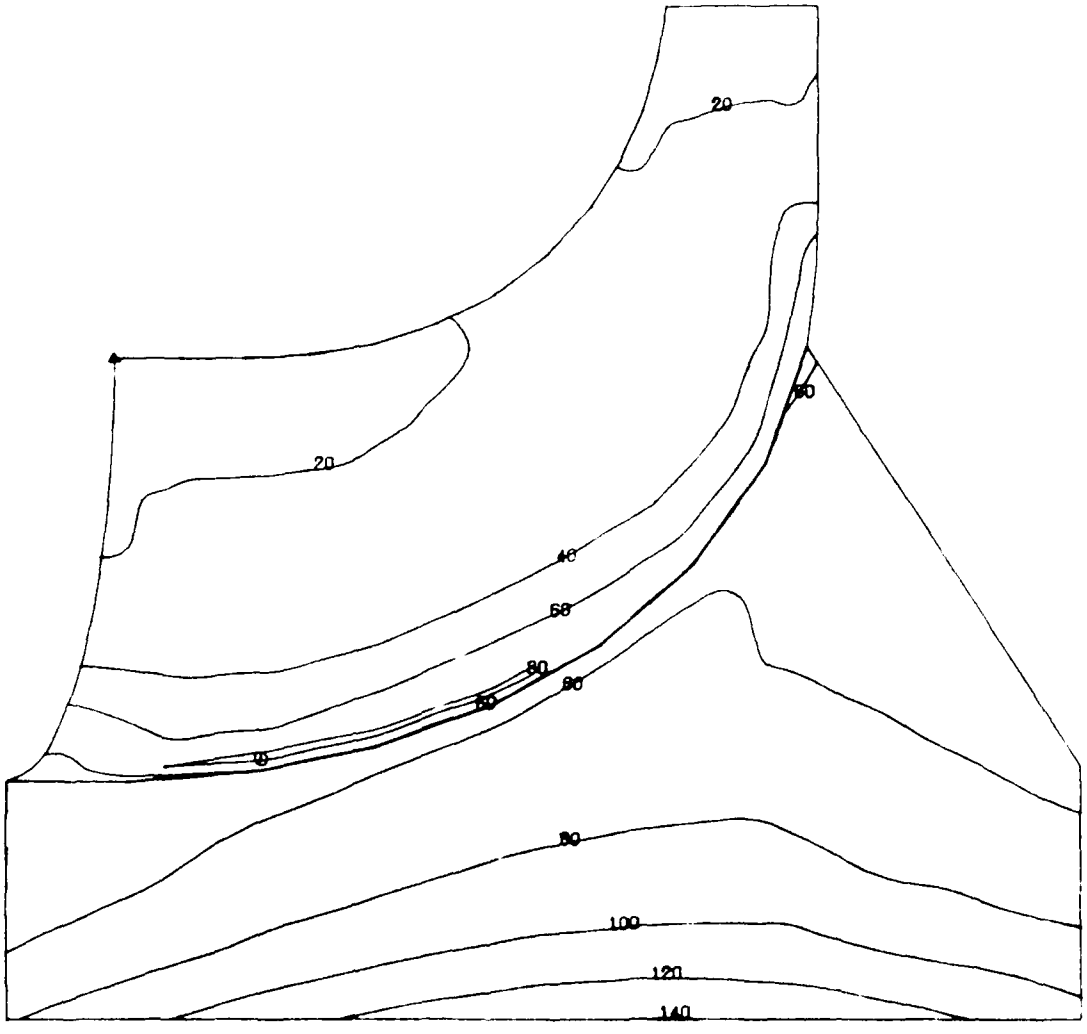

Figure 45. 3-D Equivalent Stresses (KSI) at 73,380 rpm and Room Temperature on Pressure Surface ot Blade with Corresponding Disk (View Rotated 180°).

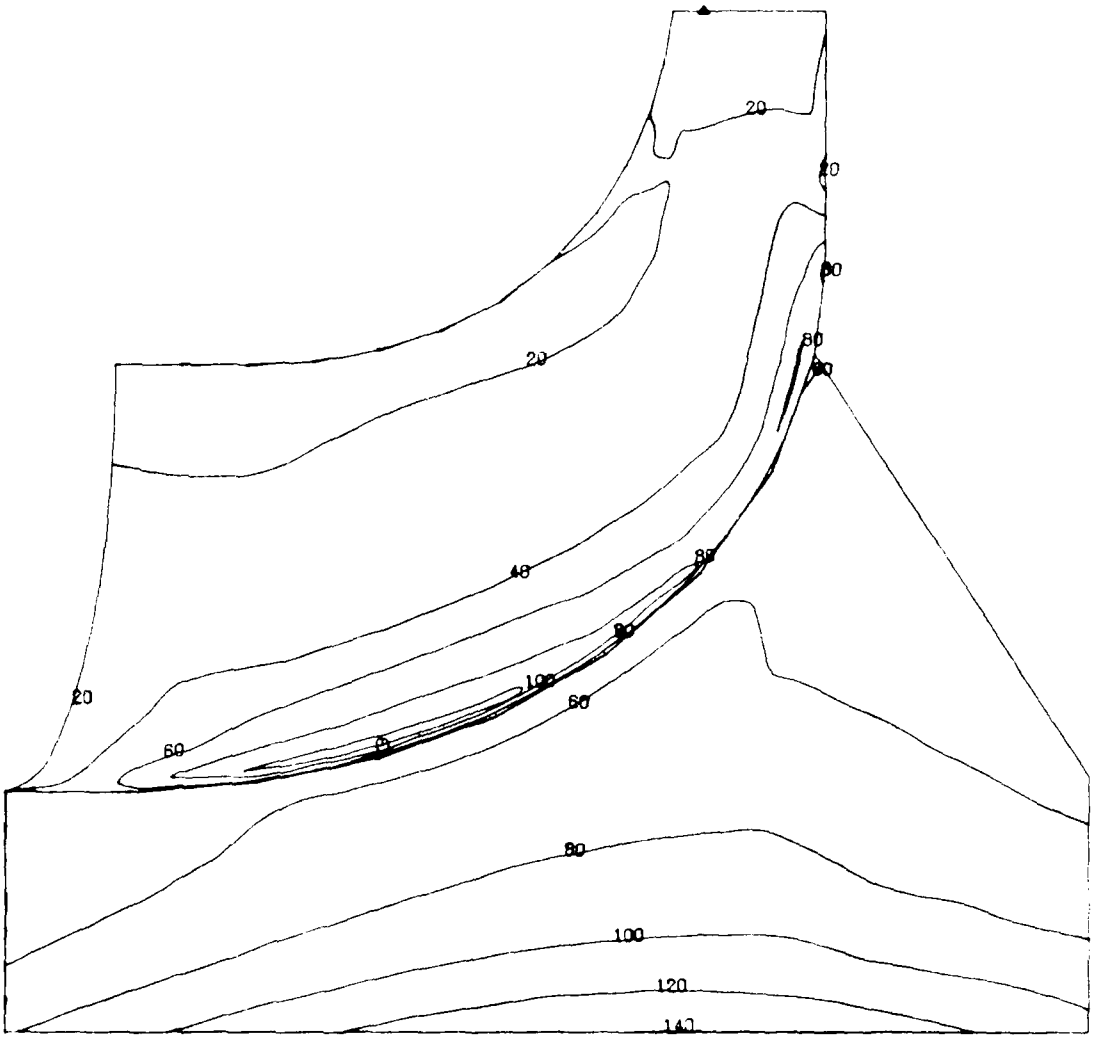

Figure 46. 3-D Equivalent Stresses (KSI) at 73,380 rpm and Room Temperature on Blade Suction Surface and Corresponding Disk (View Rotated 180°).

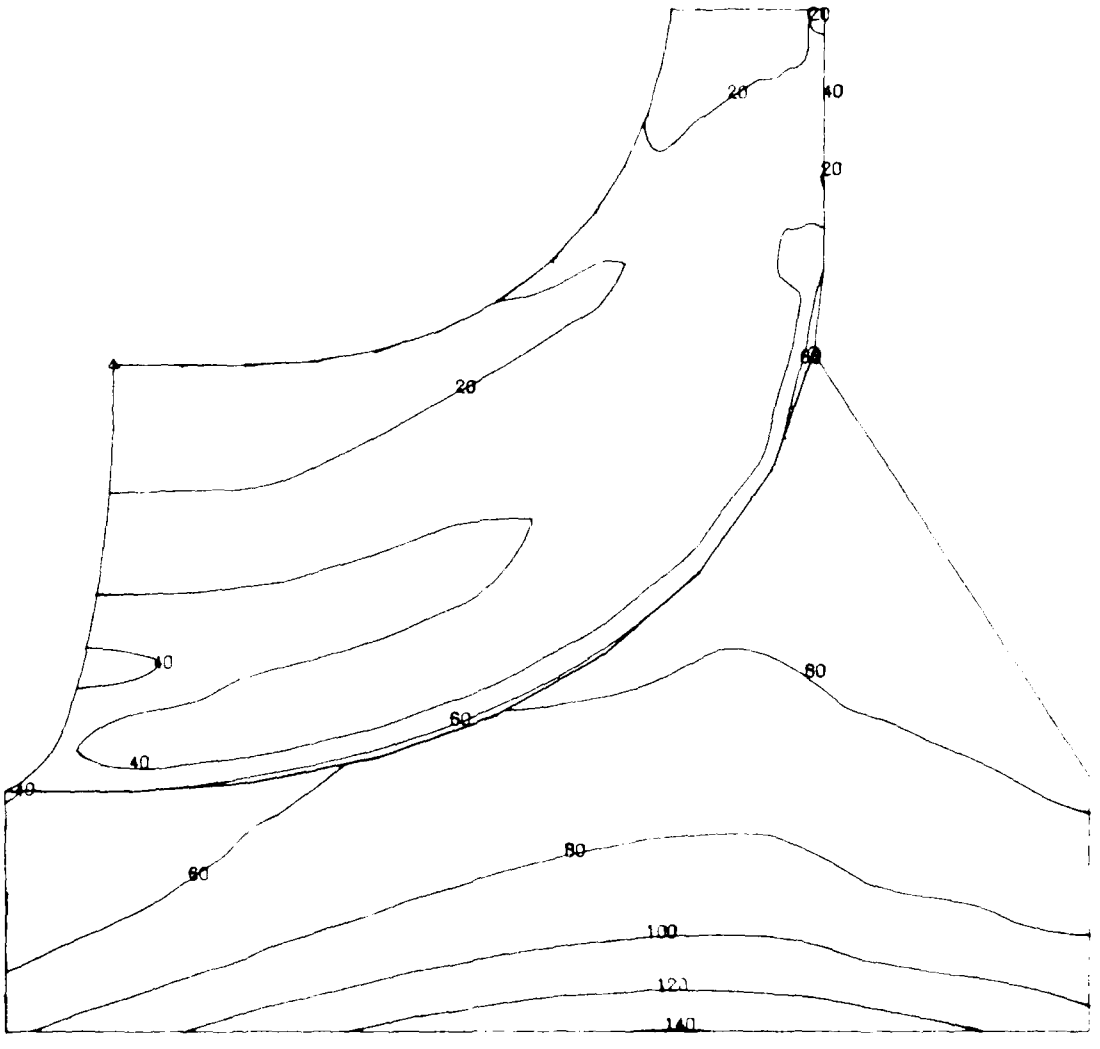

Figure 47. 3-D Equivalent Stresses (KSI) at 73,380 rpm and Room Temperature Inside Blade on Pressure-Side Cooling Passage Surface with Corresponding Disk (View Rotated 180°).

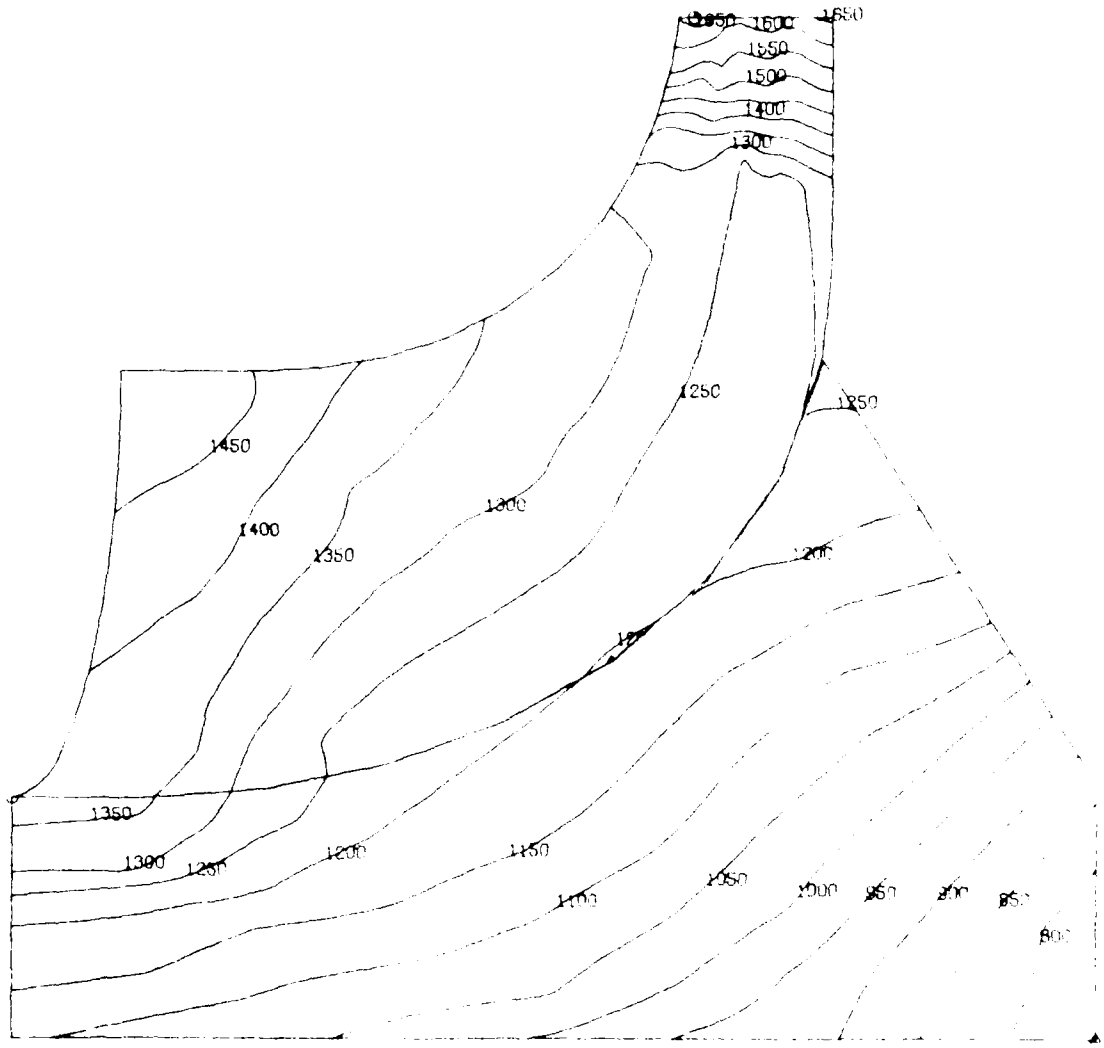

Figure 48. Blade Pressure Surface and Disk Temperatures Used in 3-D Thermal Stress Analysis (View Rotated 180°).

AD-A098 120 GHENT RIJKSUNIVERSITEIT (BELGIUM) LAB FOR EXPERIMENTA--ETC F/G 21/5
COOLED, LAMINATED RADIAL TURBINE DEMONSTRATION PROGRAM.(U)
FEB 81 R W VERSHURE, G D LARGE, L J MEYER DAAJ02-77-C-0032
UNCLASSIFIED 21-3684 USAAVRADCOM-TR-81-D-7 NL

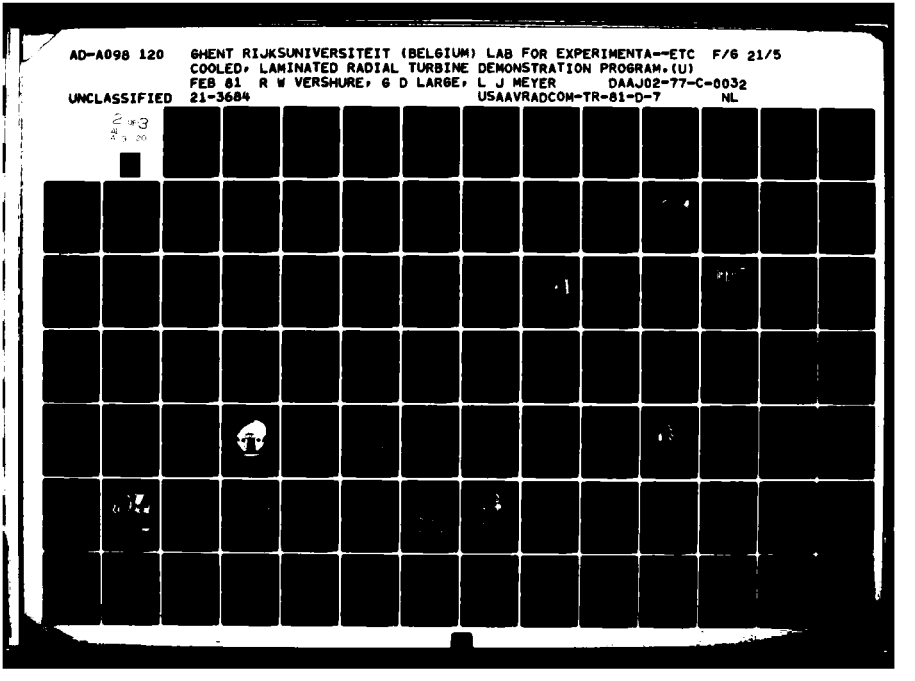

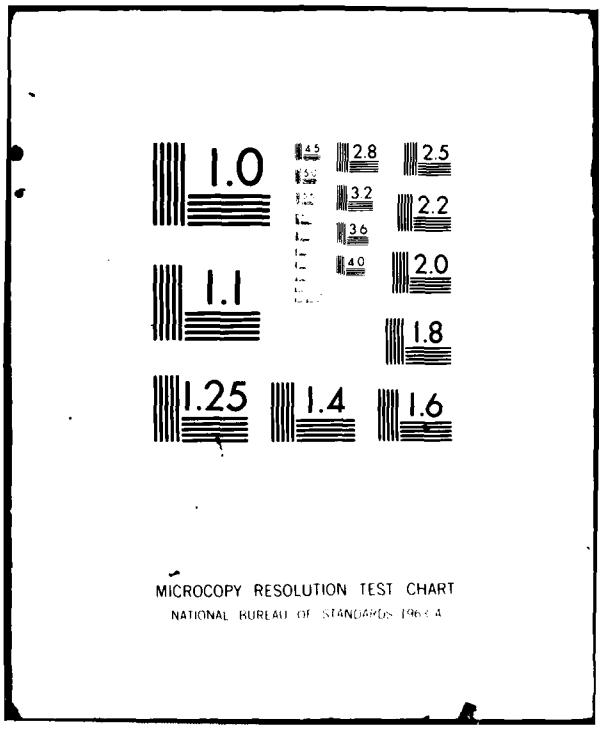
1.0
1.1
1.25
1.4
1.6
1.8
2.0
2.2
2.5
2.8
3.2
3.6
4.0
4.5
MICROCOPY RESOLUTION TEST CHART
NATIONAL BUREAU OF STANDARDS 1963-A

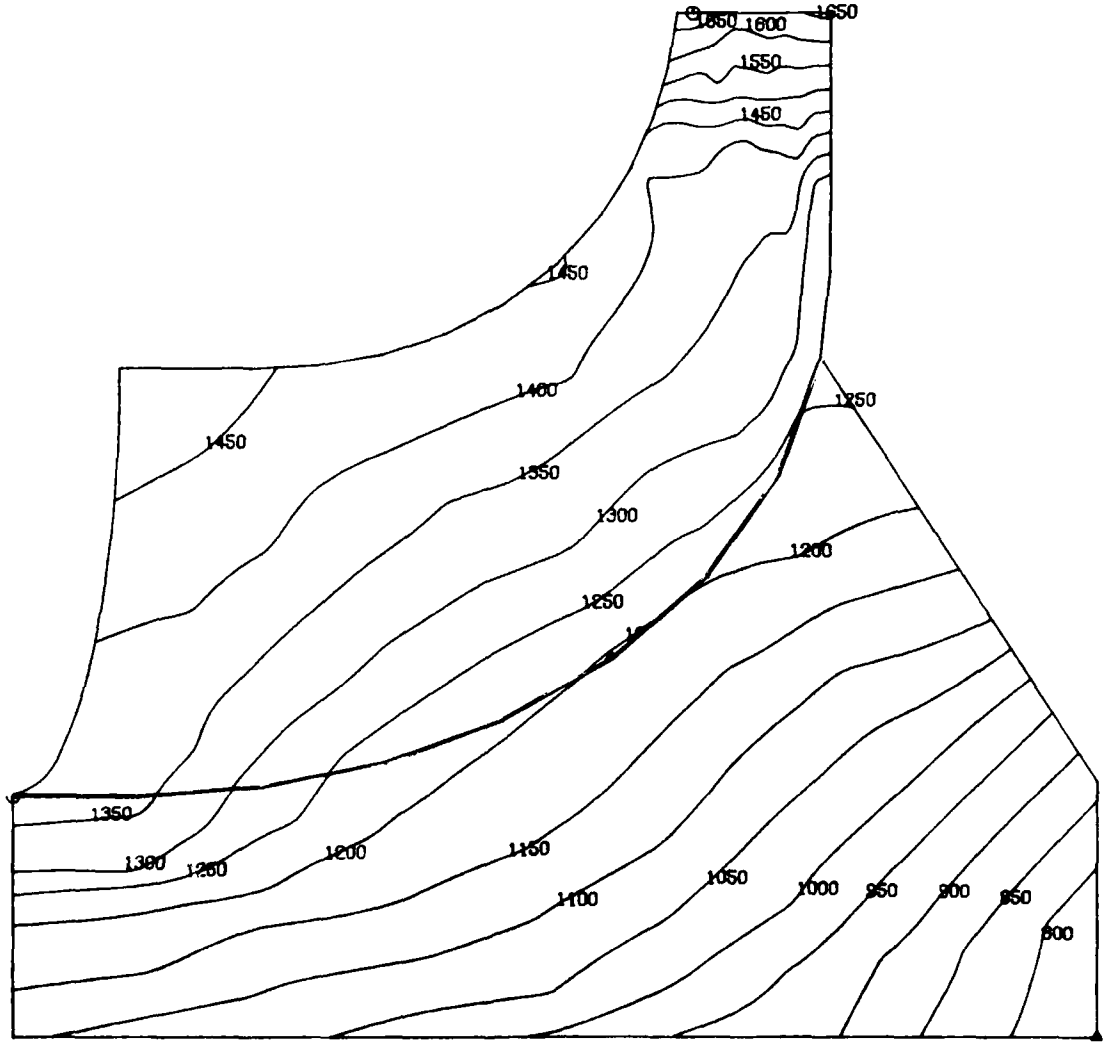

Figure 49. Blade Suction Surface and Disk Temperatures Used in 3-D Thermal Stress Analysis (View Rotated 180°).

for the combined effects of rotation and temperature are included in Figures 36 through 38, and the radial growths are illustrated in Figure 50. By including thermal effects, the maximum equivalent stress in the wheel increases from 140 ksi to 175 ksi. The location for this maximum stress is at the bore of the disk.

Results of Life Analysis

Stress Rupture

The wheel is required to achieve a stress-rupture life of 5000 hours for the following cycle:

Percent Speed	Percent Time
100	20
75	50
55	20
35	5
Idle	5

Standard AiResearch practice was used to predict the stress-rupture life of the wheel. Calculated blade metal temperatures were increased by 50°F to account for variations in operating temperatures, and the centrifugal steady-state stresses were increased by 20 percent to include blade-to-blade variations in geometry. The linear cumulative damage law was used to evaluate the stress-rupture damage for the different conditions in the table above.

Materials tests conducted for the Air Force Laminated Axial Turbine Wheel Program, Contract F33165-75-C-5211, have shown that stress-rupture properties in the plane of the laminates are nearly identical to stress-rupture properties for forged Astroloy. Therefore, the stress-rupture curve for forged Astroloy, Figure 51, was used in the analysis.

Using the approach outlined above, the blade stress-rupture life was calculated to be greater than 5000 hours everywhere in the blade except at one localized area at the interface between the blade and the disk (Figure 52). Because this region of low stress-rupture life is localized, the stresses will redistribute with time and a rupture problem will not be realized. This local region of high stress is probably caused by modeling inaccuracies in the 3-D finite-element model. To keep the model relatively simple in the disk, the stress results in this one local area are likely to be subject to calculation error.

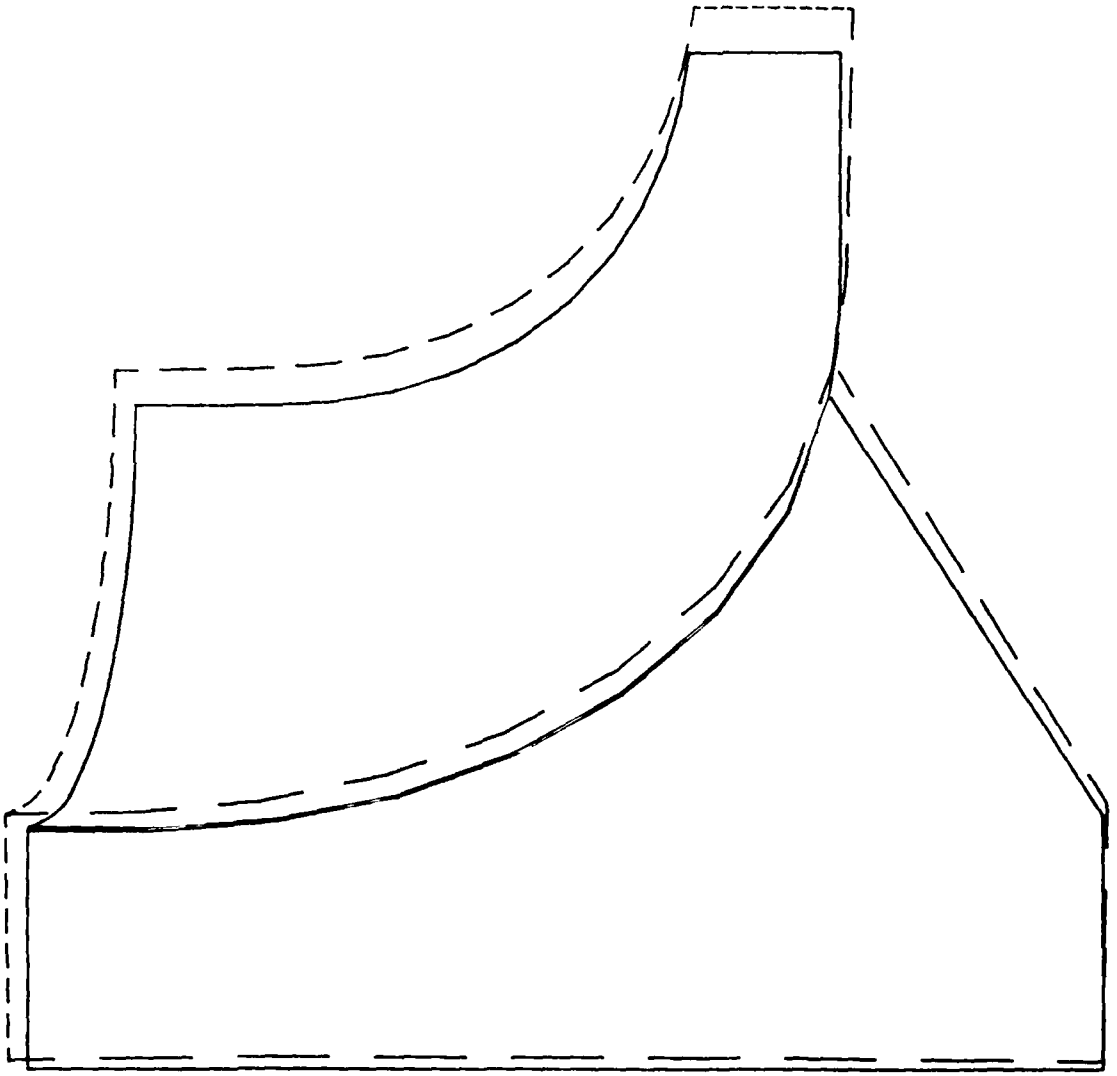

Figure 50. Radial Growth (inches) for Combined Effects of Rotation (77,380 rpm) and Temperature (View Rotated 180°). Deflection Scale: 1 inch = 0.12 inch of Deflection.

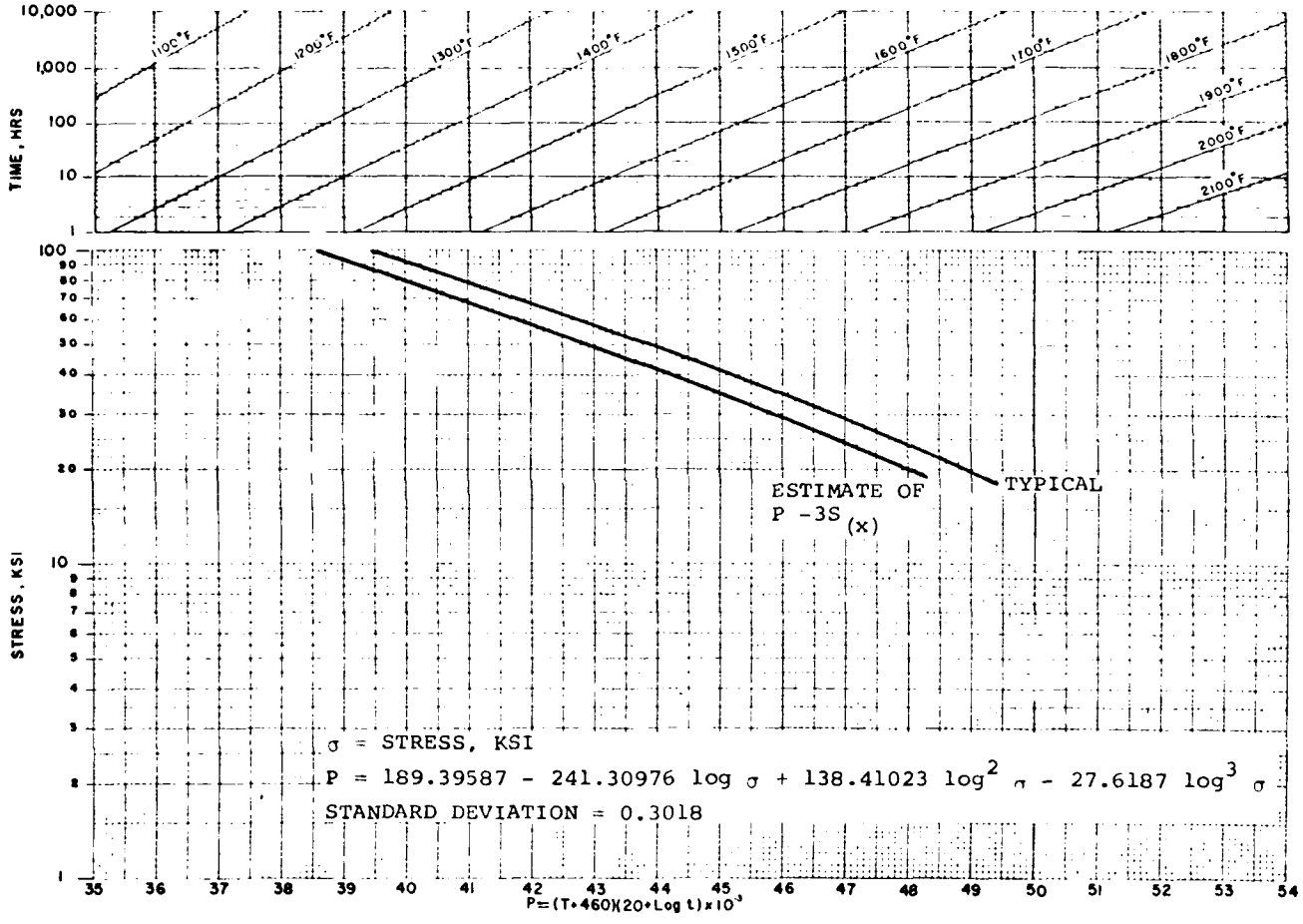

Figure 51. Typical Larson-Miller Stress-Rupture Curve for Astroloy Forgings.

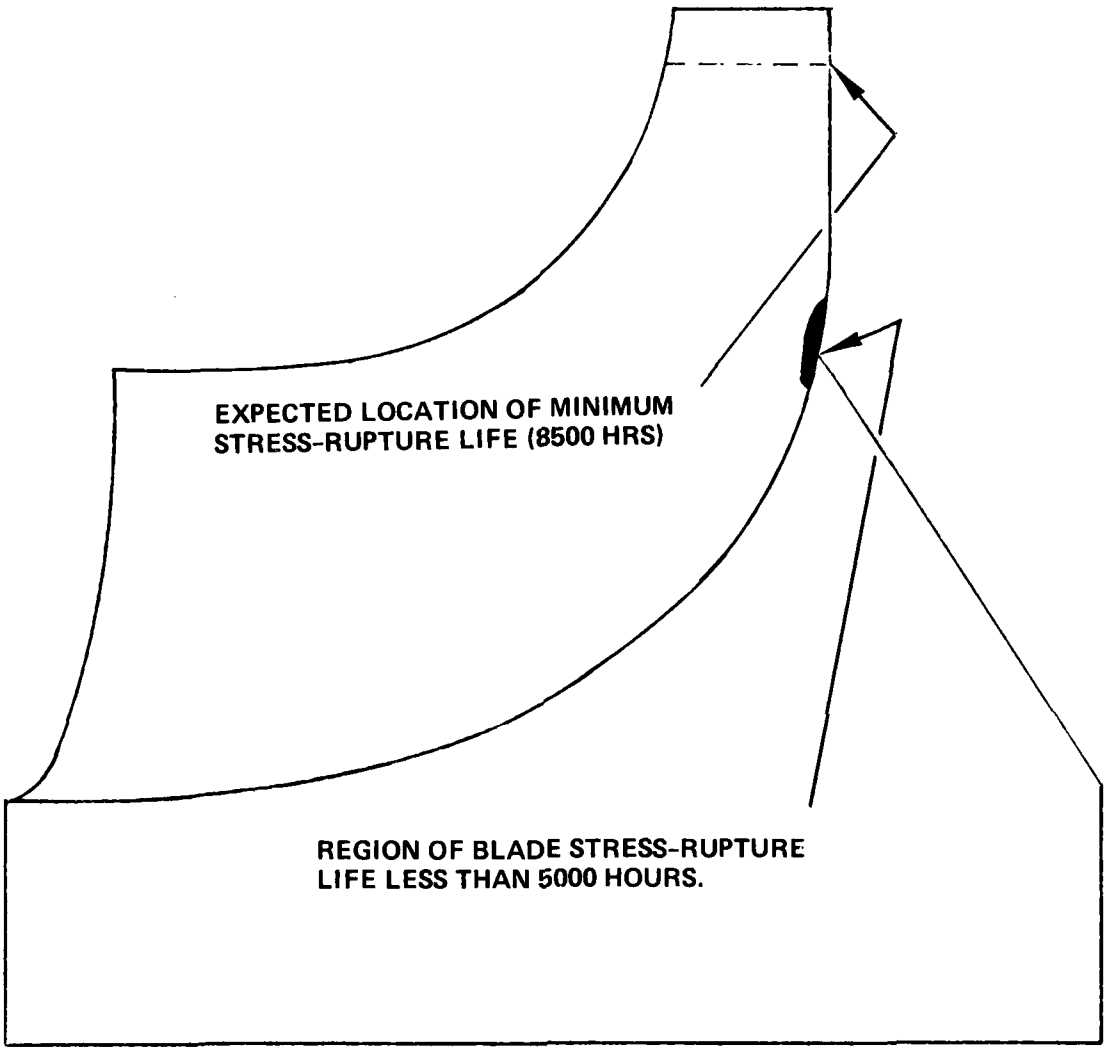

Figure 52. Local Region of Blade Stress-Rupture Life Less than 5,000 Hours at 73,380 rpm and Steady-State Operating Temperatures.

The minimum expected stress-rupture life of the blade is 8500 hours at a tip radius of 2.856 inches (Figure 52). This location is immediately below the solid tip section of the blade. All the significant stress-rupture life will be consumed at the 100-percent rated power condition. At the critical stress-rupture location in the wheel for the 75-percent rated power condition, the steady-state stress is decreased by 9 percent and the metal temperature is decreased by 110°F. This stress and temperature combination for the 75-percent rated power condition increases the stress-rupture life by more than an order of magnitude.

Low-Cycle-Fatigue Life

A rigorous low-cycle-fatigue life analysis requires calculated stress ranges from a transient thermal stress analysis. Such an analysis was not feasible for this wheel without knowing the environmental boundary conditions provided by a specific engine design. Therefore, the steady-state stresses for the combined effects of temperature differences and rotation were used to make low-cycle-fatigue life predictions. Because the maximum stress components, radial and tangential, are in the planes of the laminates, low-cycle-fatigue properties for forged Astroloy were utilized (Figures 53 and 54). By interpolating between these two material curves at the proper metal temperature, the minimum low-cycle-fatigue life was computed to be 7600 cycles at the bore of the wheel. This fatigue life exceeds the required life of 6000 cycles.

High-Cycle Fatigue

A blade vibration analysis using the 3-D finite-element program was completed at steady-state operating temperatures at 0 rpm and 73,380 rpm. The Campbell diagram, Figure 55, indicates that the fundamental frequency is between the fifth and sixtn engine orders. Experience on radial wheels at AiResearch has shown that blade vibration problems generally do not occur when the fundamental frequency is above the fourth engine order and no higher order natural frequencies correspond to the stator passing frequency. The stator passing frequency is not a concern at this time because a stator design can be chosen that will avoid interference with the lower modes and is beyond the scope of the current program.

Figures 54 through 58 illustrate the normalized deflections and equivalent stresses for the first three natural frequencies. The deflections are normalized to 10 inches and the stresses are normalized to 100 ksi.

Disk Creep

Time-dependent properties in the plane of the laminates have been shown to agree with the time-dependent properties for

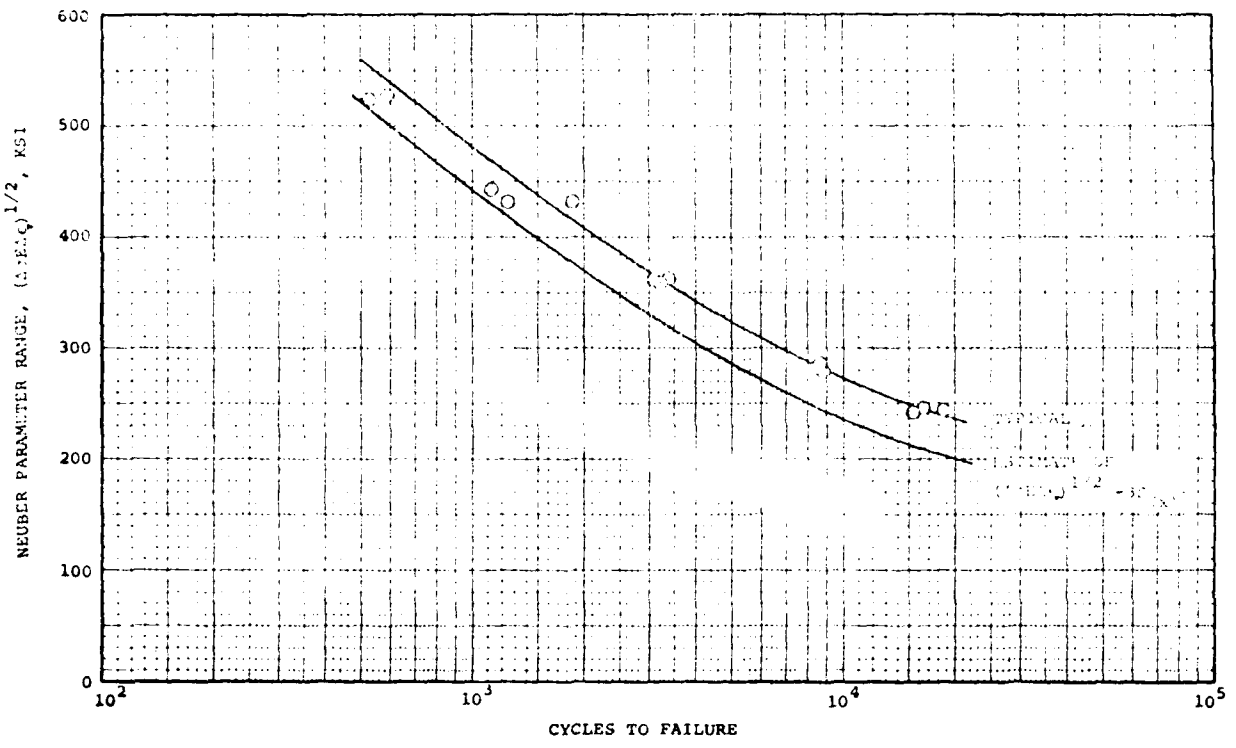

Figure 53. Typical Low-Cycle Fatigue of Astroloy Forgings at Room Temperature.

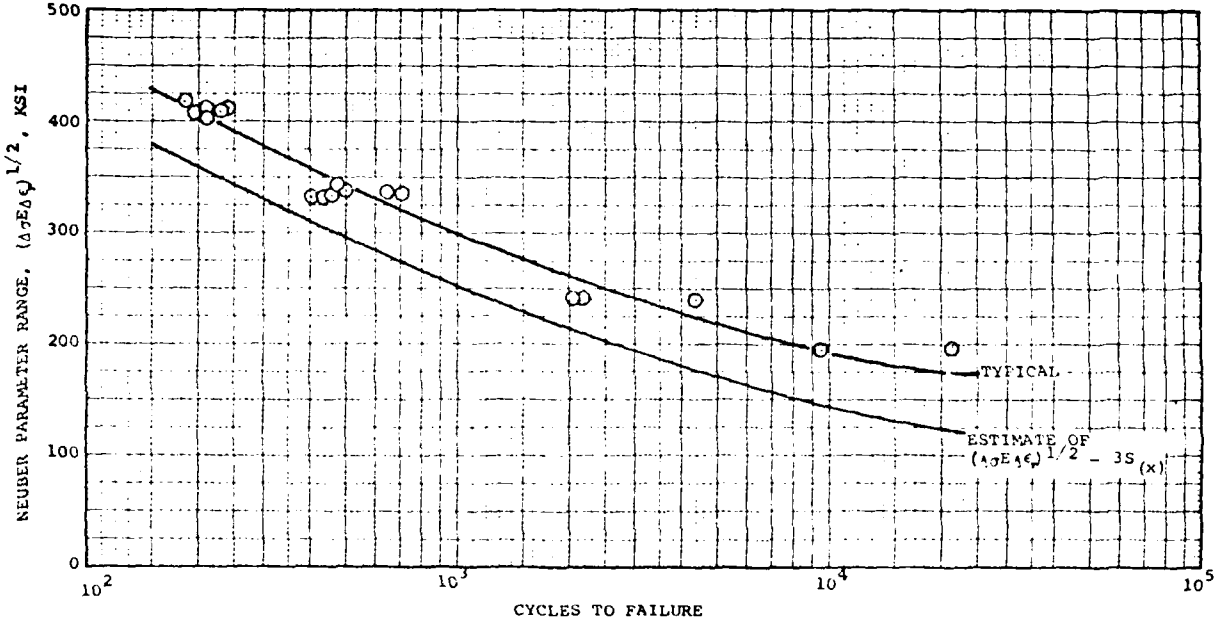

Figure 54. Typical Low-Cycle Fatigue of Astroloy Forgings at 1200°F.

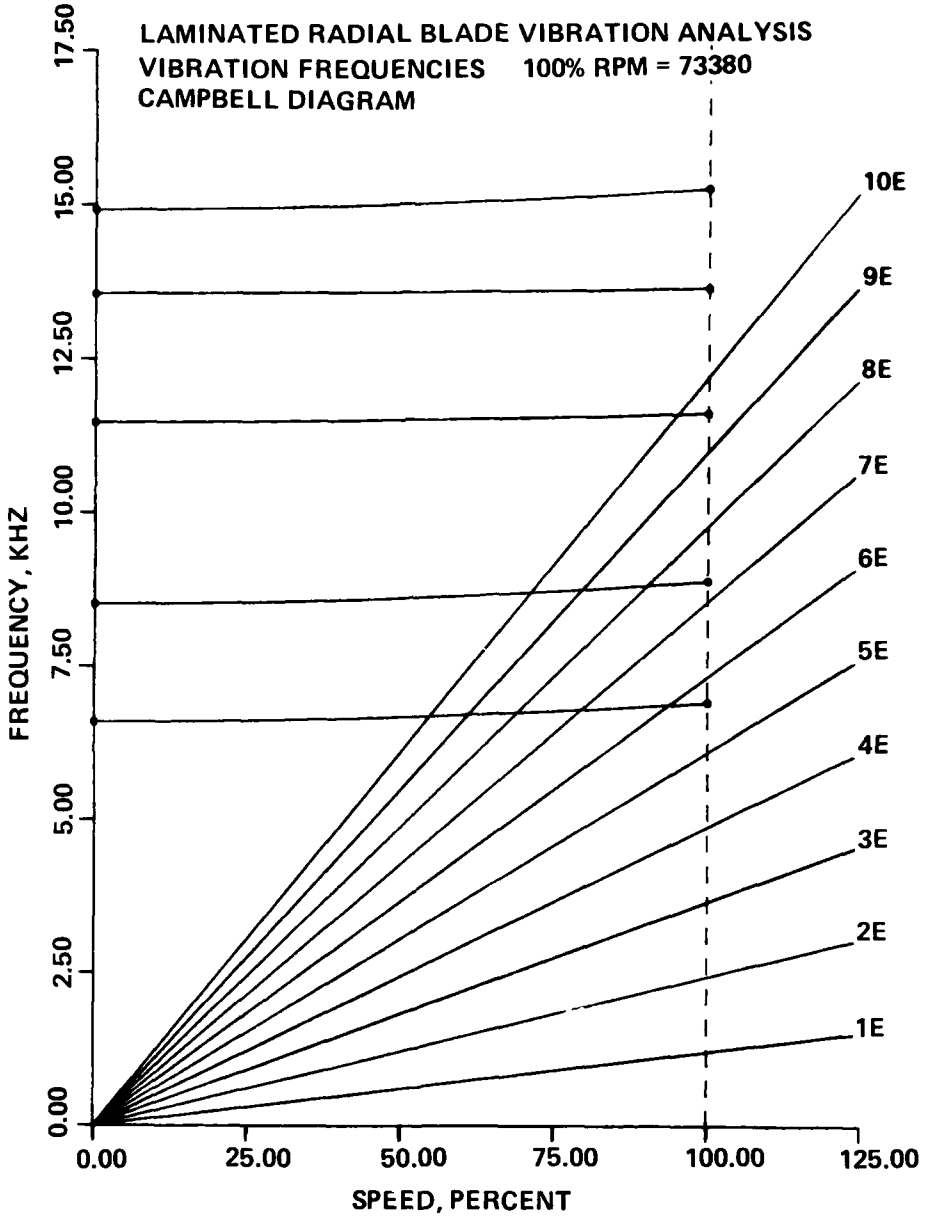

Figure 55. Campbell Diagram for First Five Natural Frequencies at Steady-State Operating Temperatures.

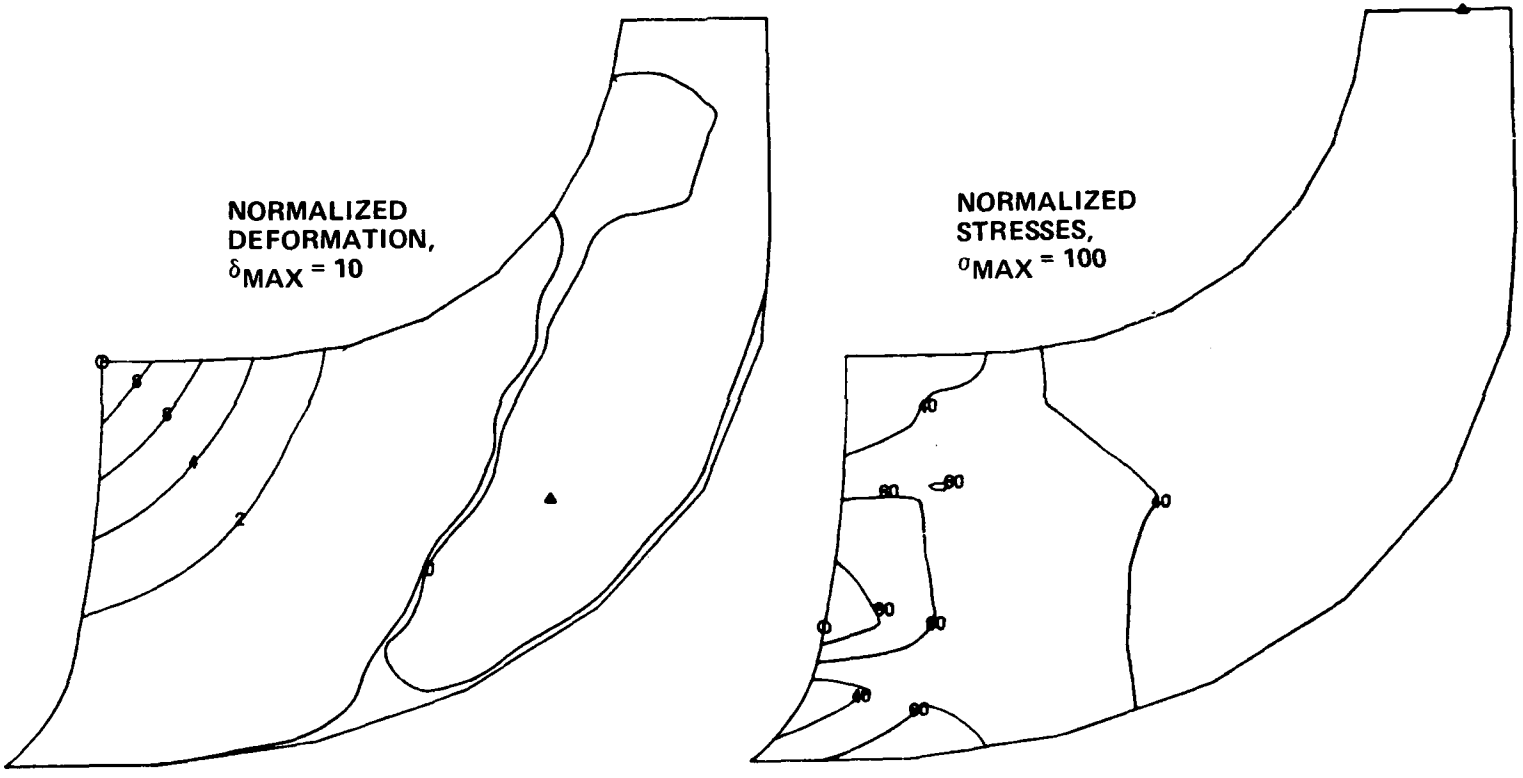

Figure 56. Normalized Deformations and Stresses for the Fundamental Blade Natural Frequency (6,916 Hz) at 73,380 rpm and Steady-State Operating Temperatures.

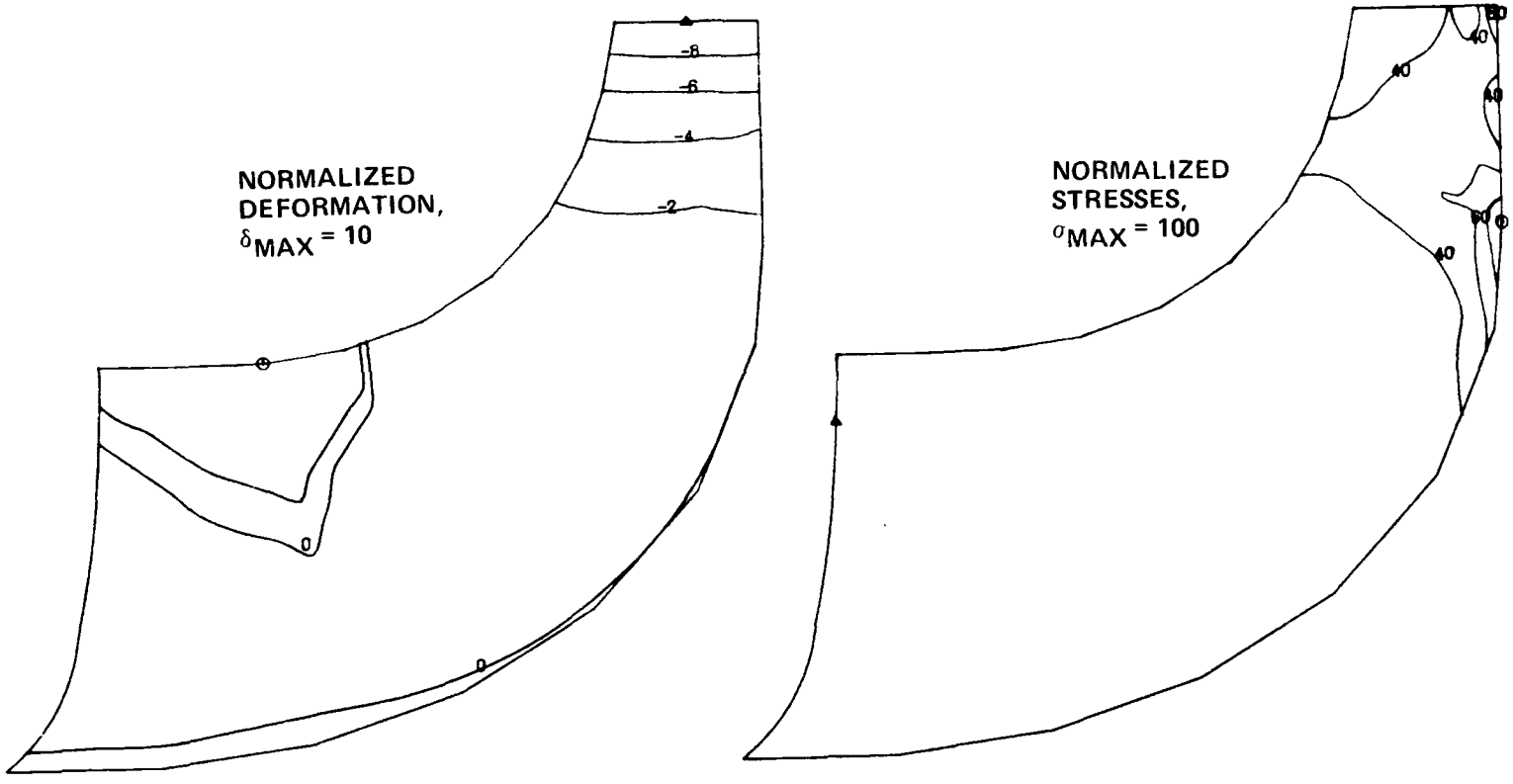

Figure 57. Normalized Deformations and Stresses for the Second Natural Blade Frequency (8,897 Hz) at 73,380 rpm and Steady-State Operating Temperatures.

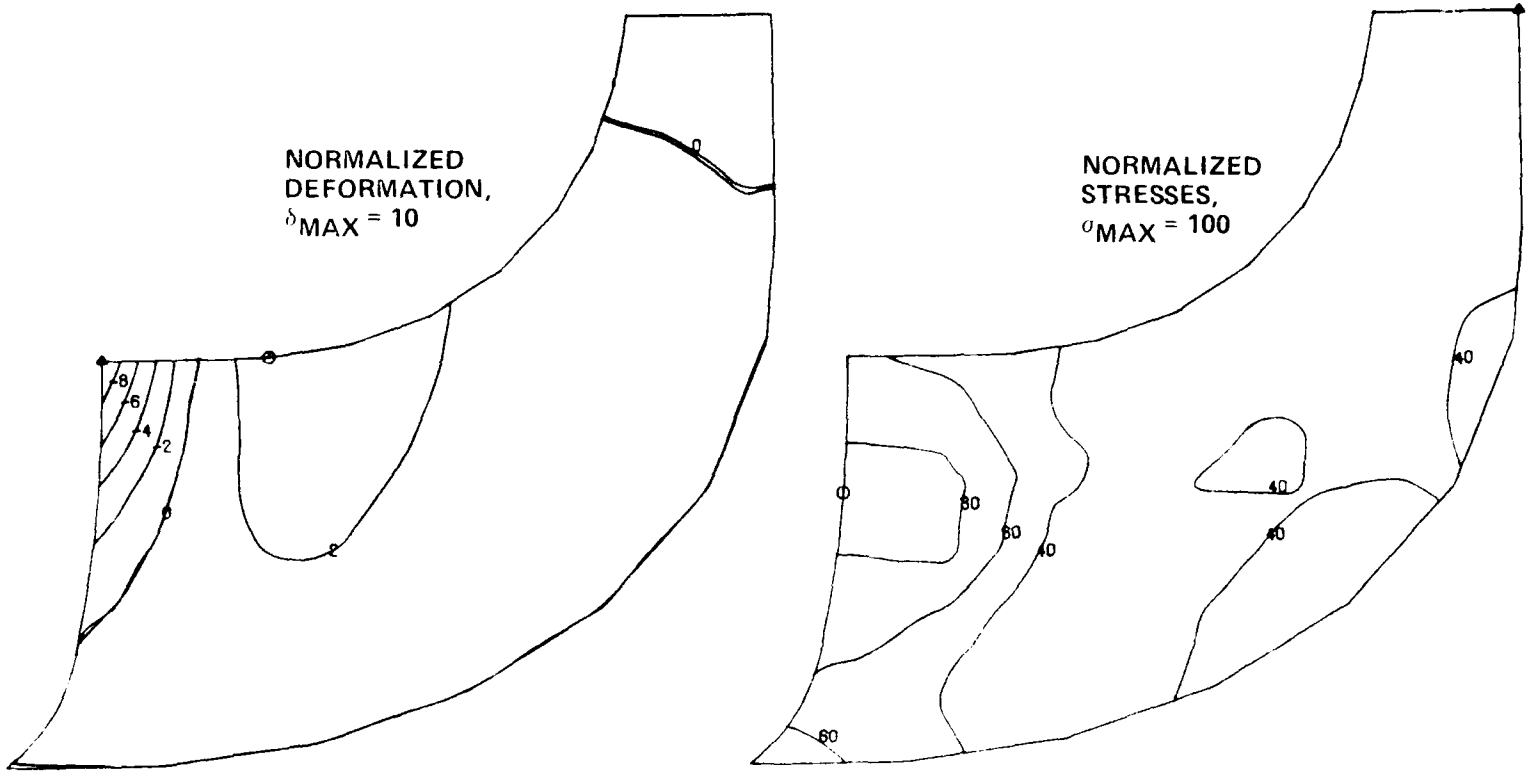

Figure 58. Normalized Deformations and Stresses for the Third Natural Blade Frequency (11,633 Hz) at 73,380 rpm and Steady-State Operating Temperatures.

forged Astroloy. Therefore, the creep properties for forged Astroloy, Figure 59, were used to evaluate the creep characteristics in the disk. Creep in the disk will not be a problem because only a small portion of the disk exceeds 0.1 percent creep during the 5000-hour design life, Figure 60.

Flaw Tolerance (NDE Critical)

The only defects that are envisioned for this manufacturing process are those that lie in the bond joint region. These can be voids, etch pits, carbides, lack of fusion, etc. In all cases the "weak" direction is presumed to be in a radial plane normal to the axis of rotation. Fortunately the stresses in the direction tending to propagate these flaws (axial stresses) are generally quite small. This can be seen in Figure 61.

Subcritical crack propagation data is not available for the bonded Astroloy laminates. However, the transverse crack growth rate (along a bond joint) is expected to be somewhat lower than for forged Astroloy, which has excellent subcritical crack growth resistance and fracture toughness. Even so, the critical crack size is expected to be large enough that brittle fracture from centrifugal and/or steady-state thermal stresses in the disk or blades does not appear to be a problem.

The propagation of flaws in the blades from high-frequency vibratory stresses coupled with low-frequency transient thermal stresses appears to be the prime failure mode of concern. Assessment of the absolute level of vibratory stresses is not practical without obtaining strain-gauge amplitudes in an actual engine environment. Transient thermal stress analysis is also not feasible without having engine environmental boundary conditions for a specific design. Cavity temperature and pressure variations with time during accels and decels need to be accurately defined in order to obtain reasonable thermal stress ranges.

Another consideration is the possible loss of cooling flow from a large number of "through the thickness" flaws connecting the cooling passages with the outer walls of the blades. Although the width of a flaw or void between laminates is expected to be on the order of 0.0005 inch or less, a large number of these in any one blade cooling passage could result in a significant loss of cooling flow, which must be made up by the compressor and results in a loss to the cycle efficiency. To prevent this from being excessive, it is proposed that no more than 5 percent of total flow area for all blades be allowed based on the summation of the maximum dimension of all flows multiplied by 0.0005 inch. Since flow area varies considerably from pass to pass and within each pass, an estimate must be made for each scan based on radial, circumferential, and axial position of each flaw. In addition, it is proposed that no more than

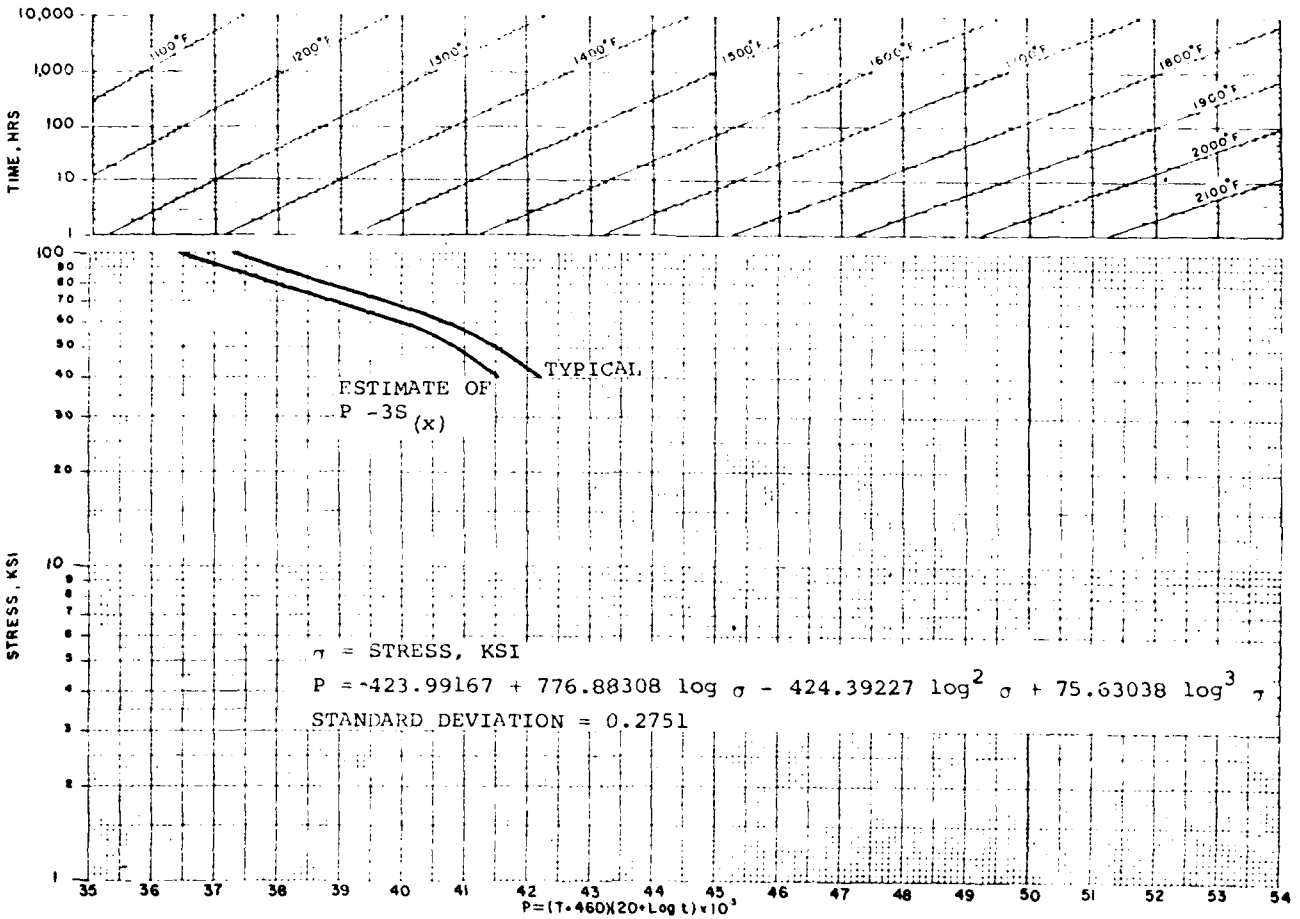

Figure 59. Typical 0.1 Percent Larson-Miller Creep Curve for Astroloy Forgings.

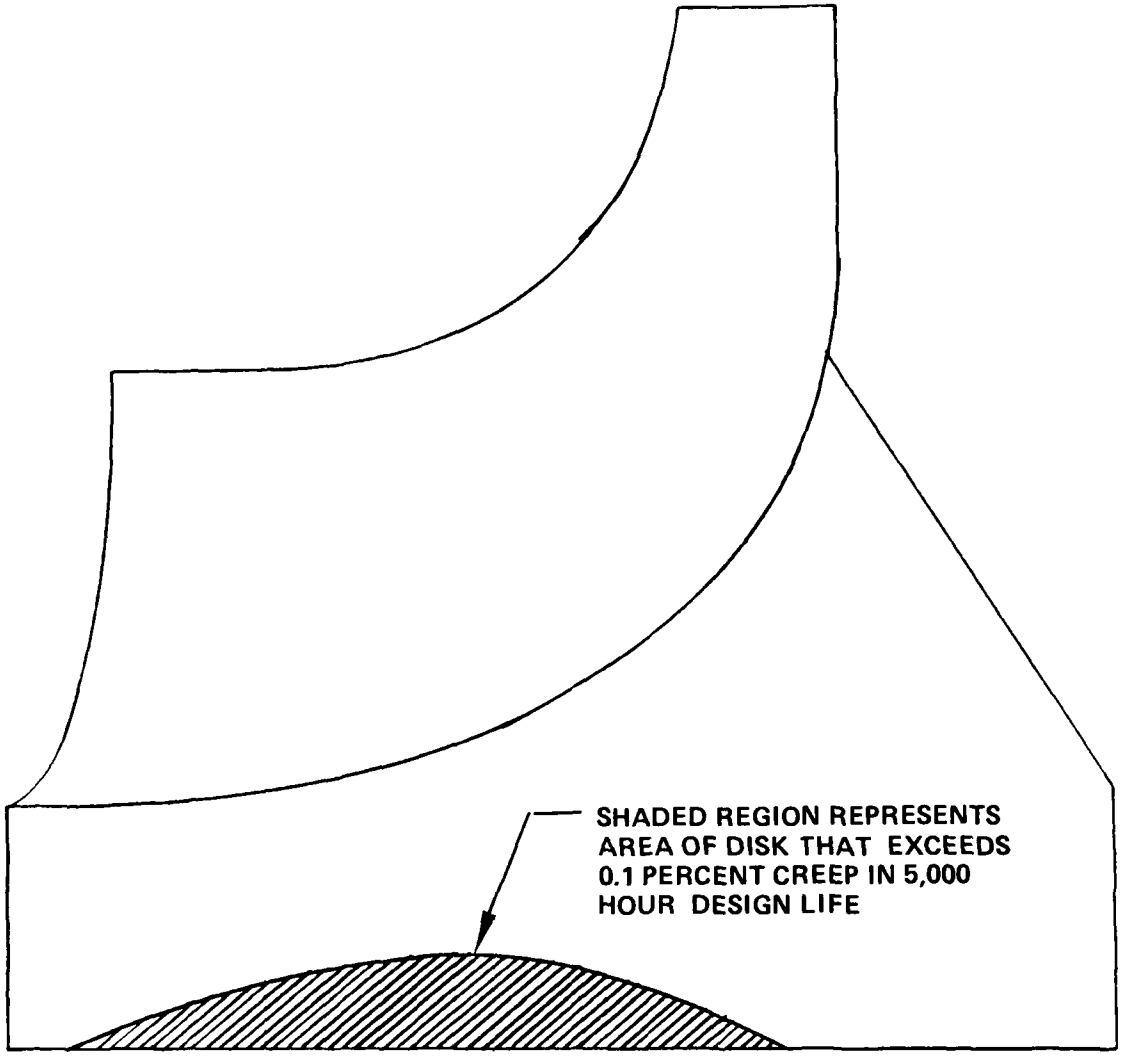

Figure 60. Region of Disk that Exceeds 0.1 Percent Creep at 73,380 rpm and Steady-State Operating Temperatures for the 5,000-Hour Design Life.

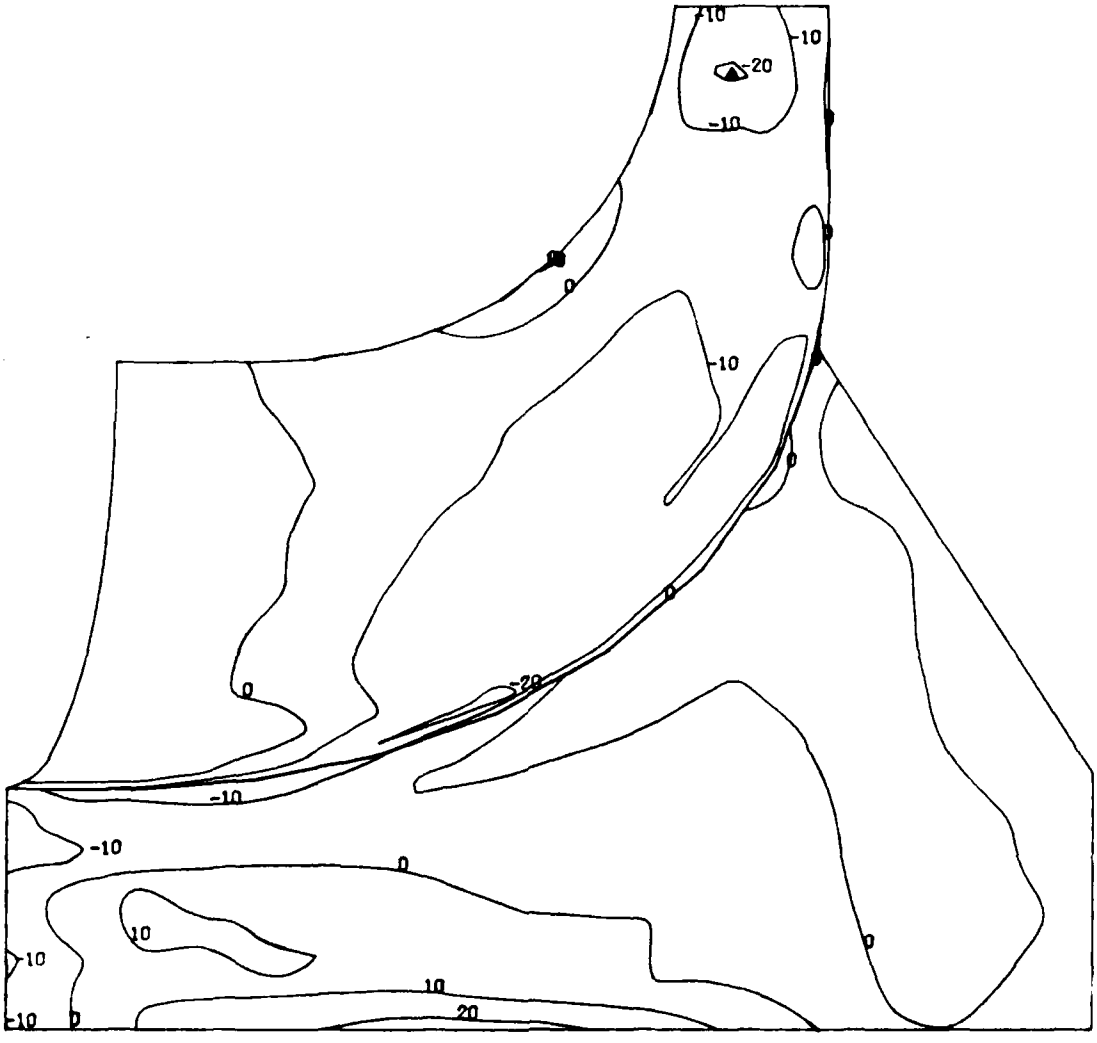

Figure 61. Typical Axial Stresses at 73,380 rpm and Steady-State Operating Temperatures.

20 percent of the total flow area in any one blade be allowed on the same basis.

To prevent any single flaw from becoming excessively large, arbitrary sizes of 0.100 inch maximum in the blade region and 0.200 inch maximum in the disk region have been tentatively selected until subcritical crack propagation data is obtained on compact tension specimens of bonded Astroloy laminates in the transverse direction.

No two flaws in the same joint or in adjacent joints should be closer to each other than 200 percent of their maximum dimension in the radial direction. Any flaw below 0.015 inch in maximum dimension will be considered uninterpretable. It is recognized that the true axial location of some flaws will be difficult to evaluate until after final machining; therefore, acceptance may depend on fluorescent, dye penetrant or radiographic inspection of the fully machined part. Individual laminates (prior to bonding) will be rejected if etch pits occur within 0.020 inch of any blade cooling passage or within 300 percent of their maximum dimension to the disk bore or other machined surface.

Conclusions and Recommendations

Based on the calculations for burst margin, blade stress rupture, low- and high-cycle fatigue, creep, and flaw growth, the final wheel configuration that meets all the design objectives is judged to be an acceptable design. In some areas these calculations are based on rather limited material properties for laminated structures.

Once a specific application for this wheel is realized and environmental boundary conditions can be obtained, a transient thermal stress analysis should be completed to better evaluate the low-cycle-fatigue life of the wheel. If low-cycle-fatigue life is a problem at the disk bore, the diameter of the bore would have to be reduced to lower the bore stresses.

Before this wheel is operated in an actual engine environment, natural frequencies should be verified experimentally by means of salt pattern or holography testing. Because the 3-D analysis cannot completely simulate the ties between the two surfaces of the blade, some inaccuracies are to be expected in the vibration analysis, especially for the higher order modes. The high-cycle-fatigue life of the blade could be severely limited if one of the lower natural frequencies corresponds to the stator passing frequency at or near the design speed. This can be avoided by careful selection of the stator count and stator-blade spacing.

Design changes to the wheel might be required if the burst factor for the wheel is determined to be less than 0.85 for test wheel No. 1, which will be used for growth and burst testing. Reduction of the bore diameter would be the recommended modification.

PHOTOCHEMICAL MACHINING TOOLING DESIGN

The design of a cooled turbine rotor from 0.020-inch laminate sheets required close attention to the approach used in making the photochemical machining tooling. As seen from the cross section of the radial turbine rotor shown on sheet 2 of Figure 62, there are 92 different photochemically machined laminates in the rotor assembly. Therefore, 92 discrete PCM tools were required to manufacture the laminates. To maintain dimensional control over the blade wall thickness, accurate PCM tooling was required to accurately position the cooling passages within the blades and to provide precise tooling pickup points for the final machining operations.

The PCM tooling design experience gained on the axial laminated turbine program (USAFAPL Contract F33615-74-C-2034) indicated the most stable PCM tooling is registered glass rather than Mylar film. This tooling is designed especially for precise chemical milling of metal parts that require etching on both sides and where resolution and registration are critical. As shown in Figure 63, two masters made from 0.190-inch, precision, photographic, glass plates are registered exactly, emulsion to emulsion, and hinged together for insertion of the sheet to be etched. Unlike registered Mylar films, the two glass plates will not shift and the exposure of the photoresist-coated metal will be consistent. Also, the precision flatness of the plate will maintain the close dimensional tolerances required on the line widths. A constant line width of 0.018 inch was chosen for all the features to be etched in the laminates. Using a constant line width ensured a constant etching rate from both sides of the part. Furthermore, the final dimensional inspection becomes the 3/8-inch-diameter center hole on each laminate, which is final inspected to a tolerance of ±0.001 inch with a go/no-go gauge.

This glass tooling was manufactured at Precision Art Coordinators Inc. (PAC), Providence, R.I. This vendor has extensive experience manufacturing this type of tooling for the photochemical machining industry and for the electronic industry in the manufacture of precision circuit boards. The precision artwork is generated using a computer-controlled photosystem with digital inputs on X-Y coordinates, which are provided. The design methodology used at AiResearch to define the coordinates for the cooling passages is currently to draw a 10 to 1 size Z section for each laminate, as shown in Figure 64, sheets 1 through 5. In the future at AiResearch, it will be possible to design the cooling passages on an interactive computer-graphics

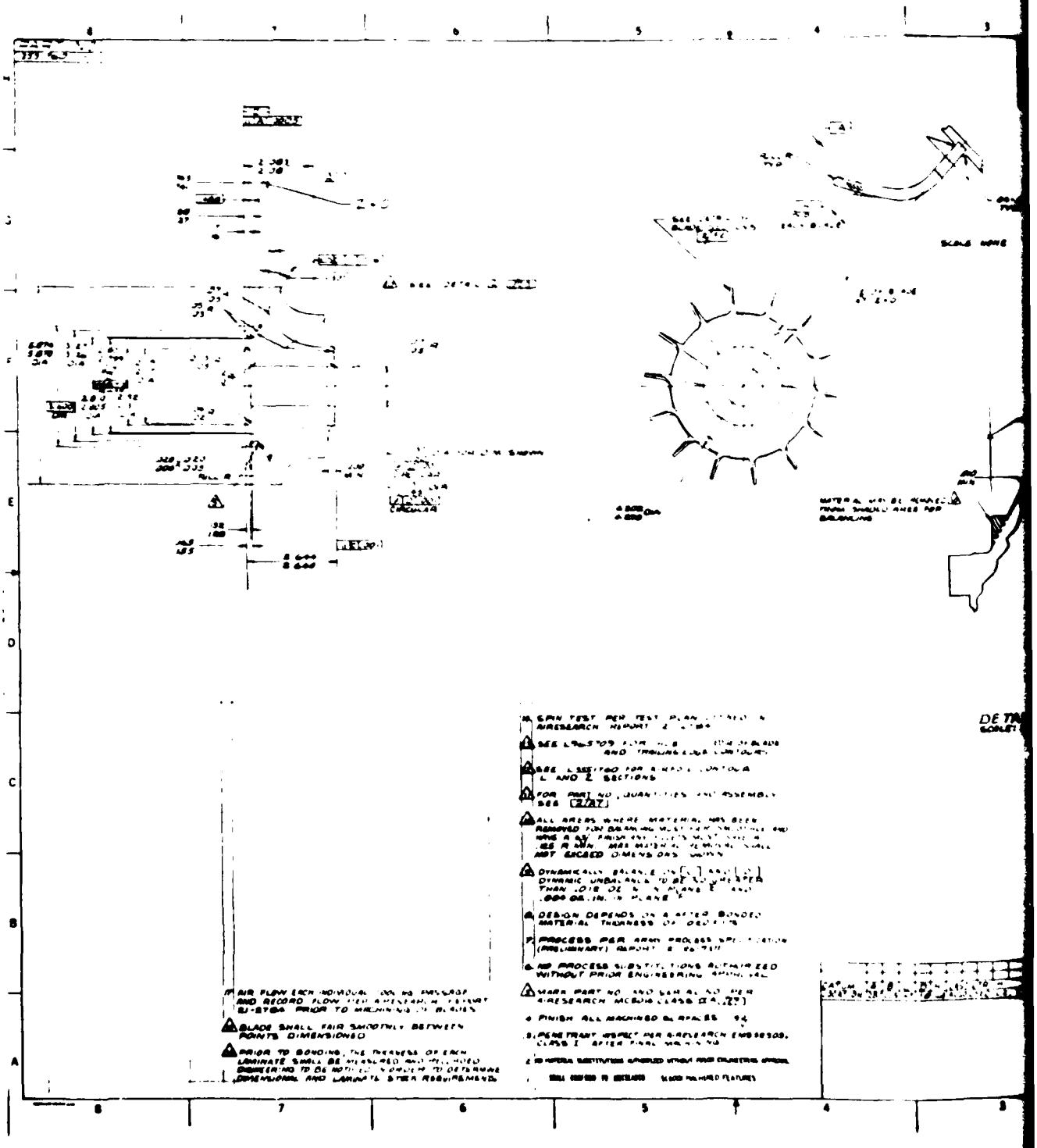

Figure 62. Wheel, Laminated Radial Turbine.

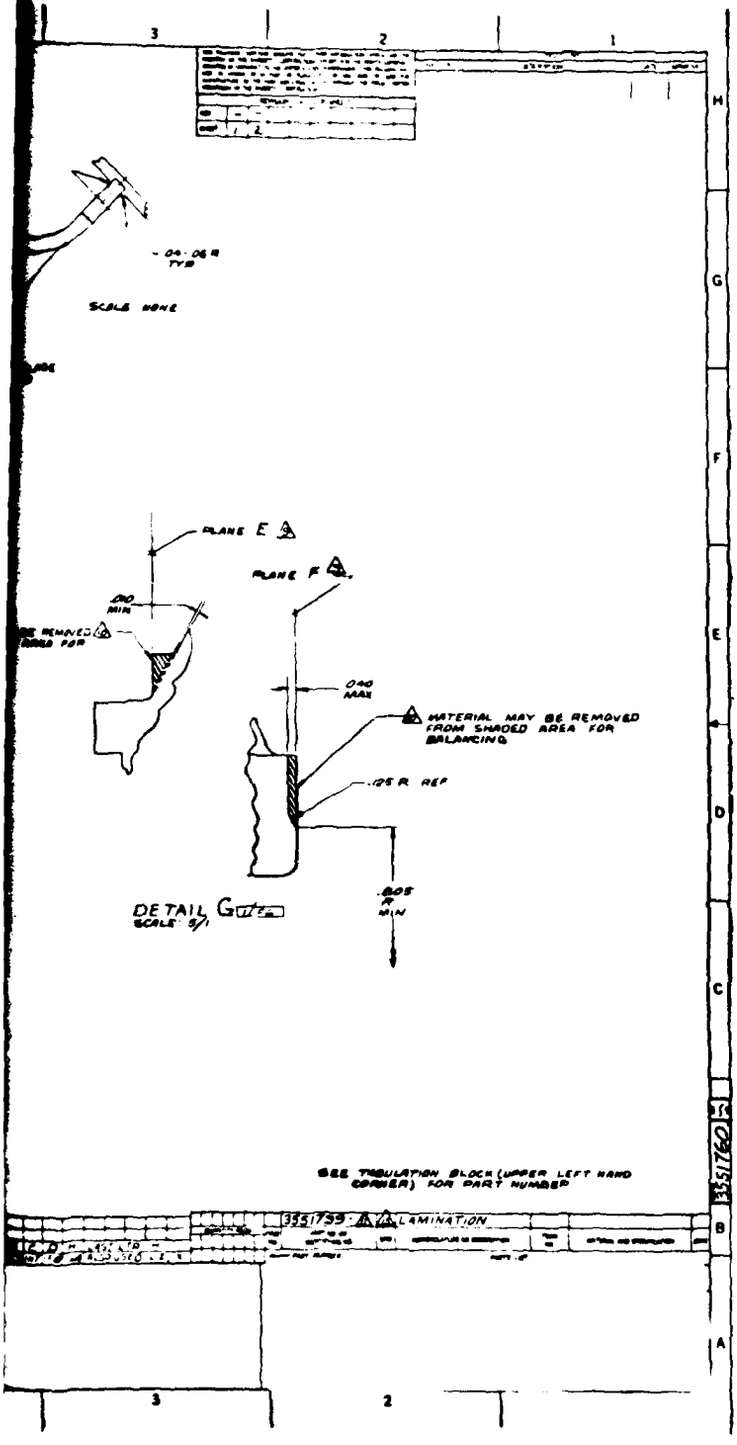
3
2
1
H
G
F
E
D
C
B
A
SCALE NONE
PLANE E
PLANE F
.040 MAX
MATERIAL MAY BE REMOVED FROM SHADED AREA FOR BALANCING
.125 R. REF
.805 R MIN
DETAIL G
SCALE 5/1
SEE TABULATION BLOCK (UPPER LEFT HAND CORNER) FOR PART NUMBER
3551739
LAMINATION
3551760

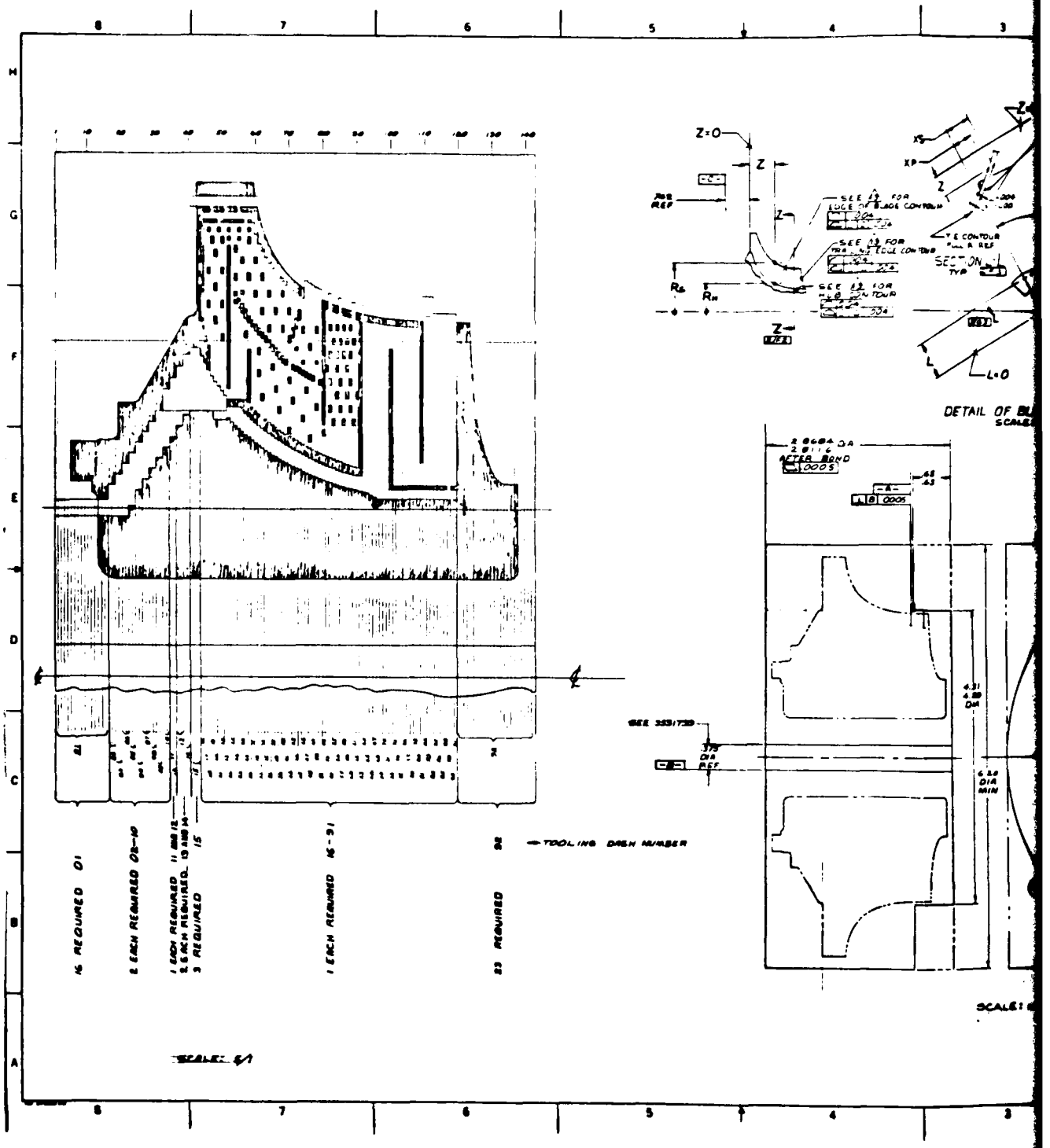

Figure 62. Continued.

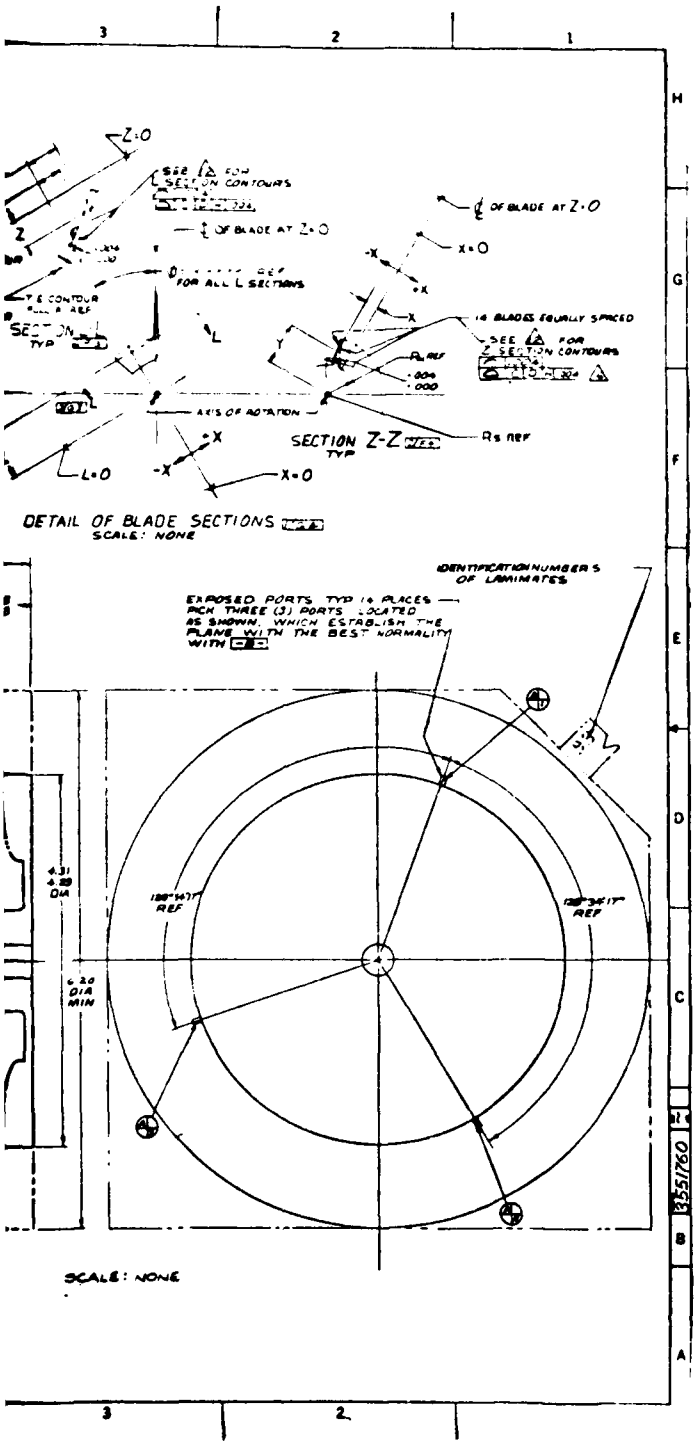
Z-0
SEE FOR SECTION CONTOURS
℄ OF BLADE AT Z-0
℄ OF BLADE AT Z-0
X-0
-X
+X
X
16 BLADES EQUALLY SPACED
SEE FOR Z SECTION CONTOURS
SECTION TYP
SECTION Z-Z
Rs REF
L-0
-X
X-0
AXIS OF ROTATION
DETAIL OF BLADE SECTIONS
SCALE: NONE
IDENTIFICATION NUMBERS OF LAMINATES
EXPOSED PORTS TYP 16 PLACES — PICK THREE (3) PORTS LOCATED AS SHOWN, WHICH ESTABLISH THE PLANE WITH THE BEST NORMALITY WITH
4.31
4.30
DIA
6.20
DIA
MIN
REF
REF
SCALE: NONE
3551760

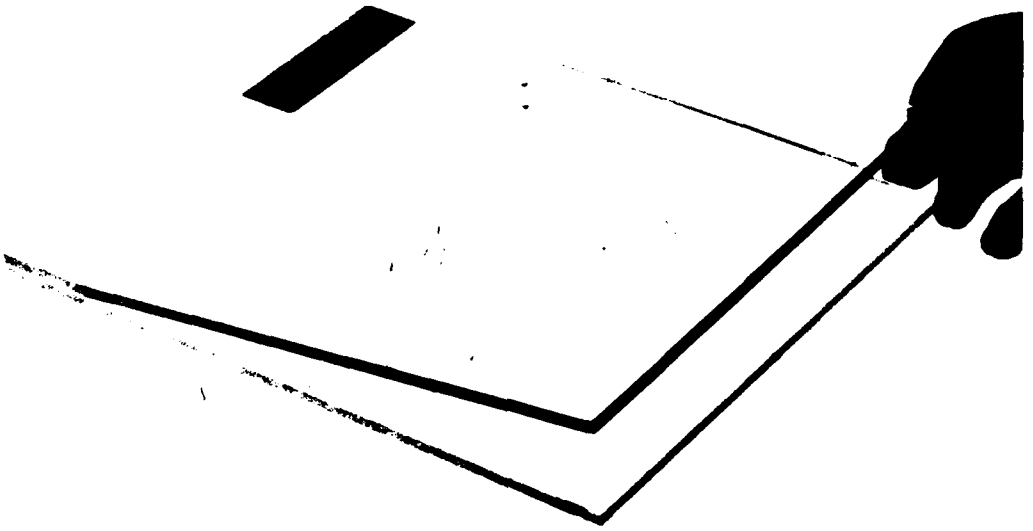

17
F

Figure 63. Two Glass Master Plates.

system and therefore interface directly with the PAC computer-controlled photosystem by transmitting the coordinates onto magnetic tape. This future method has several major advantages, including a large reduction of manual drafting and the ability to rapidly change or modify the PCM tooling in an ongoing development effort where fast turnaround of complex hardware is desired.

Sheet 2 of Figure 62 shows the envelope drawing for the bond tooling. Note that the sheet is square (6 1/4 by 6 1/4 inches). This size optimizes the tooling to the small rotor and minimizes the sheet scrap from the rolling mill. Also, the square configuration was desired in the bonding operation to provide additional column support to minimize distortion.

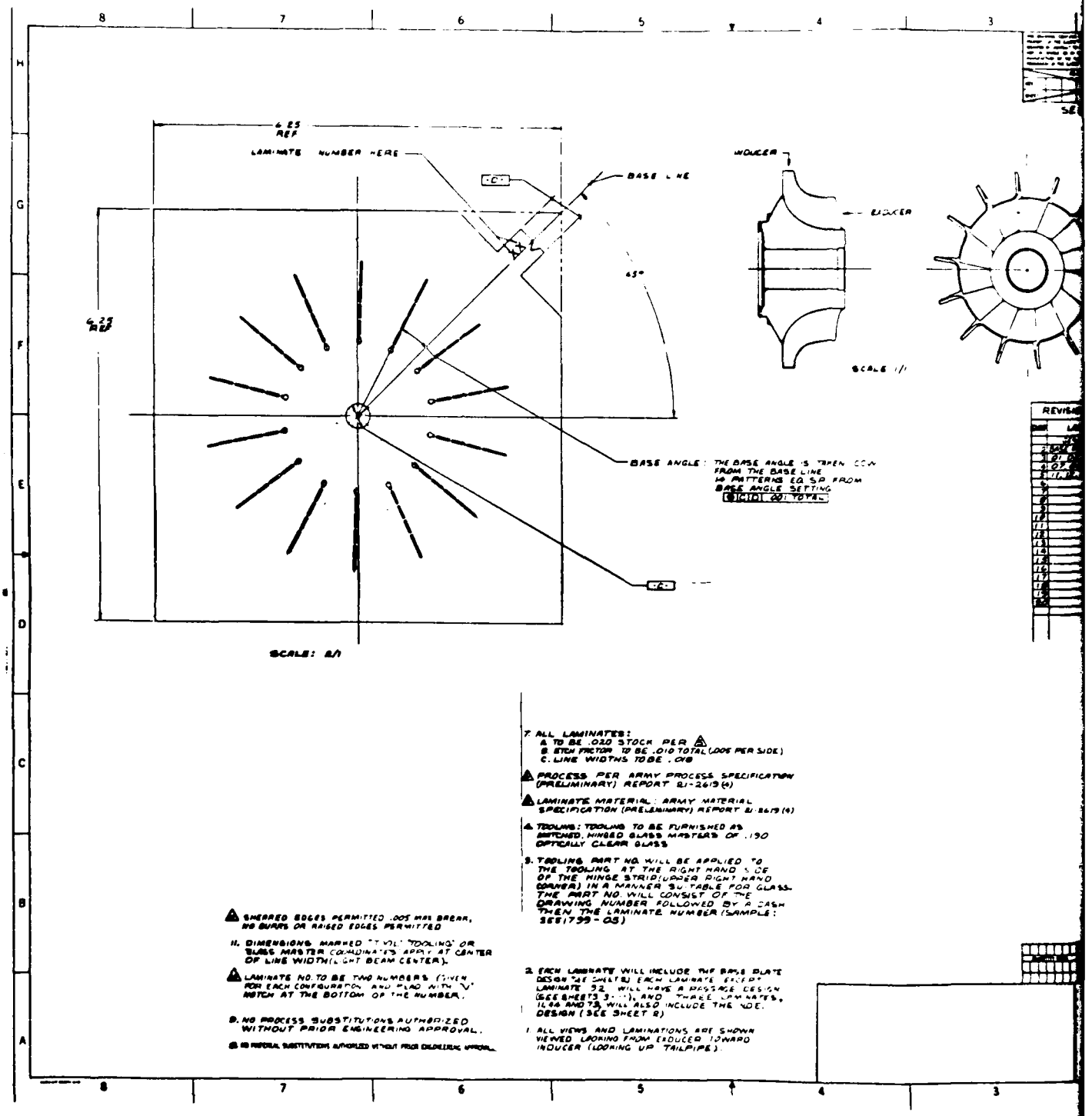

18
F

Figure 64. Lamination, Glass Master PCM Definition, Radial Wheel.

PRECEDING PAGE BLANK-NOT FILMED

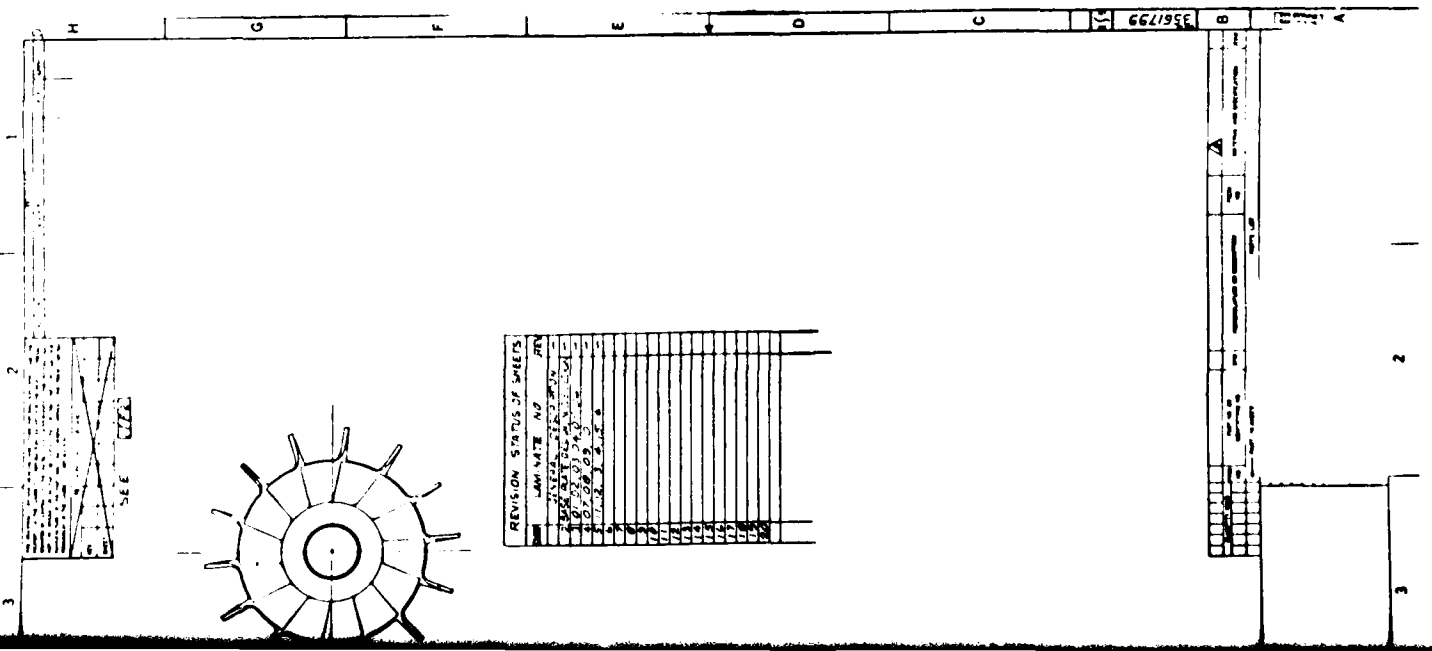

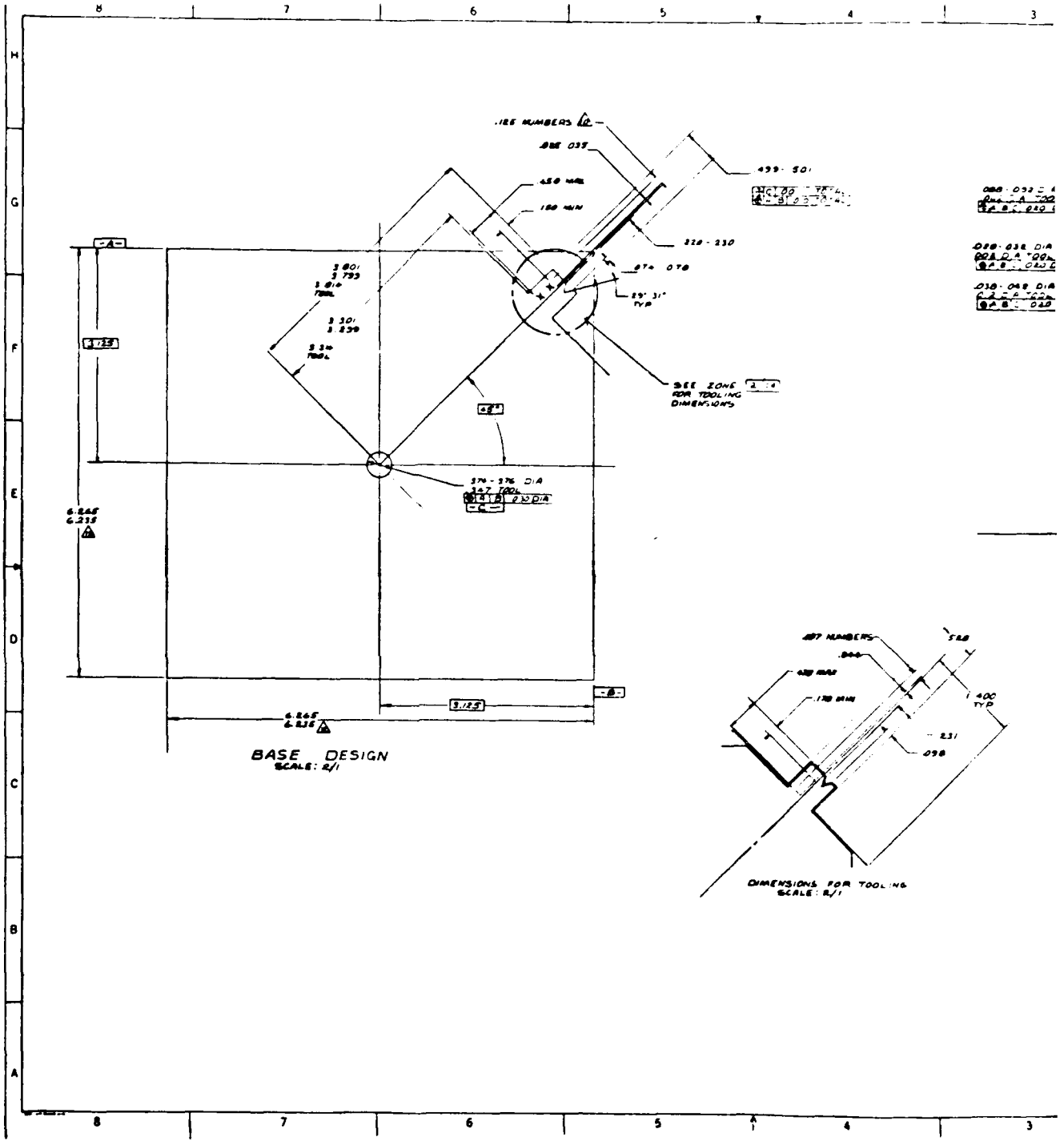

Figure 64. Continued.

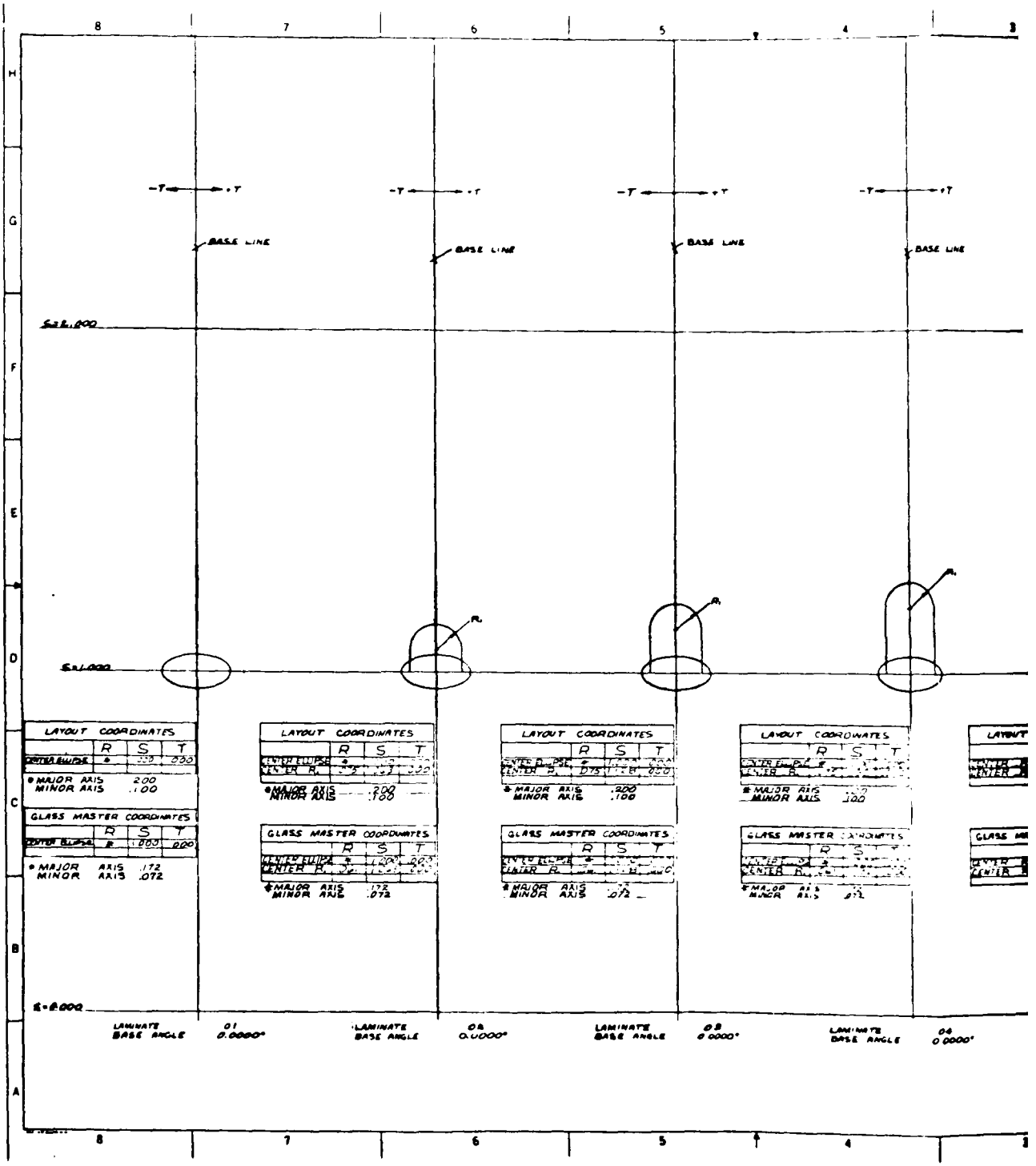

Figure 64. Continued.

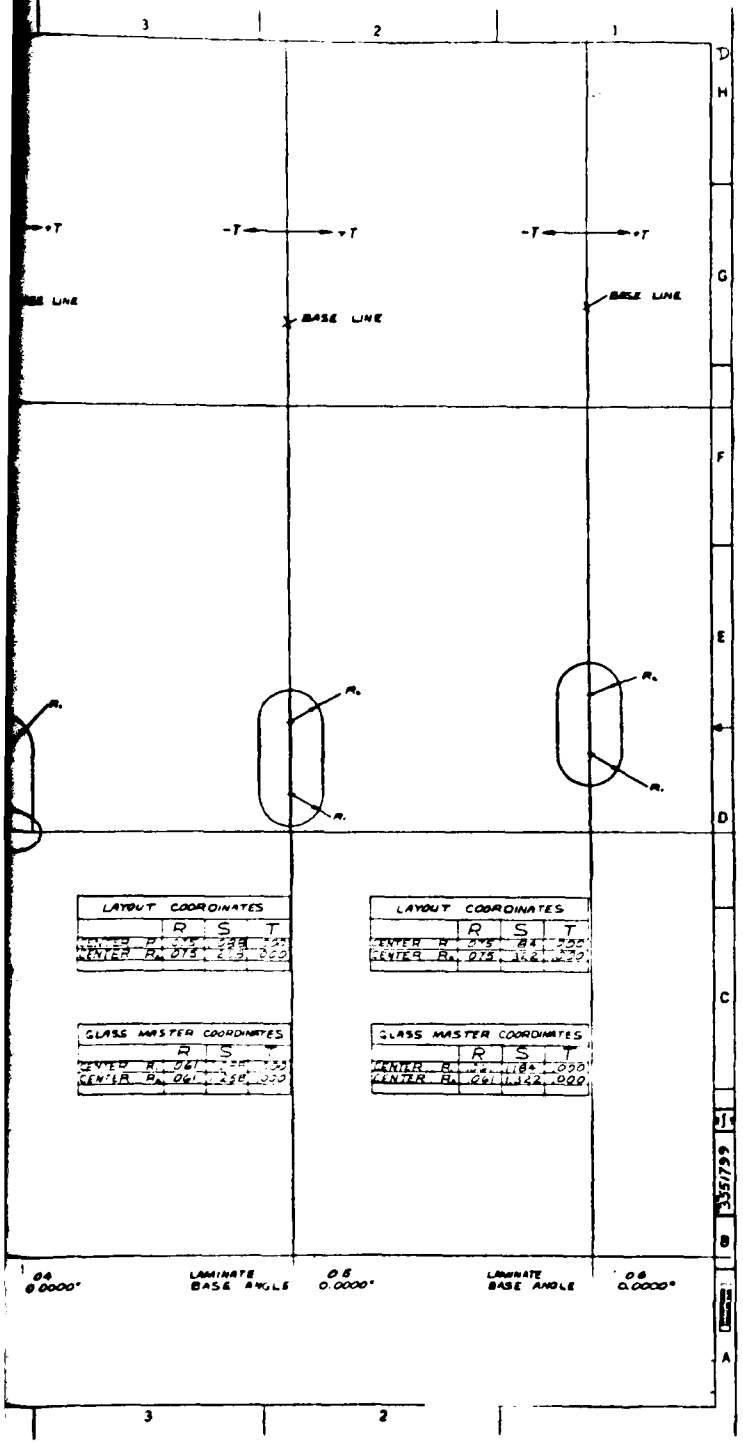
3
2
1
D
H
G
F
E
D
C
B
A
+T
-T
+T
-T
+T
BASE LINE
BASE LINE
BASE LINE
R.
R.
R.
R.
R.
LAYOUT COORDINATES
R S T
CENTER R .975 .84 .000
CENTER R .975 1.42 .000
GLASS MASTER COORDINATES
R S T
CENTER R .961 1.84 .000
CENTER R .961 1.42 .000
LAMINATE BASE ANGLE
0.0000°
LAMINATE BASE ANGLE
0.0000°
335/799

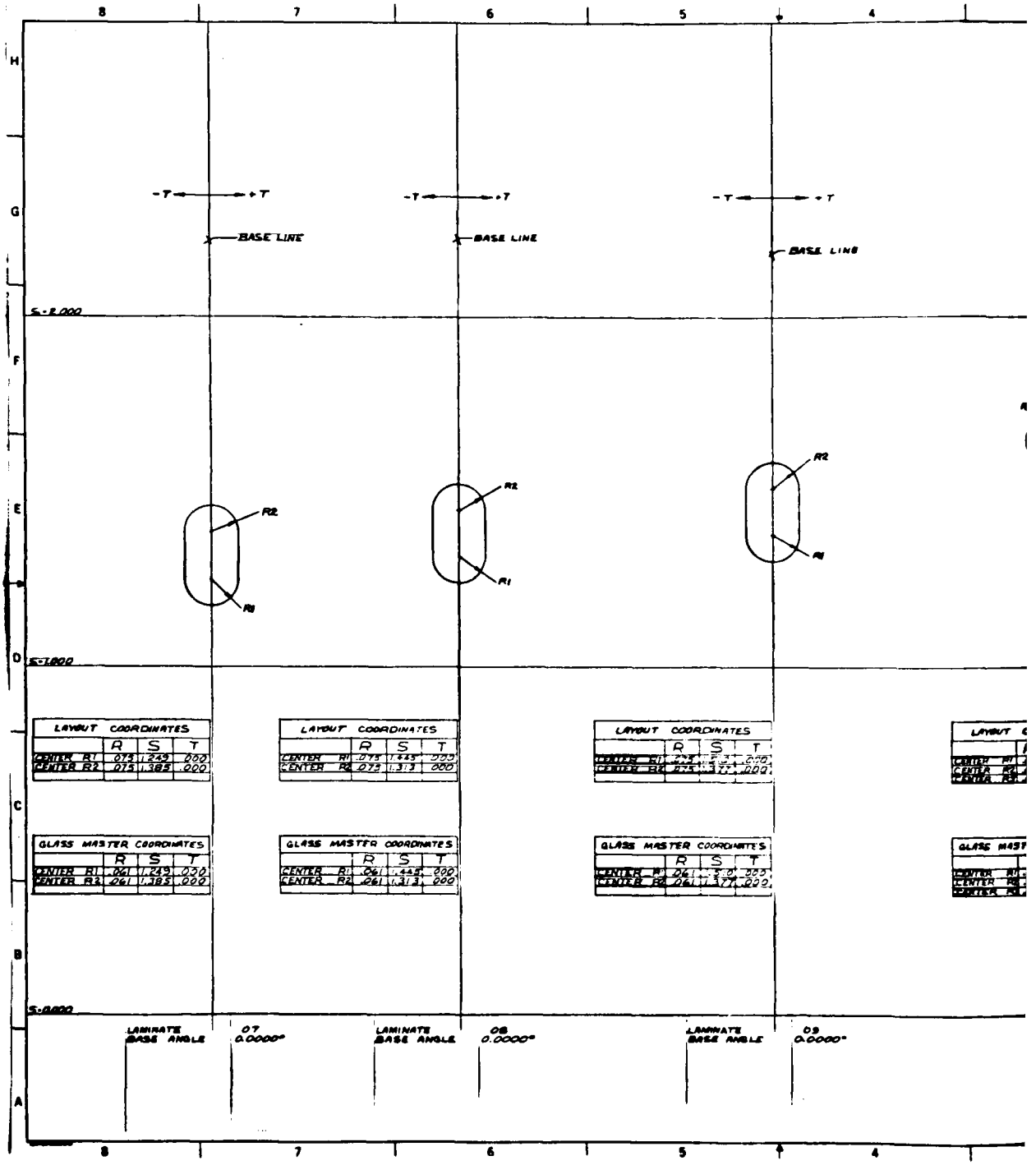

21
F

Figure 64. Continued.

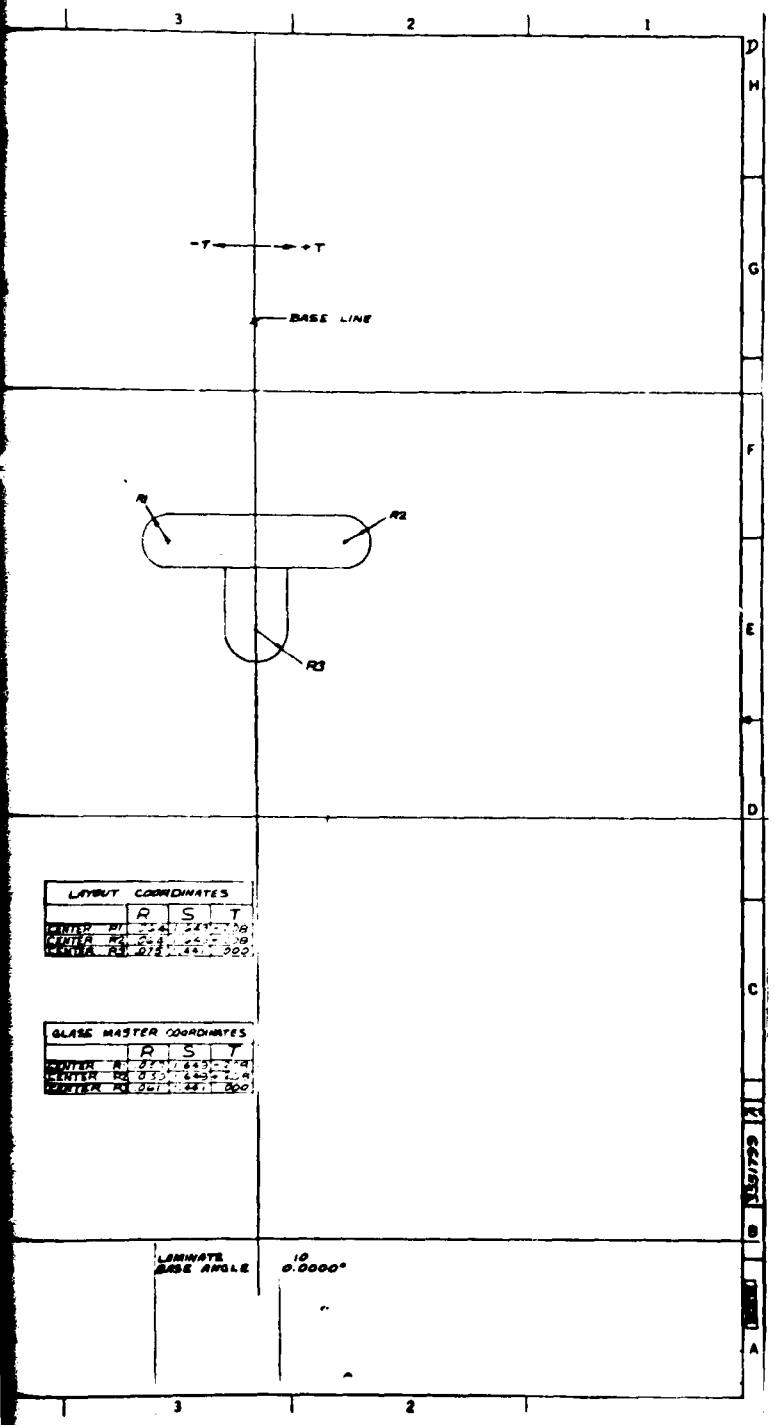
3
2
1
D
H
G
F
E
D
C
B
A
-T
+T
BASE LINE
R1
R2
R3
LAYOUT COORDINATES
R
S
T
CENTER R1
CENTER R2
CENTER R3
GLASS MASTER COORDINATES
R
S
T
OUTER R1
CENTER R2
OUTER R3
LAMINATE BASE ANGLE
10
0.0000°
3
2

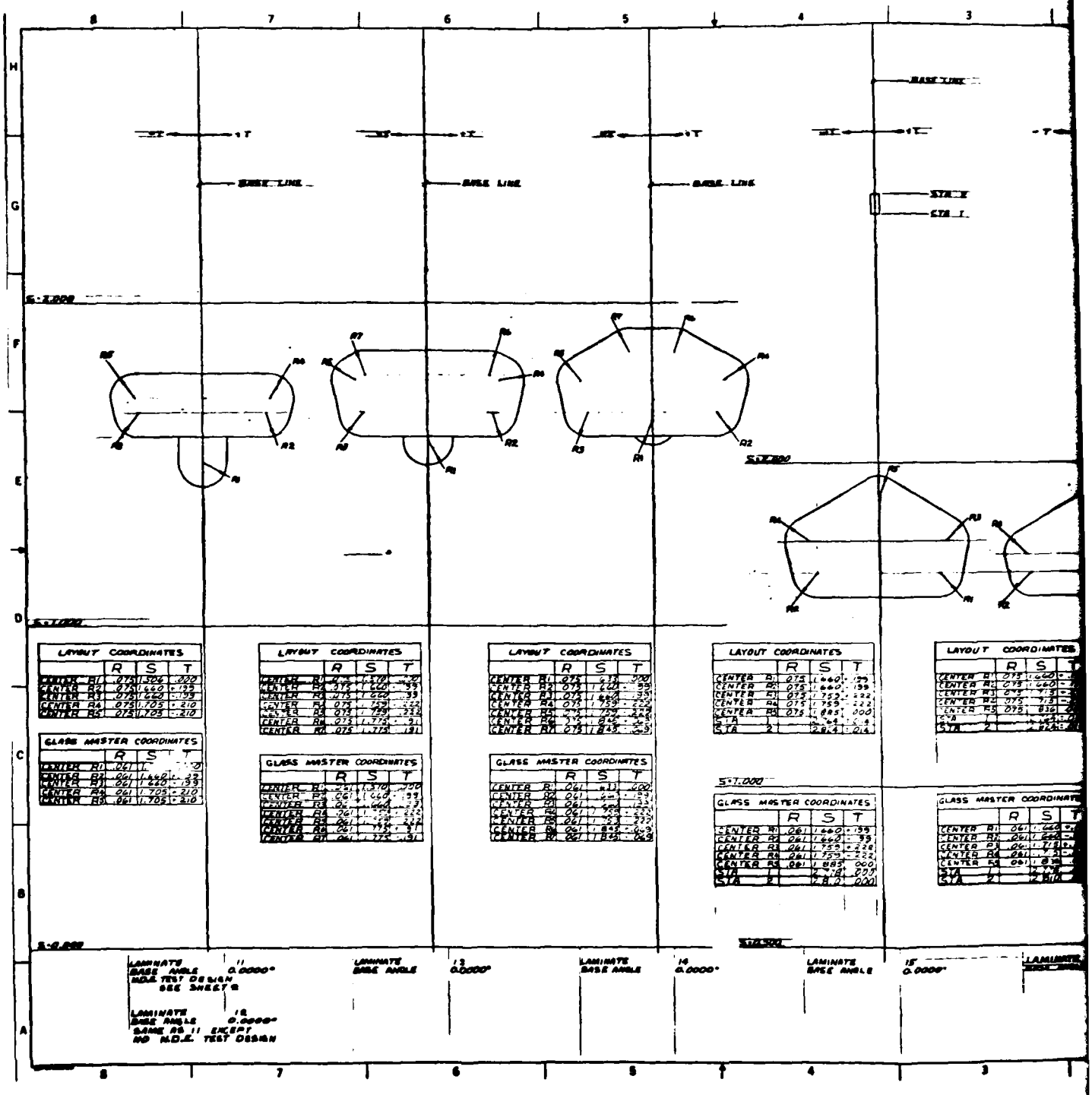

Figure 64. Concluded.

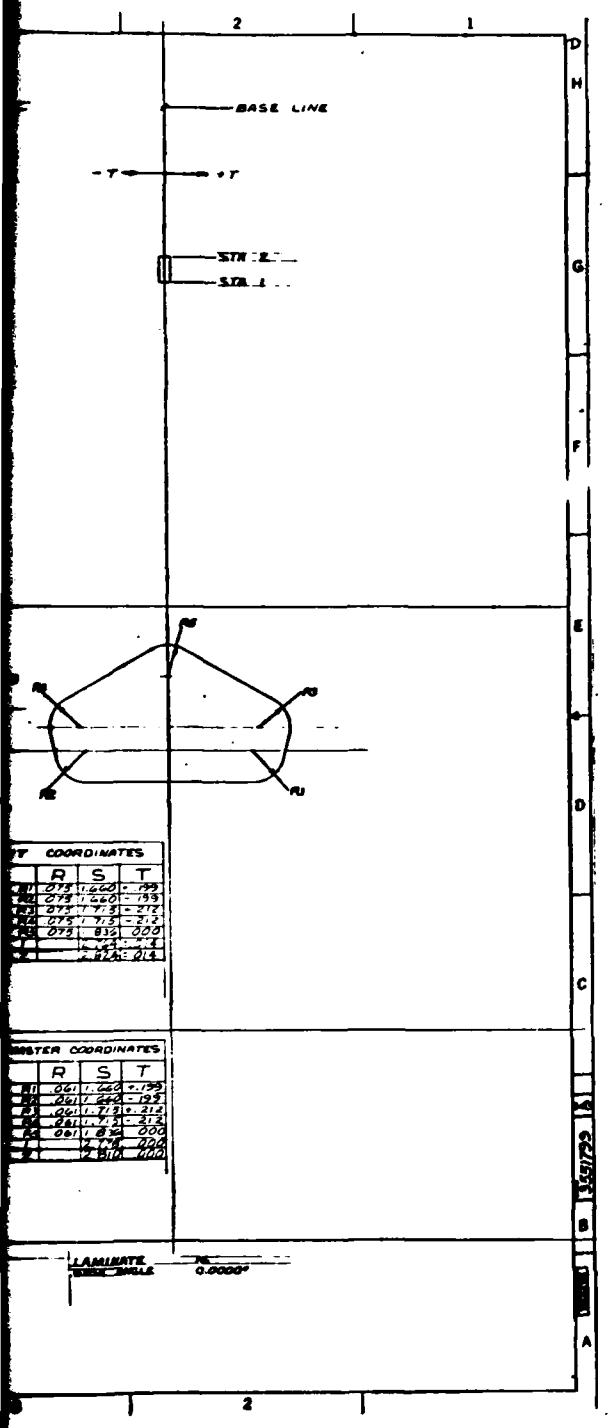
2
1
BASE LINE
-T
+T
STA 2
STA 1
RF
RB
RB
RE
RU
T COORDINATES
R S T
STER COORDINATES
R S T
LAMINATE
0.0000²
D
H
G
F
E
D
C
B
A
2

2

SECTION III

MANUFACTURING PROCESS

The manufacturing approach for the USARTL cooled laminated radial turbine drew upon technology developed under previous programs, including the AFML Cooled Axial Laminated Turbine Program (F33615-75-5211), APL Turbine Feasibility Demonstration Program (F33615-74-C-2034), and several AiResearch-sponsored research activities directed toward fabricating internally cooled structures. As the manufacturing operations progressed on the radial wheel, a gradual evolution took place as the result of new information and improved processing techniques, and experience gained with this laminated turbine configuration.

The AiResearch laminate process, as applied to the Army radial turbine, is shown in Figure 65. The process begins with procurement of precision sheet stock that was produced from forged, hot-rolled, and then cold-rolled Astroloy material. This material was deliberately procured oversize and subsequently chemically milled to the specified dimension. This was done for a number of reasons, the first of which was to achieve a clean surface, free from any "rolled in" contaminants. Another important reason for this step was that it produced a surface that allowed optimum adhesion of the photoresist systems used in later processing.

23 F

Following chemical milling of the Astroloy sheet in a modified ferric chloride solution, the sheet was coated with a photosensitive commercial preparation, which, when exposed selectively to a light source of the proper wavelength and developed, produced an acid-resistant coating except in the desired areas.

After the photoresist coating had been exposed and cured, the coated sheet was passed through a hot spray of etchant which chemically removed the exposed metal and left the desired configuration. The photoetched sheet was subsequently stripped of the photoresist coating, cleaned, and inspected for possible flaws. At this point, the sheet was called a laminate detail.

After the laminate details had been inspected, they were subjected to rigorous chemical and organic cleaning processes. Following these cleaning procedures, every other laminate detail was coated in a proprietary process, Borofuse®, which deposited a boron-rich layer on both of its surfaces. The coating was applied to the 0.0046 gram/in.^{2} level which produces consistent properties and bond results with Astroloy.

The actual bonding took place by creating intimate contact between the laminate surfaces at 2150°F in a high vacuum environment. At this temperature, the boron-enriched surfaces melted and generated a small amount of liquid at the laminate

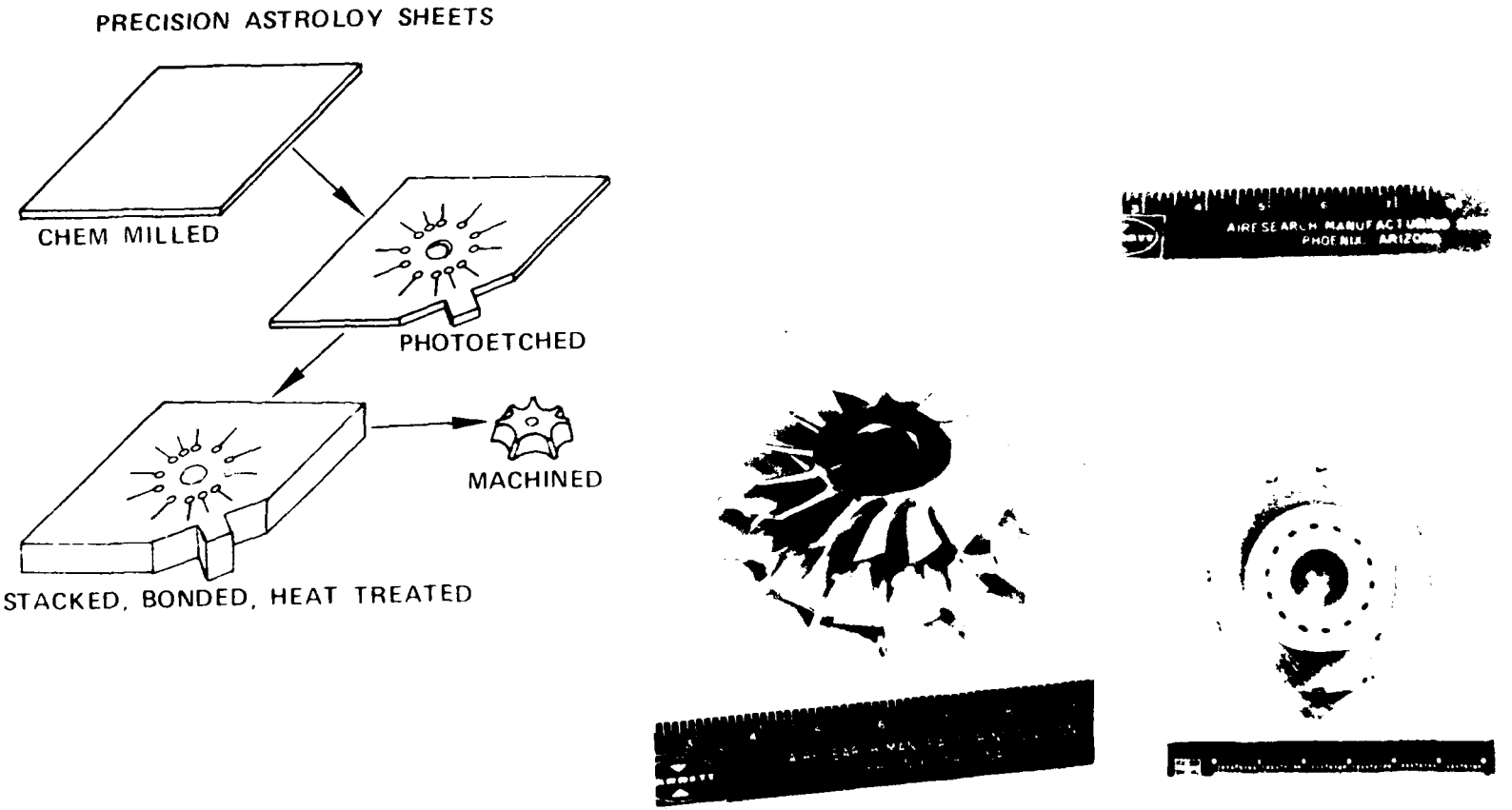

Figure 65. AiResearch Laminate Process.

interfaces which were in contact under 100 psi compressive loading. The fluid interfaces solidified isothermally due to the diffusion of boron away from the bond line. The bonding operation was conducted for a minimum of 2 hours, to fully diffuse the boron in the bond joint. A typical bond joint is shown in Figure 66.

The bonding method used to develop the radial wheel consisted of placing the laminate stack and bond tooling in a load frame, and then placing the entire assembly within a vacuum chamber. Heating was accomplished through the use of inductively heated graphite susceptors with pressure applied by the argon-filled bellows. The bond tooling is shown in Figure 67, and the bond cycle in Figure 68.

After bonding, heat treatment and nondestructive evaluation (NDE) were performed. This was followed by removal of mechanical property samples and metallographic samples from excess stock areas of the wheel blank (WB). The wheel blank was then partially machined to expose the air passages, and the airflow was checked. Final blade machining, NDE, balance and whirlpit testing completed the manufacturing process.

MATERIAL REQUIREMENTS

The Astroloy sheet from which the laminated radial turbine wheel was made conformed to AiResearch Specification EMS52338, Rev. A. Mechanical properties of the finished sheet were not made a specific requirement, due to the effects of subsequent processing (bonding and heat treatment) which the sheet material underwent in the manufacture of the finished wheel. When tested as sheet product, the mechanical properties were low, as shown in Table 8. This is primarily due to losses of reactive elements from the sheet during the rolling operations. However, after bonding, with the addition of boron the mechanical properties improved, as shown in Table 9.

Mechanical Properties

Mechanical properties of Astroloy sheet after heat treatment are given in Table 8. (Note that the heat treatment is used for the wheel blank, and is not optimized for maximum properties as a sheet metal product.)

Mechanical properties of the bonded wheel blanks are given in the following figures and tables:

- Summary of Bonded Astroloy Data — Table 9 and Figure 69
- WB No. 1 - Raw Data — Table 10
- WB No. 2 - Raw Data — Table 11
- WB No. 3 - Raw Data — Table 12
- WB No. 4 - Raw Data — Table 13

GARRETT

ASTROLOY LAMINATE BOND JOINT WITH BORIDE COATING

Figure 66. Astroloy Laminate Typical Bond Joint.

23-SVG273A

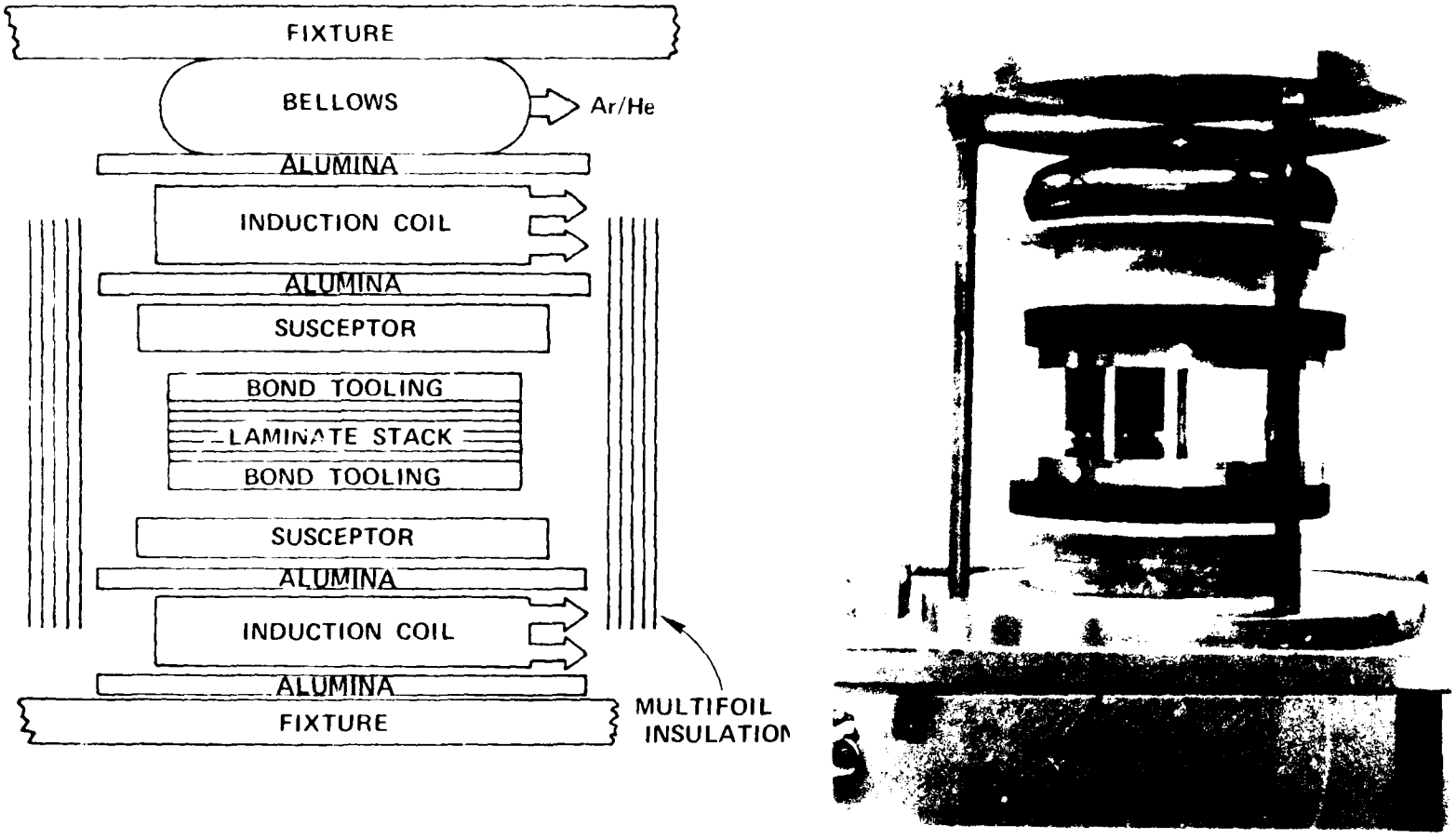

Figure 67. Fixture and Tooling for Applying Heat and Pressure During Bonding.

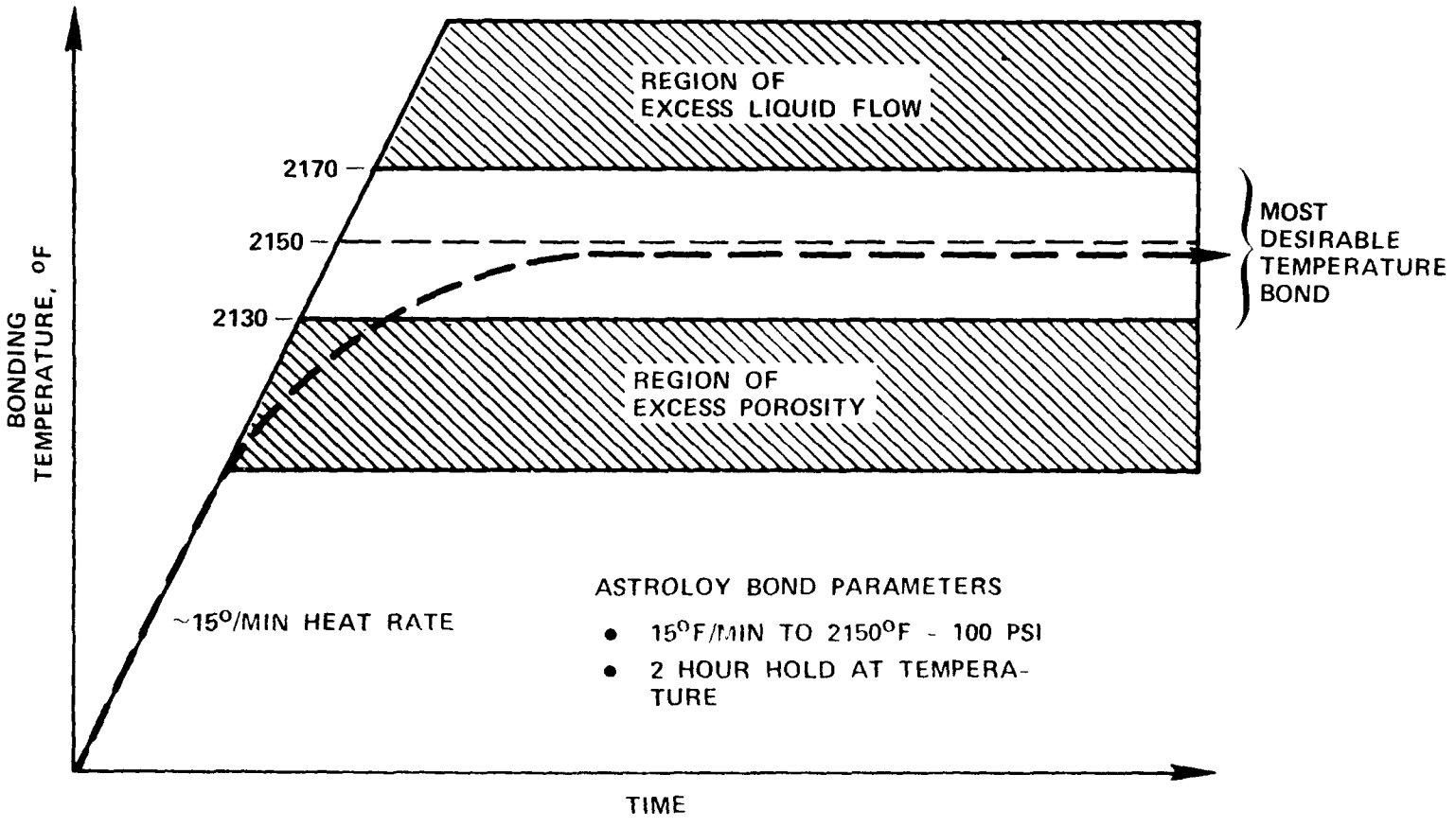

Figure 68. Bond Cycle Thermal Profile and Temperature Control.

TABLE 8. MECHANICAL PROPERTIES OF 0.020-INCH CABOT ASTROLOY SHEET MATERIAL.

	Room Temp. Tensile			1400°F Tensile			1400°F/ 80 ksi Stress Rupture		1800°F/ 20 ksi Stress Rupture	
	YS (KSI	Lo	%E	YS	UTS	%E	HR	%E	HR	%E
Heat 0036 (WB No. 1 and 2)	111	136	5	100	133	7	30	9	10	6
Heat 7092 (WB No. 3 and 4)	108	122	4	95	105	2.5	8	-	8	-

NOTE: Heat treated as follows:

2150°F - 6 hours
1975°F - 4 hours
1550°F - 24 hours
1400°F - 16 hours

To simulate wheel blank bond cycle + heat treatment

TABLE 9. BONDED ASTROLOY MECHANICAL PROPERTY DATA

SUMMARY

		Room Temperature			1300°F Tensile			Stress Rupture, Hrs	
	Wheel Blank (1)	ULT.	YD	%EL.	ULT.	YD.	%EL.	1400°F/ 80 KSI	1800°F 20 KSI
Transverse-	1	135.8	127.1	1.8	137.1	113.5	1.1	--	--
	2	150.4	133.2	2.8	147.2	117.3	1.6	--	--
	3	144.7	127.4	3.4	146.3	109.5	2.8	--	--
	4	126.8	121.3	2.3	--	--	--	--	--
	AFML DATA	141.6	129.4	1.7	133.6 (2)	114.2	1.8	50.4	36
Longitudinal-	1	195.4	134.5	14.9	--	--	--	57.5	11.3
	2	--	--	--	--	--	--	--	--
	3	180.1	125.3	12.0	--	--	--	64.3	13.3
	4	185.0	119.3	30.6	--	--	--	--	--
	AFML DATA	194.5	131.6	13.1	141.18 (2)	115.5	32.2	102	33.9

NOTES: (1) Bonding Temperature Range

No. 1 2170-2190°F

No. 2 2120-2140°F

No. 3 2130-2170°F

No. 4 2130-2155°F

AFML Data 2150 Average

(2) AFML Data Taken at 1400°F Tensile

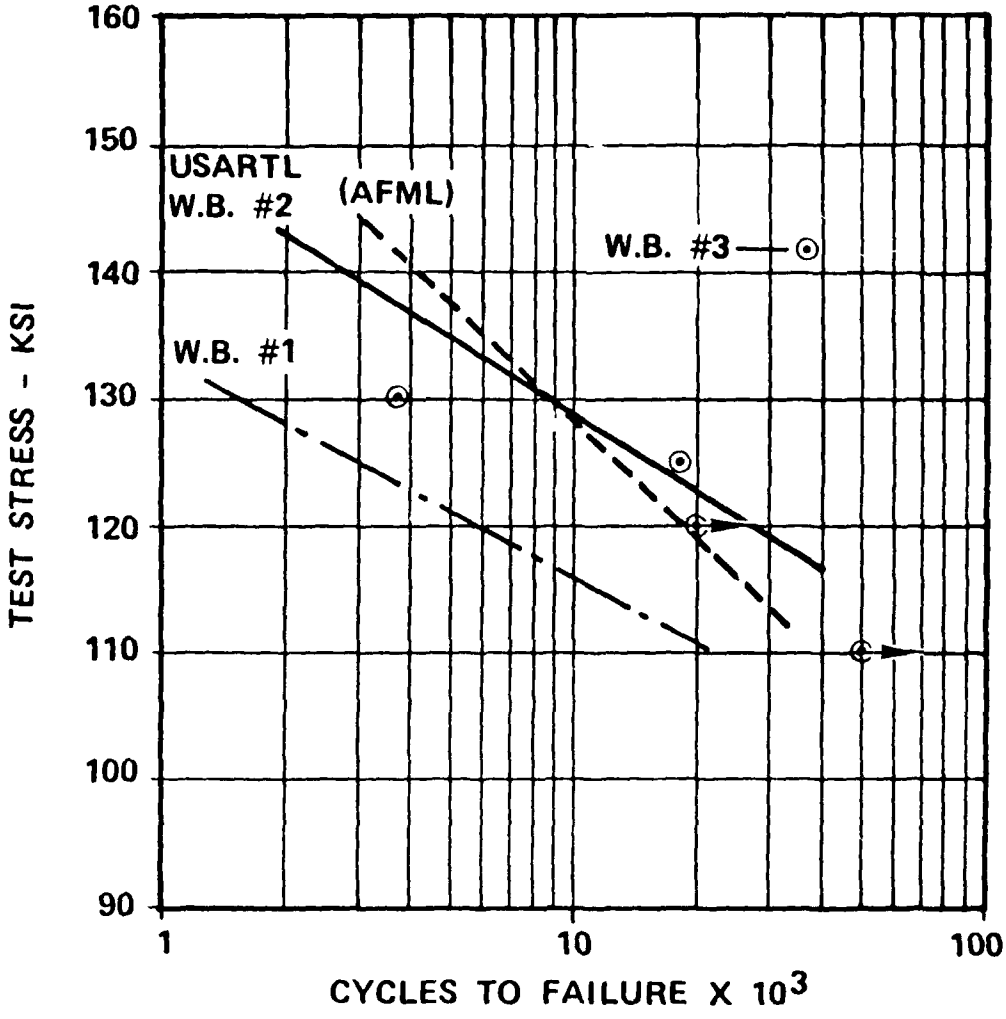

Figure 69. Summary of Bonded Astroloy Room-Temperature Low-Cycle-Fatigue Transverse Properties.

TABLE 10. USARTL MECHANICAL PROPERTY TESTS FOR WB NO. 1.

Test Bar	Location	Type of Test	Results
AWB - 1	Axial, Bore	Metallographic	100X, 400X - [illegible]
AWB - 2	Axial, Bore	75°F Tensile	Ult ksi 142.6; Yield ksi 126.4; Elong [illegible]; R.A. [illegible]
AWB - 3	Axial, Bore	A = 1 F = 20 cpm 120 ksi LCF (low cycle fatigue)	6.3×10^3 cycles
AWB - 4	Axial, Bore	140 ksi LCF	2.7×10^2 cycles
AWB - 5	Axial, Bore	1300°F Tensile	Ult ksi 135.1; Yield ksi 113.1; Elong [illegible]; R.A. [illegible]
AWB - 6	Axial, Bore	75°F Tensile	Ult ksi 129.0; Yield ksi 125.8; Elong 1.4%; R.A. [illegible]
AWB - 7	Axial, Bore	160 ksi LCF	Fail on first cycle
AWB - 8	Axial, Bore	1300°F Tensile	Ult ksi 139.1; Yield ksi 113.8; Elong 1.4%; R.A. [illegible]
AWB - 9	Axial, Rim	110 ksi LCF	1.8×10^4 cycles
AWB - 10	Axial, Rim	130 ksi LCF	1.0×10^3 cycles
AWB - 11	Axial, Rim	150 ksi LCF	Fail on first cycle
AWB - 12	Radial, Rim	75°F Tensile	Ult ksi 195.9; Yield ksi 134.3; Elong 15.1%; R.A. [illegible]
AWB - 13	Radial, Rim	S.R. (stress-rupture) 1400°F 80 ksi	51.1 hrs; Elong 24.4%; R.A. 44.[illegible]%
AWB - 14	Radial, Rim	S.R. 1400°F 80 ksi	59.1 hrs; Elong 21.8%; R.A. [illegible]%
AWB - 15	Radial, Rim	S.R. 1800°F 20 ksi	11.5 hrs; Elong 30.7%; R.A. [illegible]%
AWB - 16	Radial, Rim	75°F Tensile	Ult ksi 194.9; Yield ksi 134.7; Elong 14.6%; R.A. [illegible]%
AWB - 17	Radial, Rim	S.R. 1400°F 80 ksi	61.4 hrs; Elong [illegible]%; R.A. 40.[illegible]%
AWB - 18	Radial, Rim	S.R. 1800°F 20 ksi	11.3 hrs; Elong 27.6%; R.A. 34.[illegible]
AWB - 19	Radial, Rim	S.R. 1800°F 20 ksi	11.2 hrs; Elong [illegible]%; R.A. [illegible]

NOTE: All test bars heat treated as follows:

2 hours at bonding temp, nominal 2150°F - slow cool
4 hours at 1950°F, R.A.C. (equivalent)
24 hours at 1550°F, R.A.C. (equivalent)
16 hours at 1400°F, R.A.C. (equivalent)
All bars treated in wheel blank, then removed.

24
B

TABLE II. USARTL MECHANICAL PROPERTY TESTS FOR WB NO. 2.

Test Bar	Location	Type of Test		Results			
				ULT,KSI	Yield;KSI	% EL	% RA
AWB-2-1	Axial, bore	(2) 75°F tensiles	Top	148.2	120.4	[illegible]	[illegible]
			Bottom	[illegible]	[illegible]	[illegible]	[illegible]
AWB-2-2	Axial, bore	(2) 75°F tensiles	Top	144.2	[illegible]	[illegible]	[illegible]
			Bottom	157.9	[illegible]	[illegible]	[illegible]
AWB-2-3	Axial, bore	Metallography					
*AWB-2-4	Axial, bore	LCF 130 ksi			8.240×10^3 cycles		
*AWB-2-5	Axial, bore	LCF 140 ksi			2.800×10^3 cycles		
*AWB-2-6	Axial, bore	LCF 120 ksi			2.734×10^4 cycles		
				ULT,KSI	Yield;KSI	% EL	% RA
AWB-2-7	Axial, bore	(2) 1300°F tensiles	Top	148.6	119.4	1.5	3.3
			Bottom	149.2	121.81.4	2.8	
AWB-2-8	Axial, bore	(2) 1300°F tensile			In Testing		
*AWB-2-8B	Axial, bore	1300°F tensile		151.3	115.9	2.3	5.4
*AWB-2-8T	Axial, bore	1300°F tensile		143.8	111.9	1.1	3.8
AWB-2-9	Axial, rim	Delaminated, Metallography			-variable porosity		
AWB-2-10	Axial, rim	Delaminated - MET			-variable porosity		
AWB-2-11	Axial, rim	Delaminated - MET			-variable porosity		
				Extent of Radial major porosity, inches			
AWB-2-12	Radial, rim	Delaminated - MET			1.0 inch		
AWB-2-13	Radial, rim	Partial delamination-MET			0.5 inch		
AWB-2-14	Radial, rim	Partial delamination-MET			0.2 inch Figures 3,4		
AWB-2-15	Radial, rim	Partial delamatination-MET			0.25 inch		
AWB-2-16	Radial, rim	Partial delamination-MET			0.75 inch		
AWB-2-17	Radial, rim	Partial delamination-MET			0.75 inch Figures 3,4		
AWB-2-18	Radial, rim	Partial delamination-MET			0.55 inch		
AWB-2-19	Radial, rim	Partial delamination-MET			0.75 inch		

NOTE: All test bars heat treated as follows, in wheel blank

2 hours at bonding temperature (bore 2130°F, rim 2110°F), 11°F/min cool

2 hours at 2100°F re-solution soak, 100°F/min cool(from 2100°F to 1400°F)

4 hours at 1950°F, rapid air cool (R.A.C.) (equivalent)

24 hours at 1550°F, R.A.C.

16 hours at 1400°F, R.A.C.

*Additional data added.

TABLE 12. USARTL MECHANICAL PROPERTY TESTS FOR WB NO. 3.

Test Bar	Location	Type of Test	Results
AWB-3-1	Axial, bore	Low Cycle Fatigue(LCF) 145 Ksi	1 cycle fail
AWB-3-2A	Axial, bore	Room Temp. Tensile (RTT)	Y.S.Ksi ULT,Ksi %EL %RA 127.4 144.7 2.4 3.5
AWB-3-2B	Axial, bore	RTT	Y.S.Ksi ULT,Ksi %EL %RA 119.2 142.1 2.5 5.3
AWB-3-3	Axial, bore	LCF - 135 Ksi	7 cycle fail
AWB-3-4	Axial, bore	LCF - 110 Ksi	50,000+Cycle Runout-Uptime
AWB-3-4	Axial, bore	LCF - 130 Ksi	762 cycle fail
AWB-3-5	Axial, bore	1300°F Tensile	Y.S.Ksi ULT,Ksi %EL %RA 109.4 147.3 4.1 7.6
AWB-3-6A	Axial, bore	RTT	Y.S.Ksi ULT,Ksi %EL %RA 126.8 137.2 2.0 XX
AWB-3-6B	Axial, bore	RTT	Y.S.Ksi ULT,Ksi %EL %RA 120.2 141.4 1.7 4.1
AWB-3-7	Axial, bore	LCF - 130 Ksi	111 cycle fail
AWB-3-8	Axial, bore	1300°F Tensile	Y.S.Ksi ULT,Ksi %EL %RA 109.5 145.3 3.4 7.1
AWB-3-9A	Axial, rim	Metallography	Satisfactory
AWB-3-9B	Axial, rim	LCF - 130 Ksi	3771 Cycles to Failure
AWB-3-10	Axial, rim	LCF - 125 Ksi	17,261 cycle fail
AWB-3-11	Axial, rim	LCF - 120 Ksi	20,000 + cycle runout
AWB-3-12	Radial, rim	RTT	Y.S.Ksi ULT,Ksi %EL %RA 125.6 182.3 13.3 17.6
AWB-3-13	Radial, rim	Stress Rupture(S.R.) 1400°F/80 Ksi	Life,hrs %EL %RA 60.0 22.2 30.5
AWB-3-14	Radial, rim	S.R. 1400°F/80 Ksi	Life,hrs %EL %RA 74.4 16.9 27.3
AWB-3-15	Radial, rim	S.R. 1800°F/20 Ksi	Life,hrs %EL %RA 14.8 21.4 34.1
AWB-3-16	Radial, rim	RTT	Y.S.Ksi ULT,Ksi %EL %RA 124.9 177.9 10.7 16.3
AWB-3-17	Radial, rim	S.R. 1400°F/50 Ksi	Life,hrs %EL %RA 58.6 15.4 33.5
AWB-3-18	Radial, rim	S.R. 1800°F/20 Ksi	Life,hrs %EL %RA 13.3 30.4 31.5
AWB-3-19	Radial, rim	S.R. 1800°F/20 Ksi	Life,hrs %EL %RA 11.9 27.1 30.1

NOTE: All test bars heat treated as follows:
2 hours at bond temp., nominal 2150°F - slow cool
24 hours at braze temp., nominal 1950°F - slow cool
3 hours at HIP temp., nominal 2100°F - (36°F/min) rapid cool
4 hours at 1975°F - rapid cool
24 hours at 1550°F - rapid cool
16 hours at 1400°F - rapid cool

All bars treated in wheel blank, then removed.

TABLE 13. MECHANICAL PROPERTY RESULTS, WHEEL BLANK NO. 4.

Specimen Identity	Test Temp., °F	0.2% Offset Yield Strength, PSI	Ultimate Tensile Stength, PSI	% Elong.	% RA
		1 Transverse, Bore			
AWB-3-6 Top	75	121,400	123,200	1.4	4.8
AWB-3-6-Bottom	75	121,200	130,400	3.3	7.1
		2 Transverse, Rim			
AWB-3-9-Top	75	-	114,900	1.1	1.7
AWB-3-9-Bottom	75	-	100,200	1.3	1.9
AWB-3-11-Center	75	120,500	133,900	3.3	5.5
		3 Longitudinal, Rim			
AWB-3-22	75	118,900	184,200	14.9	20.6
AWB-3-23	75	119,800	185,800	15.7	23.6

All samples heat treated in wheel blank, as follows:

2 hrs at bond temperature, 2150°F nominal, slow cool
2 hrs resolution at 2100°F, 25°F/min cool
4 hrs stabilize at 1975°F, rapid air cool
24 hrs age at 1550°F, air cool
16 hrs age at 1400°F, air cool

It should be noted that WB No. 4 was contaminated by equipment failure during bonding and was never processed into a machined rotor. All of the other wheel blanks were finish machined and tested.

Material Specification

The material specification is contained in Appendix A.

NDE PROCEDURES

Nondestructive inspection occurred at two major points in the process. First, at the laminate detail stage, each laminate was inspected for undesirable features, such as etch pits, scratches, etc., which could affect the bonding process or be included in the finished wheel. This was a visual 100-percent inspection done at up to 10X magnification; any extra features were recorded on paper maps of the laminates. Each laminate was then reviewed against the blueprints and 10X layouts to insure that no potentially detrimental features would be incorporated in the finished wheel. (Figure 70 gives allowable feature size.)

Second, after bonding, ultrasonic inspection techniques were used to determine bond joint quality. Previously prepared laminated standards for this part configuration are scanned at the same time as the actual wheel blank. This allows direct interpretation of the 'C' scan result in terms of indicated reflections. (See Figures 71 and 72 for details of the ultrasonic calibration standard and actual laminate detail internal standards.) Ultrasonic techniques were most successful when the scan was "gated" to record only 1/3 of the wheel blank at a time, and the sensitivity was adjusted to record the 0.040-inch synthetic defect in the calibration standard.

In this process, it was possible to detect excessive porosity at the rim in WB No. 2 and at the bore of WB No. 3, as well as to discover some plugging in WB No. 1 passages. Radiography appeared to be useful for detecting plugged passages, but porosity could not be detected due to the disadvantageous orientation and physical limitations. Microfocus radiography was useful after the wheel blank was machined to examine internal blade configurations.

PROCESS SPECIFICATION

The complete process specification is contained in Appendix B.

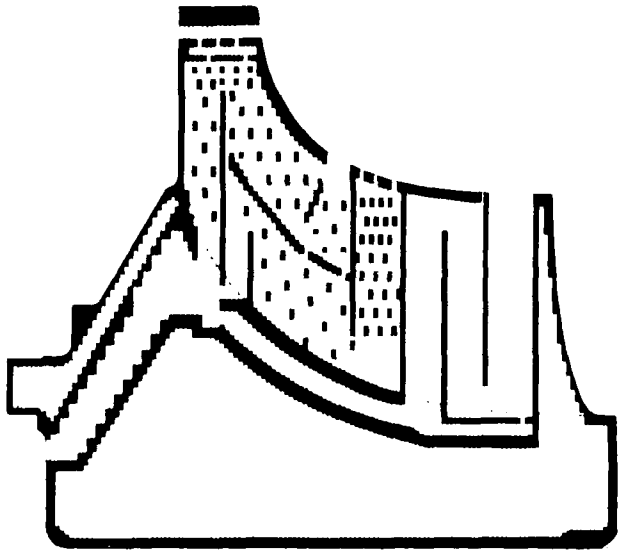

- LAMINATES WILL BE REJECTED IF ETCH PITS OR OTHER UNDESIRABLE FEATURES OCCUR WITHIN 0.020" OF ANY BLADE COOLING PASSAGE OR WITHIN 300 PERCENT OF THEIR MAXIMUM DIMENSION TO THE DISK BORE OR OTHER MACHINED SURFACE.
- UNDESIRABLE FEATURES: BLADE – 0.100" MAX. AND DISK – 0.200" MAX., WITH NO TWO FEATURES CLOSER TO EACH OTHER THAN 200 PERCENT OF MAXIMUM DIMENSION IN THE RADIAL DIRECTION. EXCEEDING THESE DIMENSIONS WILL CAUSE THE LAMINATE TO BE REJECTED.
- ANY FEATURE BELOW 0.015" IN MAXIMUM DIMENSION IS CONSIDERED UNINTERPRETABLE.

Figure 70. Army Radial Laminated Rotor Defect Criteria.

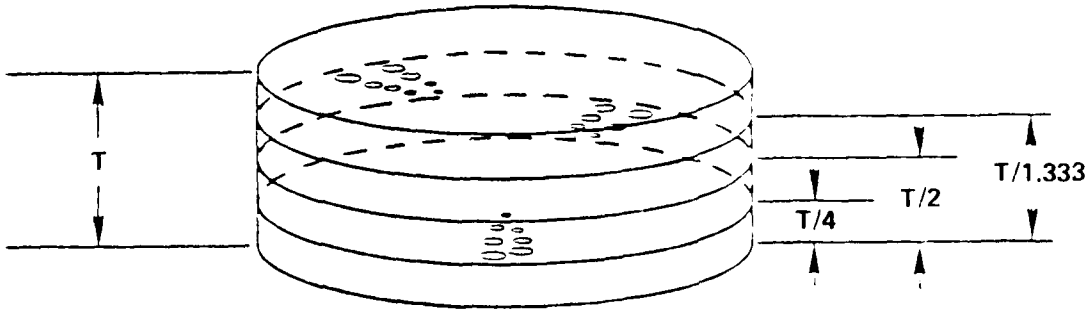

BONDED STACK (DEFECT LAMINATES ORIENTED 120° APART)

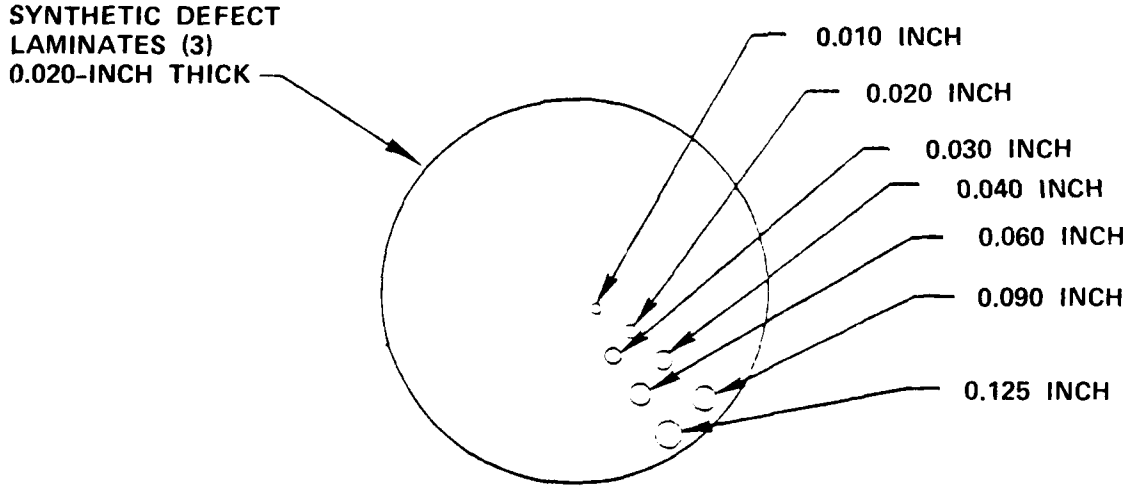

Figure 71. Laminated Astroloy Ultrasonic Calibration Standard.

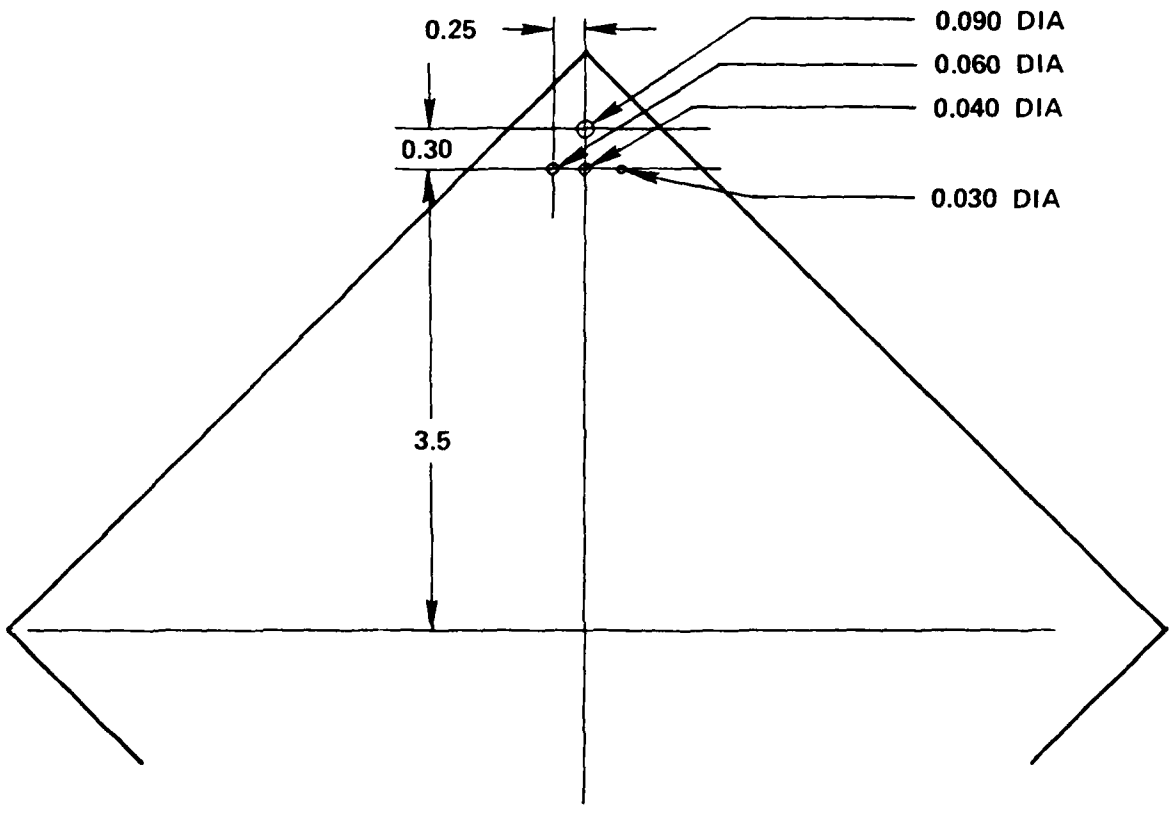

25
F

Figure 72. Synthetic Defect Locations in the Actual Laminate Detail.

HOT ISOSTATIC PRESSING

The use of hot isostatic pressing (HIP) as a repair technique for WB No. 3 was highly successful. There is justification for including HIP as a manufacturing process step rather than as a repair tool. The HIP operation will guarantee a lower porosity level in the finished weld blank that could reasonably be expected in the "as-bonded" product. This must be weighed against the additional cost of the HIP operation. For a high reliability, long life, man-rated engine, the HIP operation appears to be justifiable as a part of the fabrication manufacturing process. For this reason, it is included under "Recommended Processing and Operations" in the process specification.

SECTION IV

PHASE II - PROTOTYPE WHEEL FABRICATION

MATERIAL PROCUREMENT

Precision A-286 alloy sheet metal for constructing the cooled [illegible] rotor wheels was obtained with effort and [illegible]. Early efforts were characterized by high scrap [illegible] unfamiliarity with the production characteristics [illegible] alloy as a sheet metal product, coupled with the very [illegible] dimensional laminate quality stock. Stellite Division [illegible] ultimately produced the material from raw materials to [illegible] sheet, with the exception of one effort at rerolling [illegible] sheet stock at AMAX Specialty Metals Division. [illegible] was rejected entirely by Cabot.

[illegible] to produce acceptable material has cul[illegible] problem with reasonable yield. Areas that [illegible] these difficulties were:

a. Chemistry Control - Aluminum, titanium, and boron proved to be the most difficult elements to control to [illegible] specification. This was compounded by a real difficulty in obtaining precise chemical analysis of the aluminum and titanium contents, whether done by internal or independent laboratories.

b. Rolling Parameters - The iterative solution to obtain the reduction versus annealing schedules, proper gauge flatness, and proper surface finish [illegible] product was difficult to arrive at and [illegible] extensive documentation for their efforts in successfully [illegible] this difficulty.

c. Surface Condition - Related to the rolling reduction schedules and the annealing furnace atmosphere (dew point, [illegible] practices, etc.) for the amount of material being produced, to achieve an oxide-free surface of the sheet after [illegible]. This caused considerable early difficulty in obtaining an acceptable chemically milled surface finish. Joint experiments between Cabot and Arkansas resulted in the development of an acceptable anneal and final rolling schedule to control this problem. Later work by Arkresearch and OEA-Hunt Corporation evolved an etchant solution which may reduce this problem even further.

(d) Handling - Proper handling procedures for laminate quality stock are necessary to avoid scrappage due to mechanical defects such as scratches or dents. Cabot's recognition of this special handling requirement and implementation of adequate procedures to safeguard the material in process were needed.

FABRICATION OF BONDING TOOLING

The design of bond tooling for the laminated radial turbine wheel blanks was a complex problem that slowly evolved. Due to the limited number of parts produced (four), a satisfactory solution to the bond tooling problem was arrived at only at the end of the program. Initial constraints on the tooling, which was to serve as both assembly fixturing for the laminate stack and as the in-the-furnace bond tool, proved to be too severe to be met with existing materials.

The original tool design consisted of Waspaloy plates, pins, and locating tabs (Figure 73). This tooling proved to be dimensionally unstable at temperature and inadequate in tolerance for assembly errors. This tooling was modified to prevent assembly errors, while new higher strength and thermally stable molybdenum bond tooling was procured.

The molybdenum bond tooling was of a similar configuration but was modified to allow removal of the locating tab mechanism prior to bonding. While an improvement, this tooling also had difficulties. The last form of use of this tooling as a bond tool for WB No. 3 saw the design simplified to two flat, parallel disks with thermocouples for temperature sensing. It was still being used as an assembly tool at this point, which led to difficulties with bore porosity in WB No. 3 due to galling of the center pin upon removal at assembly prior to bonding. Simultaneous and subsequent work on both AiResearch and AFML-funded laminate programs has proved the point for separate assembly and bond tooling. To successfully assemble and bond a complex laminate structure, the following concepts must be adhered to:

(a) Assembly tooling and bonding tooling must be separate fixtures, since their functions are separate and not mutually compatible.

(b) Assembly tooling must be rigid, precise, easily cleaned, made of nongalling materials, and designed for laminate access.

(c) The laminate stack must be strip welded in compression while in the assembly tooling fixture, to make it a handleable structure prior to placement in the bond tooling fixture.

Figure 73. USARTL Bond Tooling and Assembly Fixture - Original Waspaloy Design.

(d) Bond tooling must be constructed of high-strength, high-temperature stable material, and must be kept as simple as possible. Contact between the laminate stack and the bond tooling should occur only on flat, plane surfaces to which an appropriate parting agent/diffusion barrier has been applied.

When the above concepts are employed and adequate loading devices are used in the bonding furnace, tooling-related problems are eliminated.

FABRICATION OF WHEEL BLANKS

The detailed process specification is contained in Appendix B.

Photochemical Machining of Laminates for Wheel Blanks

Each wheel blank contains 141 individual laminates, which were produced by the photochemical machining (PCM) process. Four and one-half sets of wheel blank details were produced under this contract. The extra 1/2 set was a replacement for the chemically damaged borided details of WB No. 3.

Early processing utilized the liquid-resist, KTFR method given as Method I in AiResearch Specification PC5021, Rev. B. This was the best known method at the time. Process yields were on the order of 50 percent. Later developmental work led to Method II, PC5021, Rev. B, which is the dry film photoresist process. Yield from the PCM processing step was ~90 percent with this method. Either method produces identical parts.

Cleaning and Boride Coating

After production of the laminates by PCM, all laminates were stripped of photoresist, inspected, and cleaned. The cleaning process was a rigorous one, detailed in the process specification (Appendix B). Following the cleaning and packaging operations, the laminates to be boron coated were shipped to Materials Development Corporation (MDC) in Medford, Mass. MDC applied a diffused boron coating to all surfaces of each laminate, in the amount specified. After the Borofuse ® coated laminates were returned, a trial assembly of the wheel blank was completed to verify assembly and check section heights (thickness). If sections were not correct, either of two steps could have been taken:

(a) Insert specially fabricated laminates, known as "tolerancing elements" in various thicknesses at predesignated locations (essentially, every tenth laminate is a tolerancing element). This is the most straightforward and least time-consuming method. This method would be used for production.

(b) Chemically mill the bare laminates in the discrepant section the required amount. This allows a minimum number of laminates to be fabricated, but requires that laminates be deliberately made on the "fat" side of the thickness tolerance.

Due to initial material scarcity, method (b) was used.

Final Assembly

After correct section height and trial assembly were verified, all details were given final cleaning as part of the final assembly operation. This was a clean-room operation to avoid contamination of the laminate surfaces. The laminate stack was built on the assembly tooling (formerly assembly and bond tool) according to the blueprint and laminate map package. The assembly tooling then compressed the laminate stack, and the stack was visually inspected for alignment prior to resistance tack welding using Inco 600 foil strips across the laminate edges.

The tack welded strips, which were perpendicular to the laminates, held the individual laminates tightly together and prevented any shift or misalignment in the laminate stack once the assembly tool compressive force was released. The welded strips also provided a means of securely attaching the thermocouples to the laminate stack for temperature monitoring during bonding. In the early production of wheel blanks, this was the end of preparation for bonding, since the assembly and bond tool was the same piece; the complete assembly was now ready for installation into the bond furnace load frame and insertion into the bond furnace.

As mentioned previously, separate assembly and bond tools were needed, so there was an additional step in which the rigidly strip-welded laminate stack with attached thermocouples was removed from the assembly fixture and placed in the bond tooling. The bond tooling was previously cleaned and appropriate parting agent/diffusion barrier coating applied. This completed the final assembly and the part was now ready to bond.

Bonding Equipment and Operation

Equipment

The initial bonding parameters for Astroloy laminate structures were developed under the AFML/APL programs*. Time, temperature, vacuum level, and bonding pressure were reasonably defined. These parameters were met on small Astroloy laminate stacks using laboratory vacuum hot-press equipment at

*Contracts (F33615-75-5211) and (F33615-74-C-2034)

AiResearch. The largest structures attempted under AFML sponsorship were Waspaloy laminated axial flow turbine wheels 11 inches in diameter and 1 1/4 inches thick. These were done at Rockwell International using a hot press designed for titanium superplastic forming/diffusion bonding. This equipment was temperature limited and marginal for the 2100°F Waspaloy bond temperature. It was not expected to be able to accommodate the 2150°F Astroloy bond temperature.

After the design phase of the USARTL laminated wheel program had fixed the size of the wheel, it was demonstrated that none of the laboratory equipment was capable of accommodating the size and thermal mass of the new wheel. There also was no available vendor equipment to use, given the required parameters for bonding. A decision was thus made to convert an existing piece of equipment to perform this task.

A vacuum environmental chamber was located and converted to high-vacuum use as a bonding chamber. While innovative, the equipment must be considered an expediency and not a piece of production equipment. A lengthy series of trials was required to qualify the equipment. Figure 74 shows a view of the bonding equipment.

Bonding Operation

After final assembly, the bond tooling with thermocoupled laminate stack was loaded into the load frame, which housed the mechanism for loading and heating the laminate stack. (Figure 67 contains a photograph of the fixture and a schematic of the construction of the loading/heating apparatus.) The load frame (fixture) was then installed in the bond furnace, appropriate connections were made for thermocouples and induction leads, and the chamber was evacuated.

After a sufficient outgassing period, the bond stack was run (originally with manual control, later using a microprocessor/controller) on the established bond cycle. Figure 68 gives bonding parameters. A comparison of the actual wheel blank bond runs is given in Figure 75.

After being held at temperature for 2 hours, the bonded laminate stack was cooled and removed from the bond furnace. It was then heat treated in a conventional vacuum furnace with a rapid inert gas quench capability and nondestructively inspected.

NDE, Premachining, and Mechanical Property Specimens

Following heat treatment, the wheel blank was ultrasonically inspected and radiographed prior to committing it for machining. Figures 76 through 79 show typical radiograph and ultrasonic 'C' scans from the actual wheel blanks. The last

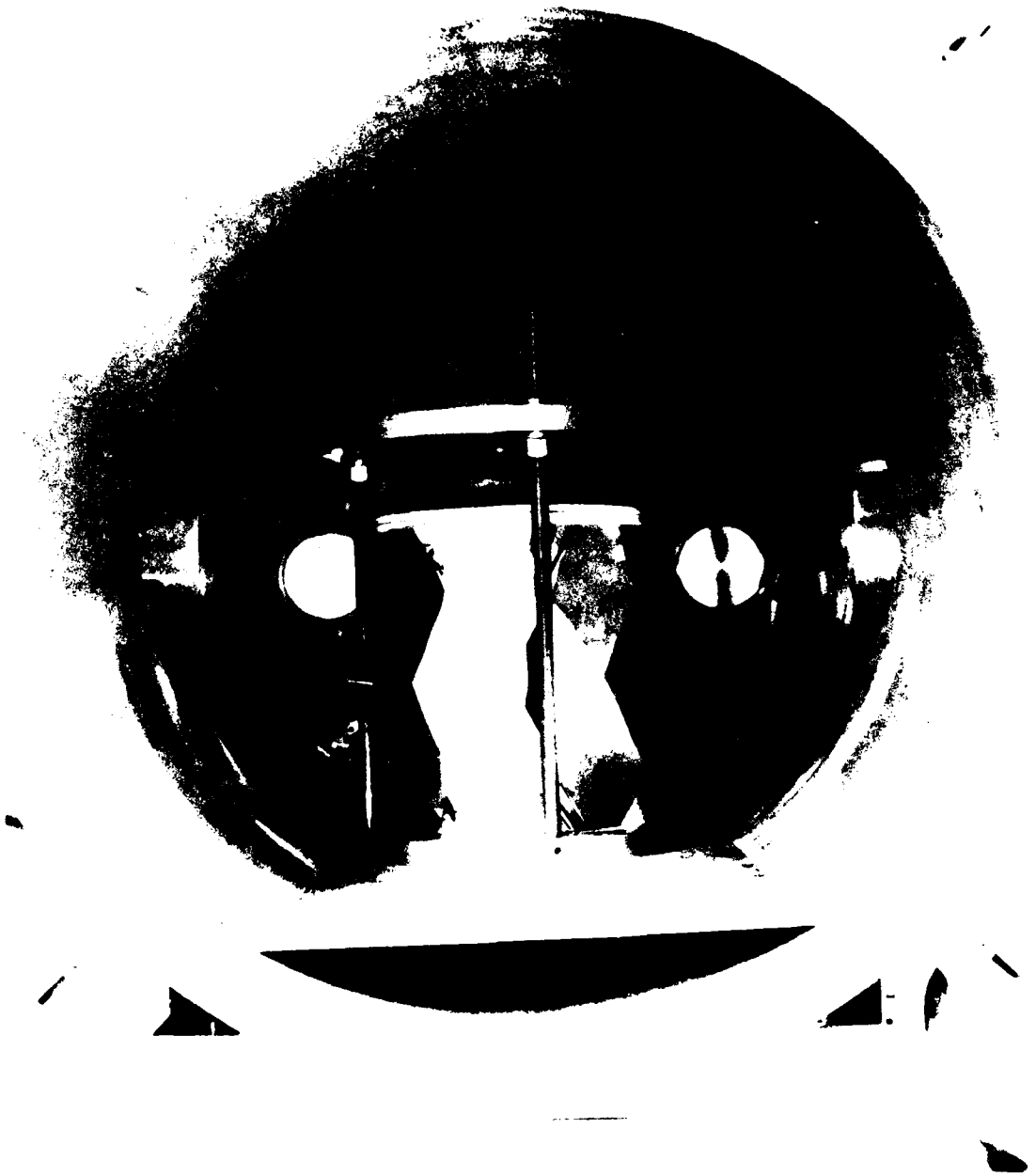

Figure 74. Bond Furnace with WB No. 3 Bond Stack in Place - Immediately after Bond run.

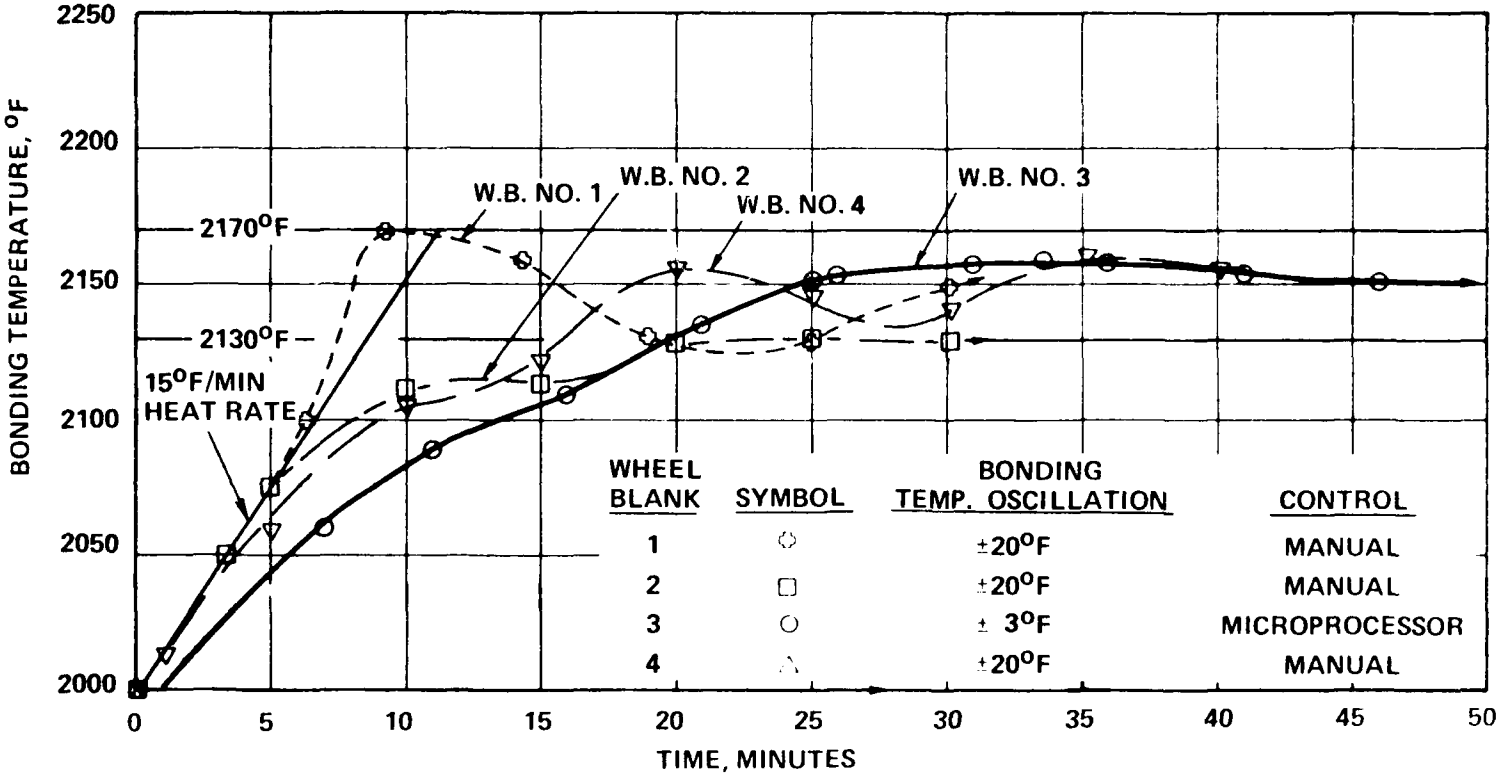

Figure 75. Wheel Blank Bond Run Comparisons.

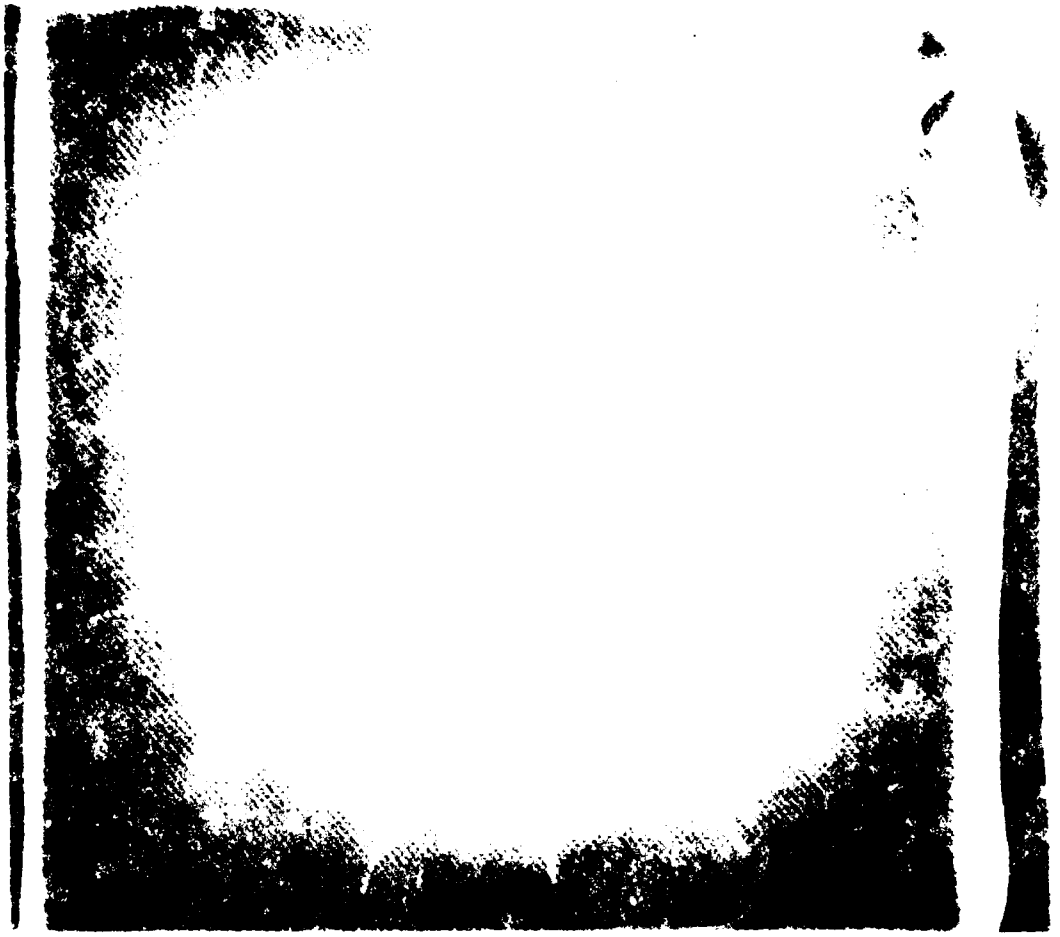

Figure 76. X-Ray Image of WB No. 3 - No Apparent Problem Areas.

Figure 77. "C" Scan of First 1/3 of WB No. 3 - Inlet Side Up (After HIP).

Figure 78. "C" Scan of Central 1/3 of WB No. 3 - Exducer Side Up (After HIP).

Figure 79. "C" Scan of First 1/3 of WB No. 3 - Exducer Side Up (After HIP).

wheel blank bonded, WB No. 3, exhibited excessive porosity in the bore area in ultrasonic testing. This wheel was successfully hot isostatic pressed (HIPped) to remove the porosity. None of the other wheel blanks underwent this HIP processing.

Wheel blanks were then premachined for airflow testing and mechanical property test specimens were removed from excess stock areas. Airflow testing was completed by AiResearch, and the mechanical property testing was completed by Joliet Metallurgical Laboratories and Metals Technology, Inc. (Actual test results are given in Section III).

Machining of Test Wheels

The blade profile machining was completed by Atlas Tool, Inc., Detroit, Michigan, in accordance with the AiResearch M.O.T. Final grind and balance was completed at AiResearch, Phoenix. Figures 80, 81, and 82 show the finish machined wheels, Serial Nos. 1, 2, and 3, respectively.

Cost Analysis Studies

A manufacturing cost estimate has been prepared for the fabrication of the cooled laminated radial turbine wheel (Part 3551760-1) in production quantities of 50 wheels per month. The costing was based on material and fabrication costs obtained from the preparation of manufacturing operations sheets, utilizing current production standards and 1980 rates.

The fabrication process utilizes 24-inch-square sheets for the photoetching process, which results in four 12-inch-square sheets, each containing four laminates. Utilizing the 12-inch-square photoetched sheet, the laminates are processed through the bond alloy application operation and the laminate wheel bonding operations in multiples of four. The end plates are bonded to the laminate wheel stacks during the laminate bonding operation, four at a time. Bonded wheel stacks are processed through the aging heat-treatment cycles 12 at a time. Machining setup times are based on a lot run of 50 wheels.

Figure 80. Finish-Machined Rotor No. 1.

Figure 81. Finish-Machined Rotor No. 2.

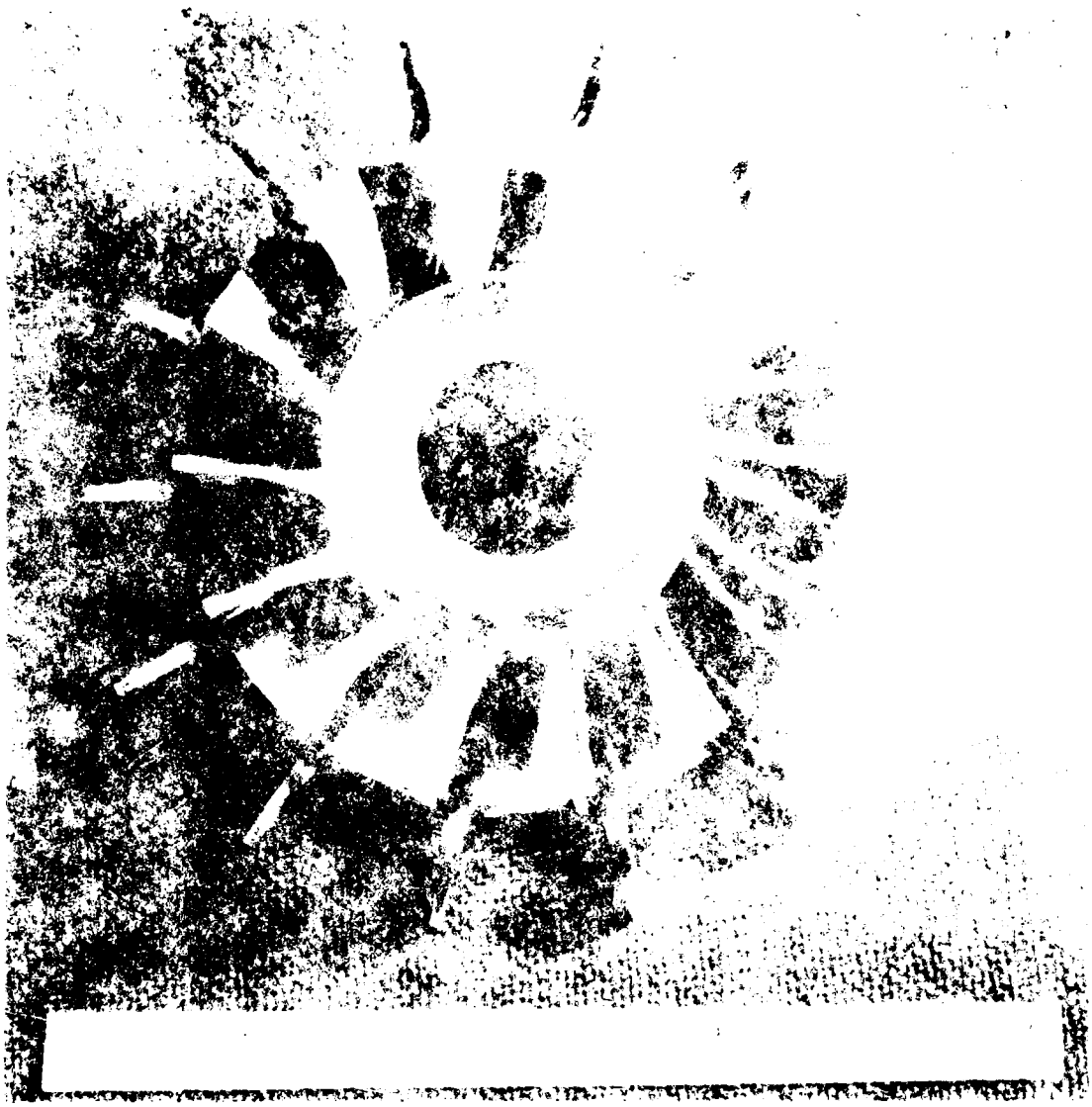

Figure 82. Finish-Machined Rotor No. 3.

The production cost for wheel is as follows:

	Material	Fabrication	Purchases	Total
Laminates	$1,575	$ 575	--	$2,150
Plating Bond Alloy Application	--	$ 200	--	$ 200
End Plates	$ 225	$ 25	--	$ 250
Assembly Bond & Heat Treat	--	$ 150	$250	$ 400
Final Machine & Test	--	$1,250	--	$1,250
	$1,800	$2,200	$250	
Estimated Total Cost to the Government Per Wheel (1980 Dollars)				$4,250

The major cost drivers in this cost breakdown are the Astroloy material costs and the final machining costs. The ECM blade profile machining assumes the use of an advanced 3-D process, and further development will be required for the radial wheel prior to production.

Further cost reductions are definitely possible, including the following:

- The use of a partial etching process will permit the use of th cker Astroloy sheet. Thus, fewer laminates will reduce cost. The use of fewer laminates not only affects material cost but requires fewer bond joints per wheel.

- Cabot-Stellite, the rolling mill supplier, has indicated that the Astroloy sheet rolling capability required for precision laminates is well within industry standards and capacity, and production scale-up should yield a cost-competitive product over that assumed in the estimates.

- In addition, a 33-percent reduction in the total number of laminates for the radial wheel is possible by using a one-piece end plate on the inducer side finish machined with 14 inlet holes and a one-piece end plate on the exducer side with a solid uncooled blade trailing edge.

- The bond alloy application costs would be further reduced over the Borofuse (R) process with the use of a plating process that is currently in development.

SECTION V

PHASE III - MECHANICAL INTEGRITY VERIFICATION

AIRFLOW TESTING

An in-process airflow test of the laminated radial wheel was completed prior to the final blade profile machining, as shown in Figure 83. A minimum flow variation blade-to-blade of ±4.2 percent on Serial No. 2 rotor and ±3.5 percent on Serial No. 3 rotor was achieved. Figure 84 shows that there is less than 2-percent difference in the flow between Serial No. 2 and Serial No. 3 rotors. A check of the Serial No. 3 rotor indicates less than ±3 percent flow variation blade-to-blade after final machining. This compares favorably to cast inserted blades, which have an allowable variation of ±10 percent. Also, zero leakage was demonstrated with the blade cavity air pressurized in a submerged water tank test. This simple in-process test procedure has established the overall integrity and conformity to the design of the cooled rotor prior to final blade profile machining.

WHIRLPIT TESTING

A series of tests was conducted in a whirlpit test facility to assess the mechanical integrity of the turbine wheel.

Stresscoat Test

The purpose of the Stresscoat test was to evaluate regions of high stress concentration in the rotor. This test was conducted in the whirlpit test facility at reduced speeds (50 and 55 krpm) and under carefully controlled temperature and humidity conditions. The stress patterns developed are shown in Figure 85 and occur primarily in the blade fillets. Small local stress concentrations occurred on several blades in the inducer-tip region of Serial No. 2 rotor. These concentrations correlated with known Zyglo and porosity indications previously established on the rotor.

Growth, Overspeed, and Burst Test

The laminated wheel was growth tested to determine the response of the wheel structure to overspeed conditions and to evaluate the burst speed margin. The results of the growth, overspeed, and burst tests are presented in Figure 86, where total diametral-bore growth has been plotted as a function of speed. A maximum total growth of 0.008 inch occurred in the bore under the inducer portion of the disk.

Figure 83. Blade Airflow Test Setup.

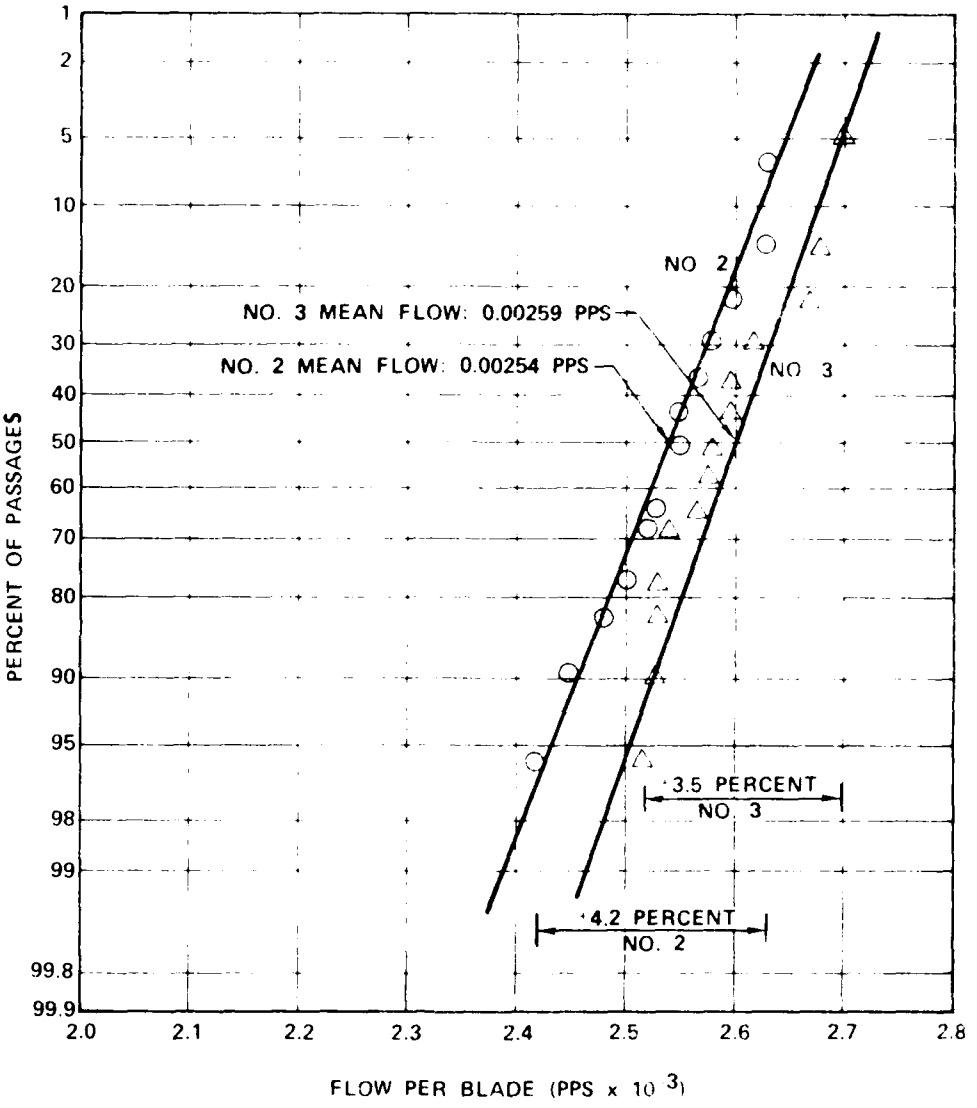

Figure 84. Airflow Test Results.

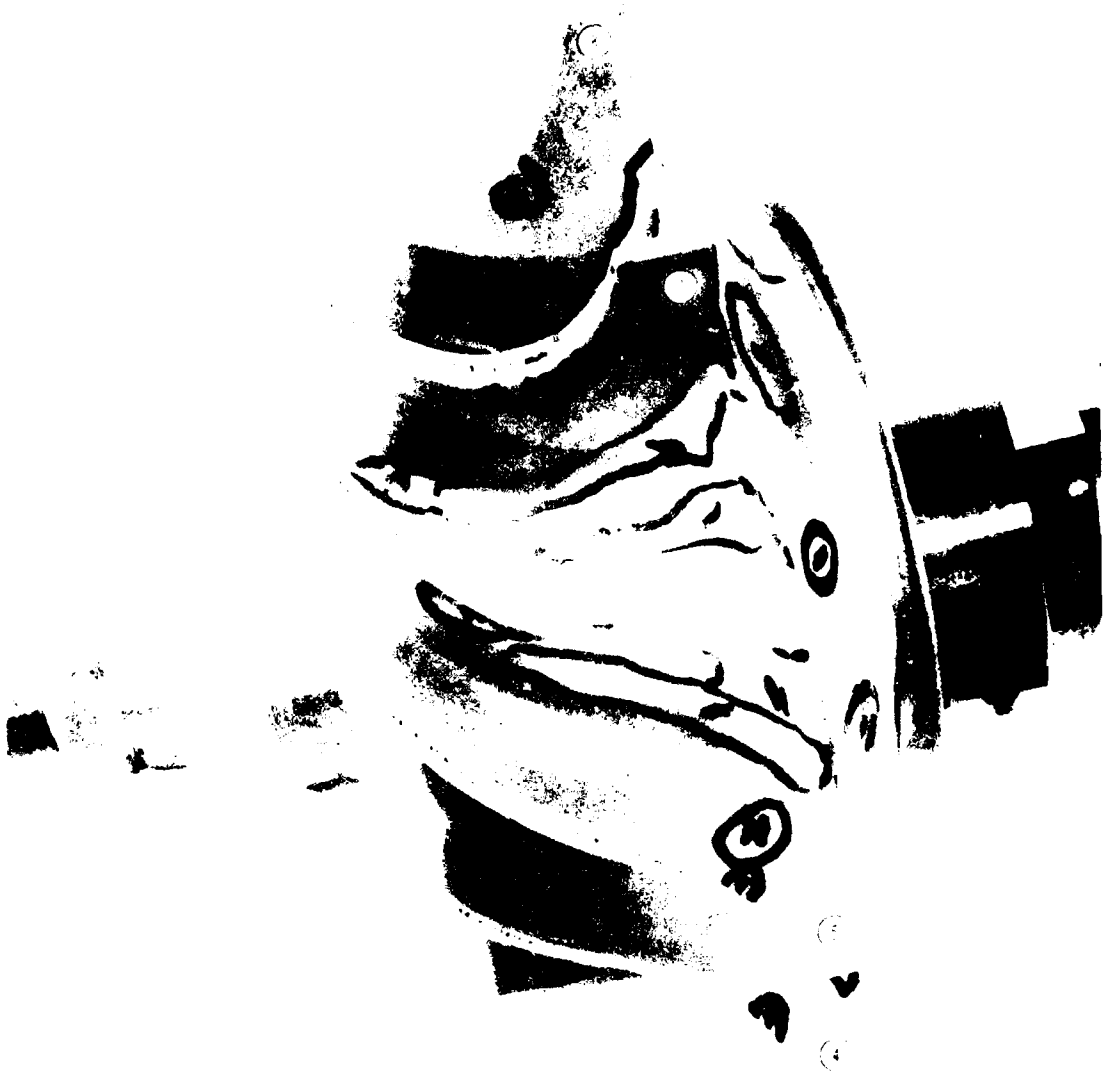

Figure 85. Stresscoat Test Result, Serial No. 2 Rotor.

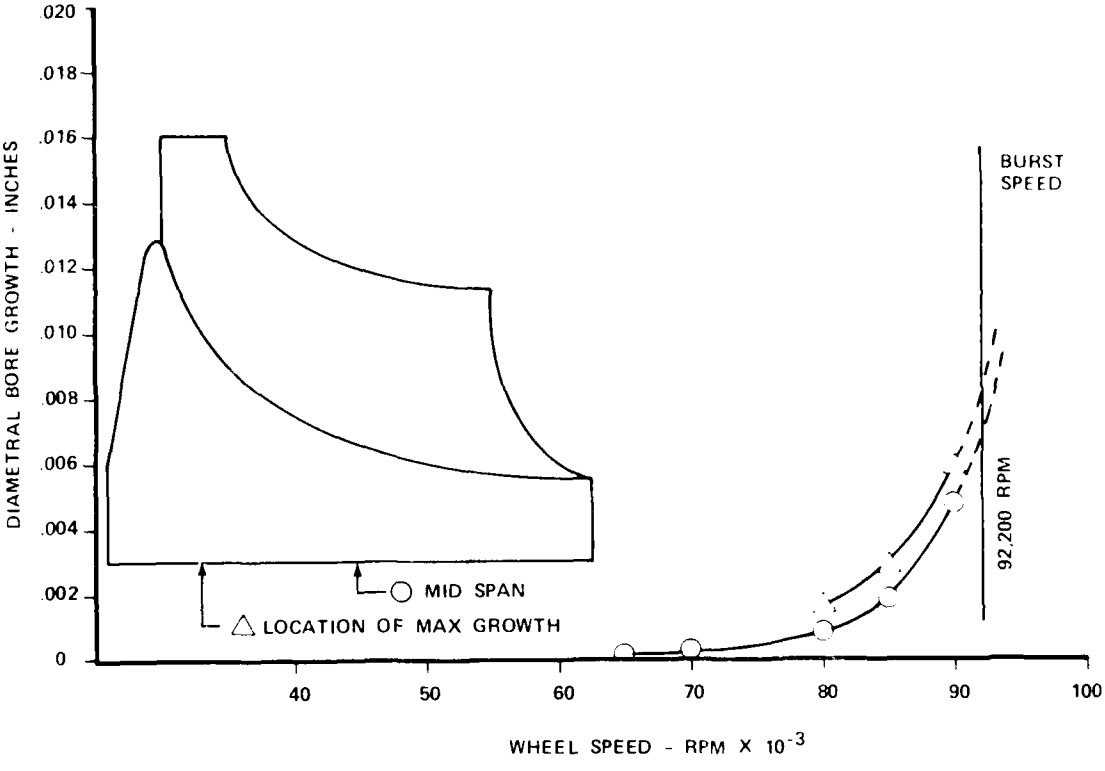

Figure 86. Radial Wheel Growth, Overspeed, and Burst Test Results.

It is theorized that the low transverse ductility in the bore of the laminated test rotor contributed to the reduced burst speed by not permitting local yielding and redistribution of the peak load. In subsequent rotors, optimization of the bond process and hot isostatic pressing to heal locally unbonded areas more than doubled the transverse ductility in the bore. The burst test established the minimum burst speed for a minimum property rotor, but subsequent rotors are expected to have a higher overall burst margin. Figure 87 shows the reassembled fragments after burst grouped in the proper orientation to show a three-piece hub burst (Sections A, B, and C). The delaminations occurred on secondary impact with the whirlpit liner. Figure 88 is a view of the reassembled fragments from the inlet and exducer sides of the rotor. A three-piece hub burst occurred, which is typical of a homogeneous isotopic material, and post-test mechanical properties were verified in the bore. The actual burst speed was 92,200 rpm, 126 percent of the design speed, which is below the design burst speed of 131 percent.

Six-Thousand-Cycle Test

A cyclic test in the whirlpit was conducted to evaluate the mechanical fatigue strength of the laminated turbine rotor. Since the proper thermal gradients in this wheel cannot be duplicated except in an engine environment, only the mechanical (centrifugal) loading was generated. Overspeed cycles were used to compensate for the lack of thermal environment and to provide a meaningful test in 6000 cycles at room-temperature conditions.

The speed increase which accounted for thermal stresses was computed by knowing the peak centrifugal stress in the bore of the disk, which was 141 ksi. The stress at this location increased to 175 ksi when steady-state thermal stresses were included. Because stress is proportional to speed squared, the required whirlpit wheel speed was

$$N = (73,380)\sqrt{\left(\frac{175}{141}\right)} = 81,750 \text{ rpm}$$

The maximum stress in the bore occurred at 1000°F and only LCF property data for Astroloy at room temperature and 1200°F was available. LCF properties at 1000°F were estimated based on a linear interpolation between the room temperature and 1200°F. Examination of LCF data from various other superalloys showed that there was very little difference in the LCF capabilities of the various superalloys. The basic difference in the LCF strengths for the different materials occurs in the very low cyclic-life ranges. Figure 89 shows the LCF properties for IN718 plotted as a function of temperature, with data available for room temperature, 1000°F, and 1200°F. LCF data for Astroloy at room temperature and 1200°F was superimposed onto this curve and cyclic life estimates for different temperatures were calculated. By crossplotting this data from Figure 89, a pseudo

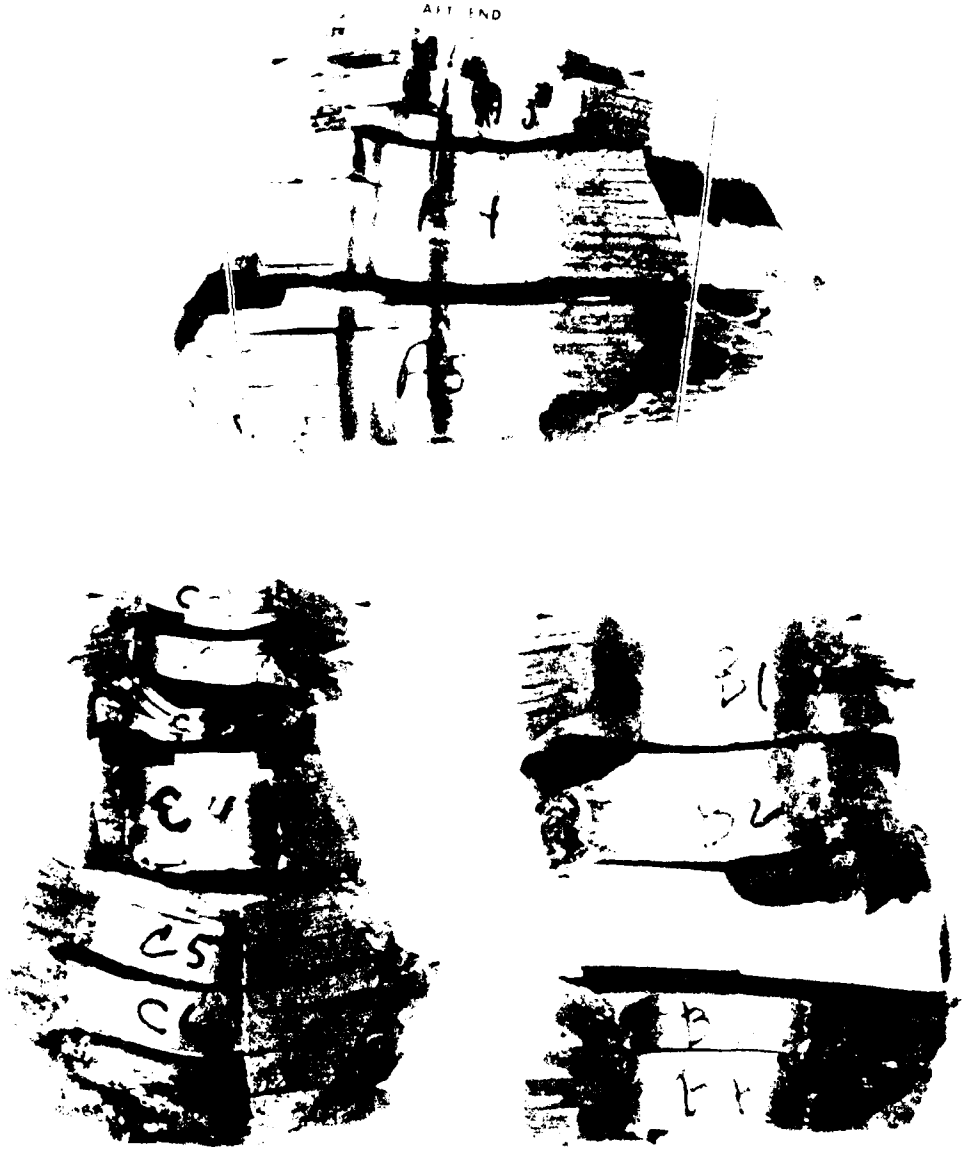

Figure 87. Laminated Radial Turbine, Serial No. 1, Reassembled Fragments After Burst Test - 3-Piece Hub Burst. Arrows Denote Mating Fracture Surfaces.

Figure 88. Laminated Radial Turbine, Serial No. 1, Reassembled Fragments After Burst Test - 3-Piece Hub Burst.

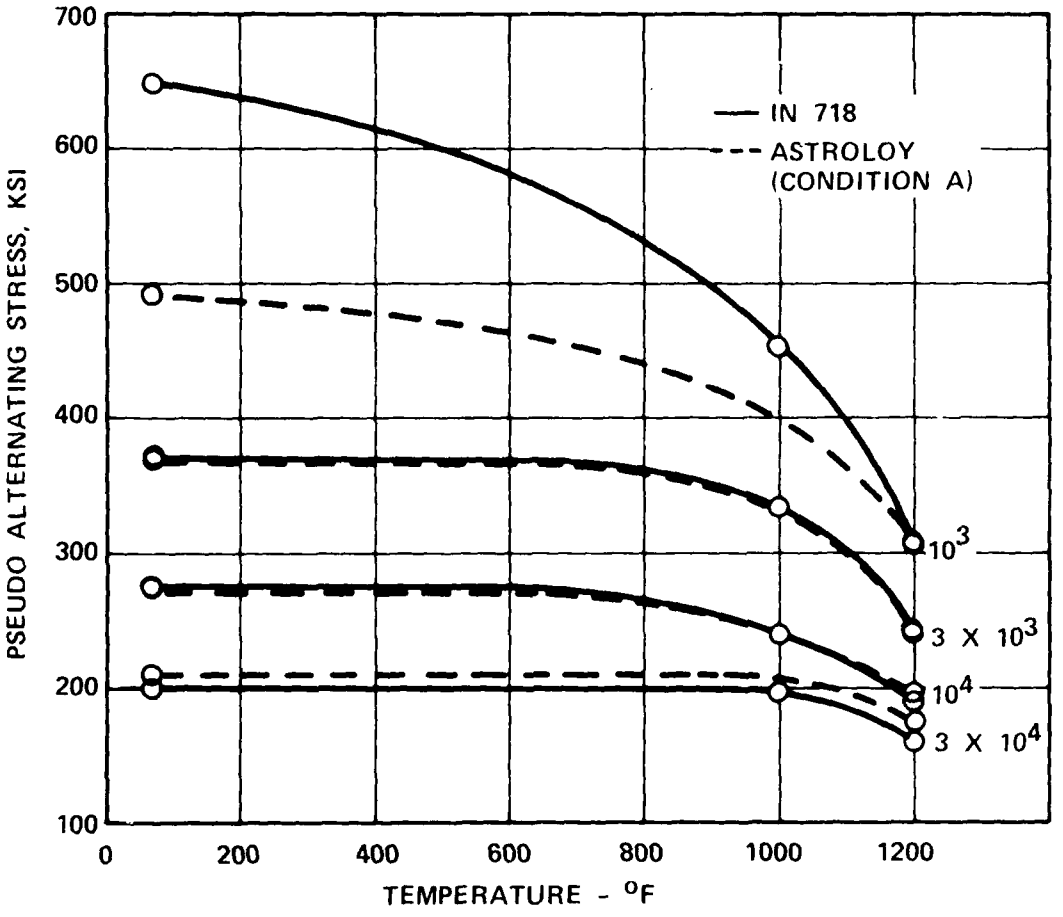

Figure 89. Pseudo Alternating Stress vs. Temperature (K_T = 1, R = -1, 20 CPM).

alternating stress - cyclic life curve was generated at 1000°F (Figure 90). The speed correction for the whirlpit test was then computed using this curve at the required 6000 cycles of LCF life.

$$N = (81,750)\sqrt{\left(\frac{310}{275}\right)} = 86,796 \text{ rpm}$$

Serial No. 3 radial laminated turbine rotor was cycled in the Site "B" whirlpit facility in Torrance (shown in Figure 91) and at a speed range from 8700 to 87,000 rpm. An automatic controller was used to continuously cycle the wheel, and the cycles were recorded on a recording strip chart. A sample of the strip chart recording is included in Figure 92. The average cycle time was 75 seconds. Initially, overspeed and growth tests were performed up to 88,000 rpm and the inducer tip diameter and bore diameters were recorded. After measurable bore growth had been observed, the maximum growth along the bore was recorded. A maximum diametral bore growth of 0.006 inch occurred at 0.80 inch from the inlet side of the wheel at 88,000 rpm. In Figure 93, the maximum diametral growth of the bore versus wheel speed is plotted and is comparable to the previous growth test performed on Serial No. 1 wheel. A Zyglo inspection (AiResearch specification EMS-52309, Class I) of the rotor was conducted and dimensional inspection completed to the following intermediate inspection schedule:

Inspection	Completed Cycles
1	1
2	10
3	35
4	100
5	200
6	350
7	500
8	1000
9	2000
10	4000
11	6000

All intermediate and final inspections indicated the rotor stayed in perfect condition throughout the test with only negligible changes in the bore and inducer tip diameters (±0.0001) and with no apparent Zyglo indications.

A preliminary cycle test was conducted on the Serial No. 2 rotor up to 100-percent design speed to check for a change in the blade porosity indications and stress concentrations identified in Zyglo and Stresscoat. Dimensional and Zyglo inspections at 1, 10, 35, 100, 200, 350, and 500 cycles were completed. No change occurred in the porosity indications; a slight change occurred in the bore and tip diameters (±0.0002 inch); and Zyglo inspection showed that the bore and disk were clean and free of defects.

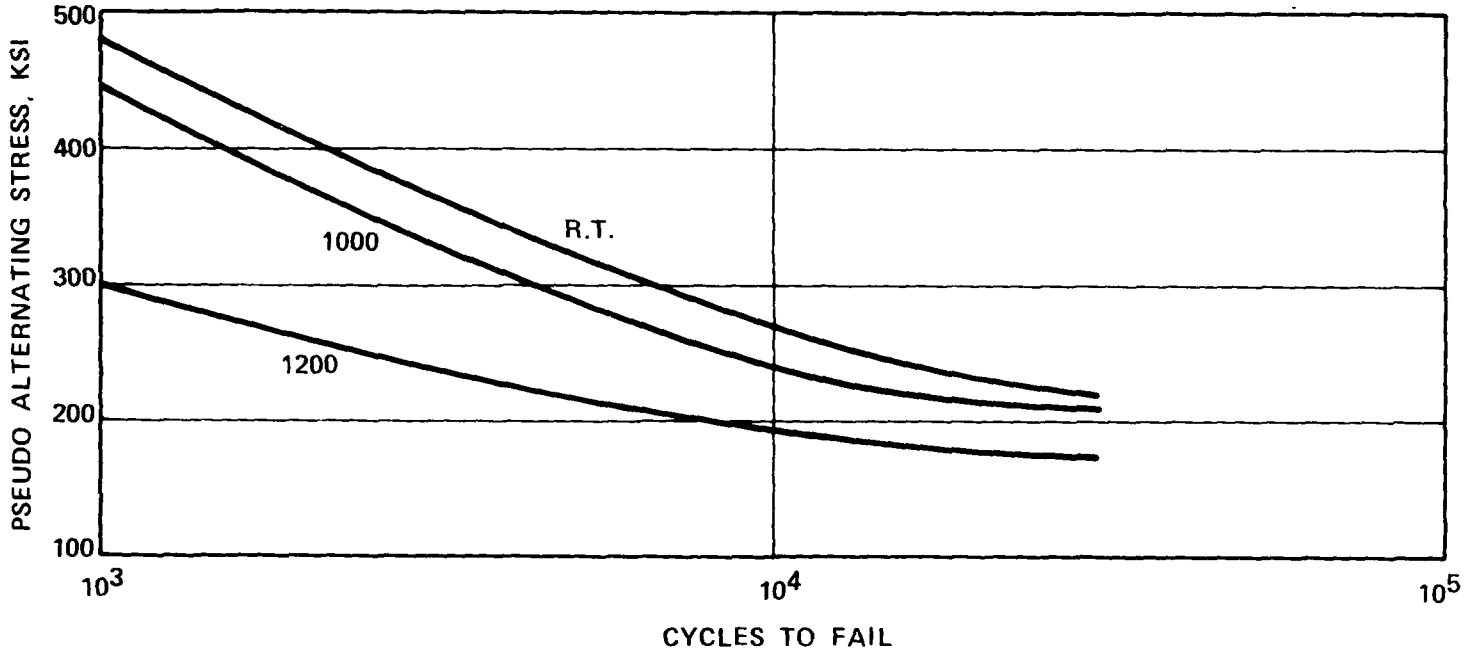

Figure 90. Astroloy (Condition A) Pseudo Alternating Stress vs Cycles to Fail (Ave.) (K_T = 1, R = -1, 20 CPM).

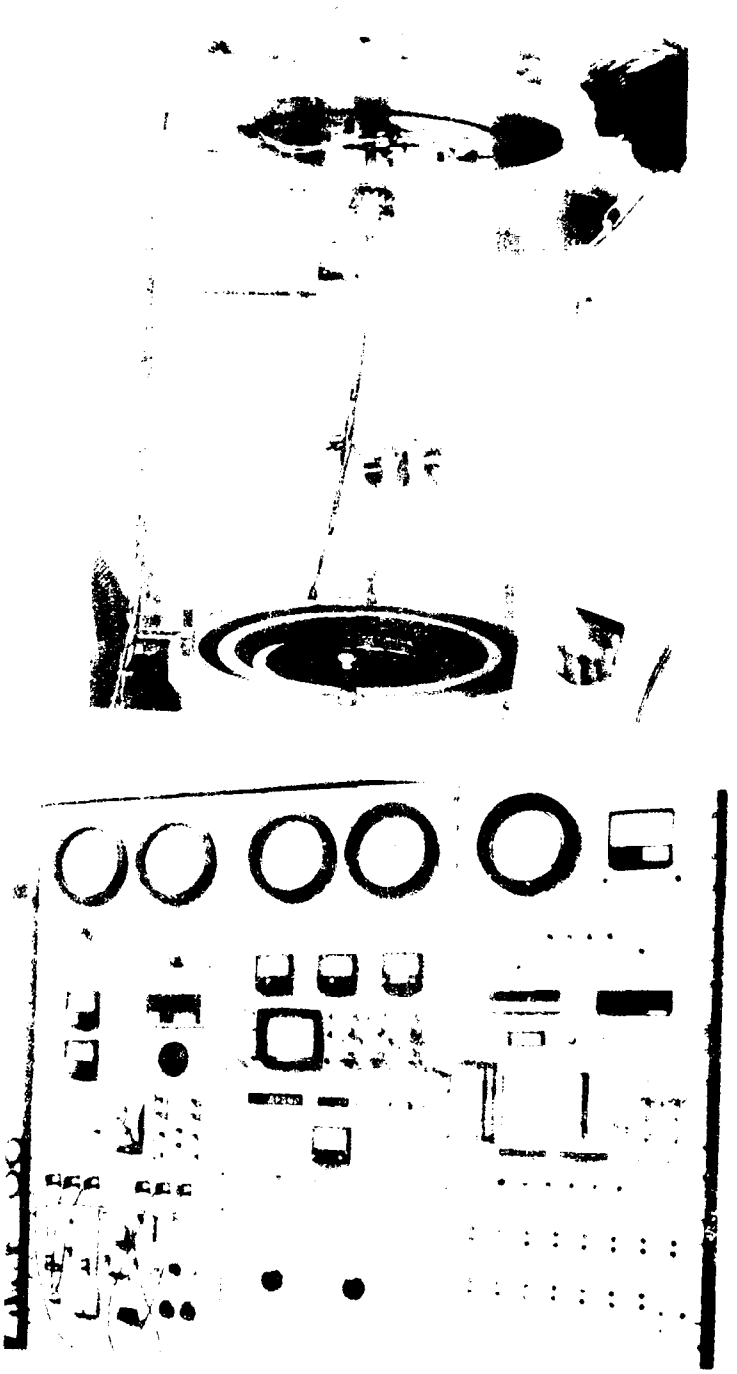

Figure 91. Site "B" Whirlpit Facility.

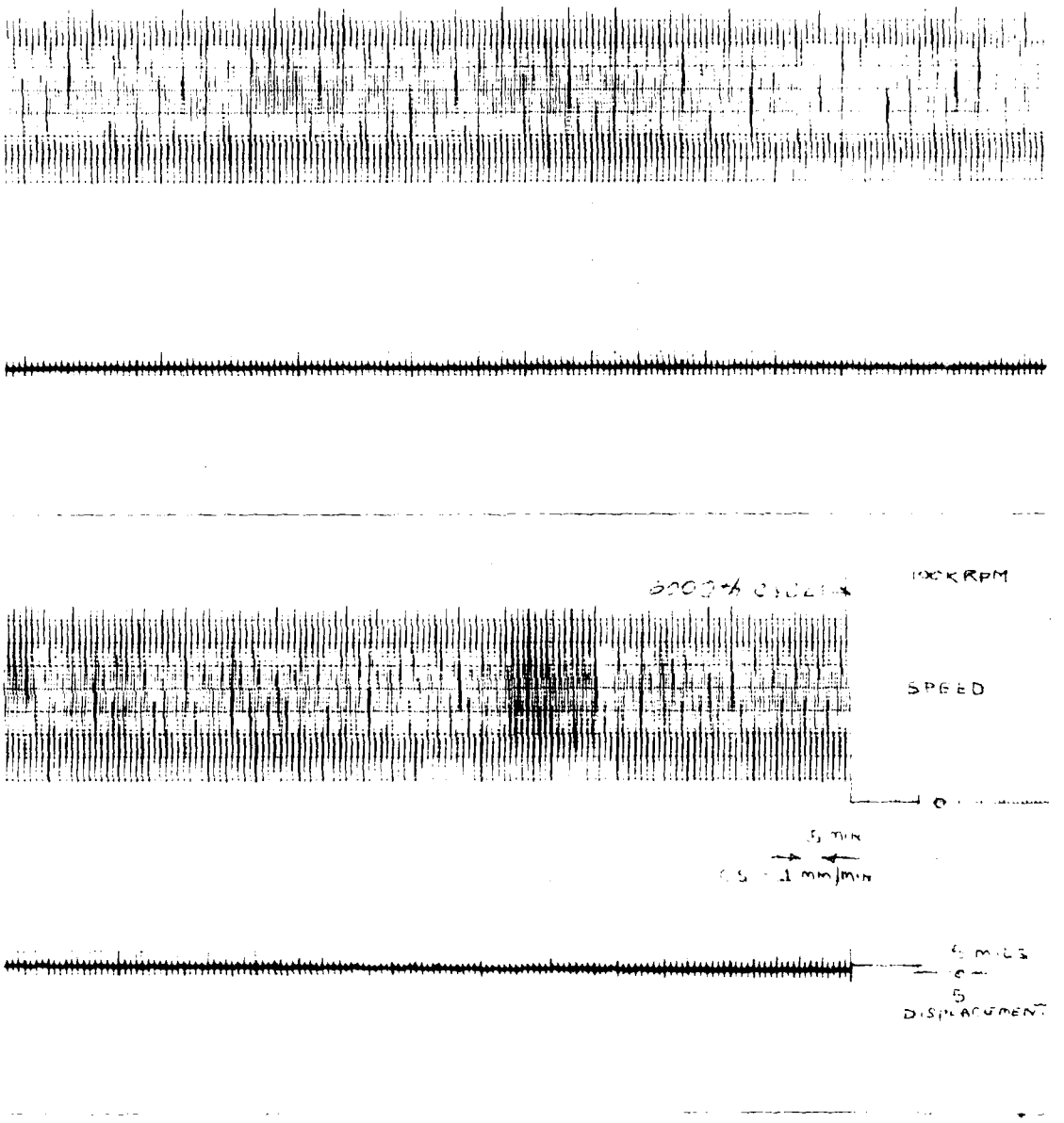

Figure 92. Sample of Strip Chart Recording.

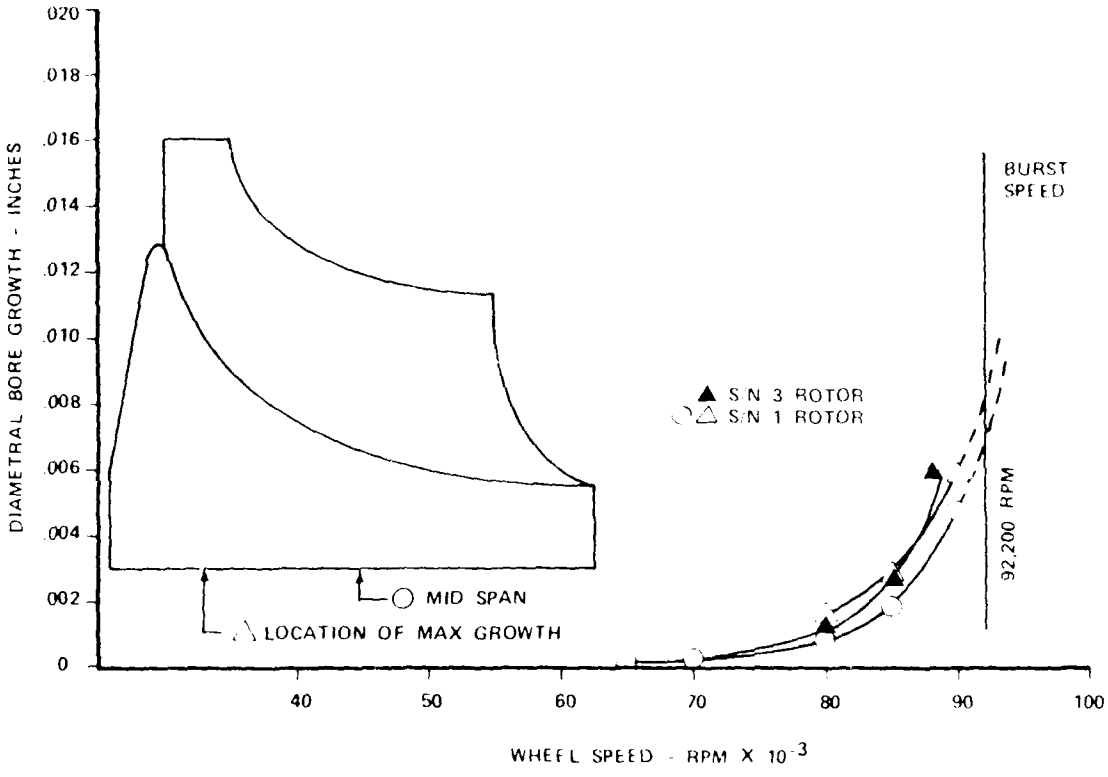

Figure 93. Permanent Growth at Bore Versus Wheel Speed.

SECTION VI

CONCLUSIONS AND RECOMMENDATIONS

This program has demonstrated the feasibility of manufacturing a small high-temperature, cooled, radial turbine utilizing the AiResearch laminate process. It has also proven that the turbine wheel has good integrity and should be given serious consideration for application to an advanced turboshaft propulsion engine. It is recommended that this manufacturing method be further developed by carefully incorporating further cost reductions with no sacrifice to the high performance or mechanical integrity achieved as follows:

- Bond Process Cost Reduction

  Bond process development is recommended using advanced materials with higher stress rupture properties than Astroloy. The potential for cost reduction exists in the laminate bonding process by combining a higher temperature bonding cycle with alternate materials such as AF2-1DA and MAR-M 247, and with a reduction in the quantity of laminates requiring the bond alloy coating system.

- Ductility Improvements

  Optimization of the bonding material systems, bond cycle, and heat treatment is recommended to further increase the transverse ductility of laminated structures. The objective being to further increase the durability and life of a cooled laminated turbine at even higher turbine operating temperatures.

An aerodynamic test of the cooled rotor is recommended primarily to establish the performance effects of rotor cooling flow and secondarily to determine the effect on overall performance of the increased exducer blockage. Heat-transfer testing should be conducted either in a high-temperature turbine rig or in a gas generator to correlate predicted characteristics with actual test results. Testing in a high-temperature environment should be conducted to further establish confidence in the wheel integrity and to determine life characteristics.

REFERENCES

1. Stanitz, J. D., "Some Theoretical Aerodynamic Investigations of Impellers in Radial and Mixed Flow Centrifugal Compressors," Trans. ASME, Vol. 74, No. 4, May 1952.

2. Dovzhik, S. A., and V. M. Kartavenko, "Measurement of the Effect of Flow Swirl on the Efficiency of Annular Ducts and Exhaust Nozzles of Axial Turbomachines," Fluid Mechanics Soviet Research, Vol. 4, No. 4, July-August 1975.

3. Rohlik, Harold E., "Analytical Determination of Radial Inflow Turbine Design Geometry for Maximum Efficiency," NASA TN D-4384, 1968.

4. Kofskey, Milton G., and Nusbaum, William J., "Effects of Specific Speed on Experimental Performance of a Radial-Inflow Turbine," NASA TN D-6605, 1972.

5. Nusbaum, William J., and Charles A. Wasserbauer, "Experimental Performance Evaluation of a 4.59-Inch Radial-Inflow Turbine over a Range of Reynolds Number," NASA TN D-3835.

6. Penny, N., "Rover Case History of Small Gas Turbines," SAE Paper No. 634A, Jan. 1963.

7. Futral, S. M., Jr., and D. E. Holeski, "Experimental Results of Varying the Blade-Shroud Clearance in a 6.02 Inch Radial-Inflow Turbine," NASA TN D-5513, 1970.

8. Calvert, G. S., and U. Okapuu, "Design and Evaluation of a High-Temperature Radial Turbine," Phase I Final Report, USAAVLABS Technical Report 68-69, U.S. Army Aviation Materiel Laboratories, Ft. Eustis, Va., Jan. 1969, AD 688164.

9. Daily, J. W., and R. E. Nece, "Chamber Dimensions Effects on Induced Flow and Frictional Resistance of Enclosed Rotating Disks," J. Basic Eng., Vol. 82, No. 1, Mar. 1960, pp 217-232.

10. "Turbine Design and Application", NASA SP-290, Vol. 2, pp. 131-138.

11. Benedict, R. P., N. A. Carlucci, and S. D. Swetz, "Flow Losses in Abrupt Enlargements and Contractions," Journal of Eng. for Power, Jan. 1966, pp. 73-81.

12. Smith, L. H., Jr., "The Radial-Equilibrium Equation of Turbomachinery," Journal of Eng. for Power, Jan. 1966, pp. 1-12.

13. Katsanis, T., "Use of Arbitrary Quasi-Orthogonals for Calculating Flow Distribution in the Meridional Plane of a Turbomachine," NASA TN D-2546, Dec. 1964.

14. Sams, E. W., "Experimental Investigation of Average Heat Transfer and Friction Coefficients for Air Flowing in Circular Tubes Having Square Thread Type Roughness". NACA RME52D17, Lewis Flight Propulsion Lab., June 1952.

15. Kolar, V., "Heat Transfer in Turbulent Flow of Fluids Through Smooth and Rough Pipes", International Journal of Heat and Mass Transfer, Vol. 8, No. 4, Apr. 1965, pp. 639-653.

16. Furber, B. N., and D. N. Cox, "Heat Transfer and Pressure Drop Measurements in Channels with Whitworth Thread Form Roughness", Journal of Mechanical Engineering Science, Vol. 9, No. 5, Dec. 1967, pp. 339-350.

17. Norris, R. H., "Some Simple Approximate Heat Transfer Correlation for Turbulent Flow in Ducts with Rough Surfaces", ASME Winter Meeting, Dec. 1970, printed in ASME Publication G76 (1970), "Augmentation of Convective Heat and Mass Transfer".

18. Vershure, R. W., Jr., H. R. Fisk, and J. A. Vonada, "Demonstration of a Cooled Laminated Integral Axial Turbine", AIAA Paper 77-949. Reprinted in Journal of Aircraft, Vol. 15, No. 11, pp. 735-742, 1978.

19. Vershure, R. W., Jr., "Engine Demonstration Testing of a Cooled Laminated Axial Turbine", AIAA Paper 79-1229, June 1979.

20. Peterson, R. E., "Stress Concentration Factors," John Wiley and Sons, New York, 1974.

APPENDIX A
MATERIAL SPECIFICATION
THIN GAUGE ASTROLOY SHEET FOR LAMINATED STRUCTURES

1.0 SCOPE

This specification is intended for use in procurement of Astroloy sheet stock of sufficient quality to enable the user to fabricate laminated structures with reasonable assurance of freedom from material-induced defects.

2.0 APPLICABLE DOCUMENTS

2.1 Government Specifications - None

2.2 Non-Government Documents

The following documents form a part of this specification to the extent referenced herein.

2.2.1 AiResearch Specifications

EMS 52338, Revision A - Photochemical-Machining-Quality Thin-Gauge Superalloy Sheet.

3.0 REQUIREMENTS

3.1 General Requirements

The supplied sheet-metal stock must meet all the following requirements.

3.1.1 Character or Quality

Uniform, precision tolerance sheet stock, free from mechanical damage or contamination, must be obtained.

3.1.2 Formulation

The material shall conform to the following chemistry:

	Percent
Carbon	0.03 - 0.09
Manganese	0.15 max.
Sulfur	0.015 max.

	Percent
Phosphorus	0.015 max.
Silicon	0.10 max.
Cobalt	16.0 - 18.0
Chromium	14.0 - 16.0
Molybdenum	4.5 - 5.5
Titanium	3.25 - 3.75
Aluminum	3.75 - 4.25
Boron	0.02 - 0.03
Iron	0.50 max.
Copper	0.10 max.
Zirconium	0.05 max.
Nickel	Remainder

3.1.3 Product Characteristics

The product shall be clean, flat sheet metal of uniform thickness, free from pits, dents, buckles, wrinkles, or other defects. It shall meet all requirements of AiResearch Specification EMS 52338.

3.1.4 Chemical, Electrical, and Mechanical Properties

3.1.4.1 Chemical Properties

Not applicable.

3.1.4.2 Electrical Properties

Not applicable.

3.1.4.3 Mechanical Properties

Specimens shall be machined transverse to the rolling direction and heat treated as follows:

*2150°F (2 hrs)
1950°F (4 hrs)
1550°F (24 hrs)
1400°F (16 hrs)

*Use a temperature ~10°F less than the gamma prime solvus, as determined empirically.

Tensile testing shall be conducted at room temperature and 1400°F along with stress-rupture testing at 1400°F/80 KSI and 1800°F/20 KSI. Test results shall be reported.

3.1.5 Environmental Conditions

Not applicable.

3.1.6 Stability

Not applicable.

3 1.7 Toxic Products and Safety

Not applicable.

3.1.8 Identification and Marking

Coils or cut lengths shall be securely bundled and identified with this specification and lot number, by a durable tag attached or on the tape used to bind the coil or stack. The material shall then be boxed for shipment in a manner to prevent contamination or damage.

Material shall not be identified by marking with inks, paints, or any other material directly on sheet surfaces.

3.1.9 Workmanship

A high quality of workmanship, as evidenced by surface finish and other features described in Section 3.1.3, must be maintained.

3.2 Qualification

Qualification of material shall be determined by AiResearch through such testing as deemed necessary to ensure the suitability of the produced material for incorporation into laminated structures.

3.3 Differentiating Requirements

Not applicable.

4.0 QUALITY ASSURANCE PROVISIONS

4.1 Responsibility for Inspection

Unless otherwise specified in the contract or order, the supplier is responsible for the performance of all inspection requirements as specified herein.

4.2 Special Tests and Examinations

Not applicable.

4.3 Quality Conformance Inspection

Sheet material shall be inspected for conformance to Section 3 of this specification by means of physical measurement devices appropriate to the characteristic being measured (dimension air thickness tester, profilometer, etc.).

4.4 Test Methods

Testing shall be accomplished in accordance with applicable ASTM and/or AiResearch specifications.

5.0 PREPARATION FOR DELIVERY

Preparation for delivery shall include all steps identified in Section 3.1.8. In addition, individual sheets or coil surfaces shall be separated by placing clean paper between each sheet or coil layer.

6.0 NOTES

None.

MATERIAL SPECIFICATION	CODE IDENT NO. 99193	SPECIFICATION NO. [illegible]	REV LTR

1. [illegible]

1.1 This specification [illegible] controls and [illegible] either [illegible] forming-[illegible] [illegible] It shall apply [illegible] to [illegible] such materials [illegible] [illegible].

1.2 [illegible] is required.

1.3 [illegible]

1.3.1 The following documents form a part of this specification to the extent referenced [illegible]

1.3.1.1 Aerospace Material Specification

AMS [illegible] Plates - Nickel, Nickel-Base, and Cobalt-Base Alloy Sheet, Strip, and Plate

AMS [illegible] for Testing and Processing

1.3.1.2 American Society for Testing and Materials

ASTM E 112, Average Grain Size of Metals, Determination

2. [illegible]

2.1 Material shall be supplied in the cold-rolled condition.

2.2 All [illegible] shall meet the applicable AMS or AiResearch specification.

2.2.1 All [illegible] shall be certified by analysis of the melt and/or by analysis of the finished sheet.

2.3 Sheet mechanical properties shall meet the applicable AMS or AiResearch specification [illegible] For sized [illegible], the mechanical properties shall be [illegible]

2.3.1 Tests shall be performed on samples of [illegible] stock and heat-treated [illegible] the appropriate specification.

2.4 Stress-relief annealing temperatures shall be [illegible] so that the recrystallized [illegible] shall not be larger than ASTM 5 [illegible] than the following:

TABLE I - "[illegible]" Grain Size

Thickness, Inch	Grain Size
[illegible]	8
[illegible]	7

2.4.1 These requirements [illegible] not apply to [illegible] where [illegible] metal [illegible].

3. PROCESS [illegible]

3.1 The primary melting [illegible] may be [illegible] VIM or air melting. The secondary remelting operation shall be VAR [illegible].

3.2 During [illegible] rolling, care shall be taken to prevent scratching of the sheet surfaces.

3.3 [illegible] not permitted for [illegible].

3.4 Prior to [illegible] oxidation products [illegible] rolled [illegible] shall be [illegible] of [illegible].

3.4.1 Visual standards may be established [illegible] adherent [illegible] after examination of [illegible].

3.5 Starting stock sheet and strip shall be procured in dimensions [illegible] AMS [illegible]. Either coils or cut lengths may be acceptable, depending upon the [illegible] requirements.

3.6 Annealing heat treatment shall be performed in vacuum of 10^{-5} [illegible], hydrogen atmosphere, or an inert atmosphere such as argon. A dew point of -65 F or lower shall be maintained in all atmospheres. This is required to ensure that there is no loss of alloying elements such as boron, aluminum, and titanium at the sheet surfaces. Water quenching following annealing is not permitted.

3.6.1 If this requirement cannot be met, samples of annealed material shall be submitted to AiResearch Materials Engineering for chemical milling response. Satisfactory [illegible] of the proposed annealing practice shall be based on this test.

3.7 After the first satisfactory lot of material is produced, the [illegible] including, but not restricted to, [illegible] reduction between anneals, annealing temperatures and cycles, and [illegible] operations shall be documented and [illegible] for the "fixed process" [illegible].

3.7.1 That portion of fixed process information considered proprietary by the supplier must be listed on a master [illegible] shall be available to authorized AiResearch personnel upon request.

3.7.2 Changes in the fixed process [illegible] prior AiResearch approval. Process changes that are expected to [illegible] may be optionally submitted as [illegible].

3.8 The sheet shall be finish [illegible] rolling a minimum of [illegible] anneal. A stress relief shall be performed after the final rolling.

4. [illegible]TION

4.1 Flatness shall be determined [illegible] a sheet on a flat surface. The [illegible] curl deviation per foot of length in the free state shall not exceed [illegible].

4.2 [illegible] not permitted for [illegible].

4.3 [illegible] not permitted for [illegible].

4.4 Prior to [illegible] oxidation products [illegible] rolled [illegible] shall be [illegible] of [illegible].

4.4.1 Visual standards may be established [illegible] adherent [illegible] after examination of [illegible].

4.5 Starting stock sheet and strip shall be procured in dimensions [illegible] AMS [illegible]. Either coils or cut lengths may be acceptable, depending upon the [illegible] requirements.

4.6 Annealing heat treatment shall be performed in vacuum of 10^{-5} [illegible], hydrogen atmosphere, or an inert atmosphere such as argon. A dew point of -65 F or lower shall be maintained in all atmospheres. This is required to ensure that there is no loss of alloying elements such as boron, aluminum, and titanium at the sheet surfaces. Water quenching following annealing is not permitted.

4.6.1 If this requirement cannot be met, samples of annealed material shall be submitted to AiResearch Materials Engineering for chemical milling response. Satisfactory [illegible] of the proposed annealing practice shall be based on this test.

4.7 After the first satisfactory lot of material is produced, the [illegible] including, but not restricted to, [illegible] reduction between anneals, annealing temperatures and cycles, and [illegible] operations shall be documented and [illegible] for the "fixed process" [illegible].

4.7.1 That portion of fixed process information considered proprietary by the supplier must be listed on a master [illegible] shall be available to authorized AiResearch personnel upon request.

4.7.2 Changes in the fixed process [illegible] prior AiResearch approval. Process changes that are expected to [illegible] may be optionally submitted as [illegible].

4.8 The sheet shall be finish [illegible] rolling a minimum of [illegible] anneal. A stress relief shall be performed after the final rolling.

5. [illegible]TION

5.1 Flatness shall be determined [illegible] a sheet on a flat surface. The [illegible] curl deviation per foot of length in the free state shall not exceed [illegible].

FORM P5704-3 PAGE

30
F

MATERIAL SPECIFICATION	CODE IDENT NO. 99193	SPECIFICATION NO	REV LTR

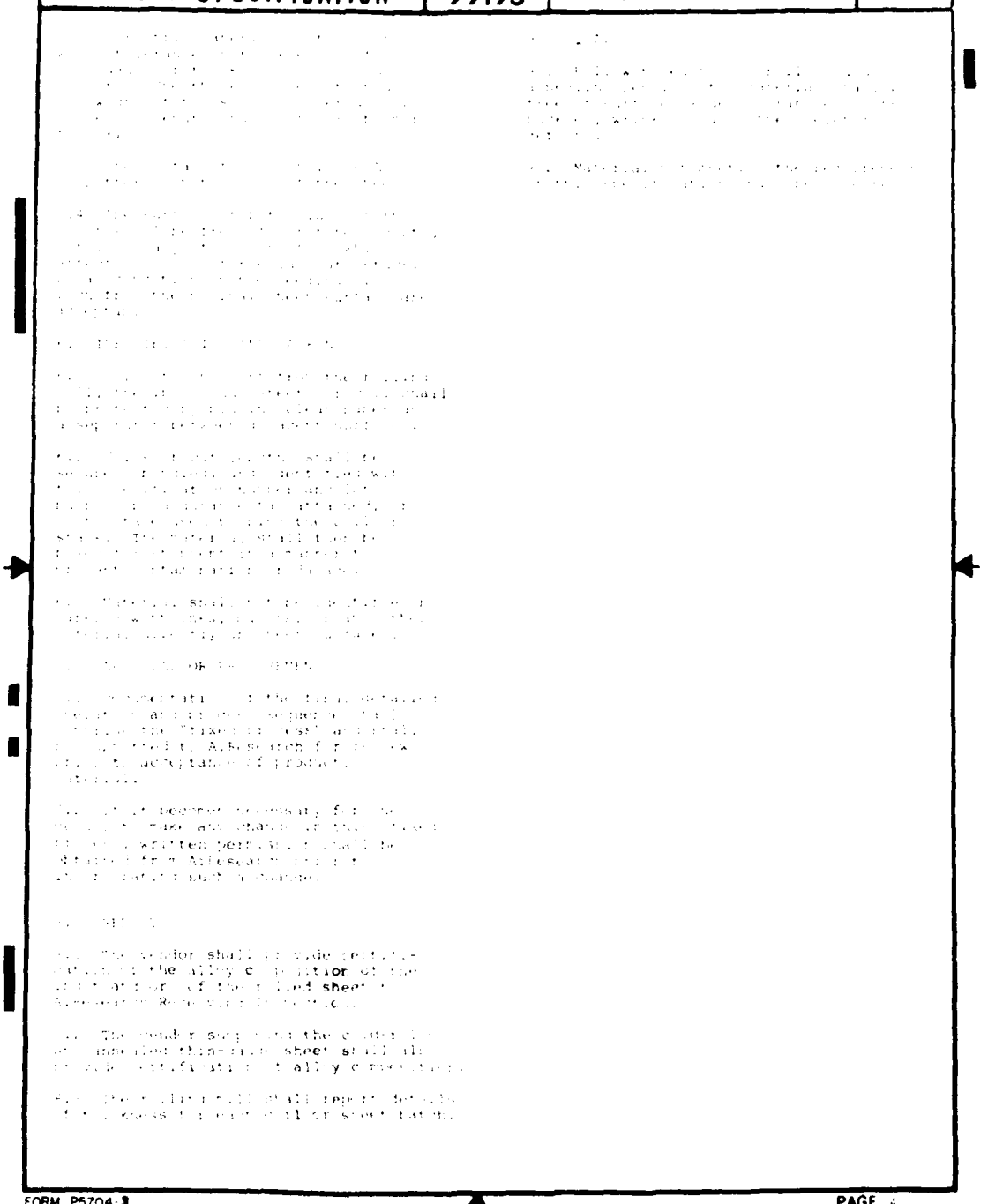

30
B

APPENDIX B

PROCESS SPECIFICATION

1.0 SCOPE

The scope of this specification is to include, but not necessarily be limited to, the fabrication of an internally cooled, laminated radial turbine wheel constructed of Astroloy sheet stock, joined by an activated diffusion bonding process, and machined to final dimensions. This specification may also be applicable to other similar laminated structures.

2.0 APPLICABLE DOCUMENTS

2.1 Government Documents

None applicable.

2.2 Non-Government Documents

The following documents form a part of this specification to the extent referenced herein.

2.2.1 AiResearch Specifications

PC5021, Rev. B - Photochemical Machining of Shapes from Superalloy sheet.

EMS 52338, Rev. A - Photochemical-Machining-Quality Thin-Gauge Superalloy Sheet

3.0 REQUIREMENTS

3.1 Equipment

3.1.1 Dry (dew point of -65°F or lower) argon or helium gas and manifolding, as required.

3.1.2 Assembly and bonding fixtures as required to hold alignment, flatness, and parallelism of the laminate stack during the bonding operation.

3.1.3 A method capable of heating and unit loading the laminate stack to the bonding temperature at the required heating rate and unit pressure, and compatible with power supplies and vacuum furnace chamber design.

3.1.4 A vacuum chamber of sufficient size and pumping system gas load capacity to meet the bonding requirements.

3.2 Materials

3.2.1 Astroloy sheet stock, 0.020 inch nominal thickness per Material Specification.

3.2.2 Solutions listed below to commercial quality standards for photoresist coating, stripping, and cleaning, unless otherwise referenced in PC5021.

(a) Dupont Riston No. 1220 Dry Film Photoresist or equivalent

(b) Kodak Micro-Resist Thinner - photoresist thinning solution

(c) Kodak Thin Film Resist (KTFR) - photoresist solution

(d) Developer solution - Kodak developer or Stoddard equivalent

(e) Hydrochloric acid (muriatic acid)

(f) Methanol

(g) Freon TF solvent

(h) Caustic permanganate solution

(i) Hydrofluoric/nitric acid solution

(j) Alkaline steel cleaner - Wyandot F.S. or equivalent solution

(k) Deionized water

(l) Turco Caviclean No. 2 soap solution

(m) Batco No. 44 photoresist stripping solution

(n) Trichlorethane 1,1,1 developer solution

3.2.3 Solution for chemical milling and chemical machining, as referenced in AiResearch Specification PC5021.

3.3 Required Procedures and Operations

3.3.1 Photochemical Etching (Blanking) of Laminates

3.3.1.1 Laminates shall be prepared by means of photochemical etching per AiResearch Specification PC5021, after the sheet material has been chemically milled to the required thickness and surface finish per PC5021.

3.3.1.2 Bore diameter of the laminates will be used for gauge purposes, unless otherwise specified.

3.3.2 Laminate Detail Preparation

3.3.2.1 The individual laminates shall be visually inspected at up to 10X magnification for defects. Those having defects that exceed the allowable limits of size and location will be rejected (see Figure B-1).

3.3.2.2 A full-size map of each laminate shall be prepared, recording location and size of any minor surface defects and identifying the condition (coated or bare) and position of the laminate in the turbine wheel assembly.

3.3.2.3 All laminates for use in the turbine wheel shall be cleaned and packaged per the following procedures prior to final assembly for bonding.

3.3.2.3.1 Chemical cleaning procedure: Place laminate details in parts cleaning racks and process through the following steps, allowing the time indicated for each step.

(a) Vapor degrease for 15 minutes.

(b) Immerse in Alkaline steel cleaner at 180°F, with air agitation, for 30 minutes (no cathodic or anodic activation allowed).

(c) Spray rinse with tap water.

(d) Immerse in 20-percent hydrofluoric/nitric acid for 30 seconds.

(e) Spray rinse with tap water.

(f) Immerse in caustic permanganate at 180°F, with air agitation, for 3 hours.

(g) Immersion rinse in 2 drag-out tanks, in sequence.

(h) Spray rinse with deionized water.

(i) Immerse in 80 percent muriatic acid for 5 minutes.

(j) Spray rinse with deionized water.

(k) Immersion rinse in deionized water for 10 minutes.

(l) Spray rinse with deionized water.

(m) Water-break-free test each detail, taking care to handle laminates with clean metallic tongs.

- LAMINATES WILL BE REJECTED IF ETCH PITS OR OTHER UNDESIRABLE FEATURES OCCUR WITHIN 0.020" OF ANY BLADE COOLING PASSAGE OR WITHIN 300 PERCENT OF THEIR MAXIMUM DIMENSION TO THE DISK BORE OR OTHER MACHINED SURFACE.

- ANY FEATURE BELOW 0.015" IN MAXIMUM DIMENSION IS CONSIDERED UNINTERPRETABLE.

- UNDESIRABLE FEATURES: BLADE – 0.100" MAXIMUM, AND DISK – 0.200" MAXIMUM, WITH NO TWO FEATURES CLOSER TO EACH OTHER THAN 200 PERCENT OF MAXIMUM DIMENSION IN THE RADIAL DIRECTION. EXCEEDING THESE DIMENSIONS WILL CAUSE THE LAMINATE TO BE REJECTED.

- ANY QUESTIONABLE AREAS WILL BE RESOLVED BY DIRECT MEASUREMENT AND COMPARISON WITH THE APPROPRIATE BLUEPRINT DRAWINGS AND 10-TIMES LAYOUT DRAWINGS OF FINISH-MACHINED CONTOURS.

- IF ANY QUESTION REMAINS AFTER MEASUREMENT AND COMPARISON, THE LAMINATE SHALL BE REJECTED.

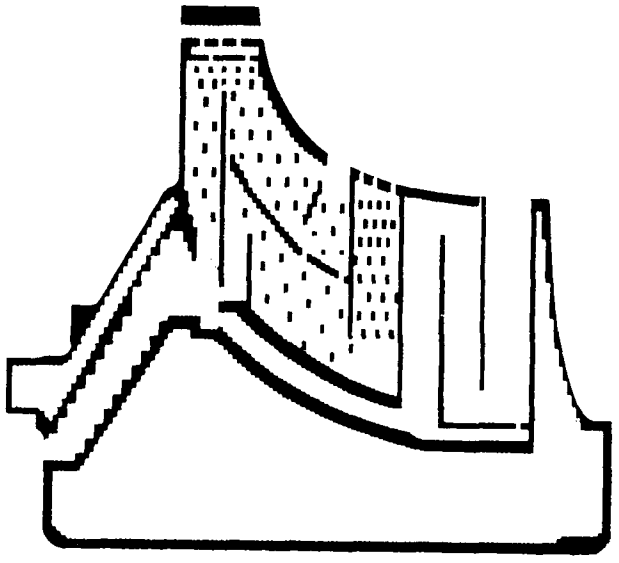

Figure B-1. Chart of Allowable Sizes and Locations of Unintentional Features.

(n) Repeat Steps (i) through (m) for any details exhibiting water-break indications.

(o) Dry laminates in a circulating air oven prior to packaging in clean protective wrap, taking care to handle all laminates with lint-free nylon gloves.

3.3.2.3.2 Organic residue cleaning procedure: This procedure is applicable to all turbine wheel blank details, prior to Borofuse® coating. Note that this is a clean room activity and all cleanliness procedures specified in AiResearch Cleaning Specification C-38 and FED-STD-209, 100,000 level clean room standards, must be observed.

(a) Immerse in Turco Caviclean No. 2 at 140°F, with ultrasonic agitation for 6 minutes.

(b) Rinse with deionized water.

(c) Immerse in 80-percent muriatic acid for 5 minutes.

(d) Rinse with deionized water.

(e) Conduct water-break-free test of each detail. Repeat Steps (a) through (d) if a water-break condition exists.

(f) Dry in circulating hot air oven.

(g) Rinse with freon TF virgin solvent.

(h) Conduct particulate material rinse test of each rack of 10 details. No detectable material allowed.

(i) Conduct nonvolatile residual (NVR) test on 10 details per 1000 ml (1 liter) of solvent. The maximum permissible NVR is 0.25 mg. Repeat Steps (a) through (i) if this limit is exceeded.

(j) Package laminate details in nylon film bags and seal with tape.

3.3.2.4 Those laminates to be coated shall be sent to Materials Development Corp., Medford, Mass. for coating with "Borofuse"® process. Boron levels shall meet a 0.0046 gm/in^2 ±0.0005 gm in^2 requirement. The vendor will be instructed to handle laminates with clean, lint-free gloves or clean metallic tongs, and no further cleaning will be permitted.

3.3.2.5 Laminates returning from the coating vendor shall be inspected for boron level and possible contamination prior to

AD-A098 120 GHENT RIJKSUNIVERSITEIT (BELGIUM) LAB FOR EXPERIMENTA--ETC F/G 21/5
COOLED, LAMINATED RADIAL TURBINE DEMONSTRATION PROGRAM.(U)
FEB 81 R W VERSHURE, G D LARGE, L J MEYER DAAJ02-77-C-0032
UNCLASSIFIED 21-3684 USAAVRADCOM-TR-81-D-7 NL

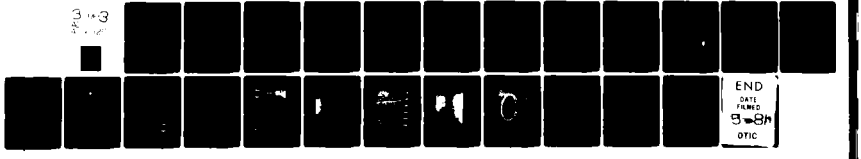

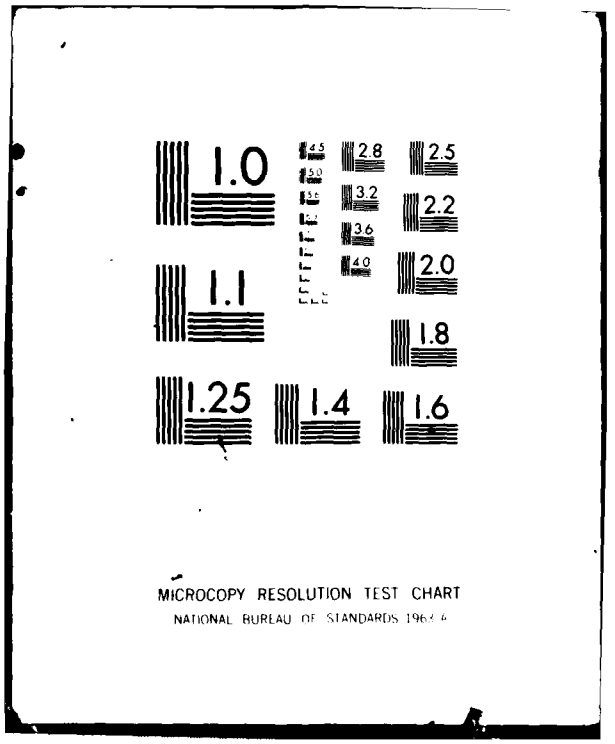
1.0
1.1
1.25
1.4
1.6
1.8
2.0
2.2
2.5
2.8
3.2
3.6
4.0
4.5
5.0
MICROCOPY RESOLUTION TEST CHART
NATIONAL BUREAU OF STANDARDS 1963-A

final assembly. This shall be accomplished by destructive examination of test samples, which shall accompany every shipment, lot, or run through the vendor's process. In addition, coated laminates shall repeat cleaning steps (g) through (i) listed in 3.3.2.3.2, organic residue cleaning procedure, prior to final assembly.

3.3.3 Assembly

3.3.3.1 The laminate details, assembly tooling, bond tooling, thermocouples, and any required tools shall all be cleaned and handled to preclude any contamination of the assembly area or the laminate assembly.

3.3.3.2 The bond tooling, a sufficient number of new Type K thermocouples, and the laminate details shall be assembled in a clean-room environment. This assembly shall either be immediately bonded or sealed in a nylon film bag until such time as the bonding can take place.

3.3.4 Bonding

3.3.4.1 The laminate stack and bonding assembly shall be placed in the vacuum chamber, along with the required loading, heating, and temperature measurement devices, and the chamber sealed.

3.3.4.2 The vacuum chamber shall be pumped down to a pressure $\leq 1.0 \times 10^{-4}$ Torr prior to starting the bonding heat cycle and maintained at a pressure level $< 1 \times 10^{-4}$ Torr throughout the bonding cycle.

3.3.4.3 The bonding cycle shall consist of heating to ~1400°F, holding for an outgassing period, followed by a steady heating rate of 15°F/minute to the specified temperature (2150°F), with a 2-hour hold at this temperature. At this time, dry argon or helium gas may be used to cool the turbine wheel to approximately ambient temperature, at which point the furnace will be unloaded and the bonded turbine wheel removed from the bond tooling.

3.3.5 Heat Treatment

Following the bonding operation, additional heat treating will be performed according to the following schedule.

3.3.5.1 Solution treat in a vacuum at 2130°F. Hold at this temperature for 2 hours, followed by inert gas fan cooling at 50°F/min to less than 1400°F. Continue to cool to approximately ambient temperature.

3.3.5.2 Stabilize in a vacuum at 1975°F for 4 hours, followed by inert gas fan cool to ambient temperature.

3.3.5.3 Age in a protective atmosphere at 1550°F for 4 hours, followed by equivalent air cool to ambient temperature.

3.3.5.4 Age in a protective atmosphere at 1400°F for 16 hours, followed by equivalent air cool to ambient temperature.

3.3.6 Inspection and Nondestructive Evaluation

After heat treatment, sequential testing will be carried out to ascertain the integrity of the bonded turbine wheel.

3.3.6.1 Dimensional inspection will be performed to determine if flatness, parallelism and thickness are within allowable limits.

3.3.6.2 Visual inspection for evidence of excessive flow will be performed.

3.3.6.3 Ultrasonic inspection for areas of disbond or other potential defects will be performed (using the techniques developed on the ultrasonic calibration standards) and 'C' scan records made, including areas of the bonded turbine wheel which contain synthetic defects.

3.3.6.4 Mechanical and metallographic test specimens will be taken from areas of excess stock in each bonded turbine wheel (bore area in an axial orientation and areas outside the blades in a radial orientation). Results of mechanical property testing will be recorded and maintained.

31
F

3.3.7 Machining

The aerodynamic blade machining profile will be duplicated on the program turbine wheels. Electrochemical machining (ECM) may also be used. Machining steps are identified in AiResearch M.O.T. 3551760-1.

3.3.7.1 Airflow Inspection

The cooling passages of the turbine wheel shall undergo a bench airflow test to verify design flows and pressure losses. Each blade flow channel shall be flow checked independently and evaluated for repeatability. This inspection shall be carried out after rough machining. Final machining will be carried out only after acceptable airflow is established.

3.3.8 Post-Machining Inspection

3.3.8.1 Each finish-machined turbine wheel shall be dimensionally inspected and dye penetrant inspected for evidence of cracking or delamination. Radiographic inspection of the blades may also be performed at this time.

3.4 Recommended Procedures and Operations

The substitution of a hot isostatic pressing (HIP) operation in place of Step 3.3.5.1 is recommended. Parameters are as follow: HIP in virgin argon gas at 2130°F and 22,500 psi pressure for 3 hours. Cool at ~50°F/min to less than 1400°F. Continue to cool to ambient temperature.

3.5 Certification

Not applicable for initial 3-rotor fabrication effort.

4.0 QUALITY ASSURANCE PROVISIONS

The following tests and examination are to be performed to ensure process conformity to the requirements set forth in Section 3.

4.1 Etchant Quality

Prior to the chemical milling of an Astroloy sheet lot, the etching rate and quality of surface finish shall be determined by chemical milling a sample from the same lot of sheet, and comparing etch rate and surface finish to the specifications and reference photographs set forth in AiResearch Specification PC5021, Rev. B.

4.2 Laminate Detail Quality

31
B

After photochemical machining, the laminate details or the corresponding maps shall be checked against an allowable defect size and location chart (Figure 1) to ensure that no undesirable features are incorporated in the turbine wheel.

4.3 Cleanliness and Bond Coating

Prior to bonding the laminate detail stack, NVR test results must conform to the requirements set forth in Section 3. The test samples which accompanied the Borofuse® coated laminate details through processing must be destructively examined and meet the requirements set forth in Sections 3.3.2.3.2 and 3.3.2.4, as well as demonstrate a contaminant-free interface after bonding.

4.4 Bonded Rotor

Prior to machining of the bonded turbine wheel stack, results of dimensional, visual, ultrasonic, and mechanical property testing must be examined for conformance to the applicable limits as set forth in Section 3 or the supplied inspection document.

4.5 Machined Rotor

Before release of the turbine wheel for performance testing, the results of dimensional, dye-penetrant, radiographic and bench airflow inspections must confirm that the rotor is within the design limits.

4.6 Responsibility for Inspection

Unless otherwise specified in the contract, AiResearch is responsible for the performance of all inspection requirements as specified herein. Unless otherwise specified, a subcontract supplier to AiResearch may utilize his own facilities or any commercial laboratory acceptable to AiResearch Quality Assurance. The Government reserves the right to perform any of the inspections set forth in the specification where such inspections are deemed necessary to assure that supplies and services conform to prescribed requirements.

4.7 Monitoring Procedures for Equipment Used in Process

Equipment used in the process shall be inspected for proper function and/or calibration at established intervals, and in addition, at any time when difficulties in the process suggest that equipment malfunction may be a contributing factor.

4.8 Monitoring Procedures for Materials

All materials used in the process shall be inspected for quality and suitability for use upon initial receipt and at any time when difficulty in the process suggests that material may be a contributing factor.

4.9 Certification of Operators or Process Technique

Not applicable to initial research and development effort.

4.10 Test Methods

All testing of materials subjected to this process shall, when applicable, be in accordance with ASTM specifications and/or AiResearch specifications, as necessary, to determine that the process has been properly performed.

5.0 PREPARATION FOR DELIVERY

This section is not applicable to this specification.

6.0 NOTES

6.1 Intended Use

The intended use of this specification is the fabrication of a laminated turbine wheel as described in Section 1.

1. INTRODUCTION

1.1 This specification describes the procedure, solutions, material, and equipment for photochemical machining nickel-base superalloys, such as Astroloy and Waspeloy, in sheet form.

1.2 Two methods of photo-resist application are covered. Each method has advantages for particular geometries and materials. Unless otherwise specified, either method is acceptable.

2. APPLICABLE DOCUMENTS

2.1 The following documents form a part of this specification to the extent referenced herein.

2.1.1 AiResearch Specifications

EMS52338 - Photoetching-Quality Thin-Gauge Superalloy Sheet

3. SPECIAL EQUIPMENT

3.1 Photo-resist dip coating tank with controlled-speed withdrawal.

3.2 Infrared drying oven with temperature controls and variable-speed conveyor system. (Glo-Quartz Corp.)

3.3 Exposure system for polymerizing photo-resist coating.

3.4 Developing tank providing mild agitation and contaminant-free solution without solid particles (use filter and recirculating pump).

3.5 Spray-etching facility (Chemcut Etcher) with nozzle motion, conveyor water rinse.

3.6 No. 2 Zahn cup, for viscosity determination of photo-resist solution, or other suitable measurement device.

3.7 Convection-heated oven for drying parts.

3.8 Clean, temperature- and humidity-controlled area for application and development of photo-resist.

3.9 Dry-film laminator.

3.10 Dupont "A" processer for dry-film photo-resist.

4. MATERIALS

4.1 Photo-resist solution - KTFR (Kodak Thin Film Resist).

4.2 Micro-Resist thinner - Kodak.

4.3 Developer solution - Kodak or Stoddard solvent.

4.4 Etchant solution - high-quality $FeCl_3$, 44-46°Be, with additions of $NiCl_2$ and HCL as necessary to achieve a smooth, uniformly etched surface, as detailed in Appendix I.

4.5 Stripping solution - Batco #44 or equivalent.

4.6 Mylar photonegative tooling.

4.7 Dry-film photo-resist, Dupont Riston #1220 or equivalent.

4.8 Developer solution - 1,1,1-trichloroethane.

5. GENERAL INFORMATION

5.1 The purpose of this process is to provide dimensionally accurate, smooth-walled parts. Process steps outlined herein have demonstrated ability to produce acceptable parts; however, deviations from this process are permitted as long as the required dimensions and surface finish are obtained.

6. MANUFACTURING OPERATION

6.1 Method 1

6.1.1 Material of quality conforming to EMS52338 shall be used.

6.1.2 Punch holes in four corners of sheet to facilitate handling.

6.1.3 Clean sheet in accordance with the following procedure. (Note handling precautions under Process Control section of this specification.)

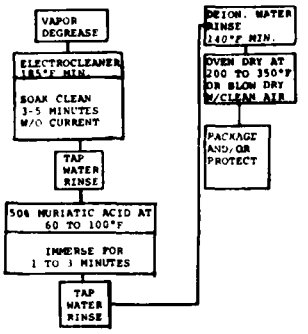

6.1.4 Strain out solid particles larger than 25 microns diameter immediately prior to use of photo-resist solution. Dip coat the sheet with photo-resist. The photo-resist viscosity must be maintained at 0.30 minutes/#2 Zahn cup. Withdrawal rate should be 11-12 inches per minute (30 setting on Gyrex dip coater).

6.1.5 Bake sheet in an infrared oven at 250°F nominal, and 18 setting (11 in/min) conveyor speed. Temperature may be adjusted 10° higher or lower to compensate for surface finish and thickness of sheet. Dark surface finishes require the lower temperature, as do thinner sheets; shiny surfaces or thick sheet require higher temperatures. Once the required temperature level has been established for each particular lot of sheet, the temperature must be controlled ±2.5° during the baking process. Sheets should be baked twice, as required, for best resist adhesion without promotion of heat-fogged areas.

6.1.6 Thick sheets, or the presence of dust particles, necessitate double dipping. Sheets which are to be doubled-dipped should be turned top to bottom (180°) prior to second coat to achieve a uniform coating density. After dipping, repeat the bake cycle above.

6.1.7 Expose sheets, using appropriate tooling, on the exposure table, making sure that vacuum holds tooling flat against sheet. Set exposure table at 3 cycles and 46 inches per minute (30 setting). This exposure promotes adhesion and full cure of photo-resist coating.

6.1.8 Remove sheet from light table and place in developer for 2 minutes, then rinse thoroughly with water spray. If defective resist images appear at this point, strip sheet and repeat procedure, starting with the cleaning operation.

6.1.9 Bake sheet for 20 minutes at 250°F ±15 in a convection-heated oven for maximum toughness of the photo-resist coating. If maximum toughness is not required to prevent resist breakdown, a two-hour air-dry cycle may be substituted; this alternate drying cycle will allow easier stripping after etching.

6.1.10 Calculate time necessary to etch through sheet, using thickness of stock and etch rate determined by previous measurements on a sample part. Set conveyor speed on etcher to allow part to "drop out" in two passes through the etcher, alternating sides of the sheet and turning 90° between passes. Several short-duration passes may be necessary to establish total etching time required on a "first-article" basis. Dimensional inspection of the part is to be used to determine when etching is complete.

6.1.11 Parts shall be stripped after etching is complete. Immerse parts in Batco #44 stripping solution for a period of time sufficient to lift photo-resist from surface, then rinse with water spray and methanol rinse, followed by air dry. Note that bare metal surfaces are again exposed, and care must be used to avoid contamination of surfaces.

6.1.12 Inspect parts for dimensions and signs of photo-resist breakdown. Segregate and identify rejects and finished parts.

Wrap parts in clean, white tissue paper, and place in a sturdy container, along with the applicable paperwork.

6.2 Method 2

6.2.1 Material of quality conforming to EMS52338 shall be used.

6.2.2 Punch holes in four corners of sheet to facilitate handling.

6.2.3 Clean sheet using the same procedure specified for Method 1. (Note handling precautions under Process Control section of this specification.)

[illegible].4 Preheat clean sheet metal in oven maintained at 190°F ±10 for 10 to 15 minutes.

[illegible].5 Remove sheets from oven and laminate within 5 seconds. Laminator settings are 250°F ±10, roll air pressure 40 psi ±2, roll speed 5 fpm ±0.5 (may be setting 3.4). Trim excess resist from edges of sheets and allow to cool to room temperature before exposure.

[illegible].6 Expose sheets, using appropriate masters, on the Cyrex Vertex II exposure unit. Ensure that the vacuum holds tooling flat against sheet on both sides, and expose one cycle at a speed control setting of 10. Remove sheet and allow to stabilize 15 minutes minimum before developing.

[illegible].7 Remove protective Mylar film from resist on both sides, and slit into developer inlet banner of the Dupont "A" processor. Insure developer (1,1,1-trichloroethane) is at 68°F ±2. Set timer for 50 seconds and start spray developer cycle. After 50-second cycle is complete, remove sheet from chamber, immerse sheets in clean 77°F ±5 1,1,1-trichloroethane and agitate. Do not exceed 20 seconds immersion in trichloroethane, and immediately place sheets in water spray rinse chamber for 1.5 minutes ±0.5. Remove panels from banner, blow excess water from surface with air (<50 psig) pressure air, and allow sheets to air dry for at least one hour prior to baking.

[illegible].8 Cure sheets in convection oven, using a slow heating rate to prevent blistering of the photo-resist. Heat from room temperature (77°F) to 250°F ±10 at a rate not to exceed 1°F per minute. A 30-minute soak at 250°F ±10 is required. Remove sheets and allow to cool to room temperature before etching.

[illegible].9 Inspect sheets for areas of incomplete resist adherence, poor image quality, or extra resist (missing or chipped resist). Sheets with no defects should be stripped and recycled to step 6.2.3 for reprocessing. Sheets that exhibit small areas of missing resist in noncritical areas may be touched up by applying General Electric "Red Crystal Resist Enamel" with an artist's brush. Allow 15-minute minimum air dry between touch-up and etching.

6.2.10 Etch parts as described in Method 1, step 6.1.10. Note that dry film resist is sensitive to thermal shock and "drying up" of the resist after etch is initiated. For this reason, a hot-water (120°F ±20) rinse and holding tank are required for parts that are not being actively etched.

[illegible].11 Proceed as in Method 1, step [illegible].

[illegible].12 Proceed as in Method 1, step [illegible].

7. [illegible]

7.1 Handle sheets with clean, lint-free, white cotton gloves. Clean surgical gloves are optional. Fingerprints or other contaminants must be avoided at all points in the manufacturing sequence.

7.2 Method 2 only - Viscosity of the photo-resist solution shall be checked at least every 8 hr hours while in use. Addition of thinner or unthinned photo-resist shall be made until the correct viscosity is obtained.

7.3 (Method 2 only - Temperature of developer shall be maintained at 68°F ±2. Developer shall be changed at regular intervals based on usage as determined for a process by area-meter. Developer change shall be made every 100 hours of service.

7.4 The etchant solution shall be changed and the etcher cleaned prior to retailing when the etching rate drops below a reasonable level, typically half the etching rate of a fresh solution. Etching rate of fresh solution is approximately 0.0015 in. per thickness reduction when chemical milled from both sides. The etchant shall meet the requirements of Appendix A.

7.5 All exposure and master material, sheet storage and handling devices, and any surfaces or material with which these parts, devices, or materials may come in contact must be free of dust and contaminants. All processing, as well as storing of sensitive materials, must be performed in a temperature and humidity-controlled area. Lighting must be controlled to avoid inadvertent exposure of photosensitive materials. An adequate area is met by the following description: cold fluorescent lighting, non-dust-generating work surfaces, good housekeeping practices, and 10-micron filtered air at 70°F ±5° and <40% relative humidity. A specific exception to this is the etching and chemical milling area which, because of its corrosive nature, must be separated from the controlled-environment area.

8. [illegible]

8.1 Prior to photo-resist application, sheet material shall be visually inspected for condition and freedom from any particulate contamination. Material shall be free from oil and grease as determined by a water break-free test.

8.1.1 Water break-free test shall be performed by applying distilled water to cover approximately one square inch of the sheet; the water shall remain as a film and not form drops for at least ten seconds.

8.2 The applied photo-resist coating shall be uniform in thickness, and free from pinholes, blemishes or foreign matter. The coating shall demonstrate tight adherence and full-cured resistance to attack in the etching process, as determined by running a test sample through the etching cycle and inspecting at up to 10X for pitting, lifting, flaking, or other evidence of breakdown.

8.3 The finished parts shall be smooth-walled and dimensionally accurate.

9. QUALITY ASSURANCE

9.1 The nature of thin-film resist systems available and the aggressiveness of the etchant required for cold-worked superalloy sheet dictate that careful control of each process step be maintained.

9.2 Photographs in Appendix I shall be used as criteria for acceptance/rejection of parts based on surface condition.

9.3 Parts not meeting the requirements of this specification shall be rejected.

PROCESS SPECIFICATION	CODE IDENT NO 99193	SPECIFICATION NO PC5021	REV LTR B

APPENDIX I

REQUIRED SURFACE FINISH, UNIFORMITY AND APPEARANCE OF ETCHED SURFACES FOR PHOTOCHEMICAL MACHINING AND CHEMICAL MILLING - ASTROLOY AND WASPALOY

1. It is necessary to obtain smooth, even etching in both chemical milling (thickness reduction) and photochemical machining (chemical blanking) operations. If an even etch is not obtained, dimensional tolerances cannot be met, and scrap rates will approach 100%.

1.1 Always run a sample of the material to be etched prior to running the parts. Do not run parts unless the required etching quality has been obtained on the sample.

1.2 Typical Etchant Solution:

10% by volume HCl at 20° Be
Balance $FeCl_3 \cdot 6H_2O$ at 44-46° Be
(Additional HCl or $NiCl_2$ as necessary)

2. The following photographs (Figures 1-12) shall be used as a guide for acceptable surface finish, appearance, and uniformity.

PROCESS SPECIFICATION	CODE IDENT NO 99193	SPECIFICATION NO PC5021 (APPENDIX I)	REV LTR B

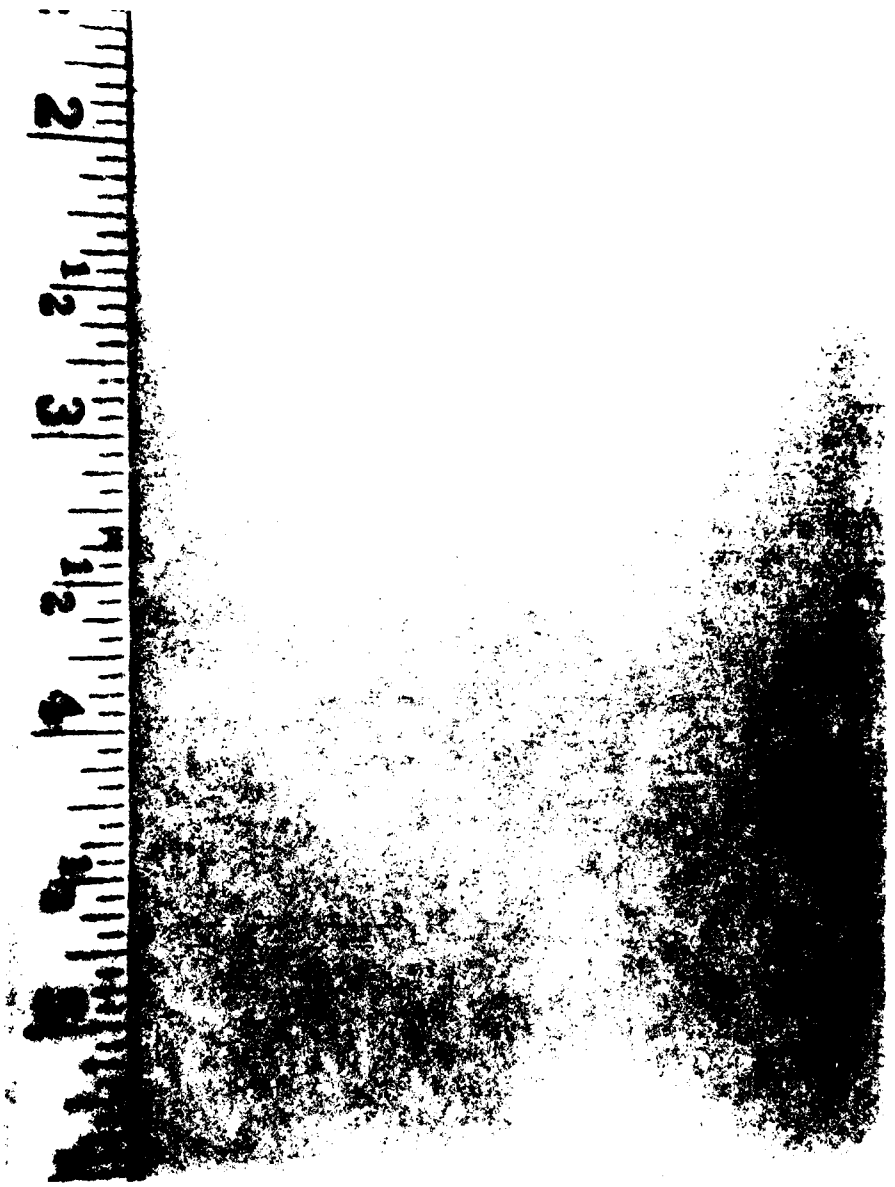

FORM PS704 1

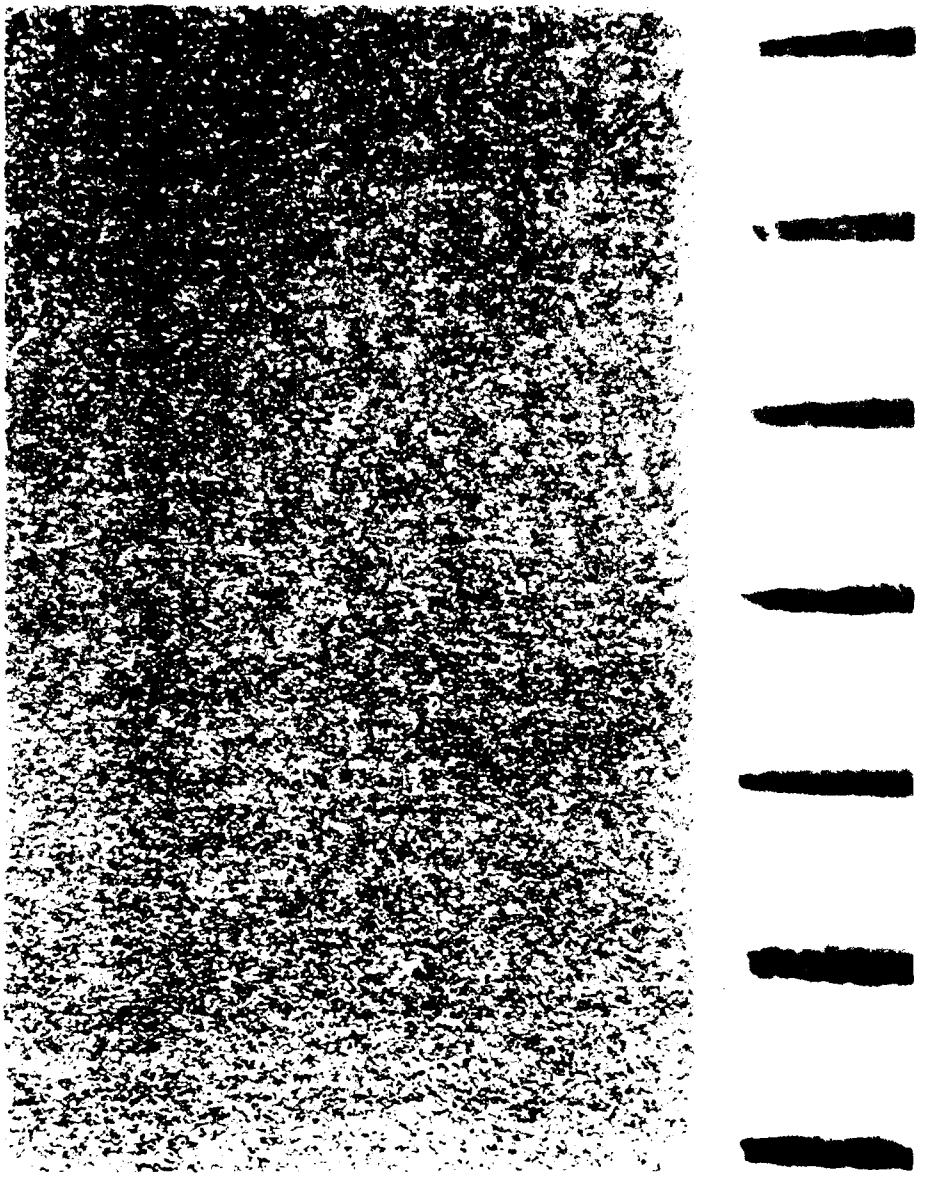

Figure 2 - (X) Acceptable

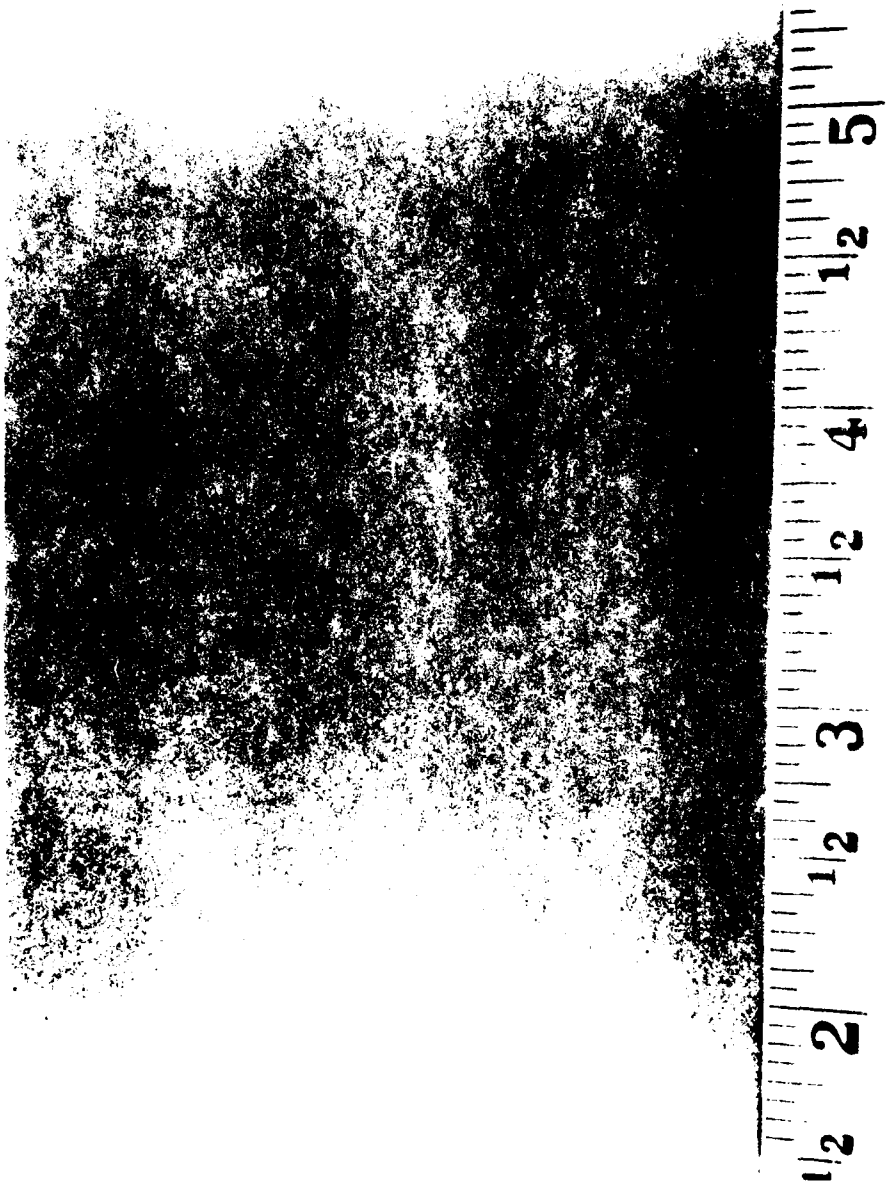

Figure 3 - (3X) Acceptable

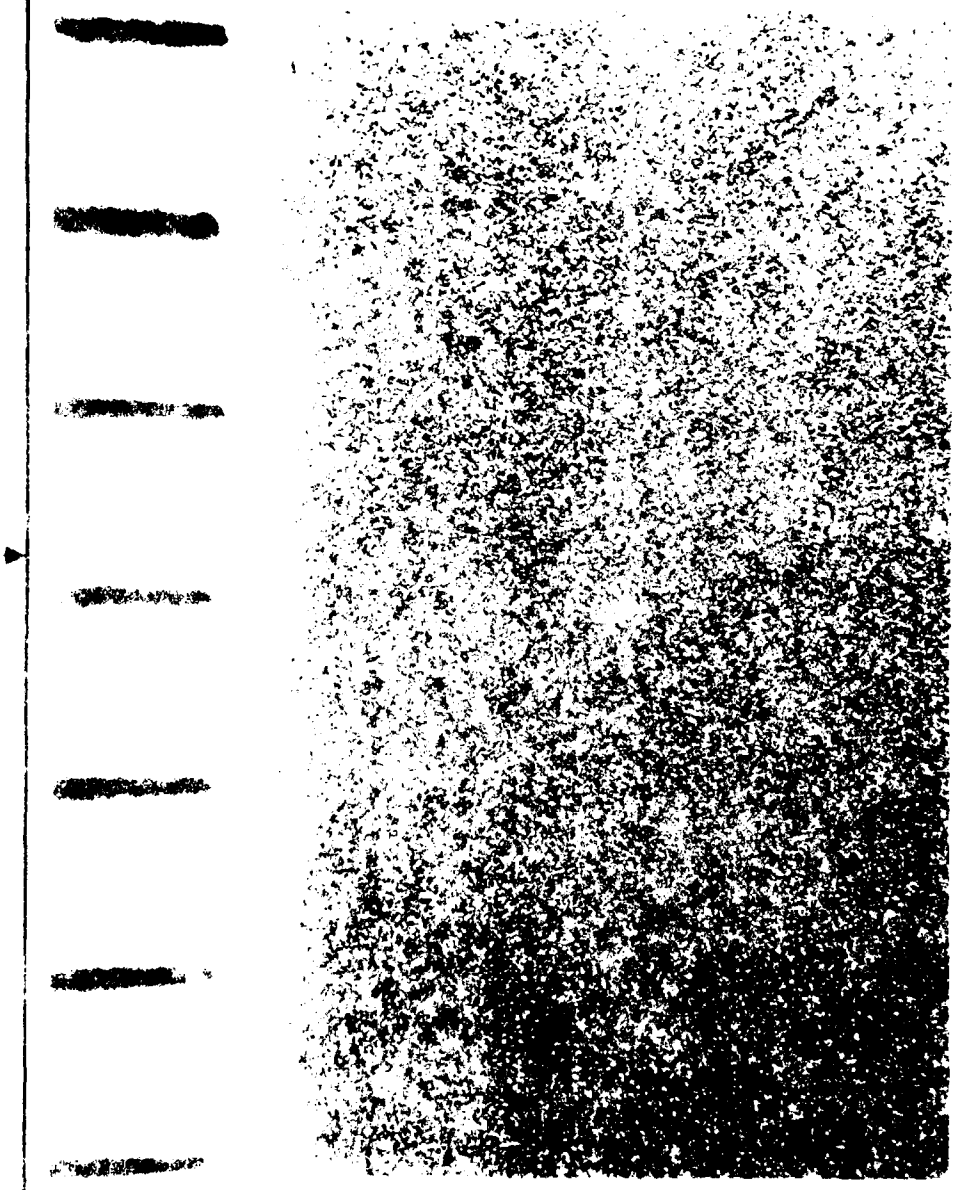

Figure 4 - (20X) Acceptable

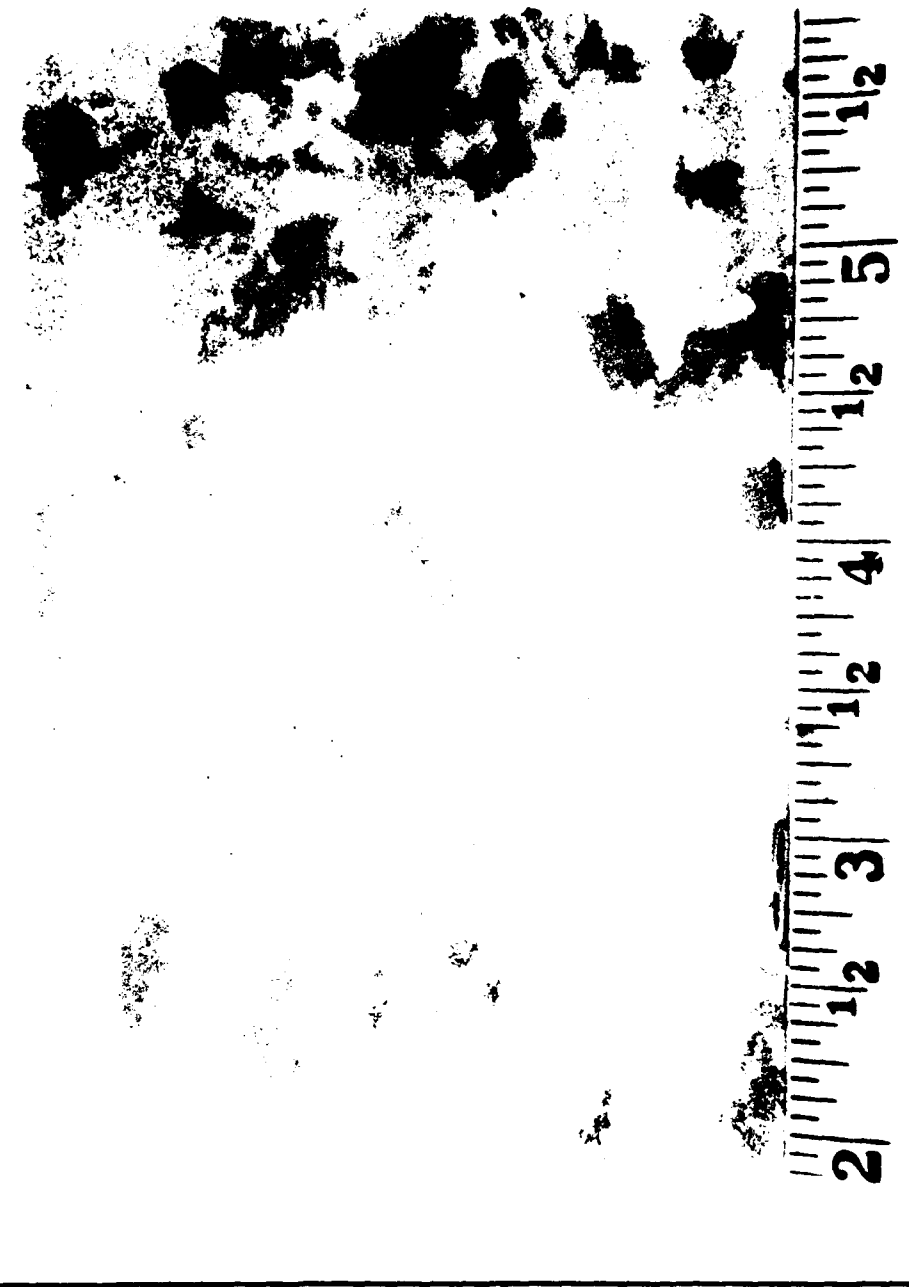

Figure 5 - (2X) Marginal, Coarse, Acceptable for Photochemical Machining, Not Acceptable for Chemical Milling

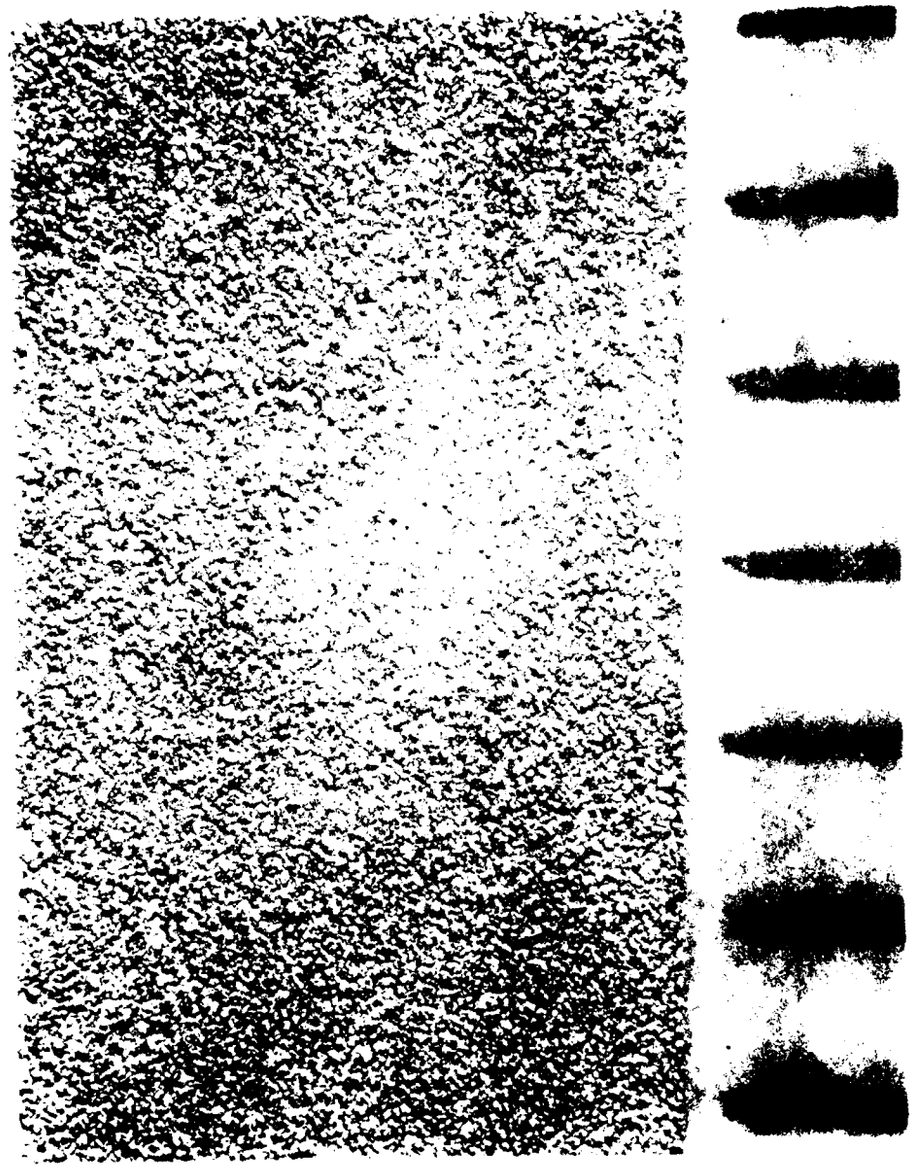

Figure 6 – 100X Marginal, Coarse, Acceptable for Photochemical Machining, Not Acceptable for Chemical Milling

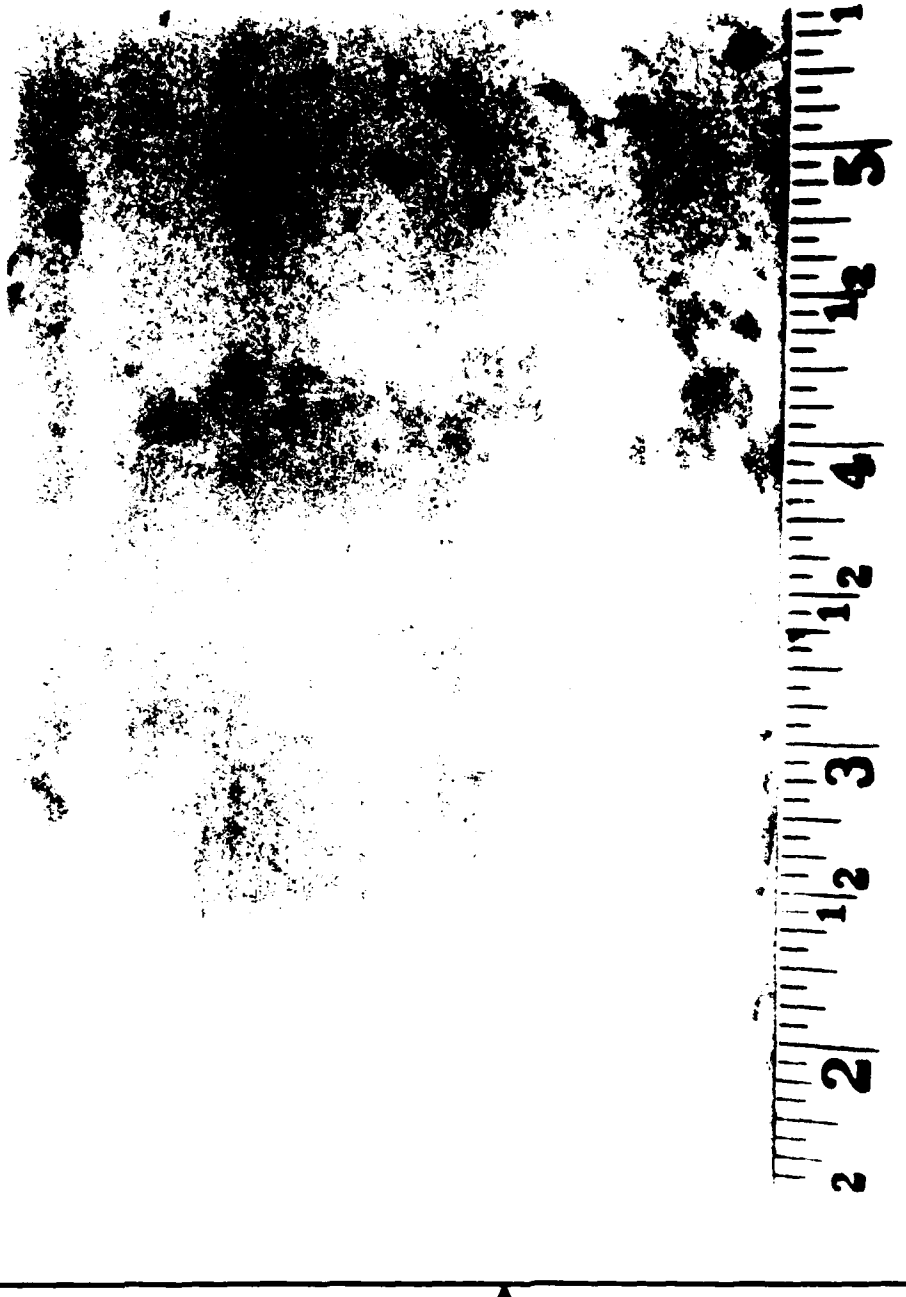

Figure 7 - (2X) Not Acceptable, Coarse, Nonuniform

PROCESS SPECIFICATION	CODE IDENT NO 99193	SPECIFICATION [illegible]	REVISION B

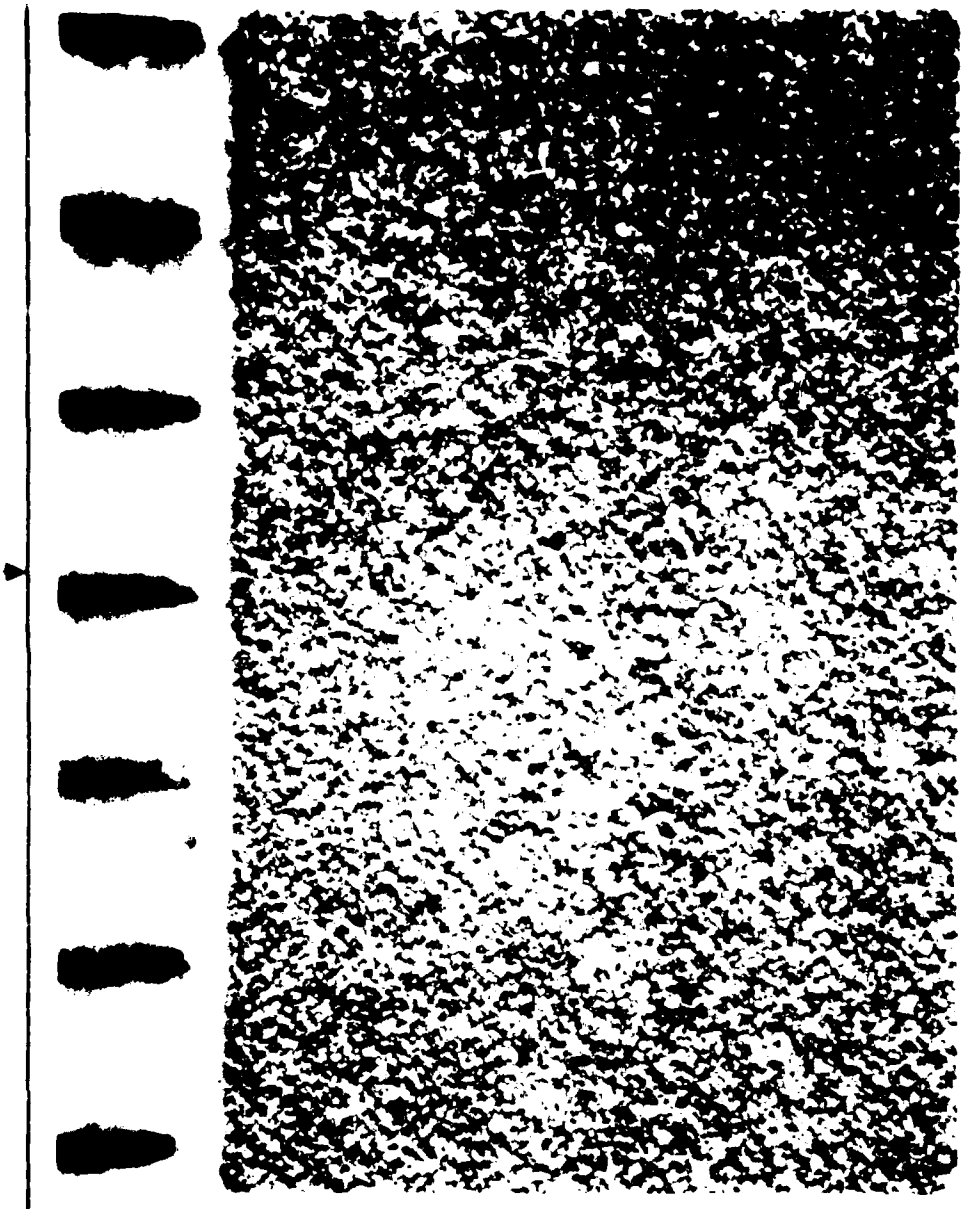

PAGE [illegible]

Figure 9. (XX) Not Acceptable - Pitted, Nonuniform

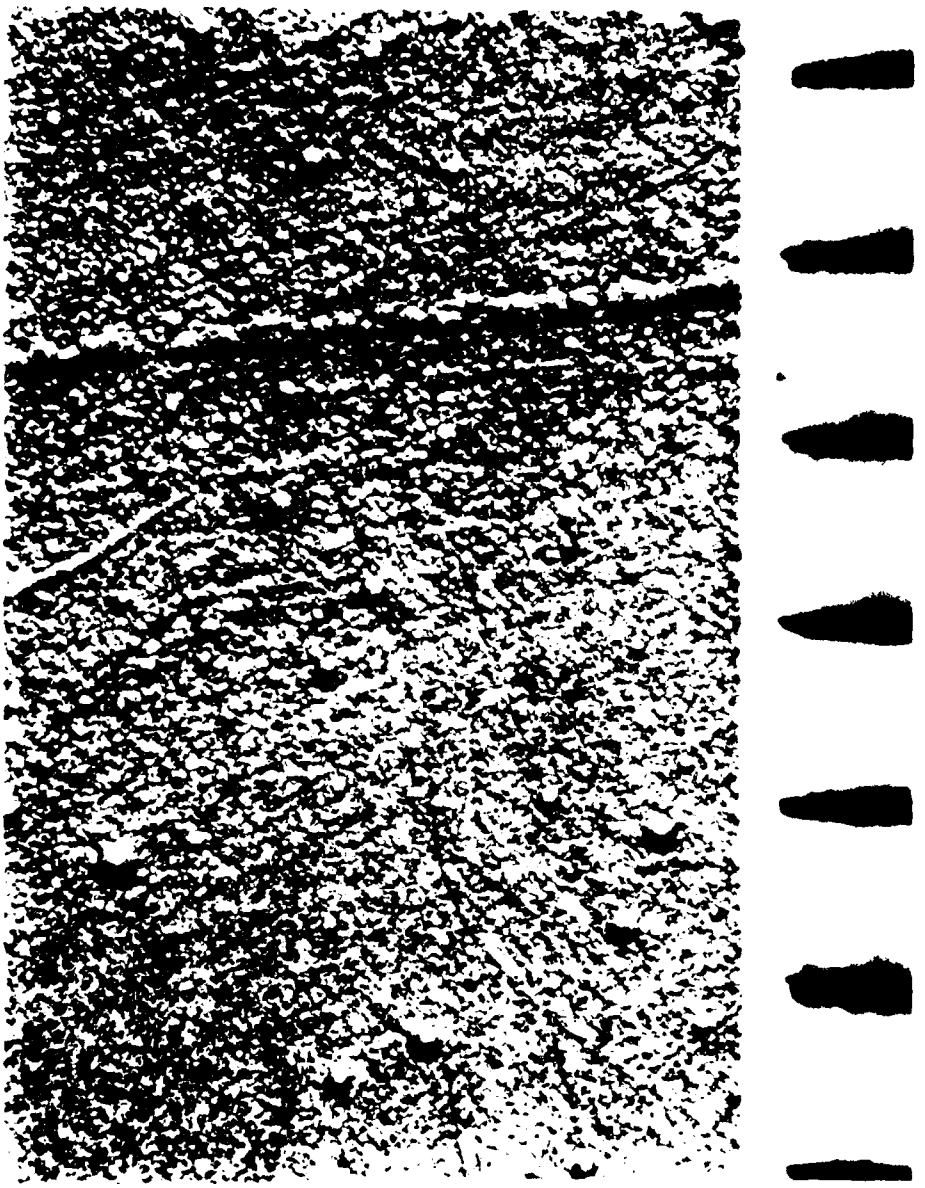

Figure 10 - (20X) Not Acceptable - Pitted, Nonuniform

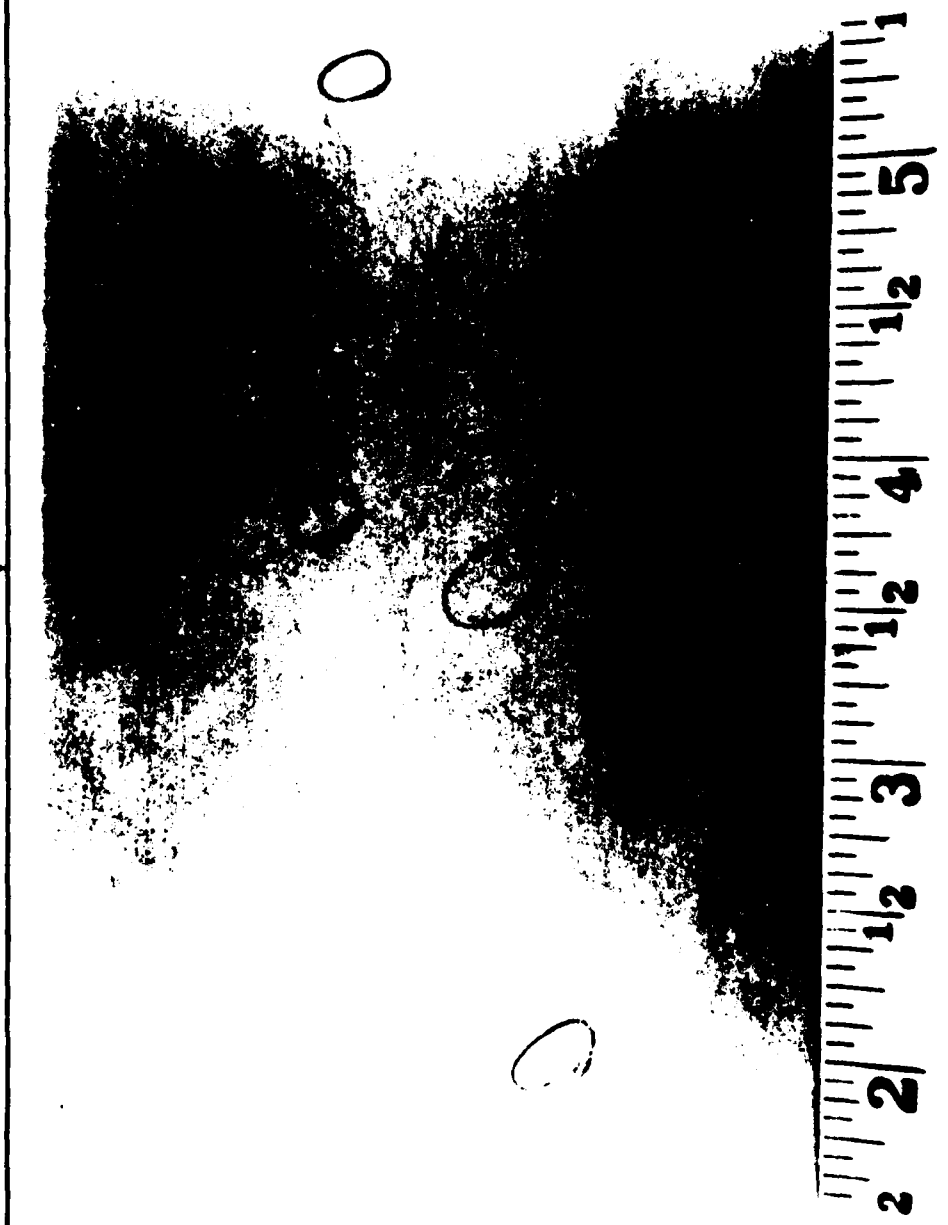

Figure 11 - (2X) Not Acceptable - Unetched Peaks (Due to Oil Contamination)

Figure 12 - (20X) Not Acceptable - Unetched Peaks (Due to Oil Contamination)

LIST OF SYMBOLS

A_{cr}	Critical velocity
C_p	Specific heat
E	Elastic modulus
g	Gravitational constant
H	Isentropic specific work
J	Mechanical equivalent of heat
K	Rotor exit mean-to-inducer-tip radius ratio
K_T	Stress concentration factor
M_{NR}	Relative Mach number
N	Rotational speed
N_s	Specific speed
$N/\sqrt{\theta}$	Corrected speed
$P_{R_{t-t}}$	Total-to-total pressure ratio
P_s	Static pressure
Q	Volume flow rate
R	$\frac{\text{Minimum stress}}{\text{Maximum stress}}$
R_e	Reynold's number
$R_{e,base}$	Base Reynold's number of specific speed curve
R_{H3}	Rotor exit hub radius
R_{T3}	Rotor exit tip radius
R_{3M}	Rotor exit mean radius
$S_{(x)}$	Standard deviation of x
T	Temperature
U	Rotor wheel speed

LIST OF SYMBOLS (CONTD)

U_{t3}	Rotor exducer tip wheel speed
U_2	Inducer tip speed
V	Absolute velocity
V_M	Meridional velocity
V_R	Absolute radial velocity
V_u	Absolute tangential velocity
V_x	Absolute axial velocity
W	Relative velocity
W_c	Cooling flow
W_p	Rotor inlet primary flow
W_u	Relative tangential velocity
$\frac{W\sqrt{\theta}}{\delta}$	Inlet corrected flow
Z_{tip}	Axial distance along rotor tip

LIST OF SYMBOLS (CONTD)

GREEK SYMBOLS

α	Absolute flow angle
β	Relative flow angle
ΔE_T	Total strain range
ΔH	Stage specific work
$\Delta H/\theta$	Corrected stage specific work
$\Delta \sigma$	Total stress range
ΔS	Change in entropy across rotor
γ	Ratio of specific heat
η_t	Total efficiency
$\eta_{t,base}$	Base total efficiency from specific speed curve
η_{t-t}	Total-to-total efficiency
λ_{STG}	Stage work coefficient
$\lambda_{2,i}$	Ideal rotor inlet work coefficient (from slip factor criteria)
$\lambda_{2,OPT}$	Optimum rotor inlet work coefficient (with tip speed limitation)
λ_{3M}	Rotor exit mean work coefficient
$\bar{\omega}$	Interstage duct loss coefficient with swirl
$\bar{\omega}_{min}$	Minimum interstage duct loss coefficient

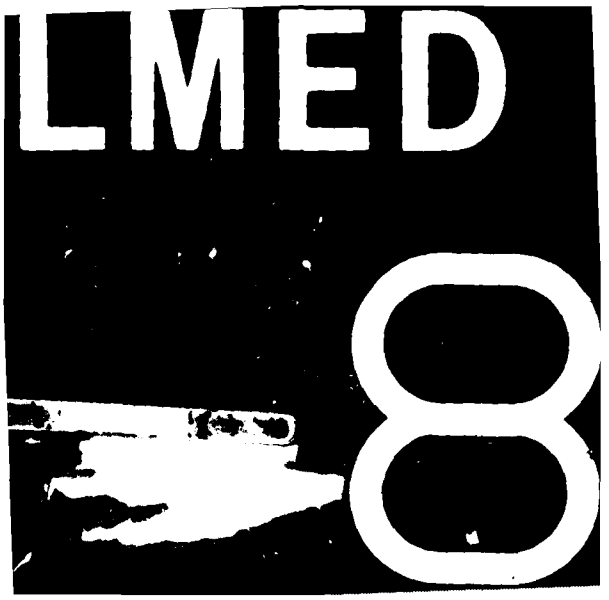
LMED
8